

**Ministry of Higher Education and Scientific Research
University of Baghdad
Institute of Laser for Postgraduate Studies**



Design and Performance Investigation of Smartphone Based Colorimetric Sensor

**A Thesis Submitted to the Institute of Laser for Postgraduate
Studies, University of Baghdad in Partial Fulfillment of the
Requirements for the Degree of Doctor of Philosophy in Laser
/ Electronic and Communication Engineering**

By

Taif Aied Faisal

B.Sc. Laser and Optoelectronics Engineering - 2013

M.Sc. Laser and Optoelectronics Engineering - 2017

Supervisor

Asst. Prof. Dr. Zainab Fadhil Mahdi

2021 AD

1442 AH

Certification

I certify that this thesis was prepared under my supervision at the Institute of Laser for Postgraduate Studies, University of Baghdad, in a partial fulfillment of requirements for the degree of a Doctor of Philosophy in Laser / Electronic and Communication Engineering.

Signature:

Name: **Dr. Zainab Fadhil Mahdi**

Title: **Asst. Professor**

Address: Institute of Laser for Postgraduate Studies

University of Baghdad

Date: / / 2021

In view of the available recommendation, I forward this thesis for debate by Examining Committee

Signature:

Name: **Dr. Hanan Jaafar Taher**

Title: **Asst. Professor**

Address: Head of the scientific committee

Institute of Laser for Postgraduate Studies

University of Baghdad

Date: / / 2021

Examining Committee Certificate

We certify that we have read this thesis "Design and Performance Investigation of Smartphone Based Colorimetric Sensor" and as examination committee we examined the student in its contents and in our opinion it is adequate with standards as a thesis for the degree of a Doctor of Philosophy in Laser / Electronic and Communication Engineering.

Signature:

Name: **Dr. Bassam G. Rasheed**

Title: Professor

Address: College of Engineering,
Al Nahrain University

Date: / 05 / 2021

(Chairman)

Signature:

Name: **Dr. Shelan K. Tawfeeq**

Title: Asst. Professor

Address: Institute of Laser for
Postgraduate Studies, University of
Baghdad

Date: / 05 / 2021

(Member)

Signature:

Name: **Dr. Mohammad K. Dhahir**

Title: Asst. Professor

Address: Institute of Laser for
Postgraduate Studies,
University of Baghdad

Date: / 05 / 2021

(Member)

Signature:

Name: **Dr. Hanan J. Taher**

Title: Asst. Professor

Address: Institute of Laser for
Postgraduate Studies, University of
Baghdad

Date: / 05 / 2021

(Member)

Signature:

Name: **Dr. Shaymaa R. M. Ali**

Title: Asst. Professor

Address: College of Engineering,
Al Nahrain University

Date: / 05 / 2021

(Member)

Signature:

Name: **Dr. Zainab F. Mahdi**

Title: Asst. Professor

Address: Institute of Laser for
Postgraduate Studies, University of
Baghdad

Date: / 05 / 2021

(Supervisor)

Approved by the deanship of Institute of Laser for Postgraduate Studies, University of Baghdad.

Signature:

Name: **Prof. Dr. Hussein A. Jwad**

Title: Dean

Address: Institute of Laser for Postgraduate Studies, University of Baghdad

Date: / 05 / 2021

Dedication

At this moment in time, I dedicate my efforts to the people who put me ahead of themselves and did make everything possible for me to do my work -My family- being a lucky son to be born and raised by the most encouraging father and the most caring mother, the friendliest environment for me to make this work into existence.

I hope my family will be proud of this moment to celebrate the final achievement of their elder son to hold the PhD certification.

Acknowledgment

I would proudly mention the people whom I express my deepest respect, and appreciation. My supportive, astounding and caring supervisor *Asst. Prof. Dr. Zainab Fadhil Mahdi*, in which simple plane words are not enough for me to express my sincerest gratitude and acknowledgment.

To the current dean of the Institute of Laser for Postgraduate Studies *Prof. Dr. Hussien A. Jawad*, for teaching me and making things go smoothly during the research period.

To the past dean of the Institute of Laser for Postgraduate Studies *Prof. Dr. Abdul Hadi M. Al-Janabi*, for his existence as a godfather with caring, motivating, and supportive advices whenever I needed, for making my scholarship program go smoothly, with all my respect and appreciation.

To the head of the Department of Industrial and Engineering Applications *Asst. Prof. Dr. Mohammad K. Dhahir*, for being very helpful and encouraging and always providing optimism with his blissful smile.

To the instructors whom provided me with their best efforts the latest information available during the study period and the seminars sessions, *Asst. Prof. Dr. Shelan K. Tawfeeq, Dr. Rabab Al-Darraji, Asst. Prof. Dr. Tahreer S. Mansour, Asst. Prof. Dr. Hanan J. Taher, Dr. Mahmoud S. Mahmoud, Dr. Ziyad A. Taha, and Dr. Jwad A. Hassan*.

To the kind and helpful *Dr. Rawaa A. Faris*, for her fruitful discussions, suggestions, and helpfulness always.

To the staff of the Institute of Laser for Postgraduate Studies, for making everything go easily. To the Iraqi Ministry of Higher Education and Scientific Research, and the University of Baghdad, for acknowledging the scholarship. To the Italian Ministry of Foreign Affairs and International

Cooperation (Rome, Lazio). For funding me with a 9-month scholarship. To the "*La Sapienza University of Rome*" for hosting me for nine months in the university.

To *Prof. Dr. Roberto Beraldi*, La Sapienza University of Rome, for collaborating with me in the thesis work throughout the research period, giving advices, suggestions and paving the way towards new insights in the research field, always being motivating and encouraging. I highly appreciate his input to my work.

To *Prof. Dr. Francesca Cuomo*, La Sapienza University of Rome, for teaching me Smart Environments and supervising me with project work. To my Italian colleague the PhD student, *Gabriele Proietti Mattia*, for his input and great discussions with the research work.

To the Iraqi Embassy in Rome, and the Iraqi ambassador, *Safia Al-Suhail*, for being helpful during the COVID-19 pandemic. To the Italian Embassy in Baghdad, and especially, *Dr. Antonio Puggioni*, and *Dr. Alessandro Mignini*.

To *Asst. Prof. Dr. Anwaar Aldegazly*, *Dr. Fatima H. Rajab*, *Prof. Dr. Raad Sami Fyath* Al Nahrain University, Laser and Optoelectronics Engineering Department, for recommending me to the scholarship.

Taif Alawsi

Abstract

Recently, smartphone-based imaging and sensing made possible the applications of multidisciplinary fields to come through a unique platform in which all the processes happen rapidly and smoothly. The utilization of smartphone-based approaches made significant advancements being a reliable tool for rapid testing, diagnostics, on-site measurement and monitoring.

In this research, a smartphone-based colorimetric sensor was realized and experimentally verified and demonstrated, the colorimetric sensor of both hardware and software aspects was implemented experimentally for measurement and imaging of multi-biomaterials including whole blood, urine, glucose, triglycerides, urea, HDL, and bilirubin. These measurements and imaging were done on the existing laboratory devices, as well as with software only and with both smartphone-based colorimetric sensor hardware and software.

For software only and laboratory instrument work the samples of glucose and triglycerides, were prepared with concentrations of (100, 200, 300, 400, 500 mg/dL) and urea concentrations were (10, 30, 50, 100, 150 mg/dL). The measured wavelength ranges were for glucose (350 – 640 nm), triglycerides (400 – 680 nm), and urea (500 – 780 nm). Resulting in an absorbance and transmittance regression coefficient (R^2) for the colorimetric sensing application were 0.9825, and 0.9899; 0.9405 and 0.9502; 0.9431 and 0.8597, respectively. While for the spectrophotometer measurement the (R^2) values were 0.9973 @560 nm and 0.9793 @600 nm; 0.952 @620 nm and 0.9364 @410 nm; 0.9948 @570 nm and 0.9827 @530 nm, respectively.

The feasibility of the novel smartphone-based 3D printed design was demonstrated with the aid of an Android application intended solely to measure the concentration of multiple biomarker samples based on the

colorimetric detection approach. The optical and electronic elements inside the adapter provide a reliable imaging platform for image acquisition, analysis, rapid testing, and measurements. 3D printed smartphone-based adapter design has been implemented and tested for colorimetric applications in biomarkers including glucose, urea, triglycerides, bilirubin, and HDL.

Results showed that the linear regression coefficient (R^2) values for the absorbance curve of glucose using the illumination sources of 405 nm; 532 nm; 650 nm; WLED; WLED+BF; WLED+GF; WLED+YF; and WLED+RF are 0.9922; 0.9983; 0.9898; 0.7004; 0.9518; 0.9313; 0.9567; and 0.9407, respectively. Following the same order of illumination sources, the R^2 of urea 0.9332; 0.9818; 0.8829; 0.9464; 0.6615; 0.9161; 0.9567; and 0.7502. For triglycerides the R^2 values are 0.9496; 0.9725; 0.7749; 0.8395; 0.8192; 0.9313; 0.9567; and 0.944. For bilirubin the R^2 values are 0.7858; 0.9422; 0.7791; 0.9124; 0.9326; 0.6192; 0.5894; and 0.324. For HDL the R^2 values are 0.8248; 0.7831; 0.7902; 0.8332; 0.9077; 0.8071; and 0.998.

For transmittance curves the R^2 values with the same order of illumination sources and biomarkers are (0.9915; 0.9965; 0.9862; 0.6997; 0.9398; 0.916; 0.9545; and 0.9398), (0.9263; 0.9818; 0.8829; 0.9464; 0.6615; 0.9161; 0.9567; and 0.752), (0.9035; 0.955; 0.9859; 0.8333; 0.8063; 0.9298; 0.9545; and 0.9533), (0.7123; 0.9446; 0.8971; 0.9241; 0.9289; 0.563; 0.6669; and 0.3565), (0.7658; 0.8003; 0.8364; 0.8418; 0.9108; 0.9044; 0.7954; and 0.9575), respectively.

The limit of detection (LOD) for glucose, urea, triglycerides, bilirubin, and HDL was 0.57 mg/dl or 0.03135 mM, 1.34 mg/dl or 0.2278 mM, 7.79 mg/dl or 0.0879 mM, 0.008 mg/dl or 0.14 μ M, and 0.86 mg/dl or 0.02224 mM, respectively.

Contents

No.	Subject	Page
	Abstract	i
	Contents	iii
	List of abbreviations	v
	List of symbols	vii
	List of tables	viii
	List of figures	ix
	Chapter One: Introduction and Basic Concepts	
1.1	Motivation	1
1.2	Lab-on-Chip	2
1.2.1	Smartphone-Based Adapter (Hardware)	3
1.2.1.1	Smartphone	3
1.2.1.2	Optical Components	7
1.2.1.3	Illumination Sources	7
1.2.1.4	3D Printing	8
1.2.2	The Software	9
1.2.2.1	SolidWorks	10
1.2.2.2	Cura Ultimaker	11
1.2.2.3	Android Studio	11
1.3	Sensors	12
1.4	Biosensors in the Smart Environment	14
1.5	Biomarkers	14
1.6	Colorimeter	16
1.7	Image Processing	18
1.8	Smartphone 3D Printed Adapter Design Guide	23
1.9	Performance Characterization of Smartphone Adapters	26
1.10	Literature Review	28
1.12	Aim of the Work	32
1.13	Thesis Outline	33
	Chapter Two: Materials, Methods, and Experimental Work	
2.1	Introduction	34
2.2	Materials and Methods	34
2.3	The Components	35
2.4	Material Preparation	37
2.5	Experimental Work	39
2.5.1	Smartphone-Based Bioimaging of Whole blood and Urine (Microscopy)	39
2.5.2	Colorimetric Analysis for Biochemical Samples with Android Smartphone Application	41

2.5.3	Smartphone-Based 3D Printed Design with the Aid of Android Application	47
2.6	Complexity Analysis	48
2.6.1	Hardware	49
2.6.2	Sample Preparation and Measurements	50
2.6.3	Software	51
	Chapter Three: Results, Discussion, Conclusions and Future Work	
3.1	Introduction	53
3.2	Smartphone Bioimaging 3D Printed Adapter (Microscopy)	53
3.2.1	Using 532 nm Laser Diode	53
3.2.2	Using White LED	55
3.2.3	Using 650 nm Laser Diode	56
3.3	Colorimetric Analysis for Biochemical Samples with Android Smartphone Application	57
3.4	Smartphone-Based 3D Printed Design with the Aid of Android Application	72
3.5	Performance Comparison	91
3.5	Conclusions	94
3.6	Future Work	95
	References	96-108
	Appendices	A-1-E-6

List of Abbreviations

Abbreviation	Description
3D	Three-Dimensional
ABS	Acrylonitrile Butadiene Styrene
BS	Beam Splitter
CAD	Computer-Aided Design
CL	Chemiluminescent
CMOS	Complementary Metal-Oxide Semiconductor
CNC	Computer Numerical Control
CPU	Central Processing Unit
CRP	C-reactive Protein
DC	Direct Current
DNA	Deoxyribonucleic acid
E. coli	Escherichia-coli
ELISA	Enzyme-Linked Immunosorbent Assay
GPS	Global Positioning System
GPU	Graphics Processing Unit
GUI	Graphical User Interface
HD	High-Definition
HDL	High-Density Lipoprotein
HIV	Human Immunodeficiency Virus
HPU	High Pick Up
HSV	Hue, Saturation, and Value
IOS	iPhone Operating System
IoTs	Internet of Things
ISO	International Organization for Standardization
JPEG	Joint Photographic Experts Group
LED	Light Emitting Diode
LFIA	Lateral Flow Immunoassay
LOC	Lab-on-chip
LOD	Limit of Detection
PC	Personal Computer
PCR	Polymerase Chain Reaction
PET	Polyethylene Terephthalate
PETG	Polyethylene Terephthalate Glycol-modified
PLA	Polylactic Acid
POC	Point-of-Care
PSA	Prostate-Specific Antigen
RGB	Red, Green, and Blue
TSB	Total Serum Bilirubin
TTL	Time to Live
UA	Uric Acid

USB	Universal Serial Bus
UV	Ultraviolet
Wi-Fi	Wireless Fidelity

List of Symbols

Symbol	Description
A	Absorbance
b	Sample length
B_0	Blue channel background
B_s	Blue channel sample
c	Sample concentration
C_1	Original concentration
C_2	Prepared concentration
CV%	Coefficient of Variation
err%	The absolute average error percentage
G_0	Green channel background
G_s	Green channel sample
I	Sample intensity of the RGB colored image
I_0	Background intensity of the RGB colored image
I_B	Blue channel intensity
I_G	Green channel intensity
I_R	Red channel intensity
I_{total}	Total channels intensity
n	Integer
N	Number of samples
R_0	Red channel background
R^2	Regression Coefficient
R_s	Red channel sample
S_B	Bilirubin Sensitivity
S_G	Glucose Sensitivity
S_H	HDL Sensitivity
S_T	Triglycerides Sensitivity
S_U	Urea Sensitivity
T	Transmittance
V_1	Original volume
V_2	Prepared volume
$\varepsilon(\lambda)$	Molar absorptivity

List of Tables

Table No.	Title of Table	Page
1.1	Summary of smartphone adapter design and applications	27
2.1	Parameters values for 3D model design	41
3.1	Comparison of different methods, and approaches in various techniques of concentration measurements	70
3.2	Literature performance comparison for different techniques with all reported samples	76

List of Figures

Figure No.	Title of Figure	Page
1.1	Schematic diagram of the smartphone-based adapter (Hardware)	3
1.2	Types of smartphone built-in sensors [7]	5
1.3	Schematic of the imaging CMOS camera sensor with its function [8]	6
1.4	Optical component sets for different purposes [9]	7
1.5	Different manufacturers of 3D printer [15]	9
1.6	Android Studio IDE Project template [18]	12
1.7	Classification of sensors [20]	13
1.8	Schematic of a biosensor [21]	13
1.9	Biomarkers 3D chemical structure (a) Glucose [28] (b) Urea [29] (c) Triglycerides [30] (d) Bilirubin [31] (e) HDL [32]	16
1.10	Commercial Colorimeter schematics (1) Wavelength selection, (2) Printer button, (3) Concentration factor adjustment, (4) UV mode selector (Deuterium lamp), (5) Readout, (6) Sample compartment, (7) Zero control (100% T), (8) Sensitivity switch, (9) ON/OFF switch [33]	17
1.11	The CIE 1931 color space chromaticity diagram [35]	19
1.12	RGB values for a colored image	20
1.13	RGB color component and axis coordinate [40]	21
1.14	RGB image and the components of each channel [40]	21
1.15	Biochemical applications of smartphone adapter (a) Transmission light microscope based on smartphone, [59], by Skandarajah, et al. under the Creative Commons license. (b) Smartphone-based adapter, [61], by You, et al. © copyright 2017 American Chemical Society. (c) 3D-printed device with its different parts [62], by Alvarez-Diduk, et al. under the Creative Commons license. (d) Smartphone Biochemiluminescence adapter, [63], by Roda, et al. © copyright 2014 American Chemical Society. (e) Cellphone-enabled image acquiring system, [64], by Cui, et al. © copyright 2018 American Chemical Society.	25
2.1	Prepared biochemical samples with six different concentrations labeled in the figure in mg/dl of (a) Glucose (b) Urea (c) Triglycerides (d) Bilirubin (e) HDL	38

2.2	Schematic layout of the experimental work	39
2.3	Schematic layout of the design and implementation of smartphone 3D adapter for microscopy	40
2.4	Images of biochemical samples (12 Mpx); glucose (Pink; left side images) triglycerides (Purple; middle images) urea (Green; right-side images) at 20 cm distance (a) without flash and no reflection (b) with flash (b) with flash and reflection	45
2.5	Schematic illustration of the imaging mechanism showing both background and sample image	45
2.6	Colorimetric sensing application workflows (a) with a single image background (light green box) (b) with a background image for every trial (light purple box)	46
2.7	Colorimetric sensing application layout (a) Creating a session (b) Adding a sample (c) List of samples with the same material in different concentrations	46
2.8	Schematic of the optical path from the illumination source to the CMOS camera (PS: Power Source; FL: Focusing Lens, NDF: Neural Density Filter; OL: Objective Lens; EF: Emission Filter; EYE-L: Eyepiece Lens)	48
2.9	Schematic of the colorimetric sensor design and implementation	48
3.1	Images of the smartphone adapter using 532 nm laser diode (a) Without sample (b) Urine sample (c) Blood sample (d) microscope image of the blood sample	54
3.2	Six different output images of the smartphone adapter for the same blood sample	55
3.3	Images of the smartphone adapter using white LED as illumination source (a) without the emission filter (b) with the emission filter FB530-10 (c) with the emission filter FB580-10 (d) with the emission filter FB640-10 (e) with the emission filter FB430-10	55
3.4	Image of the smartphone adapter using the 650 nm laser diode as illumination source (a) with the emission filter FB640-10 (b) without the emission filter	56
3.5	Samples of calculations using the colorimetric sensing application (a) glucose sample list (b) triglycerides sample list (c) urea sample list (d) calculations of absorbance (e) transmittance (f) error of measurements	58-62

3.6	Transmittance (a), absorbance (b), and absolute average error percent (err%) (c) of glucose sample in different concentrations	63-64
3.7	Transmittance (a), absorbance (b), and absolute average error percent (err%) (c) of triglycerides sample in different concentrations	65-66
3.8	Transmittance (a), absorbance (b), and absolute average error percent (err%) (c) of urea sample in different concentrations	66-67
3.9	Application-based results for glucose (a) Absorbance (b) Transmittance. Spectrophotometer-based results (c) Absorbance (d) Transmittance	70
3.10	Application-based results for triglycerides (a) Absorbance (b) Transmittance. Spectrophotometer-based results (c) Absorbance (d) Transmittance	71
3.11	Application-based results for urea (a) Absorbance (b) Transmittance. Spectrophotometer-based results (c) Absorbance (d) Transmittance	71
3.12	Images of glucose samples under the illumination of (a) 405 nm laser (b) 532 nm laser (c) 650 nm laser (d) LED with 430 nm Emission Filter (e) LED with 530 nm Emission Filter (f) LED with 580 nm Emission Filter (g) LED with 640 nm Emission Filter (h) White LED only	79
3.13	Images of the prepared samples in different concentrations using the smartphone adapter (a) Urea (b) Triglycerides (c) Bilirubin (d) HDL material under (a) 405 nm laser (b) 532 nm laser (c) 650 nm laser (d) LED with 430 nm Emission Filter (e) LED with 530 nm Emission Filter (f) LED with 580 nm Emission Filter (g) LED with 640 nm Emission Filter (h) White LED only	80-83
3.14	Transmittance (a) and absorbance (b) spectra for glucose, triglycerides, urea, bilirubin, and HDL using the UV-VIS spectrophotometer	84
3.15	Absorbance (a) and transmittance (b) measurement of glucose using the smartphone adapter with colorimetric sensing application in eight different illumination sources	85
3.16	Absorbance (a) and transmittance (b) measurement of urea using the smartphone adapter with colorimetric sensing application in eight different illumination sources	86

3.17	Absorbance (a) and transmittance (b) measurement of triglycerides using the smartphone adapter with colorimetric sensing application in eight different illumination sources	87
3.18	Absorbance (a) and transmittance (b) measurement of bilirubin using the smartphone adapter with colorimetric sensing application in eight different illumination sources	88
3.19	Absorbance (a) and transmittance (b) measurement of HDL using the smartphone adapter with colorimetric sensing application in eight different illumination sources	89
3.20	The regression coefficient of both absorbance (a) and transmittance (b) measurement of glucose, urea, triglycerides, bilirubin, and HDL using the smartphone adapter with colorimetric sensing application in eight different illumination sources	90
3.21	Price comparison among point-of-care devices [65]	91
3.22	Price comparison in USD as a logarithmic scale for different adapters in reported literature [65]	92
3.23	Limit of detection (LOD) in μM for reported literature [65]	92
3.24	Regression coefficient for reported literature [65]	93
A.1	Cura Ultimaker software environment	A-1
A.2	Control parameters of Cura Ultimaker software	A-1
B.1	3D model of (a) Laser casing (b) Ring holder (c) Optical density filter ring (d) Adapter holder (e) Extended support (f) Ground support (g) Sample holder (h) Sample cover (i) Sample casing (j) Optics casing (k) Slide cover of optics casing (l) Smartphone holder	B-1
B.2	Smartphone-based 3D printed adapter: source case dimensions	B-2
B.3	Smartphone-based 3D printed adapter: sample case dimensions	B-2
B.4	Smartphone-based 3D printed adapter: smartphone holder dimensions	B-3
B.5	Smartphone-based 3D printed adapter: optics case dimensions	B-4
B.6	Smartphone-based 3D printed adapter: overall dimensions	B-5
C.1	Laboratory devices (a) Centrifuge (b) Optical Microscope	C-1
C.2	(a) Slide coloring (b) Left to dry	C-1

C.3	Chemical dyes used in sample preparation	C-1
C.4	Chemical pigments (a) Leishman Stain (b) Phosphate Buffer (c) Slide treatment chemical solution	C-2
C.5	3D printer AnyCubic i3 Mega	C-2
C.6	Glucose Biosystems Datasheet	C-3
C.7	Urea Biosystems Datasheet	C-4
C.8	Triglycerides Biosystems Datasheet	C-5
C.9	Bilirubin Agappe Diagnostics Datasheet	C-6
C.10	HDL Agappe Diagnostics Datasheet	C-8
D.1	Light Emitting Diode Datasheet	D-1
D.2	532 nm Laser Diode Datasheet	D-3
D.3	405 nm Laser Diode Datasheet	D-5
D.4	650 nm Laser Diode Datasheet	D-6
D.5	Optical Density Filter Datasheet	D-9
D.6	Bandpass Emission Filter Datasheet	D-11

Chapter One

Introduction and Basic Concepts

1.1 Motivation

In the rapidly increasing age of technology, smartphones are the essential devices used in everyday life by billions of users worldwide. The processing power of these handy devices are extremely high. For comparison, the Apollo II mission -the first mission to the moon- was imitated with a computer called the Apollo Guidance Computer. It had 2048 words of memory which could be used to store “temporary results” – data that is lost when there is no power. This type of memory is referred to as RAM (random-access memory). Each word comprised 16 binary digits (bits), with a bit being a zero or a one. This means that the Apollo computer had 32,768 bits of RAM memory. In addition, it had 72 KB of read-only memory (ROM), which is equivalent to 589,824 bits. This memory is programmed and cannot be changed once it is finalized. To compare this with smartphones available today, an 8 Gigabyte of RAM, 256 Gigabyte of memory, which outperform the Apollo computer billions of times [1].

The rise of technology, with software platforms motivates enormous efforts to combine the smartphone technology with Lab-on-Chip to make the most of the research fields including imaging, sensing, measurements, and data achieving, etc. Our motivation was based on the current technology to overcome design issues of smartphone-based adapters to use them in bioimaging and biosensing applications. By designing both hardware adapter and an easy-to-use android software to make three different works including, bioimaging of whole blood and urine, biosensing with Android application, biosensing with 3D printed adapter design and Android application to measure the concentration of biomarkers.

1.2 Lab-on-Chip

A Lab-on-chip (LOC) is a miniaturized device that integrates into a single chip to perform certain analyses, that are usually done in a laboratory setting; such as DNA sequencing, bacterial recognition, cell counting, and biochemical detection. LOC technology offers tremendous advancements for outstanding research opportunities in biomedical, biochemical, electrochemical, surgical, and ophthalmic applications. In addition, material inspection, quality control, environmental monitoring, biological sample analysis, and diagnosis applications use the emerging LOC to assess, diagnose, inspect, and ensure quality measures of the targeted samples. LOC technology promises real-time signal/data monitoring, rapid inspection, precise measurements, accurate readings, and is on the market demand due to the small footprint, cheap fabrication/manufacturing/production, the ability to integrate with currently available electronic/optoelectronic chips, and smartphone integration [2,3]. To maintain trustworthy environments numerous attempts are being performed to compare the performance of the LOC devices with bulk and complicated laboratory instrumentation. Resulting in a high regression coefficient (R^2) when data comparison was performed. Thus, enabling the LOC devices as a cheap alternative will affect the market and result in cheaper costs for sample analysis, and diagnosis, which in turn, benefit the user and the patient in need. Point-of-care (POC) applications utilize the integration of several emerging fields including LoC, 3D printing technology, internet of things (IoT), smartphone applications (Apps), networking, and data analysis. Each field has a different perspective and specialization, and therefore, the POC application is a multidisciplinary research and analysis field. Introducing these fields pointing out the gaps among them and how to customize the research output according to the

integration criterion [4,5]. A LOC is composed of two main components, namely, hardware and software as detailed in the proceeding subsections.

1.2.1 Smartphone-Based Adapter (Hardware)

The hardware is the visible chip/device/adapter that contains the optical, electronic, and other components. For the purpose of LOC, the hardware can be an integrated set of chips or 3D printed adapter. The smartphone is attached to the adapter to perform the specific functions to do the necessary processes that are required by the work. A schematic diagram of the hardware is shown in Figure 1.1. In the next subsections the details of the hardware will be explored.

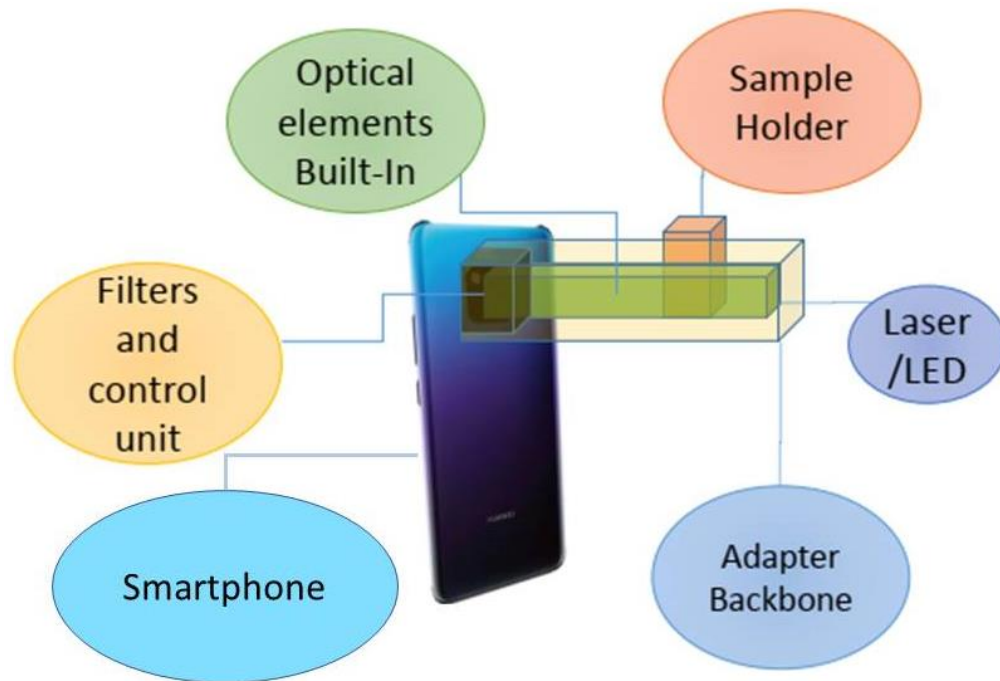


Figure 1.1: Schematic diagram of the smartphone-based adapter (Hardware)

1.2.1.1 Smartphone

Smartphones are mobile devices that combine cellular and mobile computing functions into one unit. They are distinguished from feature phones by their stronger hardware capabilities and extensive mobile operating

systems, which facilitate wider software, internet (including web browsing [6] over mobile broadband), and multimedia functionality (including music, video, cameras, and gaming), alongside core phone functions such as voice calls and text messaging.

Smartphones typically contain a number of metal–oxide–semiconductor (MOS) integrated circuit (IC) chips that include various sensors that can be leveraged by their software (such as a magnetometer, proximity sensors, barometer, gyroscope, or accelerometer), and support wireless communications protocols (such as Bluetooth, Wi-Fi, or satellite navigation). Since the emergence of smartphone with state-of-the-art technology, the demand of smartphone applications skyrocketed.

These applications make use of different aspects of the embedded technologies inside the smartphone including but not limited to GPS (Global Positioning System), CMOS camera (Complementary Metal-Oxide Semiconductor), Bluetooth, Flash LEDs (Light Emitting Diodes), memory, CPU (Central Processing Unit) and GPU (Graphical Processing Unit), USB-connectivity, wireless transmission of audio and video, etc. Each of these technologies within the palm of a hand enabled a huge industry based solely on smart applications devoted to serve the users' needs in various fields including entertainment, games, social networking, industry and management, teaching and learning, internet browsing, and scientific/research purposes.

The technology giants such as Google, Apple, Samsung, Nokia, and Huawei with their impact on the world are making the business of smartphone applications more fruitful every day. Based on fair competition of the application developers the most reliable and safe haven for the developers is Android platform since it is an open-source platform that encourages the developers to create new ideas without consent from the technology providers

in this case Google. While Apple store makes complications on the developers by harnessing their efforts in developing applications and their strict policies on privacy with their Swift platform it is always a subject of debate, though it is more convenient to use Android for developing the applications.

As more and more applications are created they impact the modern era with increasing creativity and finding more problems to be solved in the current time. Developers must use certain codes that works for the platform of interest for example, java script is mainly used to develop the Android applications [7].

A wide range of sensors are built-into the smartphone, these sensors support smartphones' functionality and ensures accurate data collection from different external stimuli, as shown in Figure 1.2.

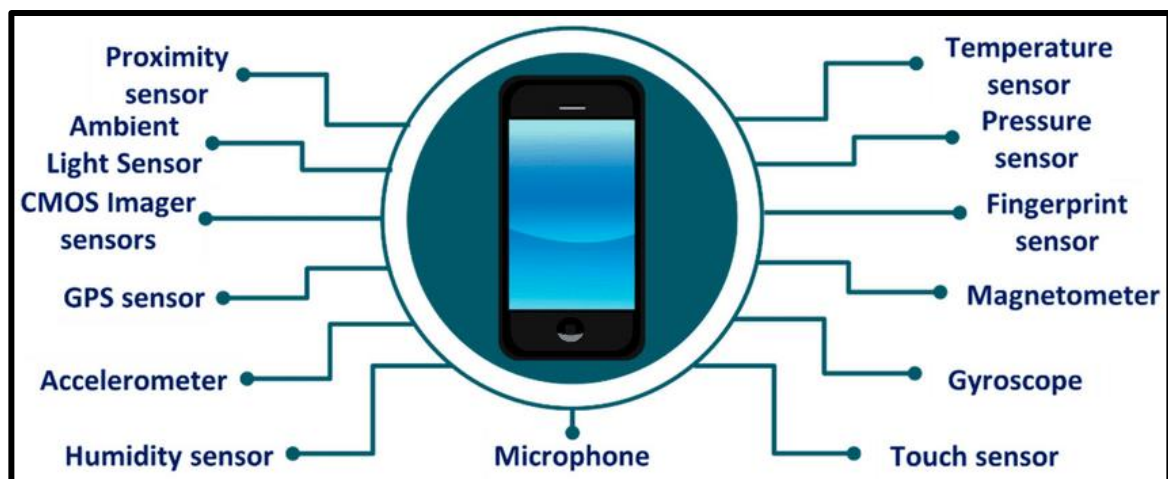


Figure 1.2: Types of smartphone built-in sensors [7]

Each sensor responds to different external stimuli, for example, a pressure sensor responds to external pressure wave, while a temperature sensor responds to an external temperature fluctuation. CMOS camera [8] responds to the visible spectrum waves and mimics the eye function of the human. Such diversity of sensors makes the smartphone being "smart". A schematic of the Imaging CMOS camera sensor is as depicted in Figure 1.3.

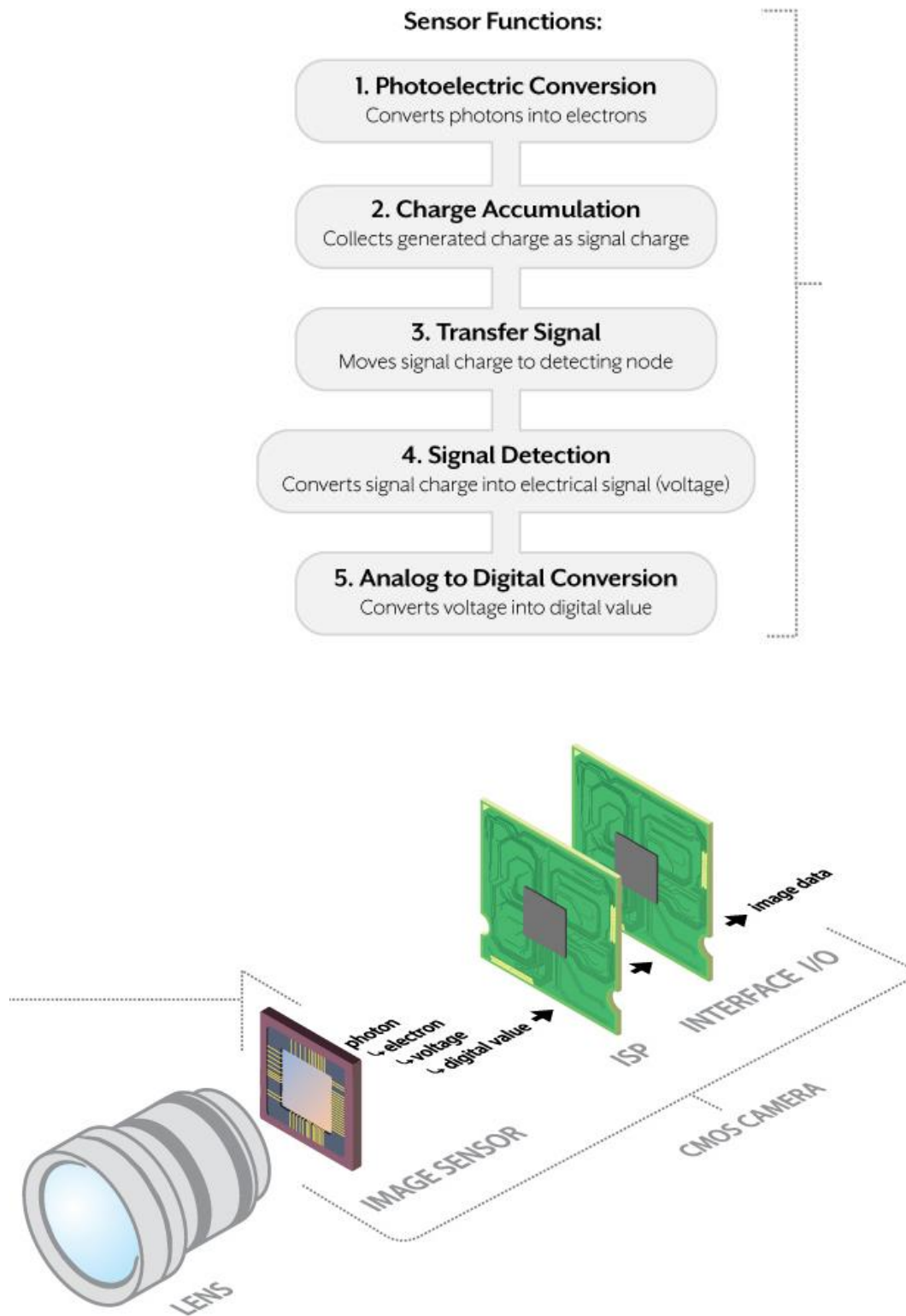


Figure 1.3: Schematic of the imaging CMOS camera sensor with its function [8]

1.2.1.2 Optical Components

The optical components are lenses, filters, interferometers, microscopes, gratings, prisms, etc. For the LOC hardware, optical components vary by the required function of the LOC chip, for example, if the function is to magnify the image of the sample, a microscope should be placed. Other functions include, optical filtering, background noise removal, focusing, defocusing, comparison, etc. The optical components are essential parts for imaging applications and thus they are the focus of the current work [9].

1.2.1.3 Illumination Sources

They are specific light sources including light emitting diodes and lasers for sample imaging. The light emitting diode is a semiconductor light source that emits light when current flows through it. Electrons in the semiconductor recombine with electron holes, releasing energy in the form of photons. The color of the light (corresponding to the energy of the photons) is determined by the energy required for electrons to cross the band gap of the semiconductor [10]. White light is obtained by using multiple semiconductors or a layer of light-emitting phosphor on the semiconductor device [11]. They are miniaturized light sources that have the following features: wide emission optical band (covering the visible spectrum, the near ultraviolet, and the near infrared), incoherent light beam, and a highly divergent light beam.

Lasers on the other hand, emits light through a process of optical amplification based on the stimulated emission of electromagnetic radiation. They have the following features: narrow optical emission band (usually with a tolerance of 10 nm), coherent light beam (with a little background noise), and low divergence [12].

The choice of the light source is entirely dependent on the LOC function, lasers can provide more focused light source, while LEDs can provide a wide range of optical band.

1.2.1.4 The 3D Printing

The 3D printing technology offers multiple solutions for fabrication and manufacturing of 3D printed adapters for smartphones. The adapter material can be PLA (Polylactic Acid), ABS (Acrylonitrile Butadiene Styrene), HPU (High Pick Up), PET (Polyethylene Terephthalate), PETG (Polyethylene Terephthalate Glycol-modified), etc. These filaments have the ability to construct a solid foundation on the 3D printer tray. There are several manufacturers of 3D printers each supporting a certain type of software such as Cura, Repetier-Host, KISSlicer, Slic3r, and Skeinforge.

The 3D printer software works as a simulation environment for the 3D printer in which the user can control various parameters including plate temperature, nozzle temperature, filling factor, speed of operation, accuracy, support frames, and the targeted filament. To ensure the quality of the 3D model various software can handle quality measures with an accuracy reaching nanometer scale including SolidWorks, AutoCAD, SketchUp, Blender, Inventor, Rhino3D, Onshape, and DesignSpark. The 3D model should be saved as ".stl" extension in order for the 3D printer software to read the data and convert the model into the ".gcode" format which the 3D printer can handle and starts the printing operation safely. Figure 1.5, shows the most common 3D printer manufacturers. These designs differ in the printing area, type of filament to support, and type of software to operate, in addition to different supporting technologies like WiFi support, USB cable to the personal computer (PC), MicroSD card, touch screen/ button control, colored screen/ black & white screen, model accuracy, maximum printing speed, resolution of

the model, maximum extruder temperature, heat plate, and filament sensor support [13, 14].

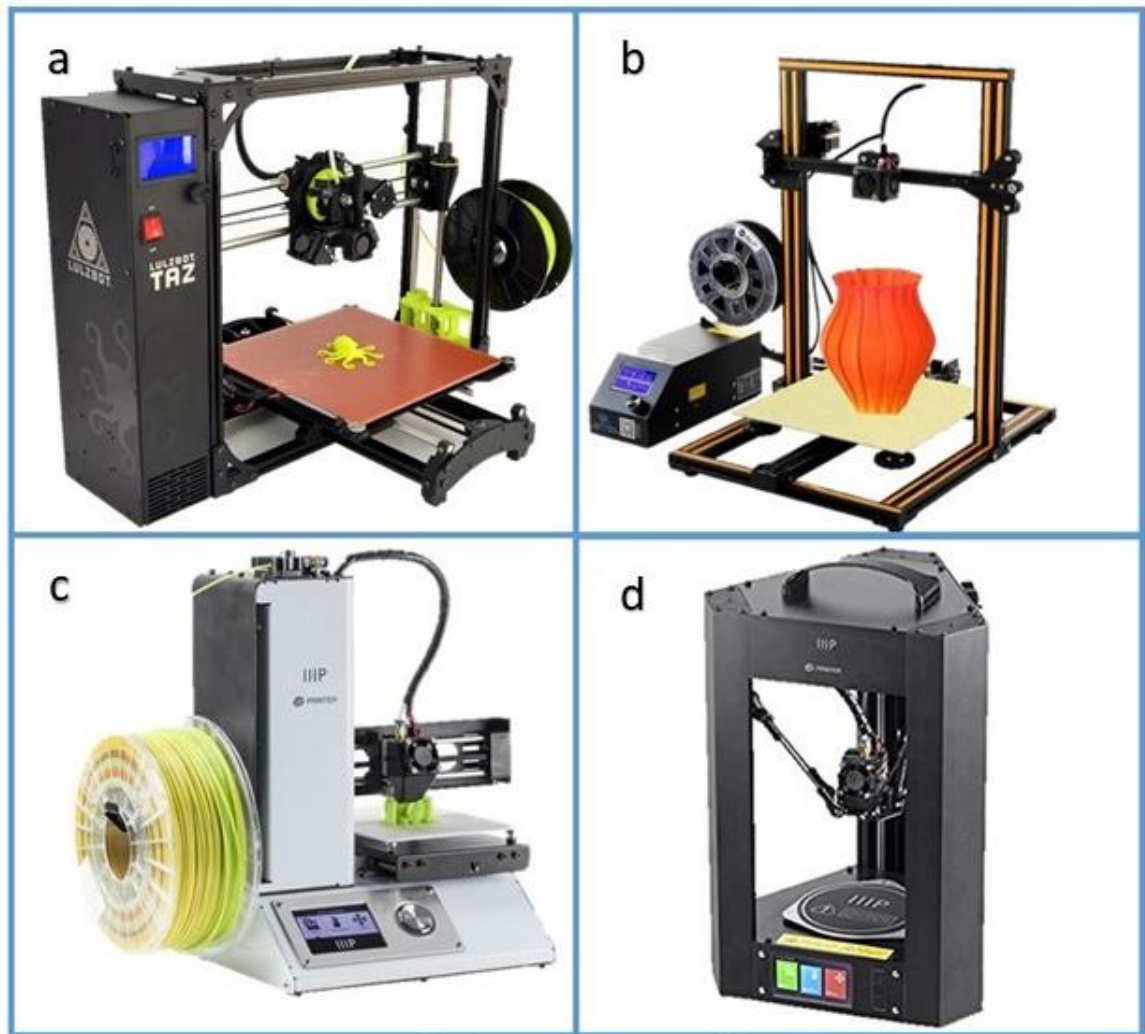


Figure 1.5: Different manufacturers of 3D printer [15]

1.2.2 The Software

The software is a set of codes, instructions, and operations that is based on computer language to perform specialized functions including graphics, voice, video, picture, text, etc.. These operations are coded in mathematical functions on a specialized platform with coding language. For example, Android Studio is the platform that accepts coding in Java script or Kotlin to produce Android smartphone application with specific functions like,

capturing an image from smartphone camera, saving the image into the memory of the smartphone, browsing the internet, recording voices, sharing information, computing formulae, creating a 3D image, tracking the smartphone location, measuring the distance, etc. [16]

In LOC settings the software is used to perform functions like, image processing, computer vision, machine learning, artificial intelligence, measurements, computations, comparison, etc.

In the following subsections the details of the software that were used in this work are introduced.

1.2.2.1 SolidWorks

SolidWorks is a computer-aided-design (CAD) software that enables the users to draw three-dimensional models within the software, the model can be assembled with other parts to make complex designs. Each part can be saved, and processed separately as well as within assembly model. The drawing tools include the basic geometrical shapes like circles, squares, cubes, triangles, cones, spheres, lines, ellipses and rectangles; by carefully designing a part a mixture of the basic geometrical shape can be produced through a set of geometrical operations like crop, enlarge, 2D and 3D surface sections, interpolation, edge rotation, alignment, etc. SolidWorks has a library of materials that can be added to the part after the geometrical shape has been drawn including glass, plastic, metals, alloys, composites, nylon, wood, paper, etc.

Other important feature is that it can simulate for the part to measure the mechanical properties like stress, strain, displacement, frequency, velocity, acceleration, safety factors, etc. in addition to mass properties and cost of manufacturing [17].

1.2.2.2 Cura Ultimaker

The Cura Ultimaker software is a 3D model based simulation software that can convert the CAD part into a “.gcode” file format which is used by 3D printers manufacturers to print the 3D model. It supports different kinds of manufactured machines (3D printers) with their dimensions to make sure that the part will mimic exactly what will happen in the printing period. It has several simulation methods used to inspect the part and simulate the process of printing before taking action to ensure a proper printing efficiency [17]. Details of the software are provided in chapter two.

1.2.2.3 Android Studio

Android Studio is the official Integrated Development Environment (IDE) for Android app development, based on IntelliJ IDEA. On top of IntelliJ's powerful code editor and developer tools, Android Studio offers even more features that enhance the productivity when building Android apps, such as: flexible Gradle-based build system, fast and feature-rich emulator, unified environment where the programmer can develop for all Android devices, apply changes to push code and resource changes to the running app without restarting it, code templates and GitHub integration to help build common app features and import sample code, extensive testing tools and frameworks, lint tools to catch performance, usability, version compatibility, and other problems, C++ and NDK support, built-in support for Google Cloud Platform, making it easy to integrate Google Cloud Messaging and App Engine, the project template activities can be basic, empty, bottom navigation, full screen, navigation drawer, and google maps as [18] shown in Figure 1.6

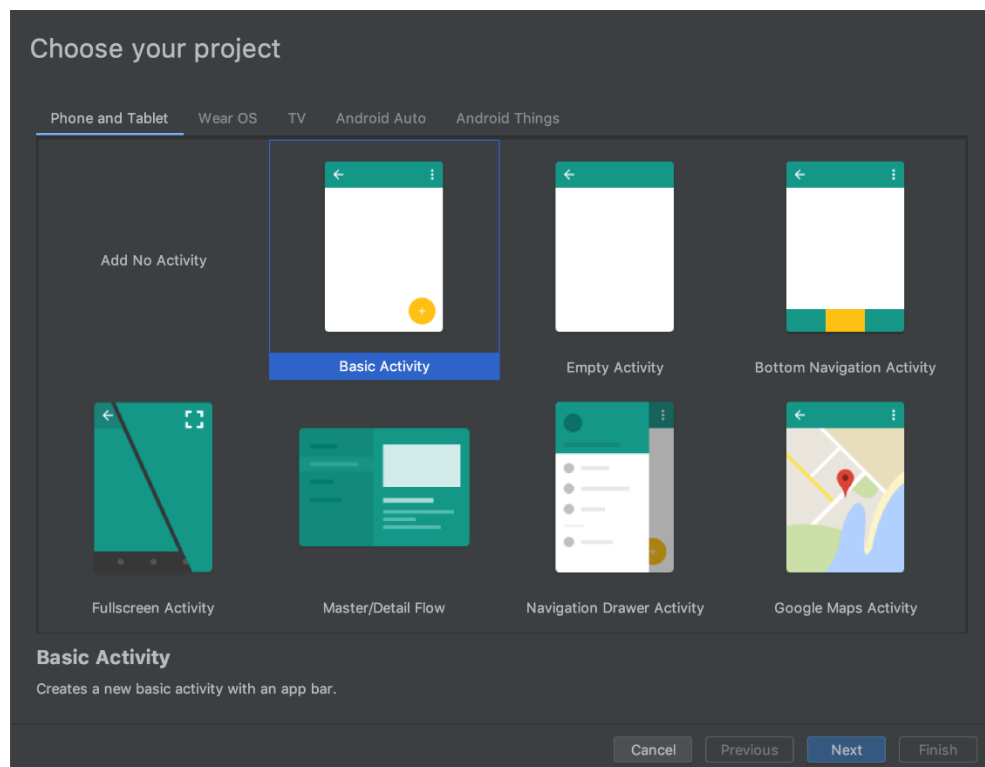


Figure 1.6: Android Studio IDE Project template [18]

1.3 Sensors

A sensor is a device, module, machine, or subsystem used to detect events or changes in its environment and send the information to other electronics, frequently a computer processor. A sensor is always used with other electronics [19]. There are many external stimuli that can be sensed like, position, motion, humidity, proximity, temperature, pressure, acoustic wave, force, optical ambient light, fluid flow, gas, level, electric and magnetic field, as shown in Figure 1.7. Biosensors shown in Figure 1.8 are sensors used in biomedicine and biotechnology. They detect analytes thanks to a biological component, such as cells, protein, nucleic acid or biomimetic polymers. Whereas a non-biological sensor, even organic (carbon chemistry), for biological analytes is referred to as sensor or nanosensor.

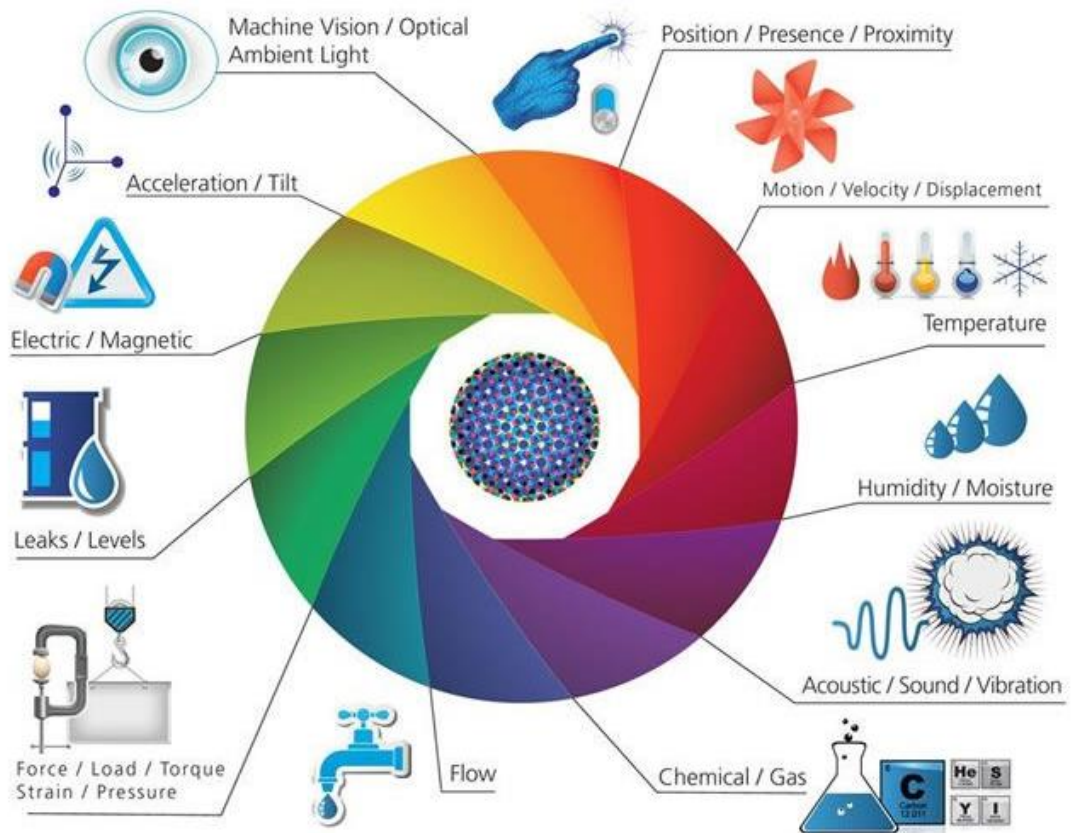


Figure 1.7: Classification of sensors [20]

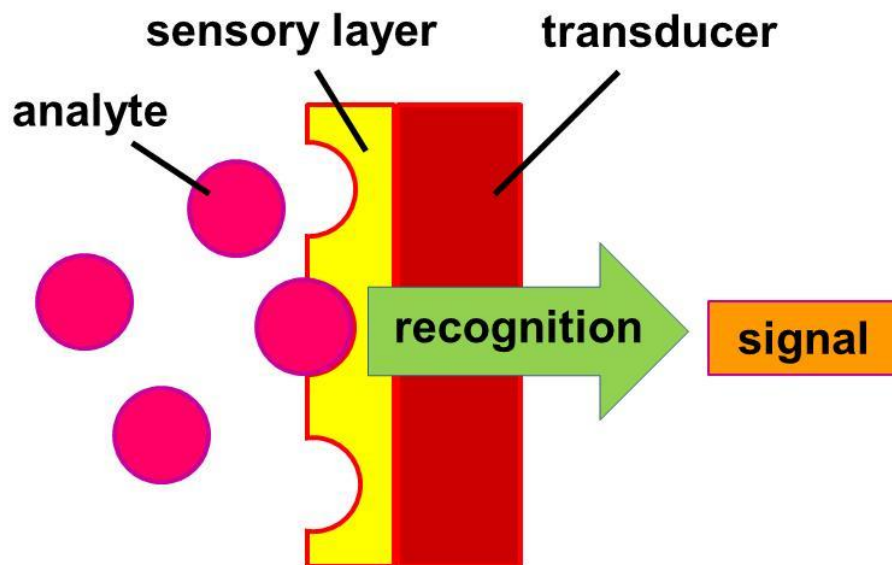


Figure 1.8: Schematic of a biosensor [21]

1.4 Biosensors in the Smart Environment

Since the development of smartphones with many tempting features in imaging, processing, storage, and other up-to-date services; the field of biosensing made use of the available technology in hand and thus new concepts started to emerge in the literature like smartphone-based sensing, smartphone-based measurement, smartphone-based imaging, smartphone-based diagnostics, and so on. These new concepts soon got the attention of researchers with different backgrounds including computer science, electronics, communication engineering, physics, biology, biochemistry, and other related fields. These fields soon progressed towards a smart environment in which testing, measurement, and diagnostics are all based on the smartphone environment. Due to huge market and engaged users of more than two-thirds of the world population, developing an easy-to-use smartphone adapter provided the possibility of on-site measurements and overcame the limitations of bulk laboratory instruments to ensure safety of patients and to come up with rapid results for on-site testing. Nowadays, this technology proved to be effective in many problems thus recommending it to the general public will be coming in the near future making more problems disappearing [22-25].

1.5 Biomarkers

A biomarker, or biological marker can be defined as a measurable indicator of some biological state or condition. Biomarkers are often measured and evaluated using blood, urine, or soft tissues [26] to examine normal biological processes, pathogenic processes, or pharmacologic responses to a therapeutic intervention [27]. There are many examples of biomarkers including but not limited to glucose, triglycerides, urea, bilirubin and high-

density lipoprotein (HDL). A rise or fall in these indicators below a certain level will indicate the corresponding effect of the biomarker.

Glucose (CH_2OH) is a diabetes biomarker, the normal range is below 140 mg/dL (7.8 mmol/L), a concentration between 140 and 199 mg/dL (7.8 mmol/L and 11.0 mmol/L) indicates prediabetes, a concentration higher than 200 mg/dL (11.1 mmol/L) after two hours indicates diabetes [28], the 3D chemical structure of glucose is as shown in Figure 1.9 (a).

Urea ($\text{CH}_4\text{N}_2\text{O}$) is the oldest prognostic biomarkers in heart and kidney failure, the adult normal range is between 10–20 (mg/dL) or 3.6–7.1 (mmol/L), the child normal range is between 5–18 mg/dL [29], the 3D chemical structure of urea is as shown in Figure 1.9 (b).

Triglycerides ($\text{C}_{15}\text{H}_{31}\text{COOH}$) biomarkers are predictors of ischemic stroke; the normal range is less than 150 mg/dL. Borderline levels are between 150-200 mg/dL. High levels of triglycerides (greater than 200 mg/dl). Higher levels come from certain conditions including obesity, low thyroid hormones, diabetes with poor control, liver and kidney diseases, alcohol consumption, and poor diet [30], the 3D chemical structure of triglycerides is as shown in Figure 1.9 (c).

Bilirubin ($\text{C}_{33}\text{H}_{36}\text{N}_2\text{O}_4$) is a biomarker of liver disease. the normal range is between 0.2-1.2 mg/dL [31], the 3D chemical structure of Bilirubin is as shown in Figure 1.9 (d).

HDL biomarkers are predictors of ischemic stroke, the normal range is between 40-60 mg/dL [32], the 3D chemical structure of HDL is as shown in Figure 1.9 (e).

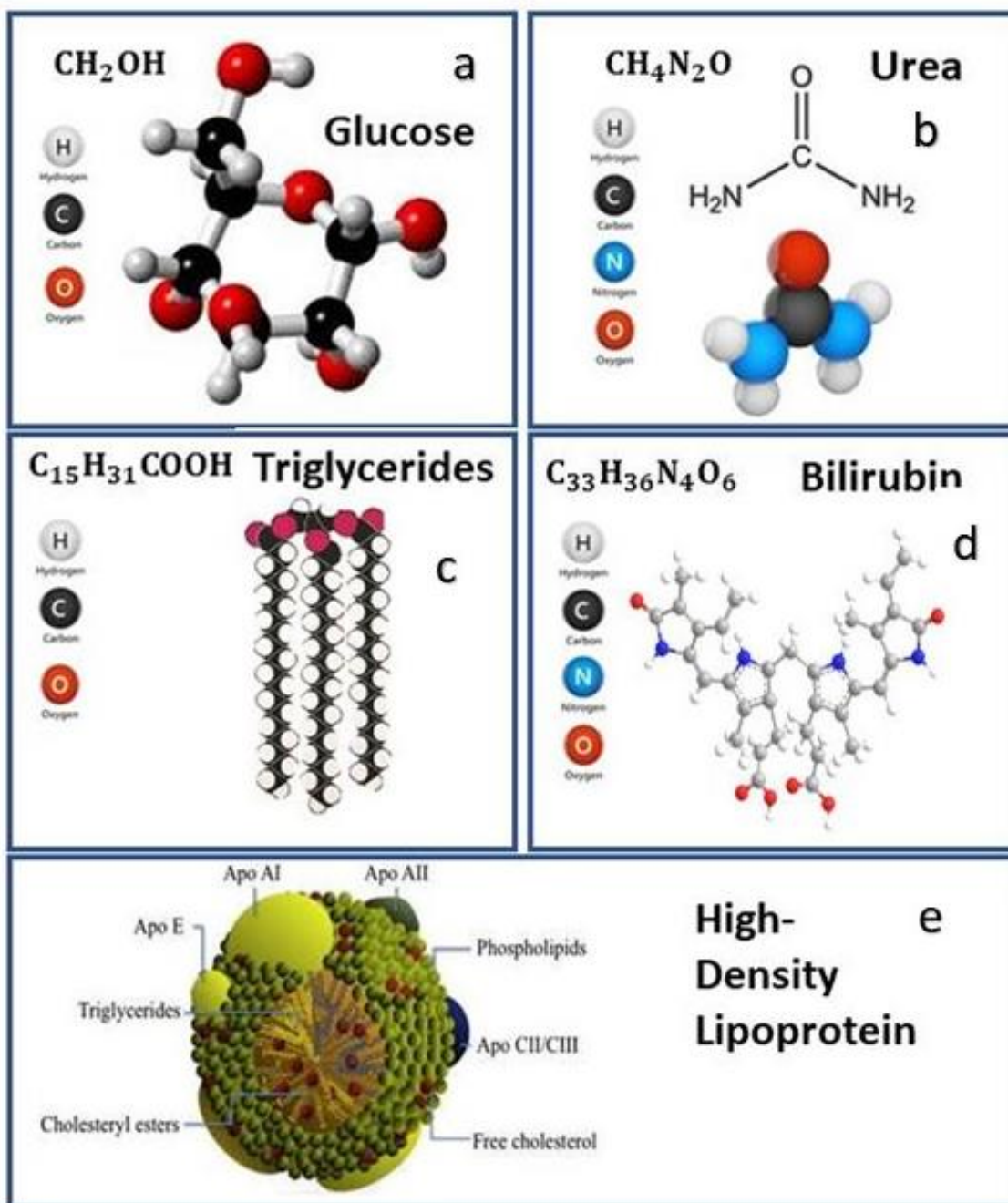


Figure 1.9: Biomarkers 3D chemical structure (a) Glucose [28] (b) Urea [29] (c) Triglycerides [30] (d) Bilirubin [31] (e) HDL [32]

1.6 Colorimeter

A colorimeter is a device used in colorimetry that measures the absorbance of particular wavelengths of light by a specific solution [33]. It is commonly used to determine the concentration of a known solute in a given

solution by the application of the Beer–Lambert law, which states that the absorbance of a solution is proportional to the concentration.

The essential parts of a colorimeter are: a light source (often an ordinary low-voltage filament lamp); an adjustable aperture; a set of colored filters; a cuvette to hold the working solution; a detector (usually a photoresistor) to measure the transmitted light; a meter to display the output from the detector. In addition, there may be: a voltage regulator, to protect the instrument from fluctuations in mains voltage; a second light path, cuvette and detector. This enables comparison between the working solution and a "blank", consisting of pure solvent, to improve accuracy.

There are many commercialized colorimeters as well as open source versions with construction documentation for education and for research [34], as shown in Figure 1.10 [33].

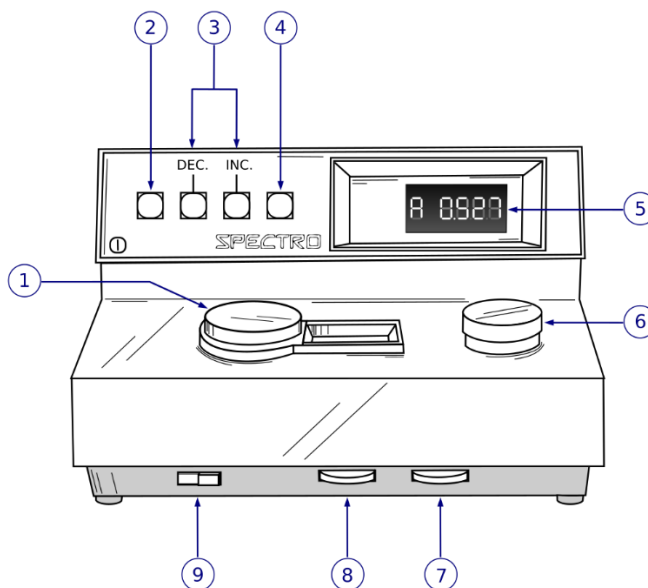


Figure 1.10: Commercial Colorimeter schematics (1) Wavelength selection, (2) Printer button, (3) Concentration factor adjustment, (4) UV mode selector (Deuterium lamp), (5) Readout, (6) Sample compartment, (7) Zero control (100% T), (8) Sensitivity switch, (9) ON/OFF switch [33]

1.7 Image Processing

Image processing are set of matrix operations on an image to make filtering, contrast adjustment, cropping, resizing, blurring, etc. These functions are coded in a software platform and applied to the image to extract features or to apply filtering and image enhancement.

For colorimetry, the image processing is related to the color wheel which is an abstract illustrative organization of color hues around a circle, which shows the relationships between primary colors, secondary colors, tertiary colors etc.

The CIE 1931 color spaces, as shown in Figure 1.11, are the first defined quantitative links between distributions of wavelengths in the electromagnetic visible spectrum, and physiologically perceived colors in human color vision. The mathematical relationships that define these color spaces are essential tools for color management, important when dealing with color inks, illuminated displays, and recording devices such as digital cameras. The system was designed in 1931 by the International Commission on Illumination [35].

The CIE 1931 RGB color space and CIE 1931 XYZ color space were created by the International Commission on Illumination (CIE) in 1931 [36]. They resulted from a series of experiments done in the late 1920s by William David Wright using ten observers [37] and John Guild using seven observers [38]. The experimental results were combined into the specification of the CIE RGB color space, from which the CIE XYZ color space was derived.

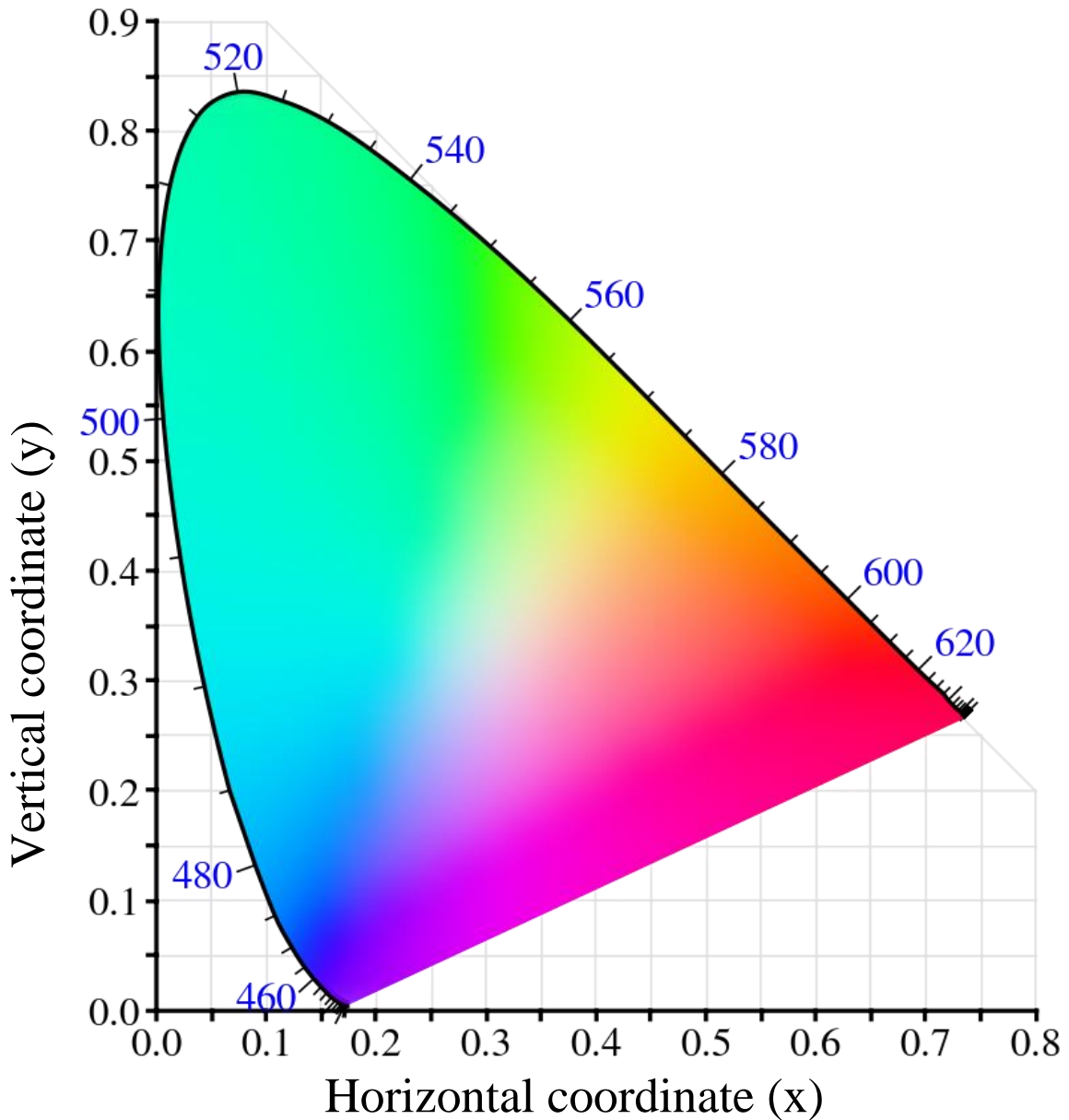


Figure 1.11: The CIE 1931 color space chromaticity diagram [35]

The outer curved boundary is the spectral (or monochromatic) locus, with wavelengths shown in nanometers. Note that the colors your screen displays in this image are specified using sRGB, so the colors outside the sRGB gamut are not displayed properly. Depending on the color space and calibration of your display device, the sRGB colors may not be displayed properly either. This diagram displays the maximally saturated bright colors that can be produced by a computer monitor or television set.

The image can be defined as a two-dimensional function $f(x,y)$ where x : is the horizontal axis and y is the vertical axis. The x and y represent the spatial coordinates of the space.

The RGB color model is the most common method for processing colored images color space, each pixel is described by how much red, green and blue intensity it contains. The color of a pixel is defined by its position in the RGB cube (a 3D scatter plot) where origin (0,0,0) is black and the (1,1,1) is white [39].

For each color in the visible spectrum, there is a pixel value ranging from 0-255 representing the color of the image for example the color white is represented as (255, 255, 255) while the black color is represented as (0, 0, 0), all other colors are sets of specific numbers in the 3D coordinate pixel (Red, Green, Blue) [39]. As shown in Figure 1.12.

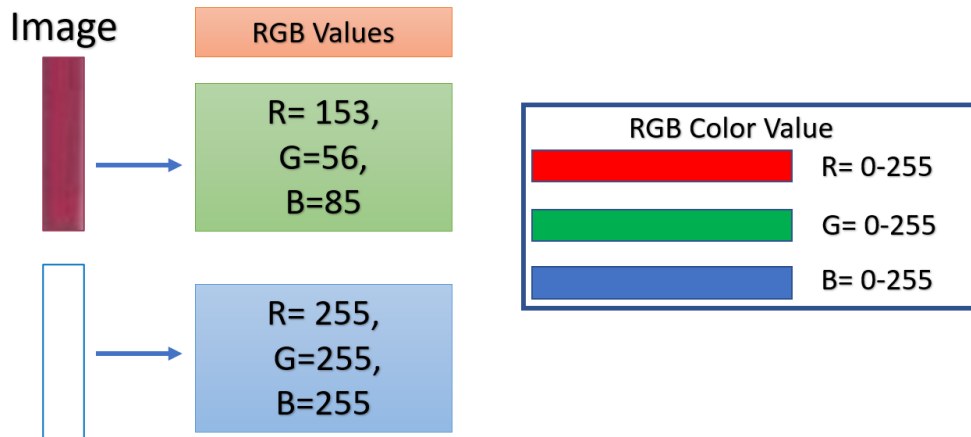


Figure 1.12: RGB values for a colored image

The mixture of red, blue and green can result in any color in the image following the coordinates of Figure 1.13. In addition, each image can be analyzed by its original RGB components as shown in Figure 1.14.

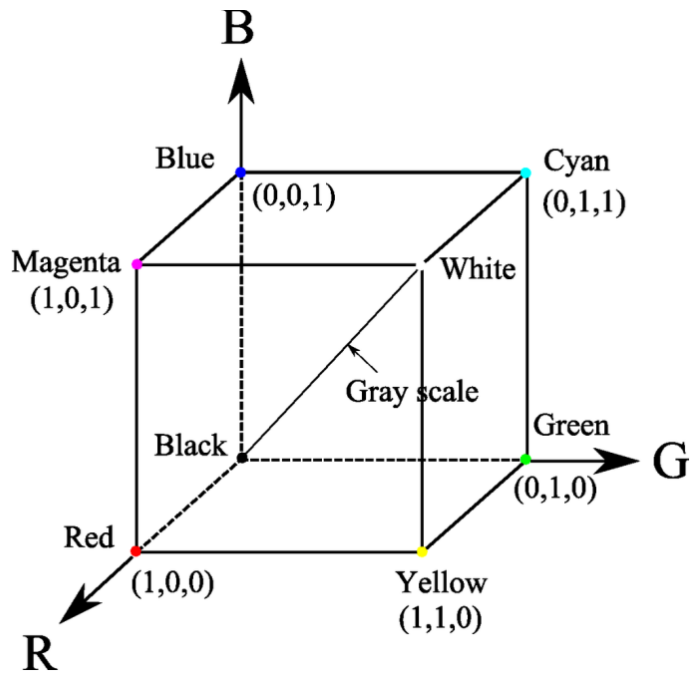


Figure 1.13: RGB color component and axis coordinate [40]

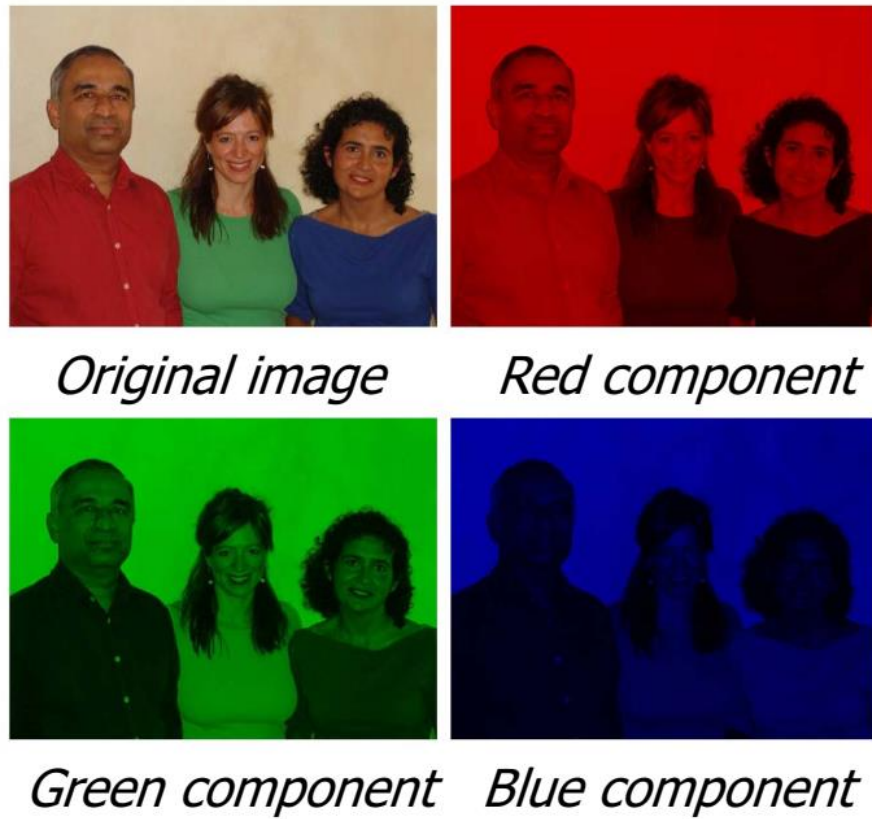


Figure 1.14: RGB image and the components of each channel [40]

The sample transmittance (T) and absorbance (A) can be evaluated using equations (1.1.a) and (1.1.b) below:

$$A = 2 - \log_{10}(T\%) \quad (1.1.a)$$

$$T\% = 10^{2-A} \quad (1.1.b)$$

And since the absorbance is equal to [41]:

$$A = \varepsilon(\lambda)bc \quad (1.2)$$

Where: $\varepsilon(\lambda)$: Molar absorptivity; b: Sample length; c: Sample concentration, and Since [41]:

$$A = -\log_{10} (I_0/I) \quad (1.3)$$

Combining equation (1.2) with (1.3), leads to:

$$I = I_0 \exp^{-\varepsilon(\lambda)bc} \quad (1.4)$$

Where: I_0 : Background intensity of the RGB colored image; I: Sample intensity of the RGB colored image.

The absolute average error percentage (err%) between measured quantities of transmittance and absorbance for the sample is calculated as shown in equations (1.5.a) and (1.5.b)

$$err\% = \sum_{n=1}^N \frac{|T_M - T_C|_n}{N} \% \quad (1.5.a)$$

$$err\% = \sum_{n=1}^N \frac{|A_M - A_C|_n}{N} \times 100\% \quad (1.5.b)$$

Where: n: Integer; N: Number of samples; the subscripts M and C denote the measured and calculated quantities respectively.

The intensity values based on the RGB images for both background and sample following this equation

$$I_R = \log_{10} R_0/R_S$$

$$I_G = \log_{10} G_0/G_S \quad (1.6)$$

$$I_B = \log_{10} B_0/B_S$$

$$I_{\text{total}} = (I_R + I_G + I_B)/3$$

Where: the subscripts 0 , and s represent the background and sample, R: Red channel; G: Green channel; B: Blue channel of the RGB image.

1.8 Smartphone 3D Printed Adapter Design Guide

Different designs have been proposed in the late literature for utilization in biology, biochemistry, and related fields. Biological objects such as bacteria [42], viruses [43], and parasites [44] are in the micrometer to submicrometer range; therefore, magnification is mandatory for visual inspection of these objects. Smartphone adapters are employed here for visual inspection, measurement, recognition [45], sensing [46], and disease diagnosis [47-49] for conditions such as diabetes, cancer [50], and malaria [51, 52]. On the other hand, chemical agents, such as hormones [53-55], biomarkers [56, 57], and reagents [58], are essential for biochemical processes; therefore, smartphone adapters were neatly designed for sensing, measuring, and monitoring these agents, as shown in Figure 1.15.

As depicted in Figure 1.15 (a), Skandarajah, et al., [59], developed a smartphone-based microscope system that is able to perform submicron imaging and compared the performance of the smartphone with that of scientific camera, resulting in comparable images when the smartphone camera resolution was more than 5 megapixels. They tested various smartphones of the iPhone and SAMSUNG series. The system is composed of

light illumination (LED), a sample holder, objective and eyepiece lenses and a plastic diffuser. The image processing software uses white-color balance before the image acquisition stage, which then involves color filtering, control, image processing, and storage.

Huang, et al., [60], developed a smartphone-based device, composed of a commercial camera, a disposable unit, an external battery, and holders, to detect the influenza virus. The device performed well, and the authors suggested improvement techniques for achieving excellent performance.

As shown in Figure 1.15 (b), You, et al., [61], developed a smartphone-based adapter with high sensitivity, low limit of detection and viable specificity for heart failure prognosis. The device included a software application enabling patients to perform remote prognoses at home.

As depicted in Figure 1.15 (c), Álvarez-Diduk, et al., [62], proposed graphene quantum dot material for the fast screening of organic compounds. The adapter consists of a plastic body, strip hole, UV LED, and USB port. It uses a smartphone for power. It includes the following: the electric circuit of a 365-nm UV LED connected to the male USB port and a nitrocellulose paper strip with wax-printed circular areas. It yields an image of the sensing platform, where the fluorescent spot is observed in the middle of a mobile phone screen, and the sensing area, with yes/no (ON/OFF) being the typical result. The UV LED was used for fluorescent imaging, and the results were fascinating in terms of the adapter response.

As depicted in Figure 1.15 (d), Roda et al., [63], developed a smartphone adapter for targeting biospecific enzymatic reactions in bioluminescence applications. The image capturing and light quantification were performed by the smartphone.

As shown in Figure 1.15 (e), Cui, et al., [64], validated the smartphone adapter for particle analysis in prostate-specific antigen (PSA) biomarkers, and their system was processed by MATLAB and a smartphone-designed application. The LOD was 0.125 ng/ml, and the smartphone-based biomarker has the potential for a wide range of biomarker detection methods.



Figure 1.15: Biochemical applications of smartphone adapter (a) Transmission light microscope based on smartphone, [59], by Skandarajah, et al. under the Creative Commons license. (b) Smartphone-based adapter, [61], by You, et al. © copyright 2017 American

Chemical Society. (c) 3D-printed device with its different parts [62], by Alvarez-Diduk, et al. under the Creative Commons license. (d) Smartphone Biochemiluminescence adapter, [63], by Roda, et al. © copyright 2014 American Chemical Society. (e) Cellphone-enabled image acquiring system, [64], by Cui, et al. © copyright 2018 American Chemical Society.

1.9 Performance Characterization of Smartphone Adapters

Adapter design requires specialized skills in optical systems and targeted applications. The design should consider the cost of the adapter, the accessories, and the integrated optical and mechanical parts. The 3D modeling and design software should have the ability to be installed on a 3D printer or CNC machine using a ".stl" file format or other types of formats depending on the 3D printer software used. SolidWorks has the advantage of being easy-to-learn and compatible with 3D printing machines, as shown in Table 1.1.

The image analysis is preferred to be integrated functionally with the smartphone application for portability and design practicality. The Xamarin platform and Ionic platform have great potential in the smartphone application industry, especially in point-of-care research. This is because both platforms can be integrated with the three main categories of smartphone software, namely, Android, IOS, and Microsoft, thus making the smartphone application available for almost every smartphone software and not just the targeted one, as shown in Table 1.1, which reveals that researchers have made astonishing advancements on only specific smartphone platforms, that is, either Android or IOS, excluding the fact that smartphone applications should be designed for all three categories.

A simulation before can be suggested to the assembly and printing of the adapter, in which optical elements are set in optimal positions to perform the specified task, e.g., focusing, filtering, or image enhancement. In this way,

the design can be optimized before the implementation of the adapter design [65].

Table 1.1: Summary of smartphone adapter design and application [64]

Application Type	Smartphone	Software Analysis	Sample	LOD	Ref.
Bacterial Sensing	HTC ONE X	Android; Cloud Computing	E. coli	10 cells/ml	[42]
Avatar DNA Recognition	iPhone touch 5 th generation	Image Quant; ColorZip-Code	DNA	NR ^[2]	[45]
Multi-reagent Immunosensor	Samsung	Android Programming	PSA; IgG; NF-κB	1 ng/ml	[46]
Barcode-like Paper Sensor	Google Nexus 5	Mobile Programming	Blood	NR	[47]
Infectious Diseases Detection	iPhone & Android	CasaXPS,	HIV p24	1.1 nM	[49]
Malaria Diagnostics	iPhone	nRF UART Application; AutoCAD; SolidWorks	Malaria	~0.6 par/μL	[51]
Malaria Detection and Reporting	iPhone 5s	MATLAB; REDCap	Malaria	20.6 par/ml	[52]
Smartphone Detection of Luteinizing Hormone	Galaxy Note 2 & Huawei Honor v8 & Xiaomi Mi	Canny Edge Detection & Fuzzy Mean Clustering	Luteinizing Hormone	2.0 mIU/ml	[53]
Salivary Cortisol Measurement	Galaxy Note 1	Android Software Developer; ImageJ	Cortisol	0.01 ng/ml	[54]
Tableting Reagents for Medical Diagnostics	iPhone 5s	MATLAB; ImageJ; SPSS	Hepatitis B Virus	10 pmol/μL	[58]

Sub-micron Imaging	iPhone; Android	Mobile App	Blood Smears	NA ^[3]	[59]
Detection of Influenza Virus	LG Nexus 5X	Android Application; ImageJ; MATLAB	Influenza A	~10 pg	[60]
Heart Failure Prognosis	Android	UC-LFS App	Brain Natriuretic Peptide; Suppression of Tumorigenicity 2	5 pg/ml; 1 ng/ml	[61]
Quantum Dots Screening	Samsung Galaxy S7	ImageJ	Graphene Quantum Dots; Paraoxon;	66.7; 23.5; 43.6; 39.7	[62]
Biochemiluminescence	iPhone 5S	ImageJ	Arsenic (As (III))	0.71 ppm	[63]
Prostate-specific Antigen (PSA) Biomarker	Android	MATLAB; App	PSA	0.125 ng/ml (3.67 pM)	[64]

1.10 Literature Review

In 2014, Hong and Chang, [66], developed a mobile application for colorimetric sensing of multi-analyte arrays. Smartphone identifies the position of the sensor then the colors measured at each sensor are digitized based on a correction algorithm; leading to concentration values by pre-loaded calibration curves.

In 2015, Jung, et al., [67], detected saliva alcohol concentration using Smartphone-based colorimetric RGB and HSV analysis. They used separate channels of color intensity values for Ethyl alcohol concentration in percentages.

In 2016, Choi, et al., [68], developed a smartphone-based urine reagent strip reader for rapid and accurate screening of leukocyte esterase (LE) and nitrite (NIT) in the urine. It was evaluated with the clinical urine samples (n =

81). The detection performance of the reader for LE and NIT was evaluated to assess the reliability of the reader.

In 2016, Kuntzleman and Jacobson, [69], described a simple protocol for teaching Beer's Law and absorption spectrophotometry using a smart phone. Materials commonly found in high school chemistry laboratories or even around the house may be used. Data collection and analysis is quick and easy. Despite the simple nature of the experiment, excellent results can be achieved.

In 2017, Ra, et al., [70], proposed an algorithm for a smartphone-based application as an alternative to delivering diagnostic results. The colorimetric detection method evaluates the captured image of the strip, under various color spaces and evaluates ten different tests for urine. Thus, the system can deliver results on the spot using both the naked eye and smartphone.

In 2017, Hosker, BS, [71], constructed a highly simplified variation spectrophotometer using a smartphone's light sensor as a detector and an app to calculate and display absorbance values. This simple version requires no need for electronic components or postmeasurement spectral analysis. Calibration graphs constructed from two molecules that absorb light maximally at different wavelengths (430 and 630 nm) demonstrate linearity with R^2 values of 0.9975 and 0.9848, respectively.

In 2018, Barnes, et al., [72], developed smartphone-based real-time loop-mediated isothermal amplification system for pathogen ID in urinary sepsis patients. The free, custom-built mobile phone app allows it to serve as a stand-alone device for quantitative diagnostics, allowing the determination of the genome copy-number of bacterial pathogens in real-time.

In 2018, Soni, et al., [73], developed a smartphone-based handheld optical biosensor for the determination of urea in saliva. The sensitivity reported was -0.005 average pixels $\text{sec}^{-1}/\text{mgdL}^{-1}$ with a (limit of detection) LOD of 10.4 mgdL^{-1} .

In 2019, Bills, et al., [74], proposed a three-layer paper device with low cost and easy fabrication. The device requires only 1-4 μl of blood per test which can be obtained from a finger prick. The device also provides on-paper mixing, capture, concentration, and separation. WBCs are captured at a predictable rate for (5%, 10% and 20%) blood dilutions.

In 2019, Yun, et al., [75], used smartphone systems and compared the results of cholesterol tests with those of existing clinical diagnostic laboratory methods. They found that smartphone-based point-of-care lipid blood tests were as accurate as hospital-grade laboratory tests ($N = 116$, $R > 0.97$, $p < 0.001$ for total cholesterol, high-density lipoprotein, and triglycerides).

In 2020, Lee, et al., [76], described the development and clinical evaluation of an automated smartphone-linked sensor capable of chemical-free, quantitative measurement of hemoglobin concentration in whole blood samples. They also established that the sensor could analyze an unprocessed blood specimen with a mean processing time of about eight seconds and results in an accuracy of about 99% against a reference analyzer.

In 2020, Hattori, et al., [77], proved that bioluminescence can be observed in an organelle in a single living cell using a smartphone camera by attaching a detachable objective lens. Through capturing color changes with the camera, changes in the number of target molecules were detected using bioluminescent indicators.

In 2020, Xing, et al., [78], developed a dual-functional smartphone-based sensor for colorimetric and chemiluminescence detection. In colorimetry, five analytes that display different colors and various intensities were detected sensitively while in chemiluminescence H_2O_2 was detected successfully. They created a smart application that allows testing and sharing of fluoride quantification results with a 3D printed smartphone adapter for RGB image detection and processing.

In 2020, Kim, et al., [79], attempted color detection of the colorimetric paper chip using smartphone-embedded LED and simple transformation calculation. This method enables the acquisition of stable color information using different smartphones by reducing the influence of external light sources.

In 2020, Liu, et al., [80], proposed a ratiometric fluorescent and colorimetric determination of H_2O_2 and glucose. A smartphone application was designed to take pictures and analyze RGB values of fluorometric and colorimetric signals, which delivered excellent analytical result for glucose.

In 2021, Vidal, et al., [81], designed a fully-functional smartphone-based spectrophotometer using 3D printing. The major advantage of this approach is its capacity to be interfaced with a variety of smartphones, allowing the use of the smartphone's camera and display, and regardless of the relative position of the camera. The analytical performance of the device was analyzed using a model dye (crystal violet), leading to a proportional response for concentrations in the $0.06\text{--}15.0\text{ mg L}^{-1}$ range, with a variability of 1.0% (intra-day) and 2.6% (inter-day). To demonstrate the functionality of the device, the degradation process of the dye by sodium hypochlorite was studied. The results obtained were applied to develop a paper-based test for

NaClO in sanitation solutions, in which the time required to bleach the dye was used to estimate the concentration of the solution.

In 2021, Mercan, et al., [82], developed a portable platform incorporating a PAD with a smartphone application based on machine learning to quantify glucose concentration in artificial saliva. The detection zones of the PAD were modified with three different detection mixtures. After the color change, the images of the PADs were taken with four different smartphones under seven different illumination conditions. The images were first processed for feature extraction and then used to train machine learning classifiers, resulting in a more robust and adaptive platform against illumination variation and camera optics. A special application called “GlucoSensing” capable of image capture, cropping and processing was developed to make the system more user-friendly. A cloud system was used in the application to communicate with a remote server running machine learning classifiers. Among the three different detection mixtures, the mixture with TMB demonstrated the highest classification accuracy (98.24%) with inter-phone repeatability under versatile illumination.

1.11 Aim of the Work

The aim of this work is to design, implement and investigate the performance of a colorimetric and imaging sensor based on smartphone. The design is aimed to be of low-cost, wide-availability, high-accuracy, portable and lightweight. Using 3D adapter laser system and an easy-to-use smartphone application to read data from samples and capture the image of the biomaterial for the use in concentration measurement of biomarkers and bioimaging applications.

1.12 Thesis Outline

This thesis is divided into three chapters in which:

Chapter One: Serves as an introductory chapter to see the motivation, the research problem, and the aim of the work. It also shows the progress of smartphone-based adapters and what are the available novel, prestigious, and mind-boggling ideas in recent literature.

Chapter Two: Shows the experimental work details and the materials and methods used in three different directions, the novel colorimetric sensing Android application and its utilization with different images of glucose, triglycerides, and urea samples with five concentrations of each material. Followed by the bioimaging of whole blood and urine samples with smartphone-based 3D printed adapter hardware for image acquisition and data collection with 532 nm and 650 nm diode lasers and white LED illumination sources. Finally, the novel 3D smartphone-based adapter for accurate and reliable concentration measurement using both hardware and software for five different materials with a total of 30 samples, namely, glucose, triglycerides, urea, HDL, and bilirubin are introduced.

Chapter Three: Illustrates the results, discussions, conclusions and future work suggestions for the previously identified three different directions. The first direction is the novel colorimetric sensing Android application. The second direction is the bioimaging of whole blood and urine samples with smartphone-based adapter. The third direction is the novel 3D smartphone-based adapter for accurate and reliable concentration measurement.

Chapter Two

Materials, Methods, and Experimental Work

2.1. Introduction

This chapter presents the materials, methods, and experimental work for three different directions. The first part deals with smartphone-based bioimaging of whole blood and urine (microscopy). The second part is, colorimetric analysis for biochemical samples with Android smartphone application. The third part is about smartphone-based 3D printed design with the aid of Android application intended solely to measure the concentration of multiple biomarker samples based on the colorimetric detection approach.

2.2. Materials and Methods

Glucose (BioSystems Co., 11503, Barcelona, Spain) samples were prepared with 11 different concentrations of 5, 10, 15, 20, 25, 30, 100, 200, 300, 400, and 500 mg/dl.

Urea (BioSystems Co., 11536, Barcelona, Spain) samples were prepared with 8 different concentrations of 5, 10, 15, 20, 25, 30, 50, 100, and 150 mg/dl.

Triglycerides (BioSystems Co., 11828, Barcelona, Spain) samples were prepared with 11 different concentrations of 10, 20, 30, 40, 50, 60, 100, 200, 300, 400, and 500 mg/dl.

Bilirubin (Total Serum Bilirubin (TSB)) (Agappe Diagnostics, 51003004, Cham, Switzerland) samples were prepared with 6 different concentrations of 0.05, 0.06, 0.07, 0.08, 0.09 and 0.1 mg/dl.

HDL (Agappe Diagnostics, 51010001, Cham, Switzerland) samples were prepared with 6 different concentrations of 10, 20, 30, 40, 50, and 60 mg/dl.

2.3. The Components

The 3D printed models are assembled and the external hardware components are integrated into the design, these components include:

Huawei mate 20 pro smartphone (Huawei, China) with 40 Mpx resolution CMOS camera was used to take images from the adapter and perform computation and analysis.

The emission bandpass filter (FB430-10, PO#T0680669; Thorlabs) was used in the adapter with white LED with central wavelength of 430 nm and a bandwidth of 10 nm (appendix D).

The emission bandpass filter (FB530-10, PO#T0648536; Thorlabs) was used in the adapter with white LED with central wavelength of 530 nm and a bandwidth of 10 nm (appendix D).

The emission bandpass filter (FB580-10, PO#T0679010; Thorlabs) was used in the adapter with white LED with central wavelength of 580 nm and a bandwidth of 10 nm (appendix D).

The emission bandpass filter (FB640-10, PO#T0672817; Thorlabs) was used in the adapter with white LED with central wavelength of 640 nm and a bandwidth of 10 nm (appendix D).

The optical density filter (NE513B, TP02047334; Thorlabs) was used in the adapter with optical density of 1.3 (5%) (appendix D).

The zoom lens LED lighted pocket microscope magnifier loupe 160x-200x magnification (MG10081-1A, 3N114A04, Luquan) objective and eye-piece lenses was used in the adapter.

The USB-to-TTL (CP2102) was used to power the adapter with 5V.

The microscope optical lens was used in the adapter with a focal length of ($f = 100$ mm).

The super wide-angle lens was used in the adapter with a magnification of 0.4x (XPSP06-RD, XP PhotoGear).

The laser diode (532 nm, 532MD-10-1250-BL, Lilly Electronics) was used as illumination source with a power of 40 mW (appendix D).

The laser diode (405 nm BANGXECT63, Osram Opto Semiconductors Manufacturing) was used as illumination source with a power of 100 mW(appendix D).

The laser diode (650 nm, BANGXECT63, Osram Opto Semiconductors Manufacturing) was used as illumination source with a power of 5 mW(appendix D).

A white LED was used as illumination source with output power of 5V and 30 mA.

The optical microscope with a magnification of 40X is shown in Figure C.1.b (appendix C) was used for image comparison.

The Labnet spectrafuge centrifuge (Spectrafuge™ 6C Compact Centrifuge, C0060, Labnet, USA) was used for sample preparation, as shown in Figure C.1.a (appendix C).

The 3D printer (AnyCubic i3 Mega, Shenzhen, China) (appendix C) with fused deposition modeling printing technology was used to perform the printing process.

The PLA (polylactic acid) filament (Mika 3D, Inc.) was used to print the 3D parts of the design.

The benchtop UV-VIS spectrophotometer (Chongqing Gold Mechanical & Electrical Equipment Co., Ltd, GD-725, Chongqing, China) was used to take the readings of the samples from 350 nm to 780 nm.

The SolidWorks software was used (SolidWorks®, premium, x64 edition, SP 1.0, 2016) to design the 3D printed adapter.

The Cura Ultimaker software (Ultimaker®, v15.04.6, x64 edition, 2020) was used to prepare the parts with the 3D printer.

The Android Studio (4.0) software was used to design the smartphone application to measure the sample concentration.

2.4. Material Preparation

Using a 1 ml of whole blood with micropipette after the centrifugation. The sample was then scanned on the slide and left for 5 minutes to dry. Using the Leishman stain to die the sample and left for 10 minutes to dry, the time was monitored using a lab timer. The slide is chemically treated with buffer phosphate to reduce the effect of the Leishman stain and left for 10 minutes to dry. The slide is washed with water and left for 10 minutes to dry. The outcome of the slide takes about 35 minutes and the slide is ready to be processed. The slide were inspected using the smartphone adapter single-source design and the ordinary laboratory microscope, more details about devices and materials are found in appendix C.

The prepared samples employ the use of equation (2.1) below:

$$C_1V_1 = C_2V_2 \quad (2.1)$$

Where: C_1 : Original concentration; V_1 : Original volume; C_2 : Prepared concentration; V_2 : Prepared volume.

To prepare glucose samples, add 1 ml of glucose reagent A, then add 3 μ l of glucose standard solution of 100 mg/dl, then incubate at 37 °C for 10 min. in a water bath, as shown in Figure 2.1.a.

Urea samples were prepared by adding 1 ml of urea reagent A1, then the addition of 5 μ l urea standard solution of 50 mg/dl, after that incubating in a water bath for 10 min., then adding 1 ml of urea reagent B, finally 10 min. incubation at 37 °C in a water bath, as shown in Figure 2.1.b.

For triglycerides samples, adding 1 ml of triglyceride reagent S.L., then adding 3 μ l of triglycerides standard solution of 200 mg/dl, then 10 min. incubation at 37 °C in a water bath, as shown in Figure 2.1.c.

Bilirubin samples (TSB) were prepared by adding a 1 ml of the reagent in a clean dry tube, then adding 20 ml of the activator to the tube, then add a 50 μ l of standard solution with 0.1 mg/dl of bilirubin, then mix and incubate for 10 minutes at 37 °C in a water bath, as shown in Figure 2.1.d.

HDL samples were prepared by adding a 300 ml of the reagent in a clean dry tube. Then adding 300 μ l from the HDL standard solution with a concentration of 50 mg/dl to the tube. Incubate for 10 minutes at 37 °C in a water bath, as shown in Figure 2.1.e.

After that, the tube is put for centrifugation using the centrifuge (see appendix A) for 10 minutes at 4000 rpm. Add 1 ml of cholesterol reagent to a dry clean tube, then add 50 μ l from supernatant to the previously prepared tube. Then incubate for 5 minutes at 37 °C in a water bath. The reaction of all prepared samples described above is stable for at least 2 hours.

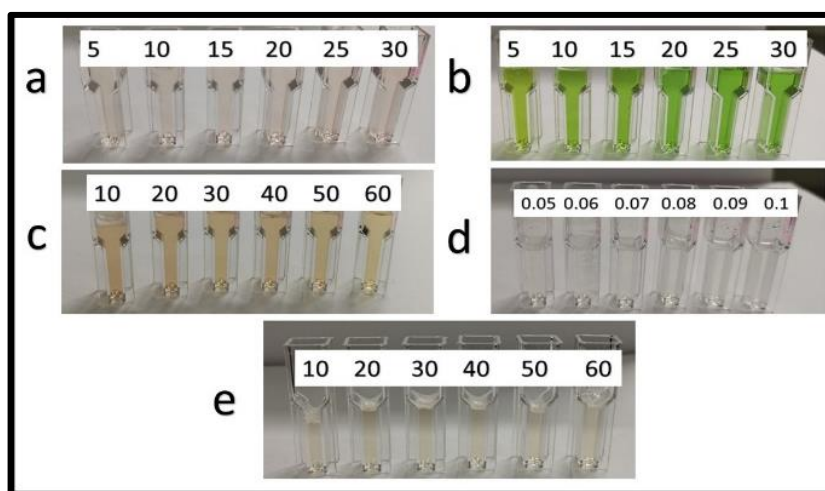


Figure 2.1: Prepared biochemical samples with six different concentrations labeled in the figure in mg/dl of (a) Glucose (b) Urea (c) Triglycerides (d) Bilirubin (e) HDL

All prepared samples were measured for absorbance and transmittance in the wavelength range of 350 nm to 780 nm using the benchtop UV-VIS spectrophotometer. The biomarkers datasheets are shown in appendix C in Figures C.6, C.7, C.8, C.9 and C.10 for glucose, urea, triglycerides, bilirubin, and HDL, respectively.

2.5. Experimental Work

The work in this thesis can be divided into three parts as shown in Figure 2.2 with each part composing of a design stage and implementation stage.

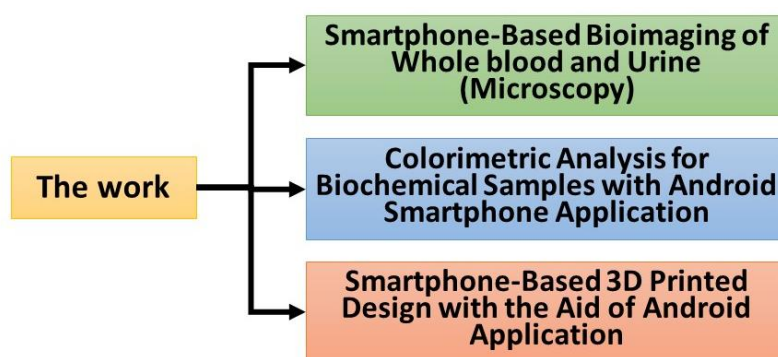


Figure 2.2: Schematic layout of the experimental work

2.5.1. Smartphone-Based Bioimaging of Whole blood and Urine (Microscopy)

Various 3D designs of the smartphone adapter were performed using SolidWorks software environment. In each design, the components were treated as drawing parts. Then, each part was "saved as" a ".stl" file format. This format is compatible with Ultimaker Cura 3D (appendix A) printer software in which the 3D printer simulation was performed. Different parameters were considered for producing the final 3D printed part. These parameters include but are not limited to, nozzle temperature, plate temperature, infill density, printer speed, support structures, in addition to filament support choice.

For convenience, the PLA filament was chosen for its compatibility and for being an environment-friendly plastic material. The part was then oriented in the most efficient direction and simulated to check the printing progress avoiding any implementation complications. The outcome of the Ultimaker Cura software is a ".gcode" file format, in which the 3D printer grasp mathematical geometrical code. The 3D printer is set for preheating matching the same input parameters in the Ultimaker Cura. The 3D printer is now ready to implement the final part. The above-mentioned technique is used for all parts in all designs.

For final assembly, all design parts were assembled to produce the final product (i.e. the smartphone adapter). Then, different parts of the hardware design including the laser, the optical density filter, the sample, the emission filter, the objective lens, and the eye-piece lens were integrated into the final hardware design. The design and implementation of the 3D adapter for microscopy is shown in Figure 2.3.

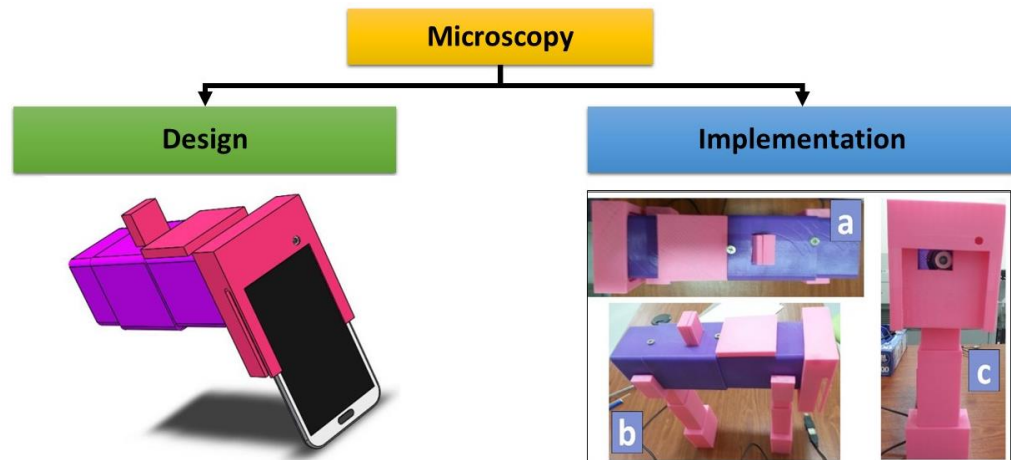


Figure 2.3: Schematic layout of the design and implementation of smartphone 3D adapter for microscopy

The software environment has different aspects such as modeling, design, simulation, and implementation. Ultimaker Cura software and SolidWorks

software were employed to perform different design aspects. Figure A.1 (see appendix A) shows the Ultimaker Cura software environment whereas Figure A.2 (appendix A) shows the control parameters in the software. The parameter choice is listed in Table 2.1.

Table 2.1: Parameters values for 3D model design

Parameter	Value
Filament Diameter	1.75 mm
Filament Material	PLA
Infill Density	20
Layer Height	0.2 mm
Nozzle Temperature	60 °C
Print Speed	150 mm/s
Printing Temperature	210 °C
Profile	Fast - 0.2 mm
Top/Bottom Thickness	0.4 mm
Travel Speed	120 mm/s
Wall Thickness	1.2 mm

2.5.2. Colorimetric Analysis for Biochemical Samples with Android Smartphone Application

The developed application can proceed in two different workflows A and B. Figure 2.6 shows the application workflow A and B. An Android application was designed and implemented, that is named "Colorimetric Sensing", using the latest version of Android Studio (4.0).

The role of the application is to implement the equations provided in (equations 1.1-1.6) but offering a user-friendly interface. Colorimetric Sensing was written in Kotlin and was tested successfully on a Huawei Mate 20 Pro.

Figure 2.10 shows the two workflows that the user can follow for generating results: the first one, workflow A, allows to use of the same background image for all the samples, the second one, workflow B allows the user to choose it for every trial of sample measurement.

Workflow A is described, so that workflow B will easily follow from that. (1) The user creates a new session (Figure 2.7a), the session can be considered as a container of all samples of the same type, for this reason when creating it the user must choose the material of interest, its absorptivity, and the linear fit when needed. In this workflow, the user is now asked to choose the background image that will be used for all the samples in the session. (2) Once the user has created a session, he can start to add samples, so he opens the session dashboard (Figure 2.7b) and adds a new sample (Figure 2.7c).

The sample image can be either already in the smartphone storage or it can be taken instantaneously from the smartphone camera. After choosing the image, the user chooses (3) the area of the image that will be used for the analysis, this area will be forced to be of the same size as the previously selected background, in order to avoid bad concentration predictions due to different image resolution.

Finally, after processing many samples of the material, the user (4) can see the absorbance, transmittance, and error estimation curves inside the application with the value of the regression coefficient (R^2) is indicated for both curves of absorbance and transmittance with linear approximation curve and the points represent the actual data collected by the application (Figure 2.7b). Moreover, the application also draws prediction error charts if the user wants to compare them with a laboratory device.

The study approach was a mixture of laboratory measurements of the biochemical materials, glucose, triglycerides, and urea. In addition to using the developed colorimetric sensing application for testing and measurement (see Figures 2.6 and 2.7). The prepared concentrations of all the samples reported here were control samples. Many variables were taken into consideration that may arise from dealing with the images of the biochemical materials. The images were taken under different lighting circumstances, with flash, reflection, and without flash to estimate the best available environment for concentration measurements. The designed application here can overcome different lighting conditions of the samples by inserting the fitting parameter to the application, in which, the molar absorptivity can be calibrated regardless of the illumination light type.

This is shown as in Figure 2.4, different lighting parameters were chosen to check for the practicality of the application to predict the concentrations of the materials under different lightening circumstances, so even when different environmental lighting is the case, the application by simple calibration of the data can overcome this issue. Therefore, discussion of different LED sources and CMOS camera characteristics are not the case, since the application work by simple calibration with a priori determined concentration values, and then the application can predict the unknown concentration of the material.

To accurately predict the concentrations of unknown samples, first, a known value must be at hand and then calibrated for the unknown material. The colorimetric sensing application can work with more materials other than just the three materials reported here. The images taken were high-resolution images with a pixel size of (without flash 960 x 540) and (with flash 528 x 960) therefore the estimation of the concentration was close to the actual concentration.

The laboratory measurement were verified based on equations (1.1a and 1.1b) after preparation with high accuracy of the material concentration in laboratory settings. The laboratory measurements were done in the visible region of the spectrum; for glucose $\lambda = (350 - 640 \text{ nm})$, triglycerides $\lambda = (400 - 680 \text{ nm})$, and urea $\lambda = (500 - 780 \text{ nm})$. The error of measurements was provided based on comparing each recorded value for absorbance and transmittance with the equation-based value (1.1.a and 1.1.b) of the measured quantity.

The error was marginal as shown in Figures 3.6c, 3.7c, and 3.8c. The absorbance and transmittance curves show the one-to-one mapping of the measured concentration, with a linear increase in absorbance and linear decrease in transmittance for all inspected materials (Figures 3.6, 3.7, and 3.8).

For the designed application, different circumstances were examined, for example, the selected area of image processing was taken into consideration to be the critical issue since in each trial of computation when choosing the material this area is subjected to minor deviation, and thus careful choice should be made when dealing with the samples.

The nature of the processed images in terms of lightening is also important and considered when designing with the application, by taking three different scenarios of image lightening (with flash, with flash, and reflection, without flash) (Figure 2.4). Finally, the background image choice is subjected to an accurate selection of the position of the pixels and cropped image size, the opportunity in the colorimetric sensing application to deal with background images in two different ways were provided.

The workflow (A) with single image background for all samples provides a solution for image comparison by subjecting all samples to the same

background, this eliminates the need for background image set up every trial, reducing the error of measurements, and provides faster image processing resulting in a rapid testing environment by reducing the processing time of concentration measurement. Figure 2.5 shows the schematic of the sensing mechanism of the colorimetric sensor.

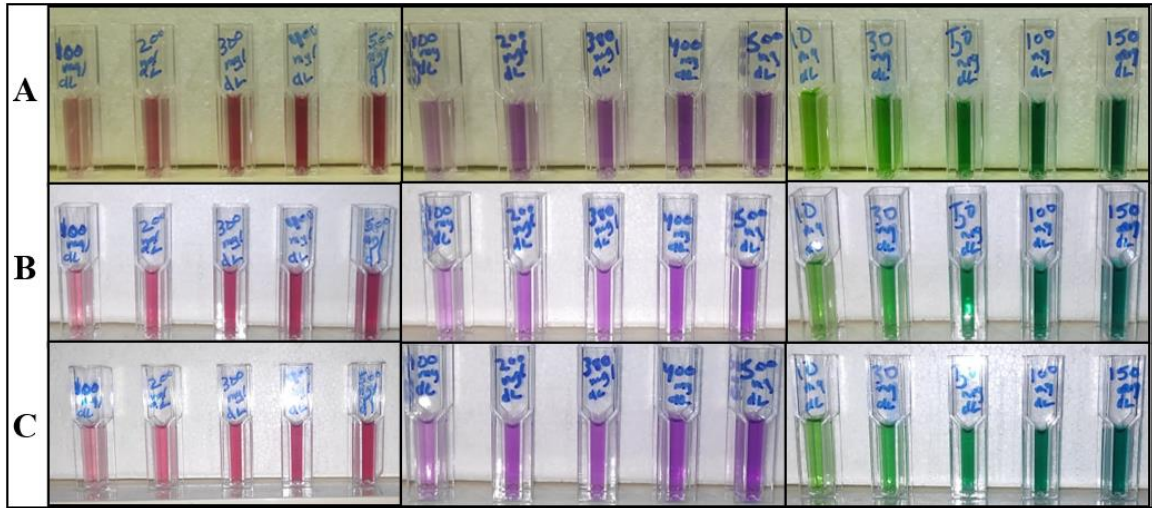


Figure 2.4: Images of biochemical samples (12 Mpx); glucose (Pink; left side images) triglycerides (Purple; middle images) urea (Green; right-side images) at 20 cm distance (a) without flash and no reflection (b) with flash (b) with flash and reflection

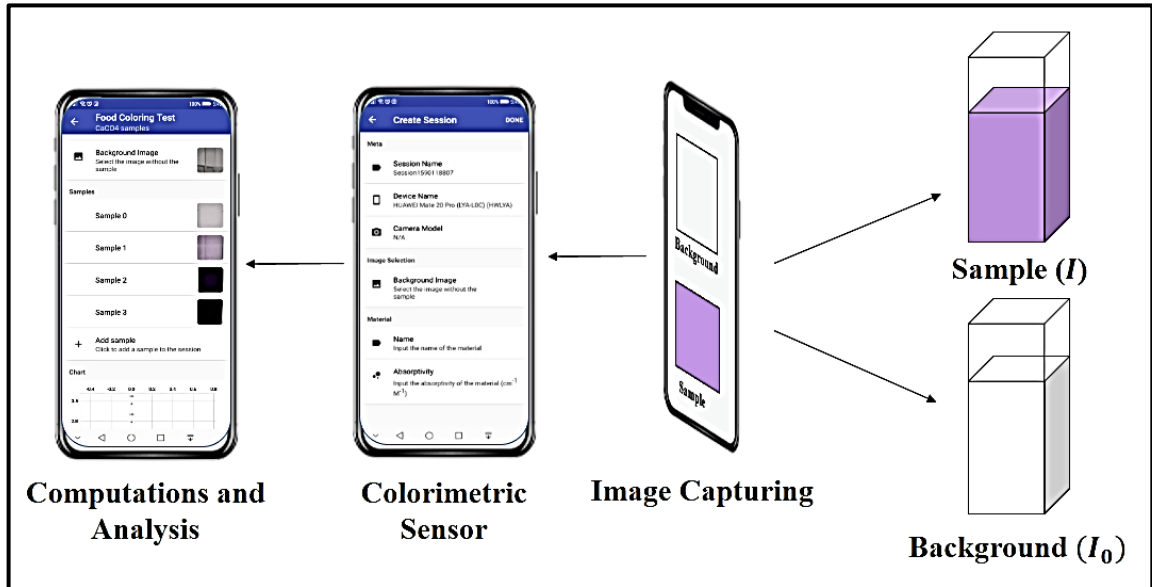


Figure 2.5: Schematic illustration of the imaging mechanism showing both background and sample image

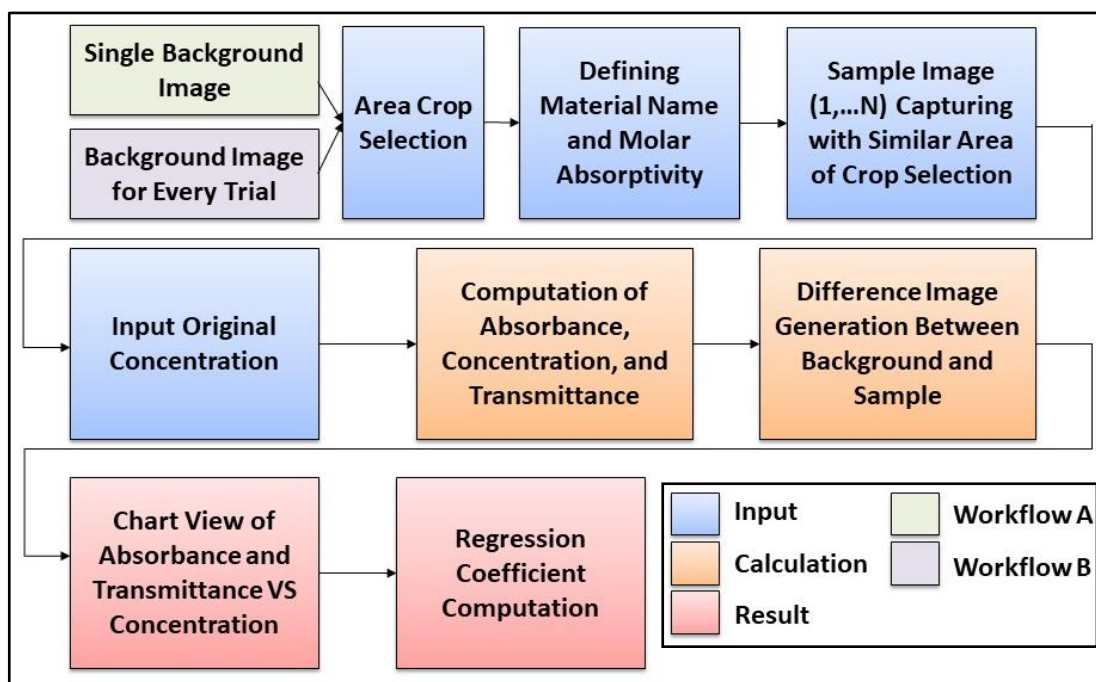


Figure 2.6: Colorimetric sensing application workflows (A) with a single image background (light green box) (B) with a background image for every trial (light purple box)

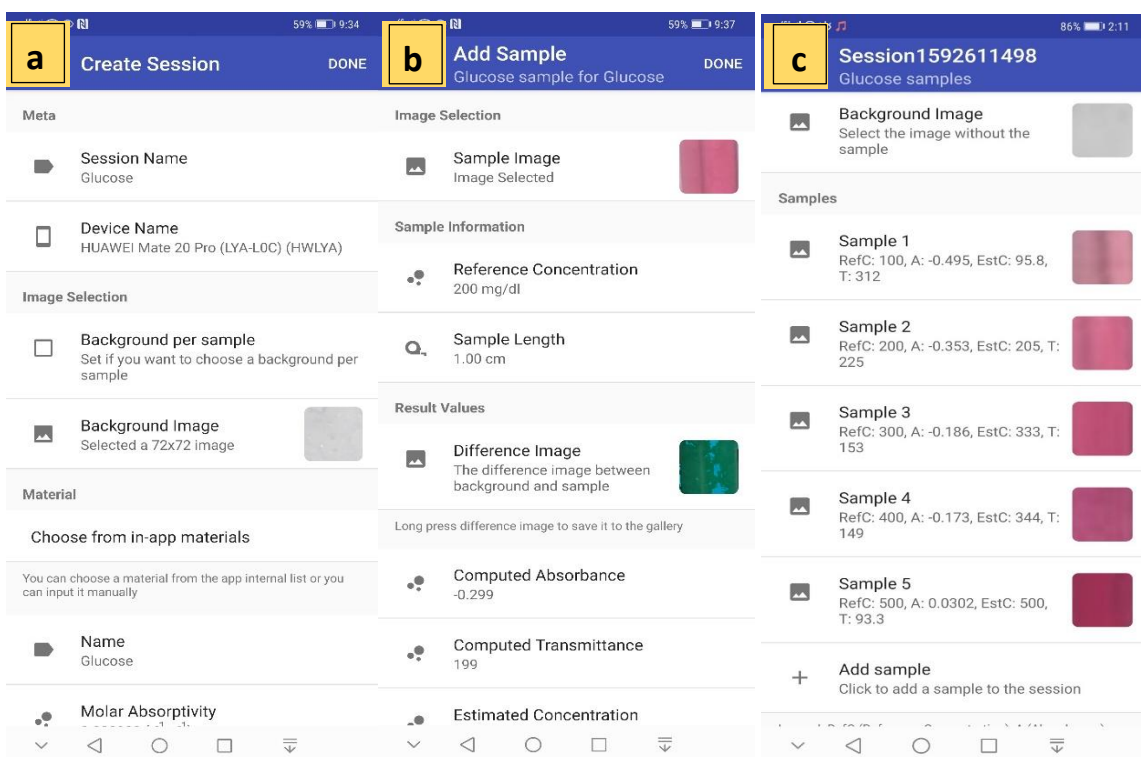


Figure 2.7: Colorimetric sensing application layout (a) Creating a session (b) Adding a sample (c) List of samples with the same material in different concentrations

On the other hand, workflow (B) with background image for every trial is useful in other cases, for example, when the user prepares the samples in different timeframes or different lightening and positioning of the cuvette, this results in changes in the background image, thus, the workflow (B) solves the issue with high accuracy.

2.5.3. Smartphone-Based 3D Printed Design with the Aid of Android Application

The 3D adapter is composed of a source case, sample case, optics case, and smartphone holder. This separate casing allows the possibility of replacement of any case with a different one. The source case has the illumination source (Laser diode or LED) and a USB-to-TTL for powering the source. Since there is a power cable for the smartphone, it can be used to power the illumination source eliminating the need for an external power source.

The light from the illumination source passes from the source case entering the sample case where a neutral density filter is there to remove the background noise and make a shield for the smartphone CMOS camera not to destroy the sensors with the focused power from laser diodes. Then the light strikes the sample in its sample holder, after that, the light travels to the objective lens in which more collimation is being done to make a brighter image. An emission filter is positioned between the objective lens and the eyepiece lens to bandpass emissions with specific central wavelengths with a tolerance of 10 nm, as shown in Figure 2.8.

The light then reaches the CMOS camera sensor in which the imaging occurs and the resulting image will be used with the developed Android application (Colorimetric Sensing) to predict the biomarkers' concentration. The design and implementation is shown in Figure 2.9.

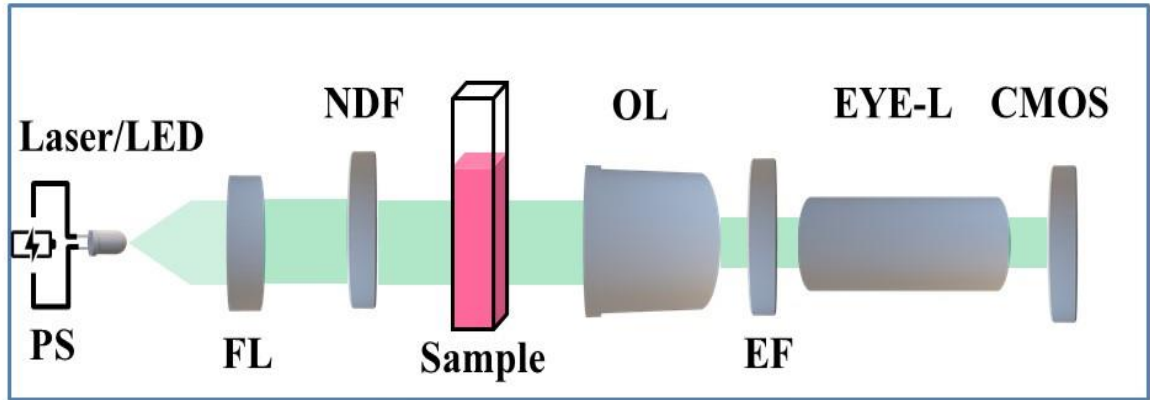


Figure 2.8: Schematic of the optical path from the illumination source to the CMOS camera (PS: Power Source; FL: Focusing Lens, NDF: Neural Density Filter; OL: Objective Lens; EF: Emission Filter; EYE-L: Eyepiece Lens)

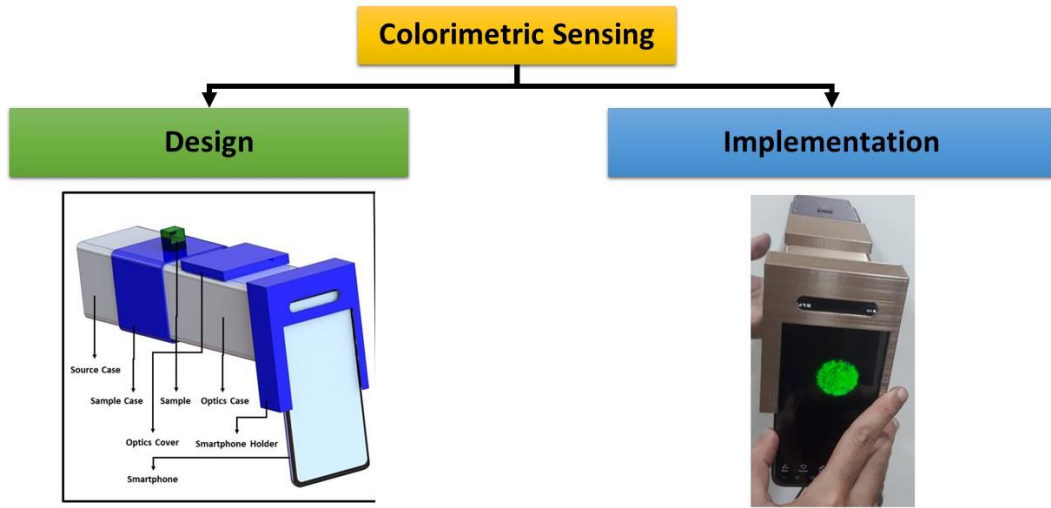


Figure 2.9: Schematic of the colorimetric sensor design and implementation

2.6. Complexity Analysis

The work in this thesis has different levels of complexity, in which design, implementation, sensing and imaging can be experimentally realized with such excellent performance over the course of the work. This analysis will cover the entire work with careful assessment of each step along the way, it can be divided into three parts, hardware, sample preparation and measurements, and software as shown below.

2.6.1. Hardware

The work in designing a hardware 3D models can be analysed for its complexity as the list below:

- 1) Design Stage - SolidWorks
 - i. Using SolidWorks to design the 3D models.
 - ii. Optimization of parts dimensions.
 - iii. Ensuring the fitting of different parts into one single design.
 - iv. Ensuring the fitting of the 3D printed parts with the external optical components.
 - v. The total number of designed parts were 360.
- 2) Design Stage – Cura Ultimaker
 - i. Using Cura Ultimaker to convert each designed part from “.stl” to “.gcode”.
 - ii. Ensuring the proper parameters for the 3D printer to operate without errors.
 - iii. Ensuring that the parts are simulated for optimum parameters.
 - iv. For each part a total of 6 simulations were done (i.e. 2160 simulations were performed).
- 3) Design Stage – 3D printing
 - i. Using AnyCubic i3 Mega to print the designed models with SolidWorks and treated by Cura Ultimaker.
 - ii. Making sure there are no errors in printing.
 - iii. Postprocessing of the 3D printed parts to eliminate the support structure put there to ensure proper printing.
 - iv. The total number of printed parts was 120 part.
- 4) Design Stage – Assembly

- i. Ensuring all printed parts are fit together and the optical elements inside it are in a great shape.
- ii. Performing different assemblies for different part to ensure more than one source and different optics are fit.
- iii. The total number of assembled designs was 20 different design.

2.6.2. Sample Preparation and Measurements

The work in sample preparation and sample measurements can be analysed for its complexity as the list below:

- a) Sample Selection and Preparations
 - i. Making sure that the sample of interest will endure a colorimetric change by different concentrations.
 - ii. Purchasing a high quality samples.
 - iii. Preparing the sample within the normal range of the human body.
 - iv. Preparing the minimum possible concentration within the laboratory settings.
- b) Sample Size

The total samples prepared for all works in the thesis are 42 samples for biosensing and 30 samples for bioimaging as follows:

- i. 11 glucose
 - ii. 8 urea
 - iii. 11 triglycerides
 - iv. 6 bilirubin
 - v. 6 HDL
 - vi. 15 urine
 - vii. 15 whole blood
- c) Performing Laboratory Measurements

- i. For 45 Samples with a range of 350 nm to 780 nm with step of 10 nm.
 - ii. A total number of 1980 reading of absorbance.
 - iii. A total number of 1980 reading of transmittance.
- d) Performing Smartphone Imaging
- i. A total number of 240 image of whole blood and urine were captured in bioimaging stage.
 - ii. A total number of 240 image of biomarkers were captured in the biosensing stage.

2.6.3. Software

The work in software design and implementation can be analysed for its complexity as the list below:

- a) Design Stage
 - i. Using Android Studio to design a smartphone application with the ability to work as a colorimetric sensor.
 - ii. Developing an algorithm based on samples of interests.
 - iii. Checking all the physics of measurements to ensure proper results.
 - iv. Employing a two-way function of the smartphone application.
 - v. The first function is to predefine a string of previously defined dataset from the Handbook of Laser Dyes.
 - vi. These data exceeds 250 materials with all their properties.
 - vii. The second function is to calibrate images with a predefined concentration values (as prepared accurately in the sample preparation stage).
 - viii. Employing another two-way function of the smartphone application.

- ix. The first function is to compare the background image with sample image everytime the user initiates a measurement.
- x. The second function is to compare a single background image with all samples making the measurement more rapid.

b) Measurements Stage

- i. The total number of measurements performed in (Software-Only) work was 900.
- ii. The total number of measurements performed with both 3D printed smartphone adapter and the software was 1200.

Chapter Three

Results, Discussion, Conclusions and Future Work

3.1. Introduction

This chapter focuses on the results obtained during the experimental work with three different parts. The first part of the work, is the design and implementation of smartphone-based 3D printed adapter for whole blood and urine imaging with three different light sources; the light emitting diode and two laser diodes with 532 nm and 650 nm, respectively. The second part of the work, is the developed smartphone Android application being the tool for image processing, data analysis, and results preview on-screen. Within the smartphone environment the analysis was done. The samples were prepared and ordinary photos of the samples were captured and then send to be analyzed within the smartphone application. All the samples were tested in a laboratory benchtop spectrophotometer with a wide range of wavelengths. Finally, the third part of the work, is the design and implementation of smartphone-based 3D printed adapter to measure the concentration of five different biomarkers with eight different illumination sources using the developed smartphone Android application.

3.2. Smartphone-Based Bioimaging of Whole blood and Urine (Microscopy)

3.2.1. Using 532 nm Laser Diode

In Figure 3.1, a 532 nm laser diode was employed. The image of the smartphone with and without the slide sample taken with a Galaxy Note II N7100 smartphone (SAMSUNG manufacturing) is shown in Figure 3.1 (a)- Figure 3.1 (c) the source (laser) can be seen from the backend of the adapter as a shining spherical spot, the Figures 3.1 (b) and 3.1 (c) shows the images of urine and whole blood sample with high details in comparison with the laboratory optical microscope in Figure 3.1 (d) .

Two different types of samples were prepared for usage in the smartphone adapter, namely, urine sample, and whole blood sample. The resulting image of the samples with 200X magnification is shown respectively in Figure 3.1 (b) and (c). The laboratory microscope image with 40X magnification is shown in Figure 3.1 (d) for comparison.

It is noteworthy to state that the position of the smartphone camera plays a significant role in the output image. Thus, proper adjustment and focusing are mandatory for good image output, as shown in Figure 3.2.

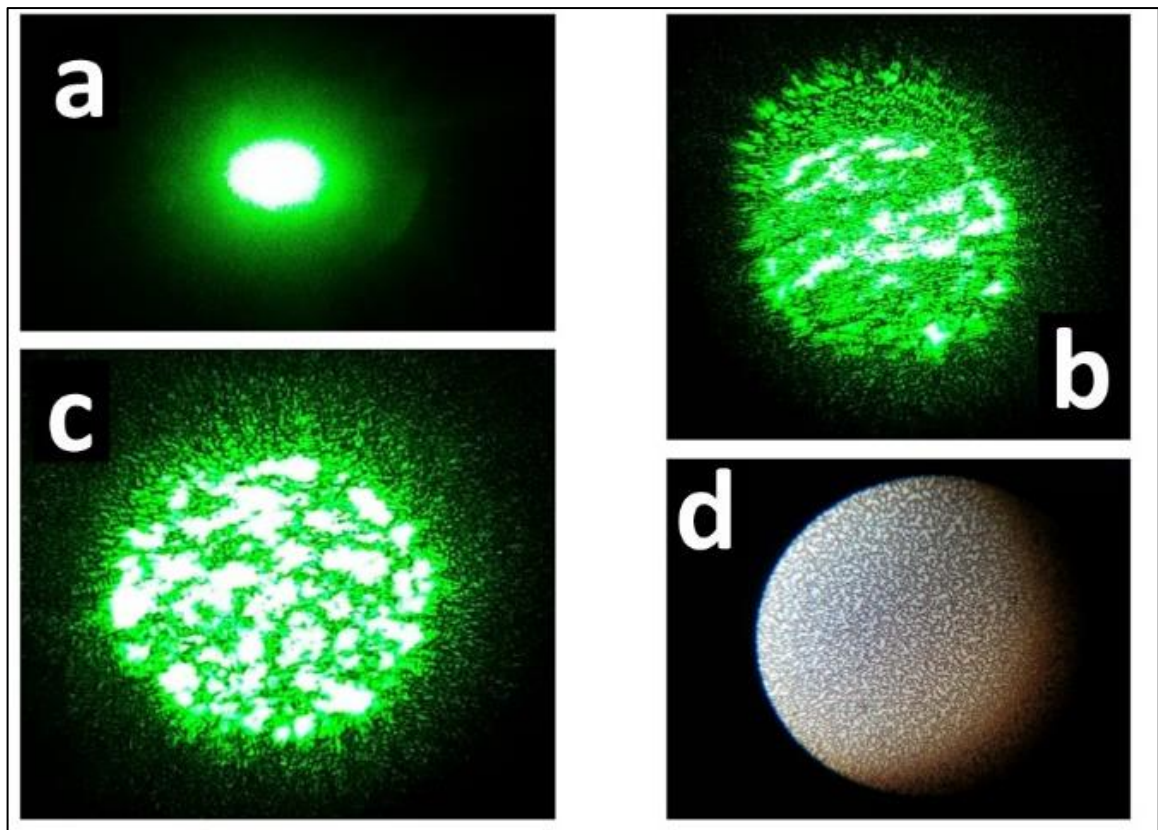


Figure 3.1: Images of the smartphone adapter using 532 nm laser diode (a) Without sample (b) Urine sample (c) Blood sample (d) microscope image of the blood sample

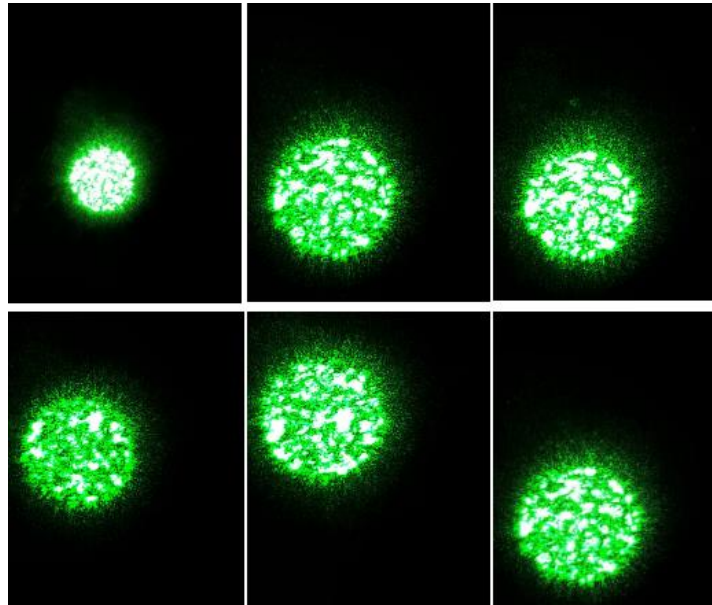


Figure 3.2: Six different output images of the smartphone adapter for the same blood sample

3.2.2. Using White LED

The white LED was used as an illumination source for the smartphone adapter resulting in poor image contrast, as shown in Figure 3.3 (a) with an image of the smartphone adapter without the use of emission filters and the sample was urine. The same sample and illumination source were subjected to the emission filters (FB530-10, PO#T0648536; FB580-10, PO#T0679010; FB640-10, PO#T0672817; and FB430-10, PO#T0680669; Thorlabs) resulting in the images, as shown in Figures 3.3 (b), 3.3 (c), 3.3 (d), 3.3 (e), respectively.



Figure 3.3: Images of the smartphone adapter using white LED as illumination source (a) without the emission filter (b) with the emission filter FB530-10 (c) with the emission filter FB580-10 (d) with the emission filter FB640-10 (e) with the emission filter FB430-10

3.2.3. Using 650 nm Diode Laser

The 650 nm diode laser was the illumination source of the urine sample, two approaches were used with the same smartphone adapter design for comparison with (FB640-10, PO#T0672817, Thorlabs) and without the emission filter, as shown in Figure 3.4 (a) and Figure 3.4 (b), respectively. Images with the emission filter show a more focused and clear view with no background noise, while the images without the emission filter show a high background noise and irregularities, indicating the proper use of the emission filter to handle the imaging operation more efficiently.

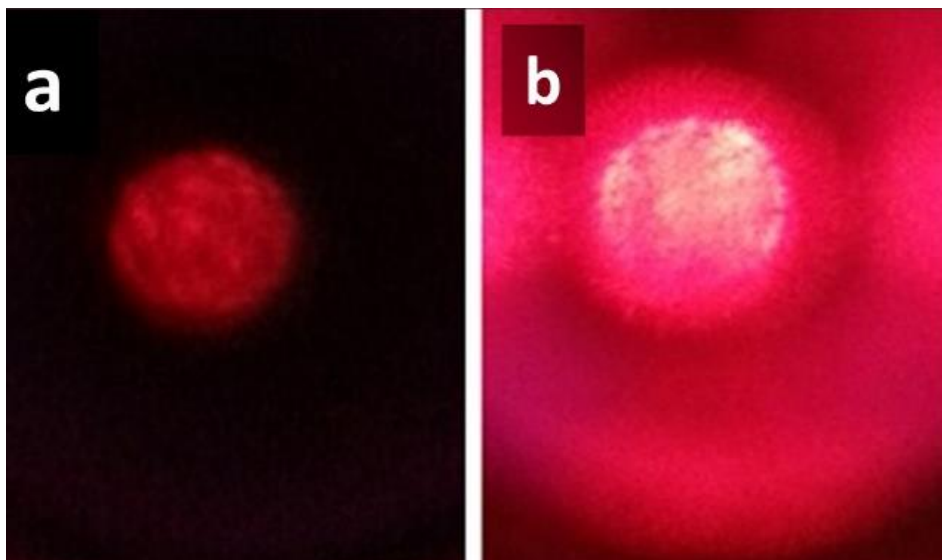


Figure 3.4: Image of the smartphone adapter using the 650 nm laser diode as illumination source (a) with the emission filter FB640-10 (b) without the emission filter

By introducing the previous work, as mentioned in chapter one, the motivation is to make an easy-to-use smartphone-based 3D printed adapter capable of capturing high-definition imagery of biosamples, a focus was made on whole blood and urine imaging with the utilization of three different illumination sources being 532 nm, and 650 nm laser diodes and a white light emitting diode with four emission filters. The results comparison is a visual one in which a high definition imagery is to be captured with portable environment,

cheap with the range of 8\$ to 7\$ per design, lightweight with a total weight of less than 200 g, small dimensions with a total dimension of less than 28 cm and a low power consumption of less than a 5 mA input power from the smartphone port.

The overall system of the smartphone-based 3D printed adapter for bioimaging purposes enables the capturing of high definition imagery when proper parameters and optical components are put in place. The results showed that the smartphone-based 3D printed adapter can overcome traditional imaging microscope with detailed imagery. The use of 532 nm laser diode showed high definitive features of the samples while the 650 nm laser diode showed a dimmer imagery with the ability to extract features from the images.

On the other hand, a white LED provided less sample features even when a wide range of emission filter where utilized to perform the imaging. Thus, a laser based imagery can provide more features than an LED source which will motivate us to bring this issue into machine learning and neural networks to develop a recognition application with a smartphone-based 3D printed adapter with a wide range of samples to be tested in the future.

3.3. Colorimetric Analysis for Biochemical Samples with Android Smartphone Application

The transmittance, absorbance, and the absolute average error curves for glucose (350 – 640 nm), triglycerides (400 – 680 nm), and urea (500 – 780 nm) with concentrations of (100, 200, 300, 400, 500 mg/dL) for glucose and triglycerides, while the urea concentrations were (10, 30, 50, 100, 150 mg/dL) are shown in the (Figures 3.6, 3.7, and 3.8). Trials of glucose, triglycerides, and urea were conducted for each material, 3 high-resolution photos were captured that were processed and a fourth trial was made by changing the background of

the third photo for all materials to establish both application workflows (A) and (B) (Figure 2.10, Chapter 2). A sample of the actual results from the Colorimetric Sensing application is shown in Figure 3.5.

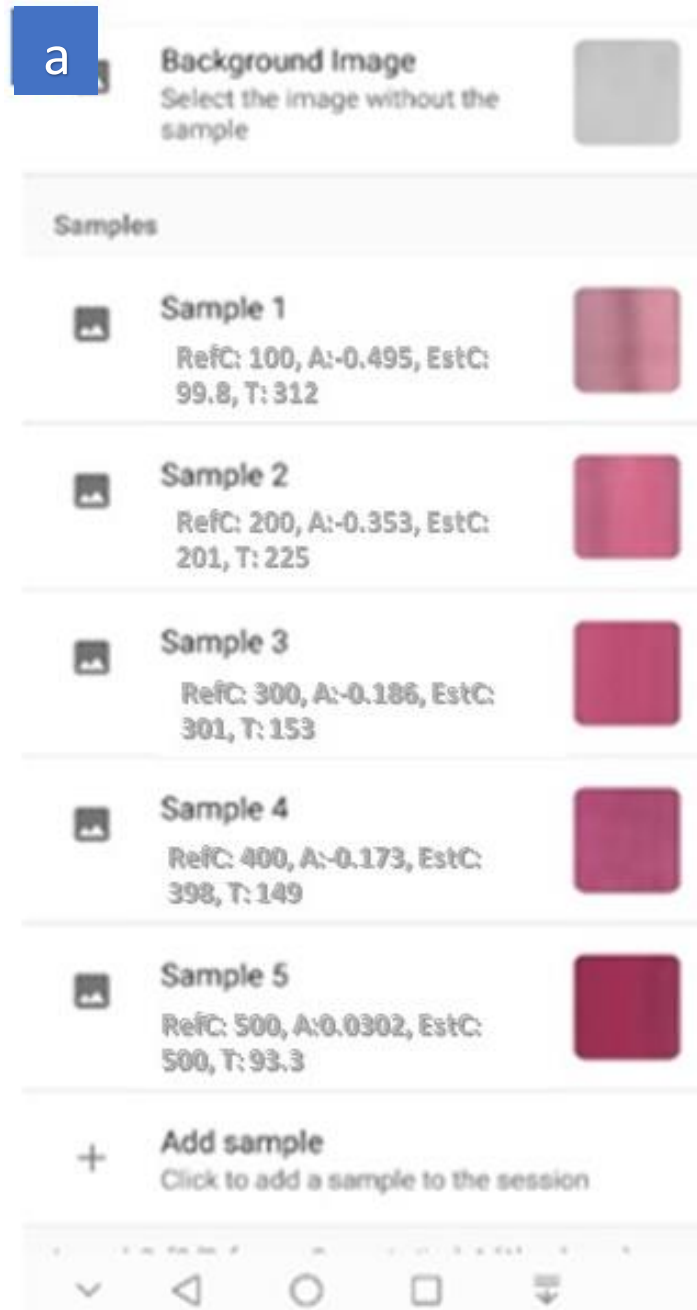


Figure 3.5: Samples of calculations using the colorimetric sensing application (a) glucose sample list (b) triglycerides sample list (c) urea sample list (d) calculations of absorbance (e) transmittance (f) error of measurements

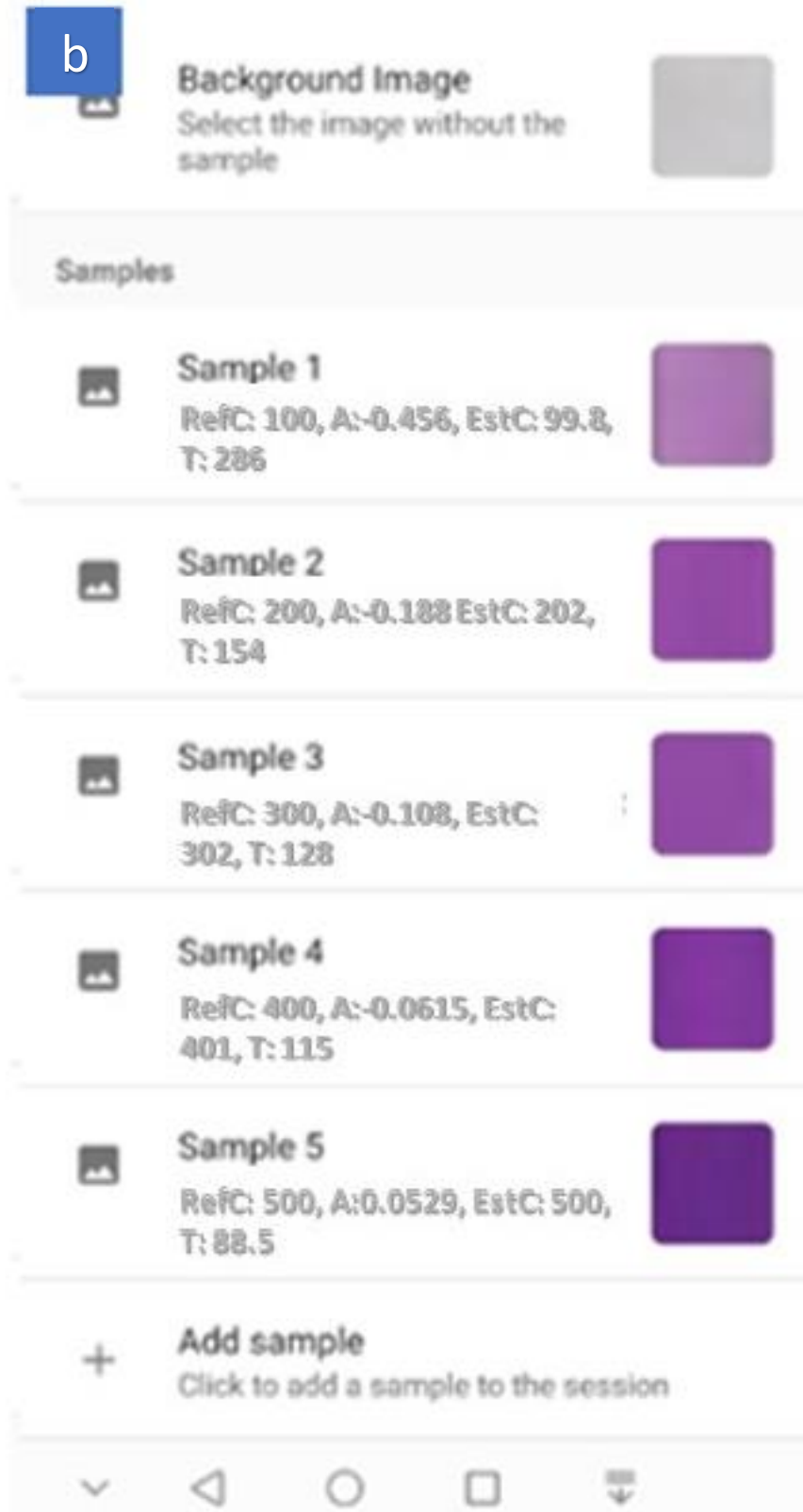


Figure 3.5: continued

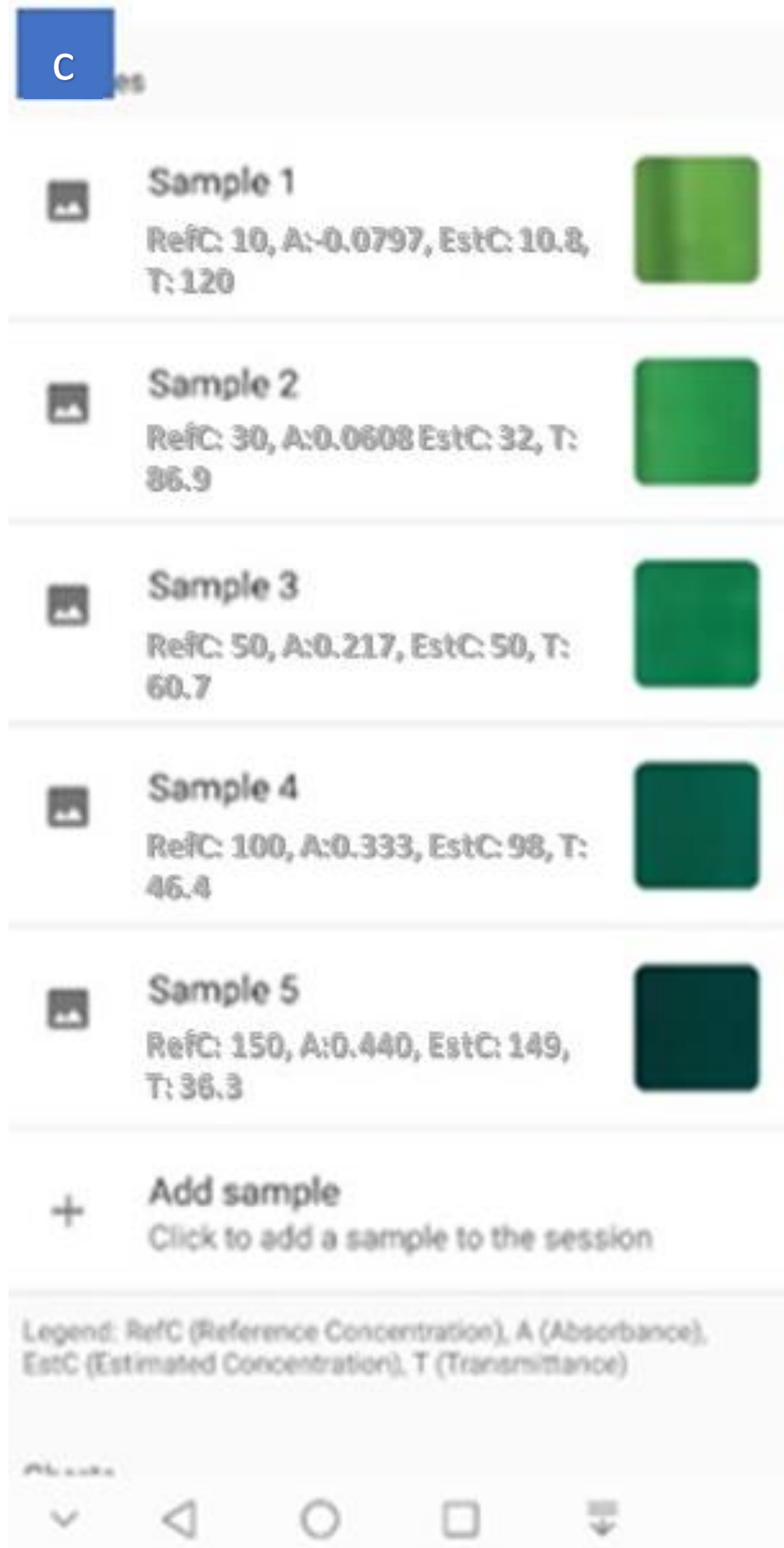


Figure 3.5: continued

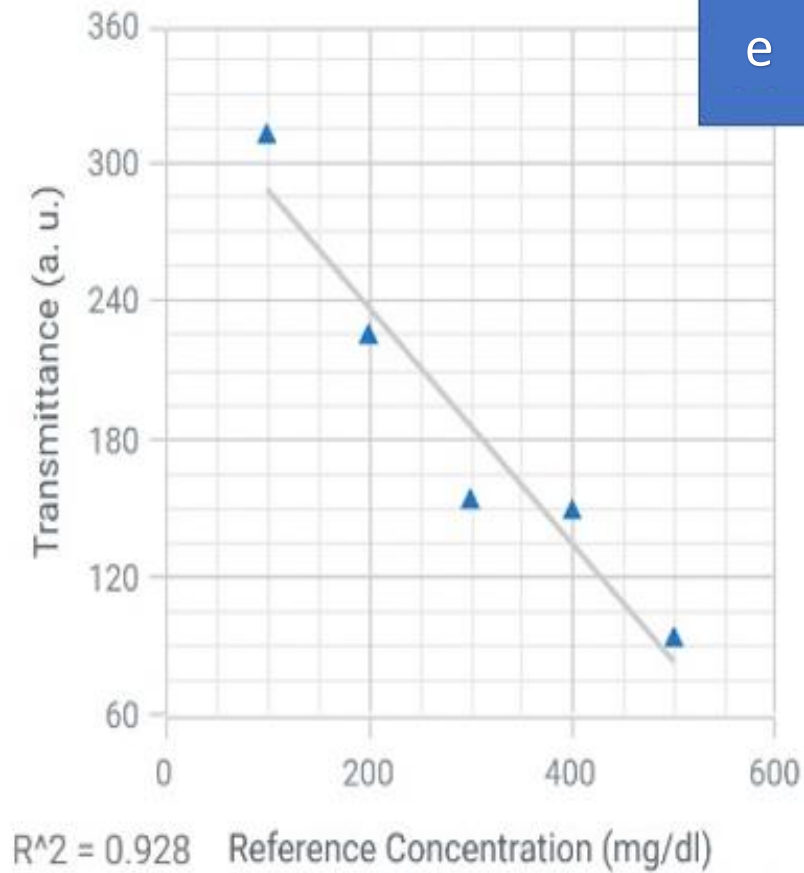
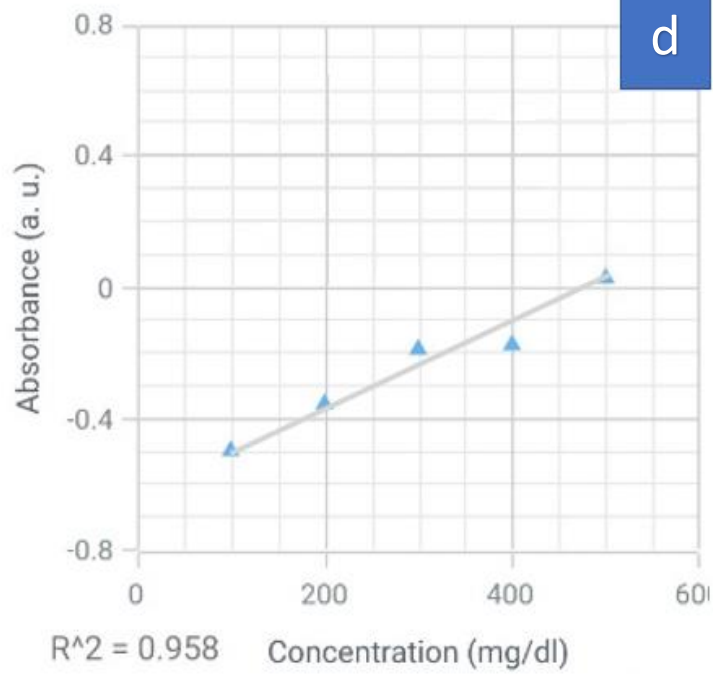


Figure 3.5: continued

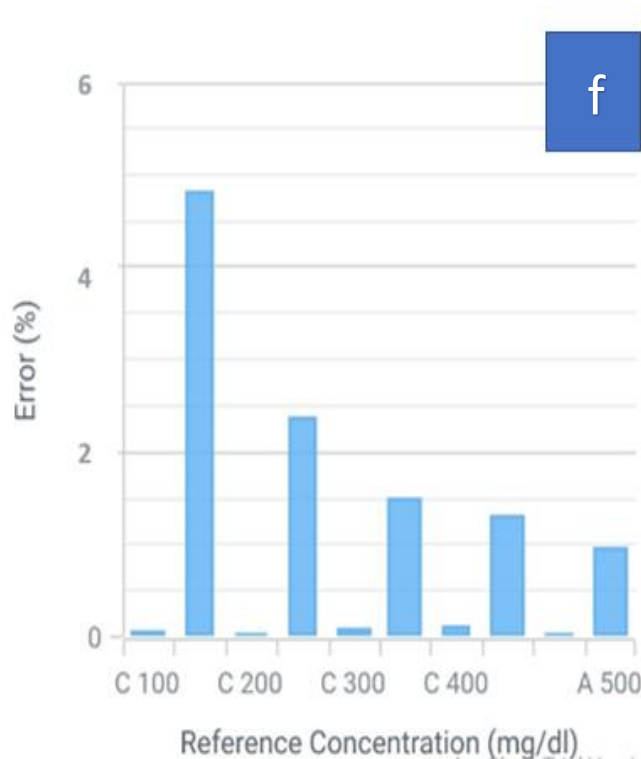


Figure 3.5: continued

The plots of transmittances, absorbances, and absolute average error percentages are shown for glucose (Figure 3.6), triglycerides (Figure 3.7), and urea (Figure 3.8). In Figures 3.6, 3.7, and 3.8, the legends are abbreviated as (T) for transmittance (A) for absorbance (M) for measured quantity using the laboratory spectrophotometer, (nm) represent nanometer, err% is the absolute average error percentage obtained using equations (1.5a) and (1.5b).

In Figure 3.6a, 3.6b, and 3.6c, the transmittance (T), absorbance (A), and error of measurement (err%) were plotted for five different concentrations of prepared glucose samples. These concentrations were for control samples of 100, 200, 300, 400, and 500 mg/dL.

Each sample was tested using the laboratory spectrophotometer for a wide range of wavelengths from 350 nm to 640 nm. The values reported for transmittance and absorbance were from the measurement with (M) (i.e.,

measuring each sample with a wavelength and reporting both absorbance and transmittance values), the measurements were done with the laboratory spectrophotometer.

The above description is also true for both triglycerides (Figures 3.7a, 3.7b, and 3.7c) and urea (Figures 3.8a, 3.8b, and 3.8c) with five different concentration each, with prepared concentrations of triglycerides of 100, 200, 300, 400, and 500 mg/dL, these measurements were in the wavelength range of 400 nm to 680 nm.

The urea concentrations were 10, 30, 50, 100, and 150 mg/dL, these measurements were in the wavelength range of 500 nm to 780 nm. All prepared concentrations for all the materials reported here were control samples, not patient samples.

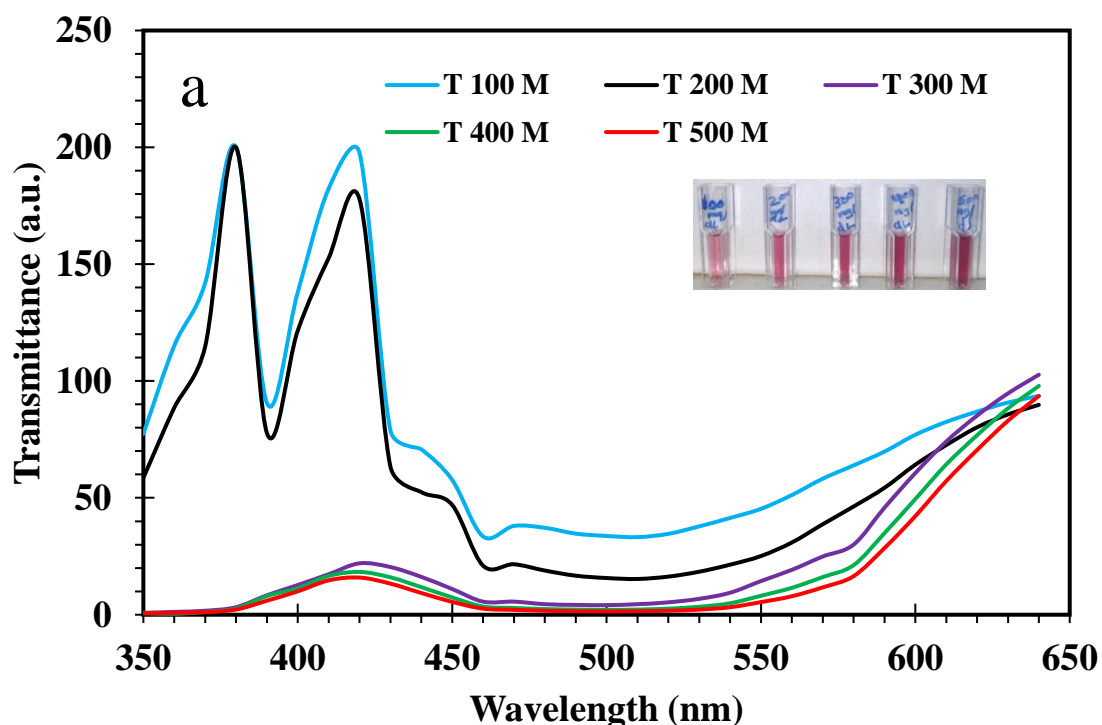


Figure (3.6): Transmittance (a), absorbance (b), and absolute average error percent (err%) (c) of glucose sample in different concentrations

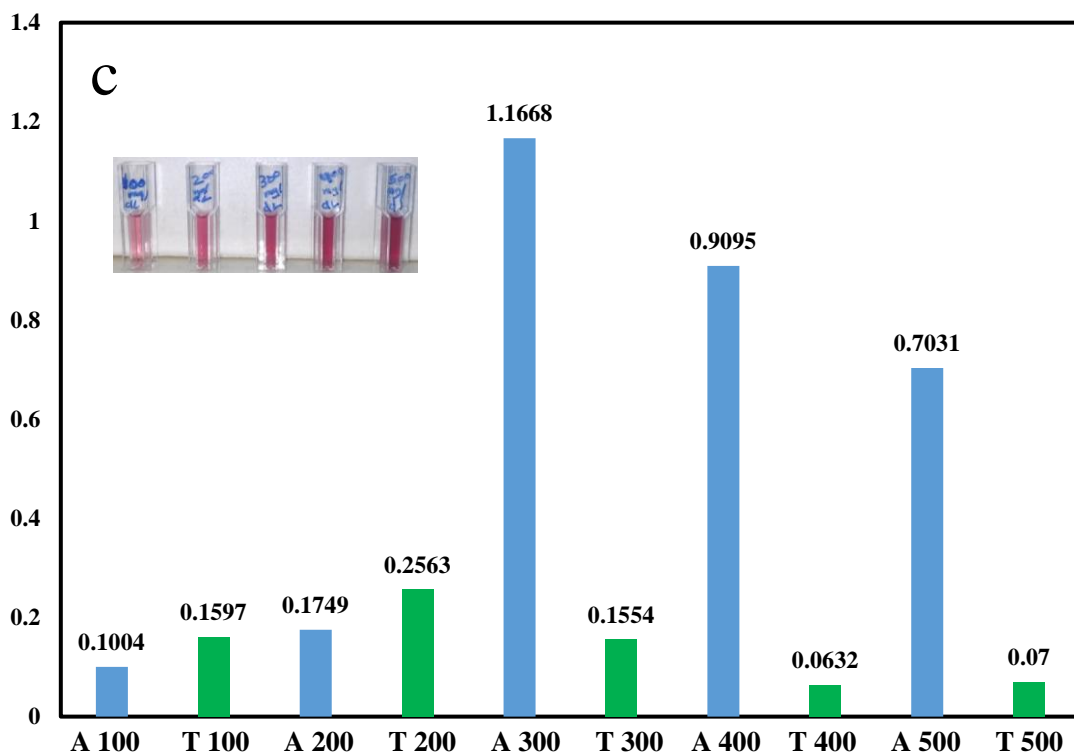
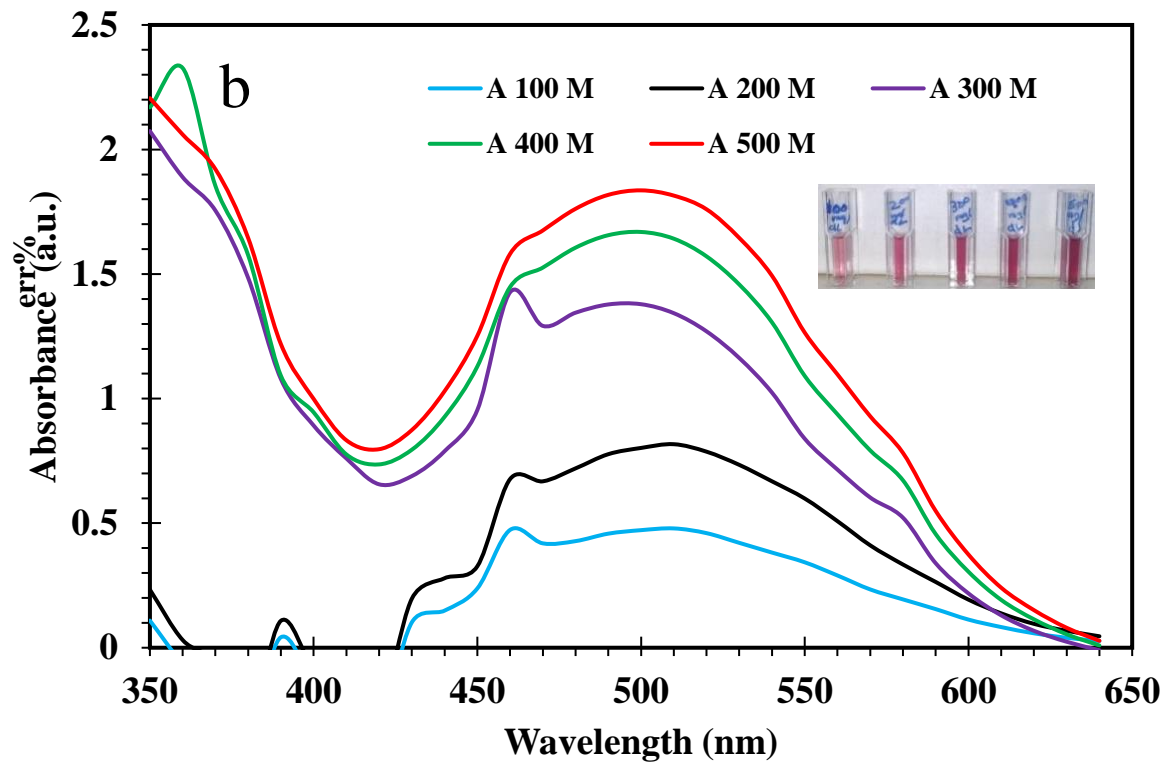


Figure (3.6): continued

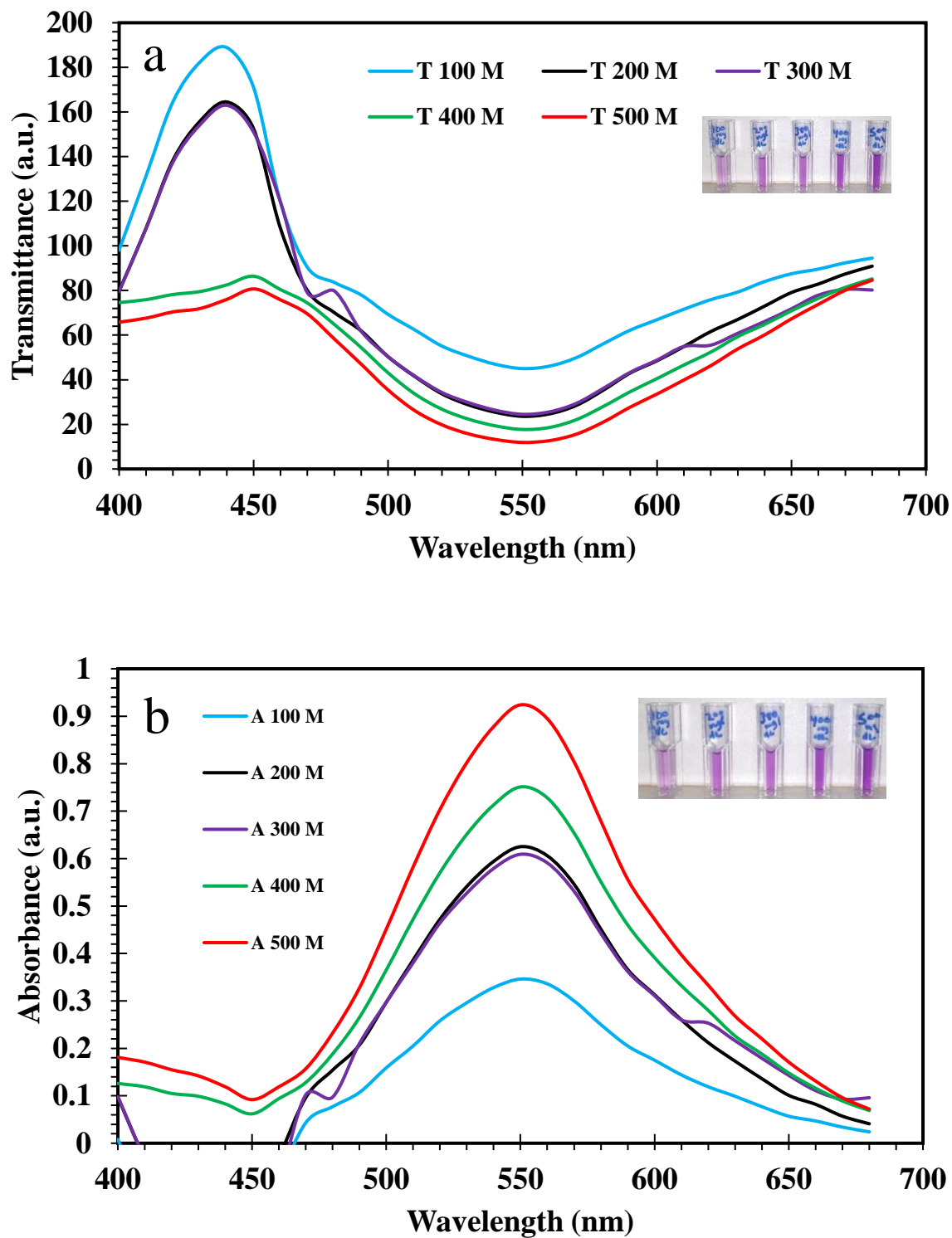


Figure (3.7): Transmittance (a), absorbance (b), and absolute average error percent (err%) (c) of triglycerides sample in different concentrations

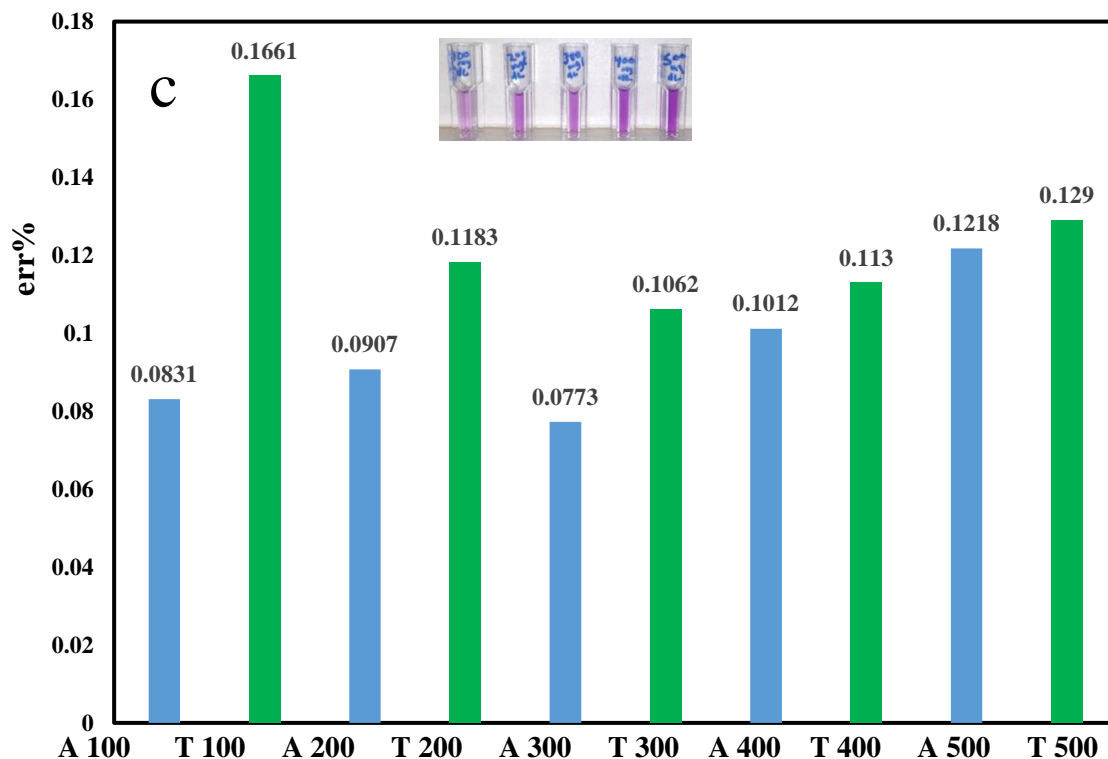


Figure (3.7): continued

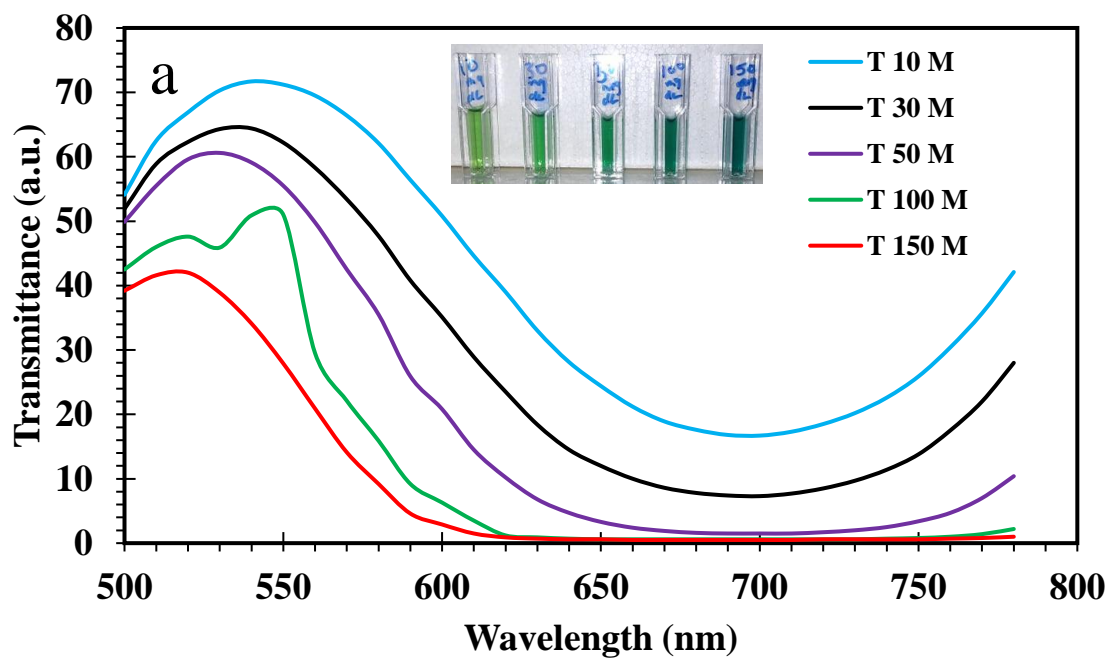


Figure (3.8): Transmittance (a), absorbance (b), and absolute average error percent (err%) (c) of urea sample in different concentrations

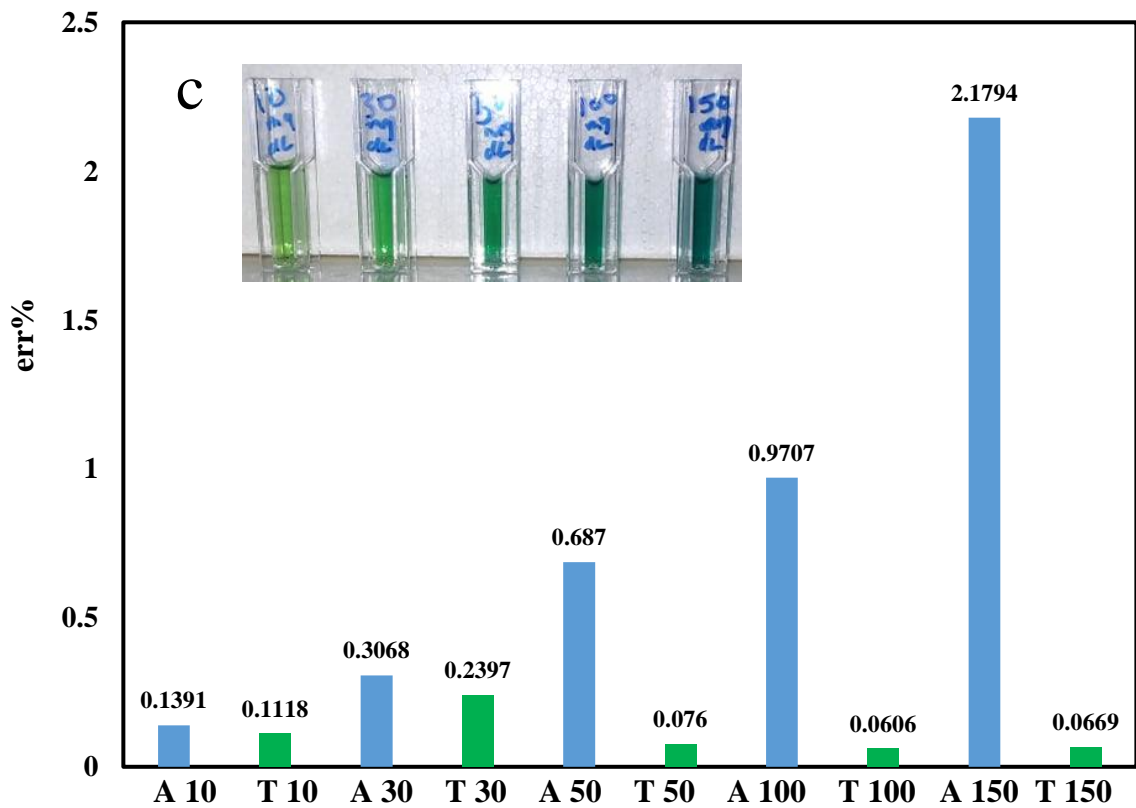
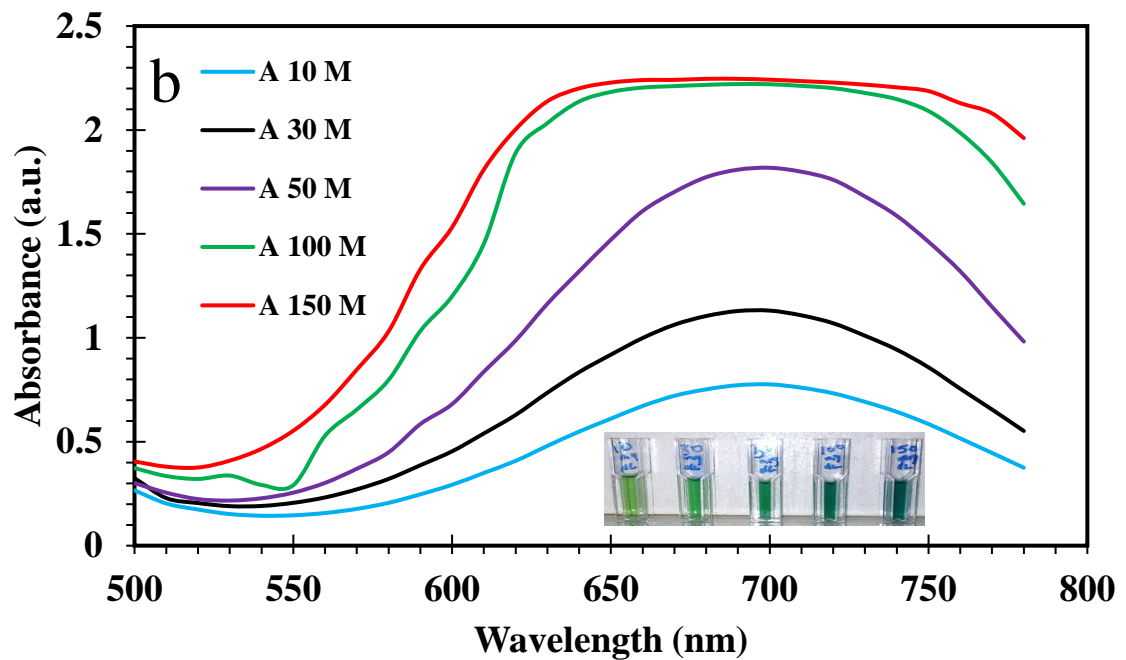


Figure (3.8): continued

The overall number of trials for all materials in all images was 900 trials. Both the absorbance and the transmittance were used for convenience, as shown in Figure 3.5 where background image, samples, concentration estimation, plots of transmittance and absorbance for all samples versus concentration in two different units, the error of measurement bar chart and the linear regression coefficient (R^2) for both A and T is depicted by the colorimetric sensing application.

Figures 3.9 and 3.10 show the absorbance and the transmittance curves for the glucose, and triglycerides materials both calculated in the colorimetric sensing application and measured in the spectrophotometer, respectively. Figure 3.11 presents the absorbance and the transmittance curves for the urea material both calculated in the colorimetric sensing application and measured in the spectrophotometer.

The results were promising since the colorimetric sensing application a linear regression coefficient (R^2) values for absorbance and transmittance for glucose, triglycerides, and urea 0.9825, and 0.9899; 0.9405 and 0.9502; 0.9431 and 0.8597, respectively (see Figures 3.9.a, 3.9.b, 3.10.a, 3.10.b, 3.11.a, and 3.11.b). While for the spectrophotometer measurements the (R^2) of the absorbance and transmittance with the same material flow was 0.9973 @560 nm and 0.9793 @600 nm; 0.952 @620 nm and 0.9364 @410 nm; 0.9948 @570 nm and 0.9827 @530 nm, respectively (see Figures 3.9.c, 3.9.d, 3.10.c, 3.10.d, 3.11.c, and 3.11.d). These results indicate a very good linear behavior and the estimation of the concentration for the materials was valid (>0.9 [83]) for testing purposes. The linearity of the samples in a laboratory setting is different from the linearity of the image processing. A spectrophotometer analyzes the transmittance and the absorbance as the measurement of the transmittance and/or absorbance by adjusting a specific wavelength to the sample with a blank

sample for calibration, these measurements use the beer's law equation (1.4). However, image processing is the basis of the application and the linear response in image processing comes with more computational complexity than with laboratory instruments used.

The colorimetric sensing application provides highly compatible concentration measurements of the materials in comparison with the laboratory spectrophotometer. The novelty of this study lies in the accurate prediction of multiple biochemical materials concentrations in various lightning effects, reducing the measurement time in an easy-to-use portable environment without the need for internet access, as the colorimetric sensing application does not require feedback from the data center for concentration measurement, also the novel approach of incorporating powerful software to tackle various issues that might arise in the traditional measurements like power consumption, heating, and calibration.

The ability to convey multiple tasks, prediction of concentration, measurement of both absorbance and transmittance, with error estimation charts and R^2 values reporting within the colorimetric sensing application as far as current knowledge there has not been any application that can provide all the capabilities of the developed application. For comprehension Table (3.1) shows a comparative analysis of the relevant literature with different approaches to the concentration calculation.

As indicated in Table (3.1) no study has reported both absorbance and transmittance with three different biochemical materials and a comparison with a spectrophotometer for reference, besides, the compatible and reliable prediction of the concentration is very compelling.

Table 3.1: Comparison of different methods, and approaches in various techniques of concentration measurements

Material	Concentration Unit	Measured Quantity	R ²	Ref
Glucose	mg.dL ⁻¹	Normalized G signal	0.983	[84]
Glucose	μmol.L ⁻¹	Absorbance @certain λ	0.9937@450	[85]
Glucose, Triglycerides, Urea	mg.dL ⁻¹	Absorbance	0.9825; 0.9405; 0.9431	*
Glucose, Triglycerides, Urea	mg.dL ⁻¹	Absorbance @certain λ	0.9973@560; 0.952@620; 0.9948@570	*
Glucose, Triglycerides, Urea	mg.dL ⁻¹	Transmittance	0.9899; 0.9502; 0.8597	*
Glucose, Triglycerides, Urea	mg.dL ⁻¹	Transmittance @certain λ	0.9793@600; 0.9364@410; 0.9827@530	*

(λ: Wavelength in nm; T: Temperature in centigrade, *: This work)

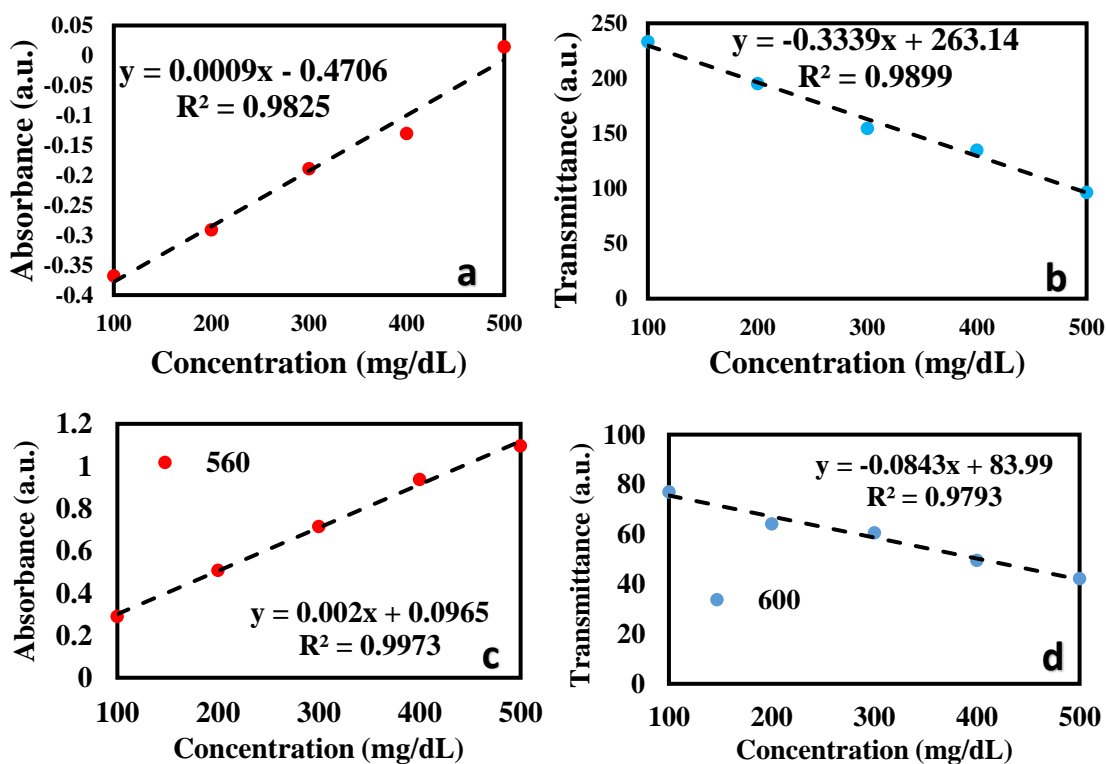


Figure 3.9: Application-based results for glucose (a) Absorbance (b) Transmittance. Spectrophotometer-based results (c) Absorbance (d) Transmittance

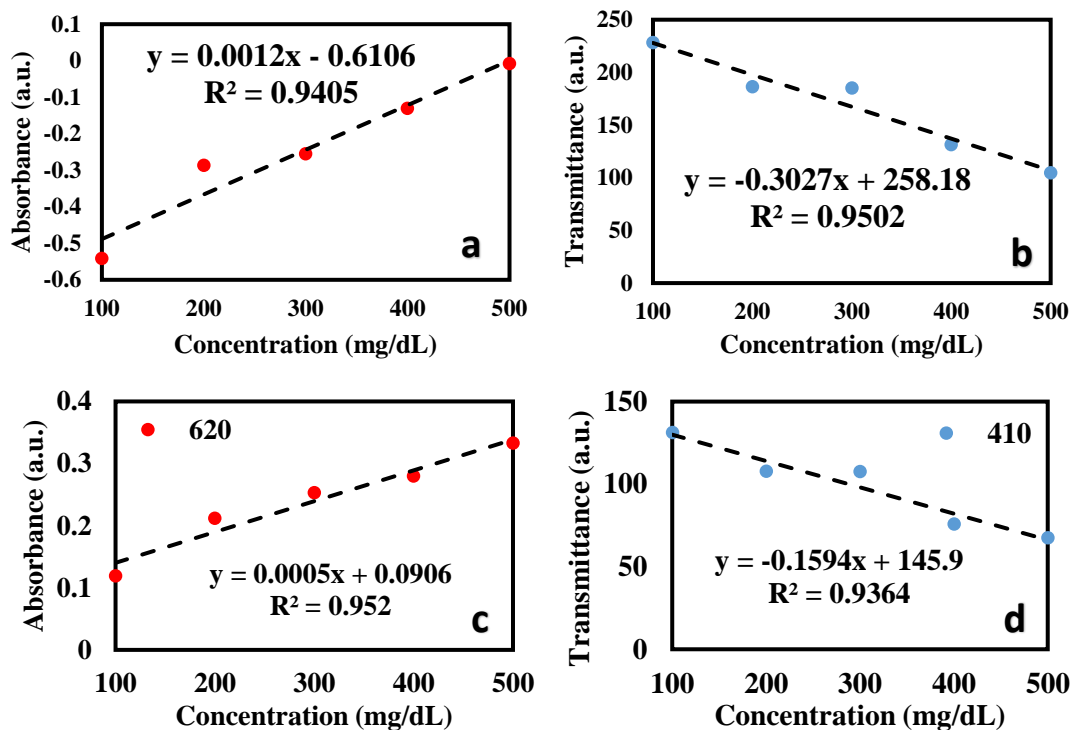


Figure 3.10: Application-based results for triglycerides (a) Absorbance (b) Transmittance. Spectrophotometer-based results (c) Absorbance (d) Transmittance

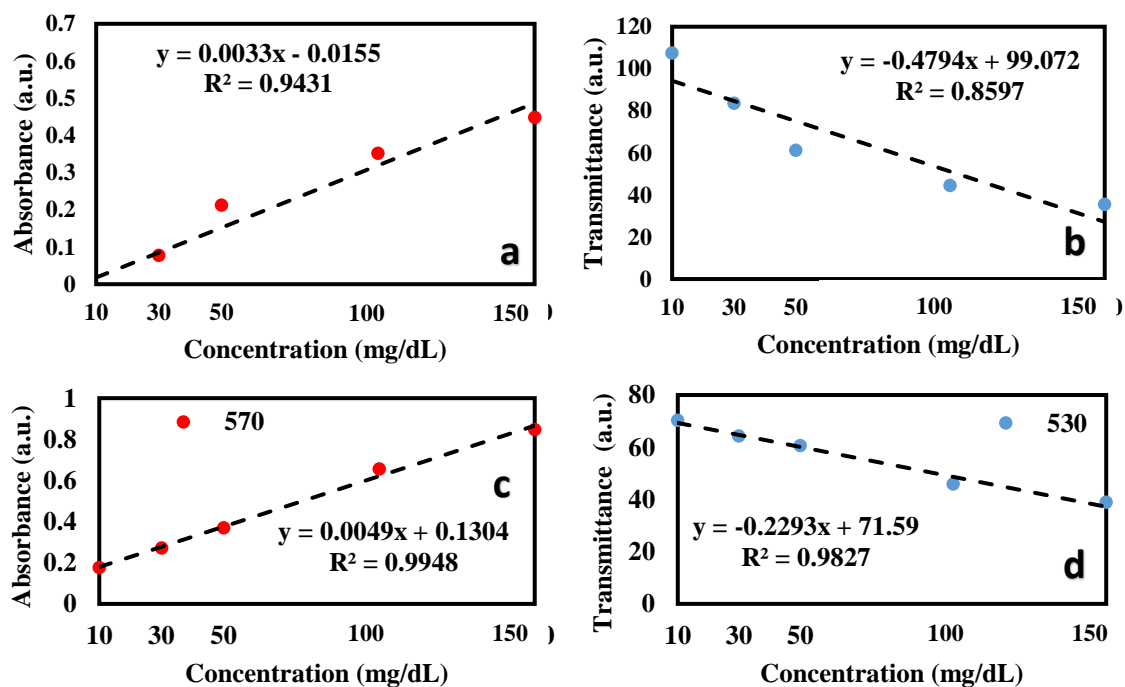


Figure 3.11: Application-based results for urea (a) Absorbance (b) Transmittance. Spectrophotometer-based results (c) Absorbance (d) Transmittance

3.4. Smartphone-Based 3D Printed Design with the Aid of Android Application

Using the smartphone adapter in Figure 2.13-2.14 (Chapter 2) with the prepared samples of Figure 2.12 (Chapter 2) the images captured with inserting the samples into the adapter are shown in Figure 3.12 and Figure 3.13. These images are the data to be used with the developed colorimetric sensing Android application on a Huawei Mate 20 Pro smartphone to predict the concentrations of the biomarkers reported here.

To see how does each biomarker behave under the spectrum, each biomarker was measured with the benchtop UV-VIS spectrophotometer. These measurements were for the wavelength range of 350 nm to 780 nm taking a 10 nm step with the measurements of both absorbance and transmittance as shown in Figure 3.14.

Different peaks were noticed near 405, 532, and 650 nm which motivate us to proceed with the smartphone 3D adapter to measure the concentrations of the biomarkers with both laser diodes of 405, 532, and 650 nm and white light-emitting-diode (WLED) with four different emission filters, the blue filter (BF) with a central wavelength (λ_C) of 430 nm, the green filter (GF) with λ_C of 530, the yellow filter (YF) with λ_C of 580 nm and the red filter (RF) with λ_C of 640 nm.

The linear regression coefficient (R^2) values for the absorbance curve of glucose using the illumination sources of 405 nm; 532 nm; 650 nm; WLED; WLED+BF; WLED+GF; WLED+YF; and WLED+RF are 0.9922; 0.9983; 0.9898; 0.7004; 0.9518; 0.9313; 0.9567; and 0.9407, respectively, as shown in Figure 3.15a.

Following the same order of illumination sources, the R^2 of urea 0.9332; 0.9818; 0.8829; 0.9464; 0.6615; 0.9161; 0.9567; and 0.7502, as shown in Figure 3.16a.

For triglycerides the R^2 values are 0.9496; 0.9725; 0.7749; 0.8395; 0.8192; 0.9313; 0.9567; and 0.944, as shown in Figure 3.17a.

For bilirubin the R^2 values are 0.7858; 0.9422; 0.7791; 0.9124; 0.9326; 0.6192; 0.5894; and 0.324, as shown in Figure 3.18a.

For HDL the R^2 values are 0.8248; 0.7831; 0.7902; 0.8332; 0.9077; 0.8071; and 0.998, as shown in Figure 3.19a.

For transmittance curves the R^2 values with the same order of illumination sources and biomarkers are (0.9915; 0.9965; 0.9862; 0.6997; 0.9398; 0.916; 0.9545; and 0.9398), (0.9263; 0.9818; 0.8829; 0.9464; 0.6615; 0.9161; 0.9567; and 0.752), (0.9035; 0.955; 0.9859; 0.8333; 0.8063; 0.9298; 0.9545; and 0.9533), (0.7123; 0.9446; 0.8971; 0.9241; 0.9289; 0.563; 0.6669; and 0.3565), (0.7658; 0.8003; 0.8364; 0.8418; 0.9108; 0.9044; 0.7954; and 0.9575), respectively, as shown in Figures 3.15b, 3.16b, 3.17b, 3.18b, and 3.19b, respectively.

Since there are many results for the R^2 of the biomarkers, comparison curves were plotted as shown in Figure 3.20 to effectively estimate the feasibility of the illumination source to be a good candidate for concentration prediction or not.

For glucose, 7 sources can give an accurate result with the 532 nm being the most significant. For urea and triglycerides, 5 sources can give an accurate result with 532 nm, and white LED with an emission filter of λ_C 640 nm being the most significant. Bilirubin and HDL both with 3 effective sources as 532

nm, WLED, WLED with an emission filter of λ_c 430 nm for bilirubin, and WLED with emission filters of 430, 530, and 640 nm for HDL.

The limit of detection (LOD) is calculated as ($S/N=3$) where S is the signal, N is the noise for all materials as detailed following most previous reports like Tabatabaee, et al. [86] and Martinkova, and Pohank [87]. From Figure 3.15a the sensitivity of glucose (S_G) can be calculated as the slope of the line from the formula $\Delta S_G=0.0052C+0.3947$ where C is the concentration, $S_G = 0.0052$ with the standard deviation (std) representing the noise (N) of 0.001004 resulting in a LOD of 0.57 mg/dl or 0.03135 mM.

From Figure 3.16a the sensitivity of urea (S_U) can be calculated as the slope of the line from the formula $\Delta S_U=0.0029C+0.5197$, $S_U = 0.0029$ with std of 0.0013 resulting in a LOD of 1.34 mg/dl or 0.2278 mM.

From Figure 3.17a the sensitivity of triglycerides (S_T) can be calculated as the slope of the line from the formula $\Delta S_T=0.0032C+0.5059$, $S_T = 0.0032$ with std of 0.00831 resulting in a LOD of 7.79 mg/dl or 0.0879 mM.

From Figure 3.18a the sensitivity of bilirubin (S_B) can be calculated as the slope of the line from the formula $\Delta S_B=2.8829C+0.3353$, $S_B = 2.8829$ with std of 0.008 resulting in a LOD of 0.008 mg/dl or 0.14 μ M.

From Figure 3.19a the sensitivity of HDL (S_H) can be calculated as the slope of the line from the formula $\Delta S_H=0.0104C+0.043$, $S_H = 0.0104$ with std of 0.003 resulting in a LOD of 0.86 mg/dl or 0.02224 mM.

The prediction of biomarker concentration within the smartphone-based 3D printed adapter and the colorimetric sensing Android application is based on averaging the three main channel intensities of the RGB image (Red, Blue, and Green) taking into account the selected region of interest (ROI) in which the prediction is based on a comparative approach between the blank sample

with the illumination source switched ON and the biomarker sample with the same illumination source.

The comparison is based on image difference by taking the absolute value of subtracting the image of the biomarker from the image of the blank. Thus, with the same size of ROI, the prediction results in a very compelling outcome. The use of multiple illumination sources is aimed to see the different effects that a light source can have on the prediction outcome.

The most accurate prediction outcome comes from the 532 nm source for glucose, urea, and bilirubin. On the other hand, the white LED with a 640 nm emission filter result in the highest prediction accuracy for triglycerides and HDL. The smartphone environment offers rapid measurement without the complications of traditional instruments, it takes only about 5 seconds to snap a shot with the camera and about 10 seconds to get the prediction outcome on the application user interface.

Table 3.2. Shows the performance comparison of a wide range of techniques used to predict concentrations of biomarkers in which the current study dominates the performance with almost all previous studies in all biomarkers.

Table 3.2: Literature performance comparison for different techniques with all reported samples

Sample	Technique	LOD	Sensitivity	R ²	Linear Range	Ref
GLOX ¹	RGB color analysis in colorimetric sensing app (A; A@560; T; T@600)	3.34 mg/dl (0.1837 mM)	0.0009 (mg/dl) ⁻¹	0.9825; 0.9973; 0.9899; 0.9793	100-500 mg/dl	[88] [§]
	Toner-based μ zone plates	0.6 mmol/l	5.1 AU ² (mmol/l) ⁻¹	0.996	0-10 mmol/l	[89]
	Smartphone- μ fluidic chemistry analyzer & image-based colorimetric assays	_____	_____	0.969	3.79-9.79 mmol/l	[90]
	Paper-based colorimetric assays with smartphone spectrometer	60 mg/dl	_____	_____	0-400 mg/dl	[91]
	μ fluidic chip-based wearable colorimetric sensor	0.03 mM	_____	_____	0.1-0.5 mM	[92]
	RGB Image colorimetric assay with smartphone	0.009 mg/ml (0.05 mM)	_____	0.996	0.039-10 mg/ml (0.2-55.6 mM)	[93]
	μ PAD Colorimetric detection in artificial saliva	29.65 μ M	_____	0.9819	0.1-1 mM	[94]
	Image analysis paper-based colorimetric device Galaxy VS iPhone	0.22 VS 0.1 mM	_____	0.9898 VS 0.9834	0-1 mM	[78]
	Ratiometric fluorometric and colorimetric determination	0.14 μ M	_____	0.9981	0.8-300 μ M	[79]
	Android VS iPhone imaging with test strips	92 VS 69 mg/dl	_____	0.99	0-300 mg/dl	[95]
	iPhone 4 VS Galaxy SII camera detection	_____	_____	_____	0-2.0 g/dl	[96]
	RGB color analysis app with iPhone 4	_____	_____	0.9994	30-515 mg/dl	[97]
	HSV and CIELAB color model	60 mg/dl	_____	_____	60-410 mg/dl	[98]
	Spiked plasma measured by sol-gel enzymatic inside bubble wrap VS reference	750 mmol/l ³	_____	0.996 VS 0.986	1-4 VS 4-16 mmol/l	[87]
UV-VIS VS Imaging with ascorbic acid into glucose	0.055 VS	0.0310 VS 0.00526	0.998 VS 0.972	_____	[99]	

¹ Glucose² Arbitrary units³ From Blue channel

		0.045 mg/l				
	3D printed adapter with colorimetric sensing app & 8 illumination sources (405 nm; 532 nm; 650 nm; WLED; WLED+BF; WLED+GF; WLED+YF; WLED+RF)	0.57 mg/dl (0.0313 5 mM)	0.0052 (mg/dl) ⁻¹	0.9922; 0.9983; 0.9898; 0.7004; 0.9518; 0.9313; 0.9567; 0.9407	5-30 mg/dl	*
Urea	RGB color analysis in colorimetric sensing app (A; A@570; T; T@530)	1.18 mg/dl (0.2006 mM)	0.0033 (mg/dl) ⁻¹	0.9431; 0.9948; 0.8597; 0.9827	10-150 mg/dl	[88] [§]
	μPAD blood urea nitrogen	10 mg/dl	————	0.9905	10-100 mg/dl	[100]
	Sol-gel colorimetric method in feedstuffs	0.1 mg/dl	————	0.99	2.5-100 & 100-1000 mg/l	[101]
	RGB color analysis of urea in saliva VS blood	10.4 mg/dl	-0.005 pixels/s/(mg/dl)	0.93 VS 0.68	10-260 mg/dl	[72]
	RGB color analysis app with iPhone 4	————	————	0.9996	2-190 mg/dl	[97]
	3D printed adapter with colorimetric sensing app & 8 illumination sources (405 nm; 532 nm; 650 nm; WLED; WLED+BF; WLED+GF; WLED+YF; WLED+RF)	1.34 mg/dl (0.2278 mM)	0.0029 (mg/dl) ⁻¹	0.9332; 0.9818; 0.8829; 0.9464; 0.6615; 0.9161; 0.9567; 0.7502	5-30 mg/dl	*
Tri	RGB color analysis in colorimetric sensing app (A; A@620; T; T@410)	20.77 mg/dl (0.2345 mM)	0.0012 (mg/dl) ⁻¹	0.9405; 0.952; 0.9502; 0.9364	100-500 mg/dl	[88] [§]
	Paper-based μfluidic device	————	————	0.9733	80-470 mg/dl	[102]
	Smartphone- μfluidic chemistry analyzer using image-based colorimetric assays	————	————	0.966	0.81-3.98 mmol/l	[90]
	3D printed adapter with colorimetric sensing app & 8 illumination sources (405 nm; 532 nm; 650 nm; WLED; WLED+BF; WLED+GF; WLED+YF; WLED+RF)	7.79 mg/dl (0.0879 mM)	0.0032 (mg/dl) ⁻¹	0.9496; 0.9725; 0.7749; 0.8395; 0.8192; 0.9313; 0.9567; 0.944	10-60 mg/dl	*
TSB	Smartphone- nanosensor bioplatform with	0.19 mg/dl	————	0.9901	2-20 mg/dl	[86]

	photoluminescent bacterial nanopaper					
	Paper-based diagnosis by colorimetric diazotization	1.2 mg/dl (20.52 μ mol/l)	_____	0.9915	0-22 mg/dl (0-376.2 μ mol/l)	[103]
	Paper-based colorimetric device based on in-situ formation of gold nanoparticles	0.001 g/l	_____	0.973	0.005-1 g/l	[104]
	Paper-based colorimetry with color space mobile app	_____	_____	_____	0.5-3 mg/dl	[65]
	TSB VS TcB (mobile app VS analytical device)	_____	_____	0.84 VS 0.92	_____	[105]
	3D printed eye box with an app and machine learning	_____	0.897	0.89	_____	[106]
	Green VS Blue color intensity channels	4.3403 mg/dl	_____	0.8152 VS 0.3522	4.3403-6.3828 mg/dl	[107]
	TSB VS TcB image analysis	250 μ mol/l	_____	0.7056 VS 0.6561	_____	[108]
	3D printed adapter with colorimetric sensing app & 8 illumination sources (405 nm; 532 nm; 650 nm; WLED; WLED+BF; WLED+GF; WLED+YF; WLED+RF)	0.008 mg/dl (0.14 μ M)	2.8829 (mg/dl) ⁻¹	0.7858; 0.9422; 0.7791; 0.9124; 0.9326; 0.6192; 0.5894; 0.324	0.05-0.1 mg/dl	*
HDL	Paper-based μ fluidic device	_____	_____	0.9878	36-48 mg/dl	[102]
	3D printed adapter with colorimetric sensing app & 8 illumination sources (405 nm; 532 nm; 650 nm; WLED; WLED+BF; WLED+GF; WLED+YF; WLED+RF)	0.86 mg/dl (0.0222 4 mM)	0.0104 (mg/dl) ⁻¹	0.8248; 0.7831; 0.7902; 0.8332; 0.9077; 0.8071; 0.998	10-60 mg/dl	*

*This work, §Our previous work

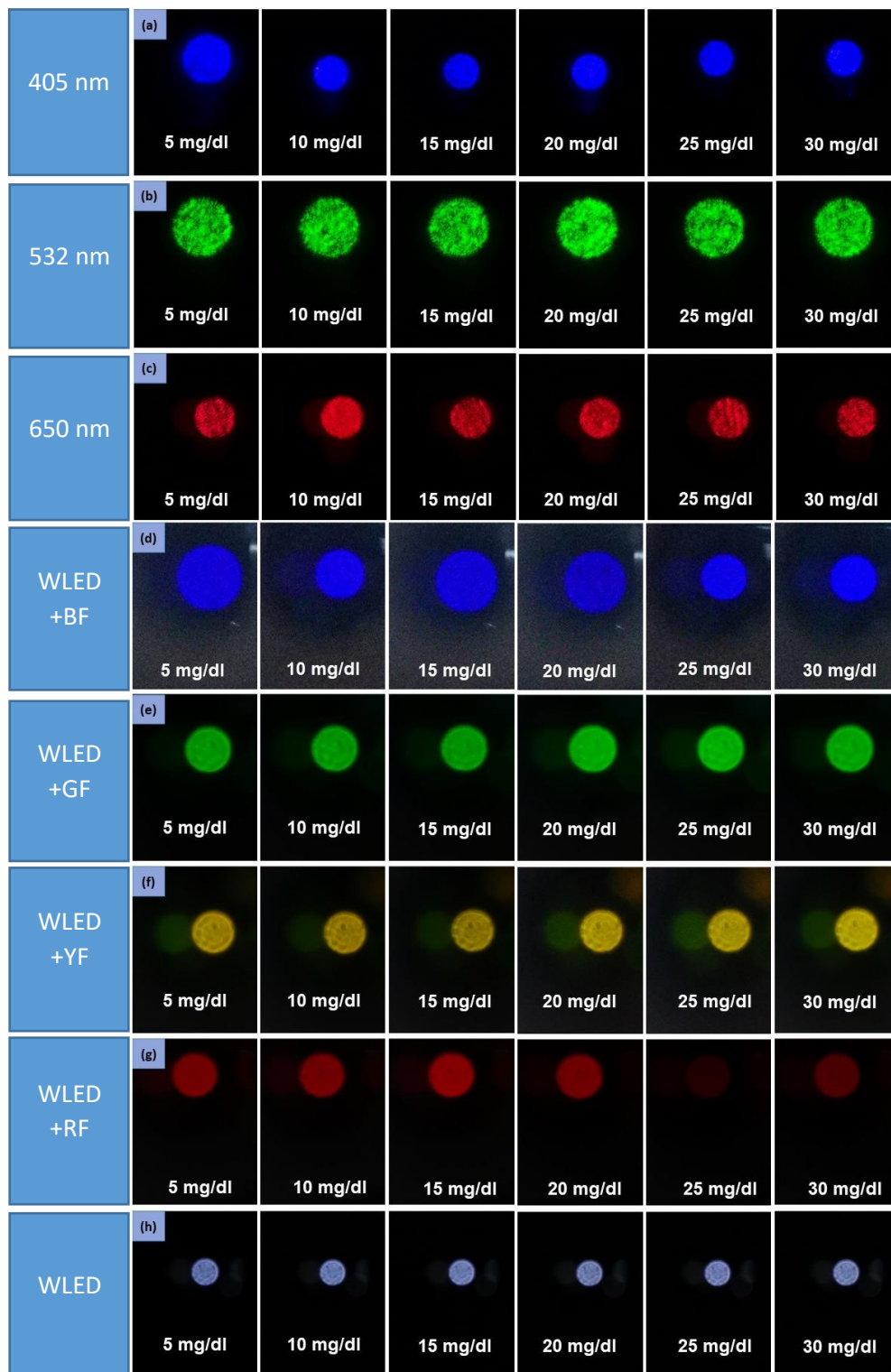


Figure 3.12: Images of glucose samples under the illumination of (a) 405 nm laser (b) 532 nm laser (c) 650 nm laser (d) LED with 430 nm Emission Filter (e) LED with 530 nm Emission Filter (f) LED with 580 nm Emission Filter (g) LED with 640 nm Emission Filter (h) White LED only

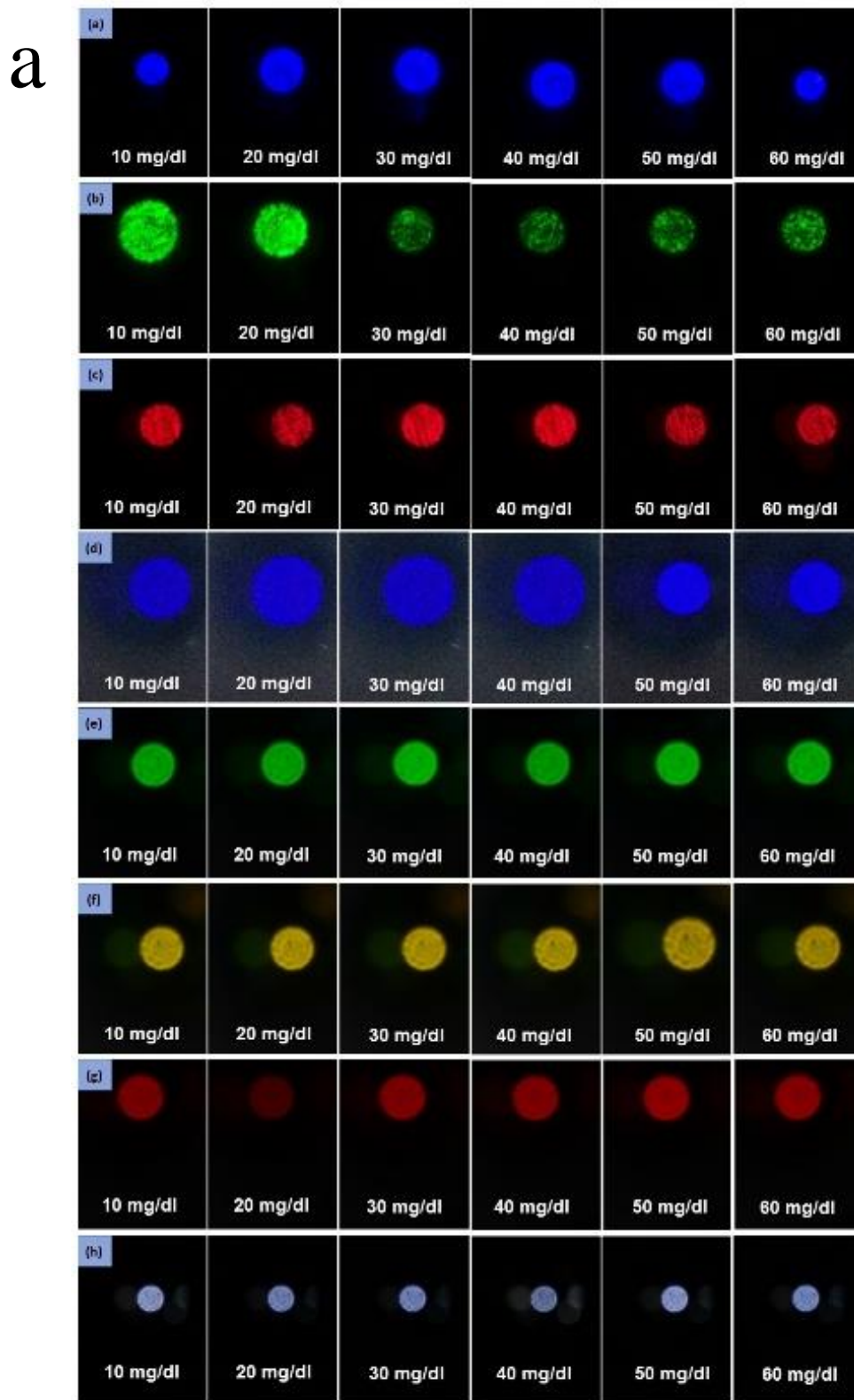


Figure 3.13: Images of the prepared samples in different concentrations using the smartphone adapter (a) Urea (b) Triglycerides (c) Bilirubin (d) HDL material under (a) 405 nm laser (b) 532 nm laser (c) 650 nm laser (d) LED with 430 nm Emission Filter (e) LED with 530 nm Emission Filter (f) LED with 580 nm Emission Filter (g) LED with 640 nm Emission Filter (h) White LED only

b

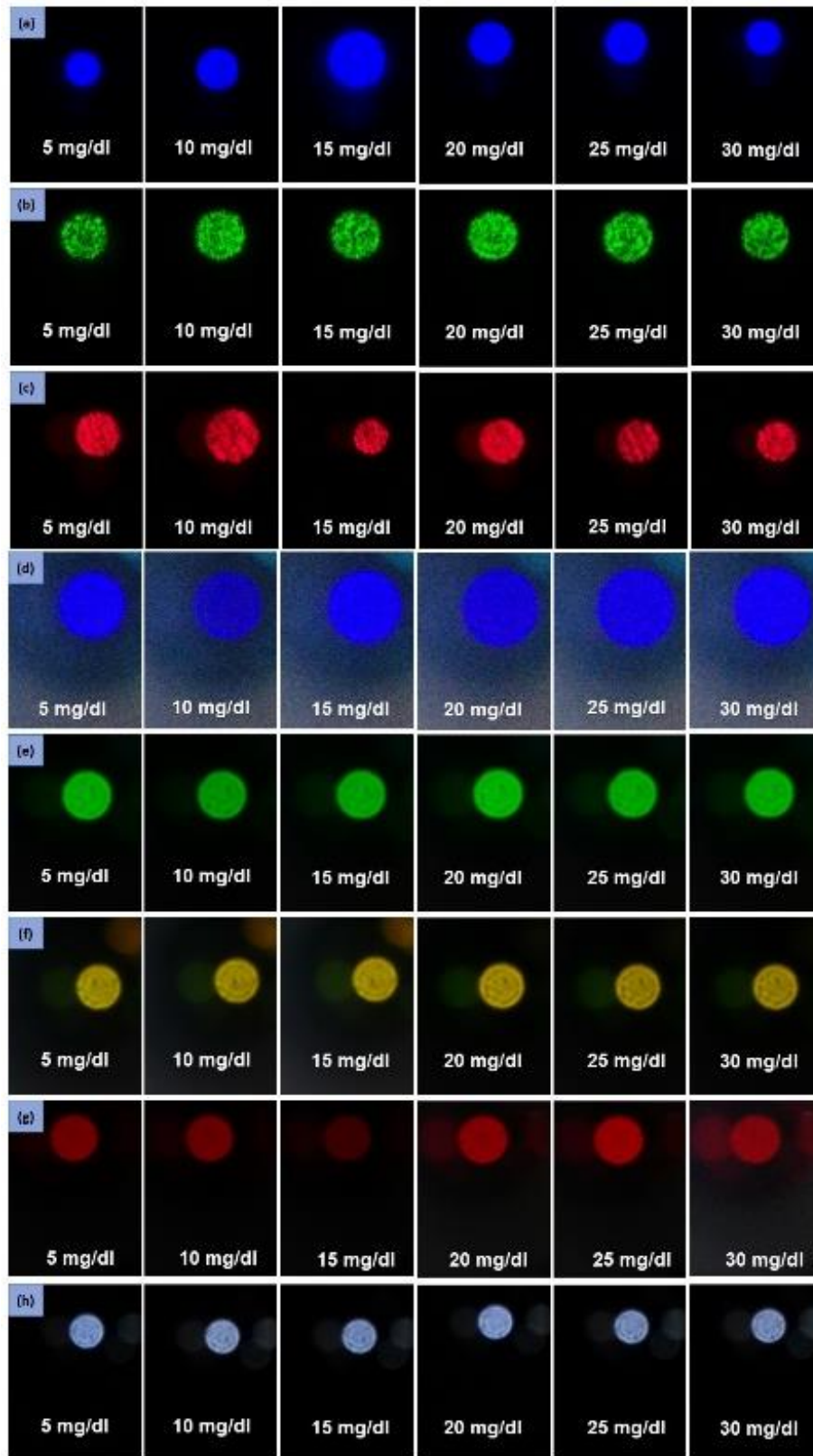


Figure 3.13: continued

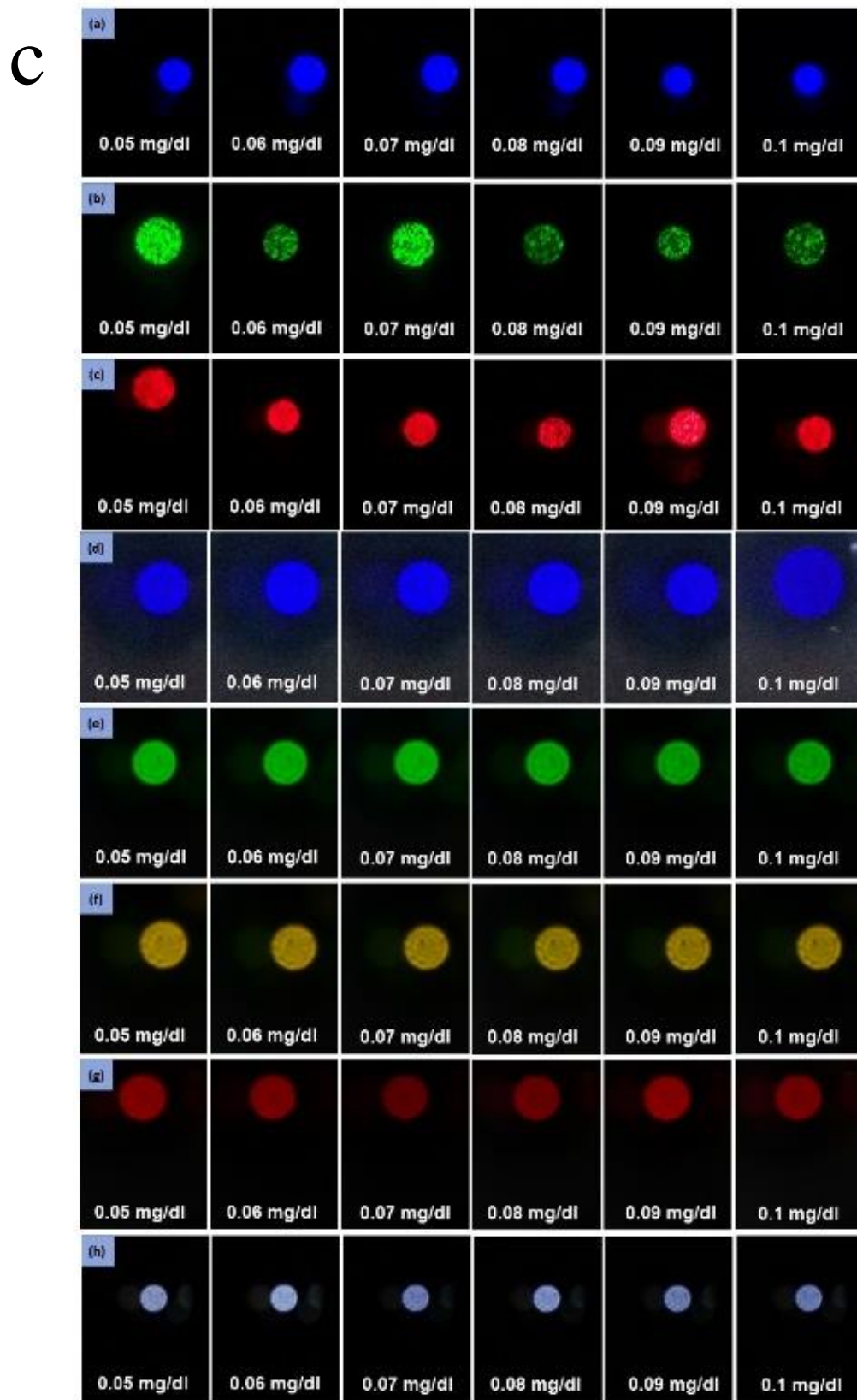


Figure 3.13: continued

d

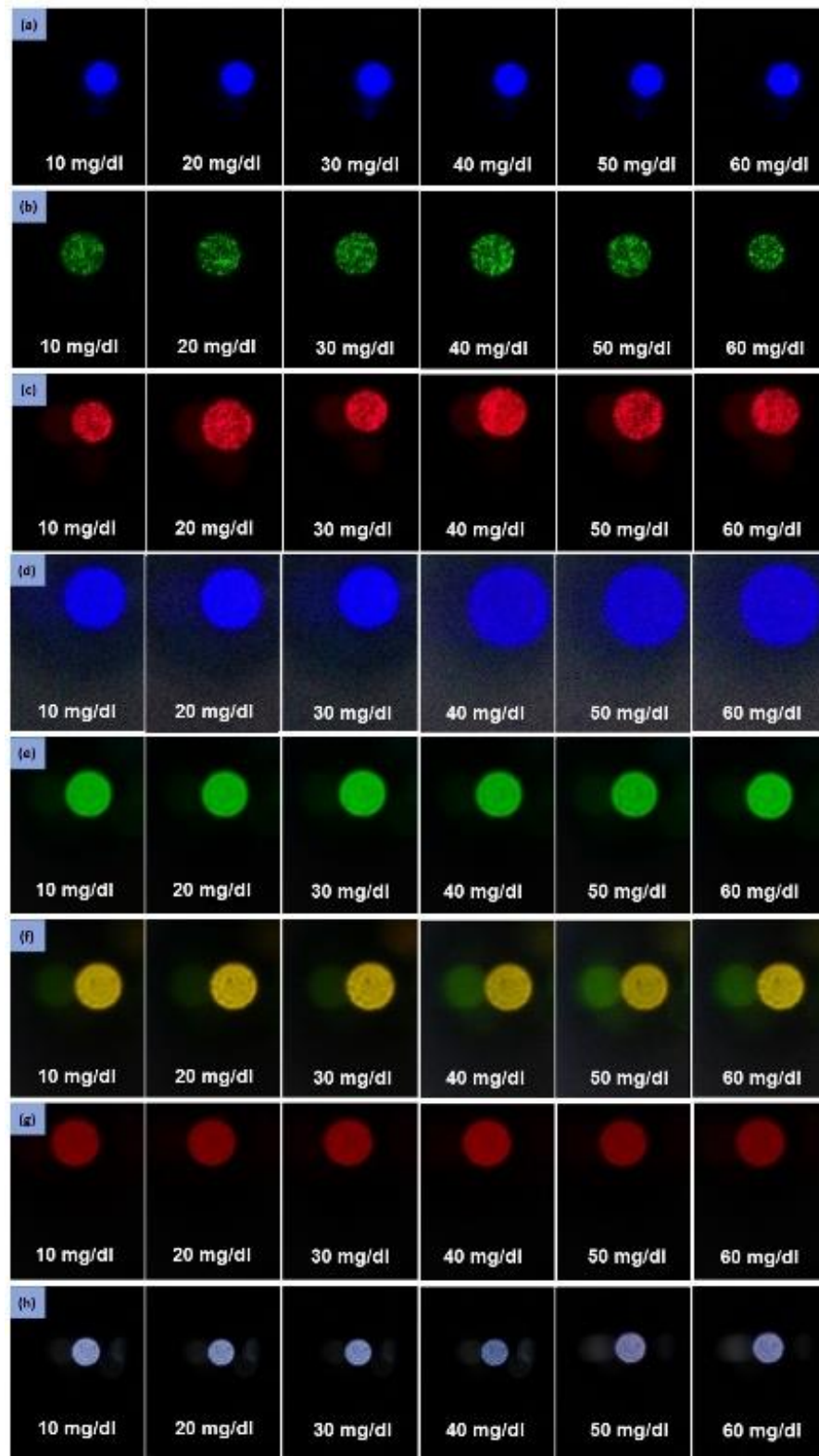


Figure 3.13: continued

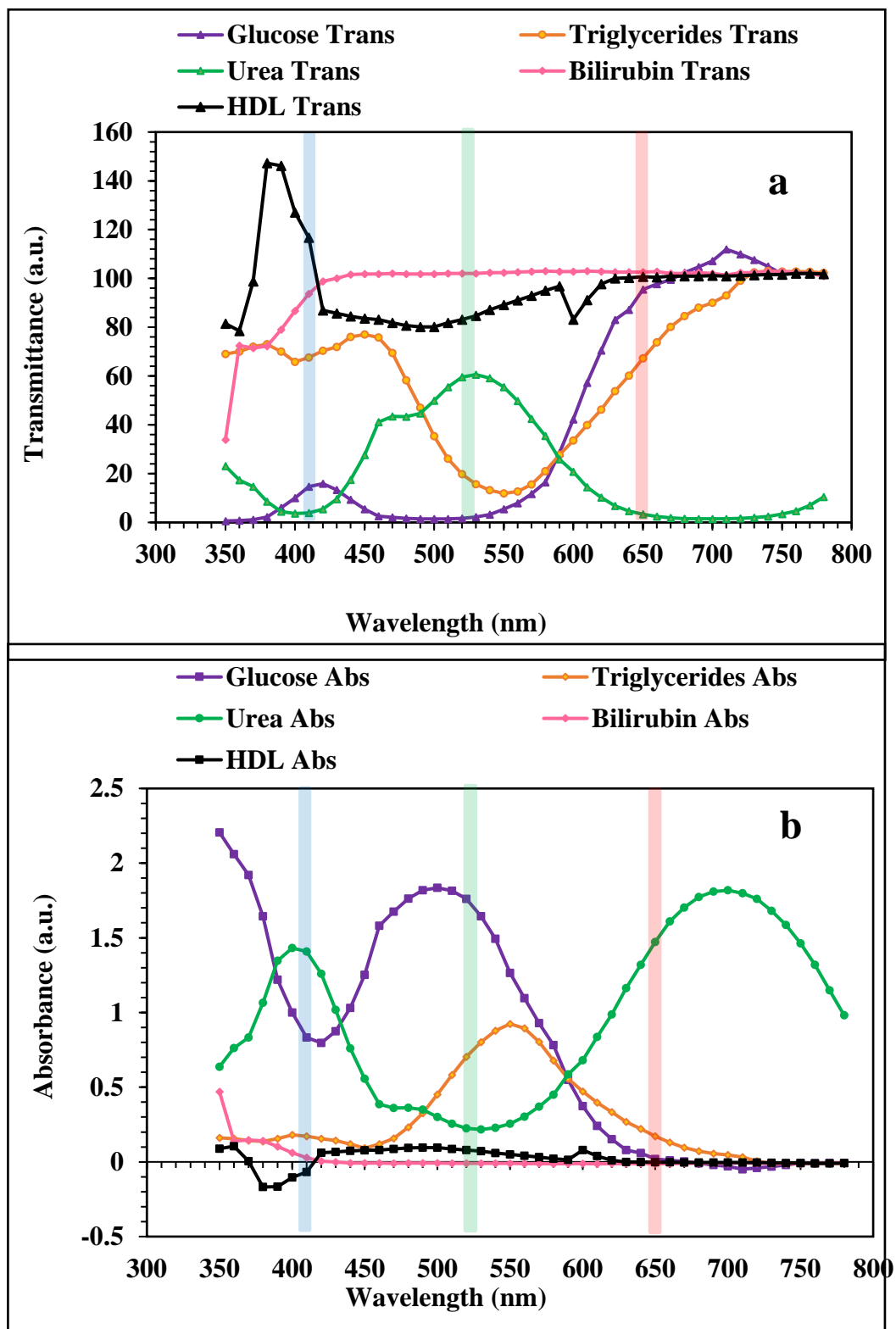


Figure 3.14: Transmittance (a) and absorbance (b) spectra for glucose, triglycerides, urea, bilirubin, and HDL using the UV-VIS spectrophotometer

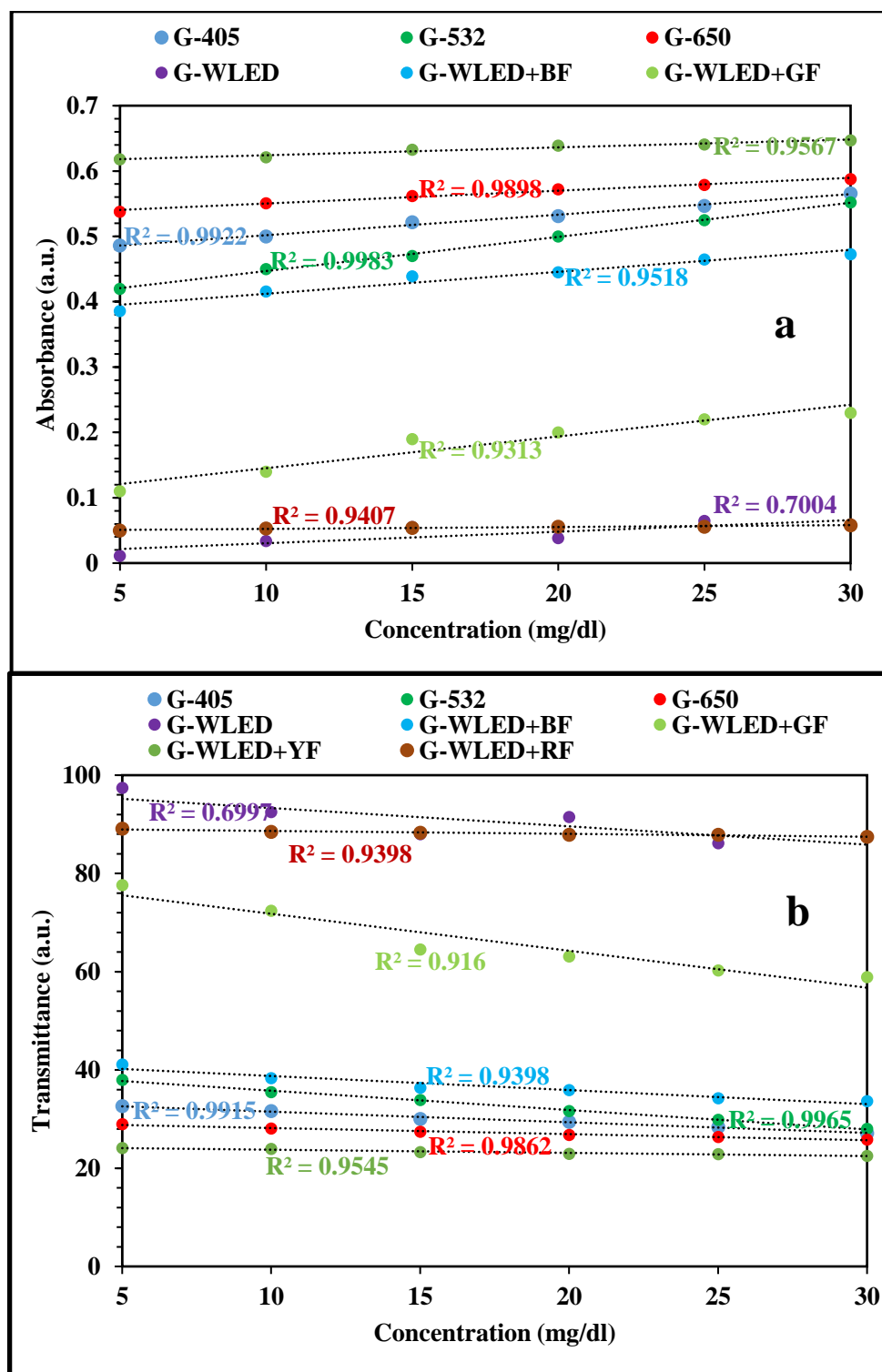


Figure 3.15: Absorbance (a) and transmittance (b) measurement of glucose using the smartphone adapter with colorimetric sensing application in eight different illumination sources

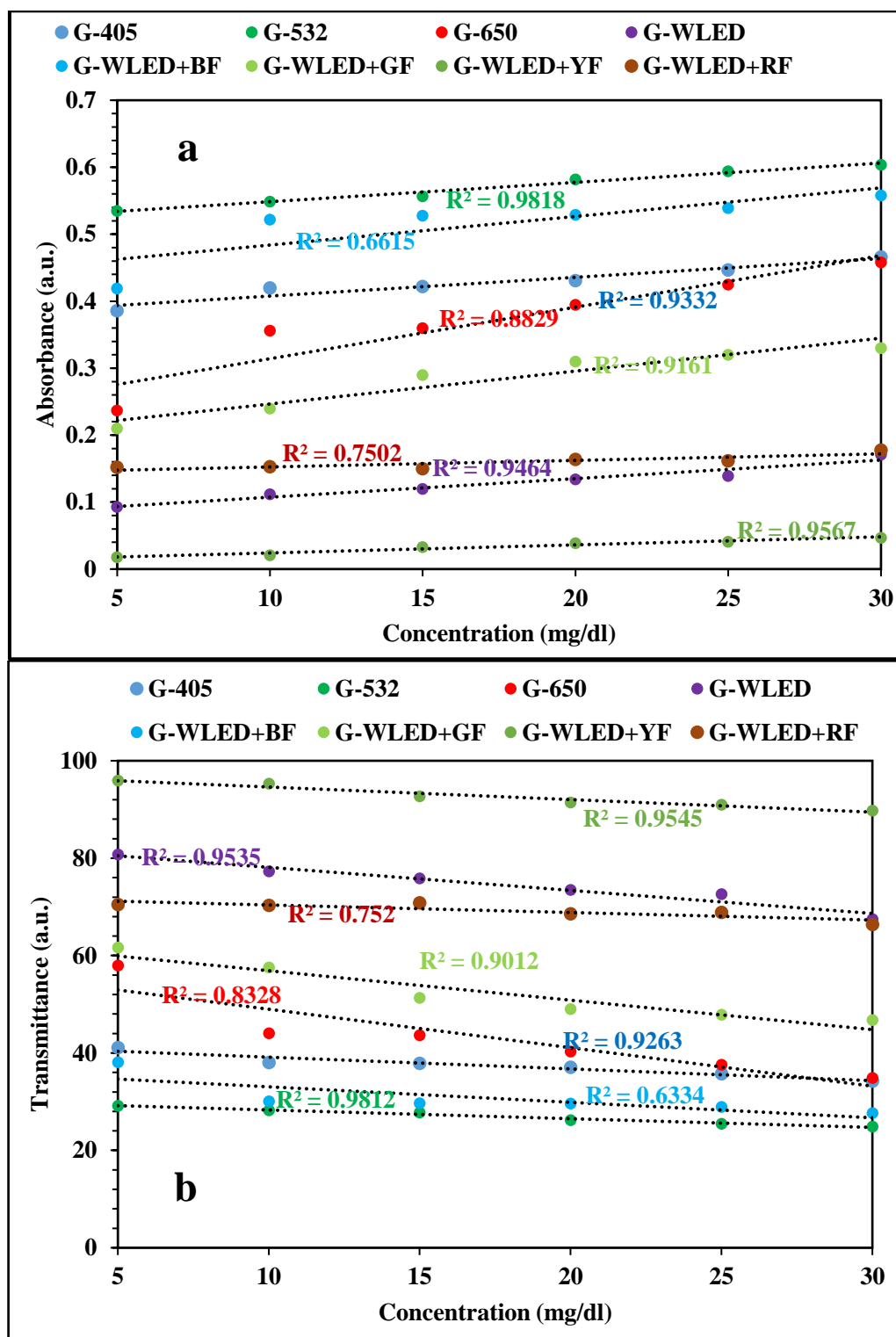


Figure 3.16: Absorbance (a) and transmittance (b) measurement of urea using the smartphone adapter with colorimetric sensing application in eight different illumination sources

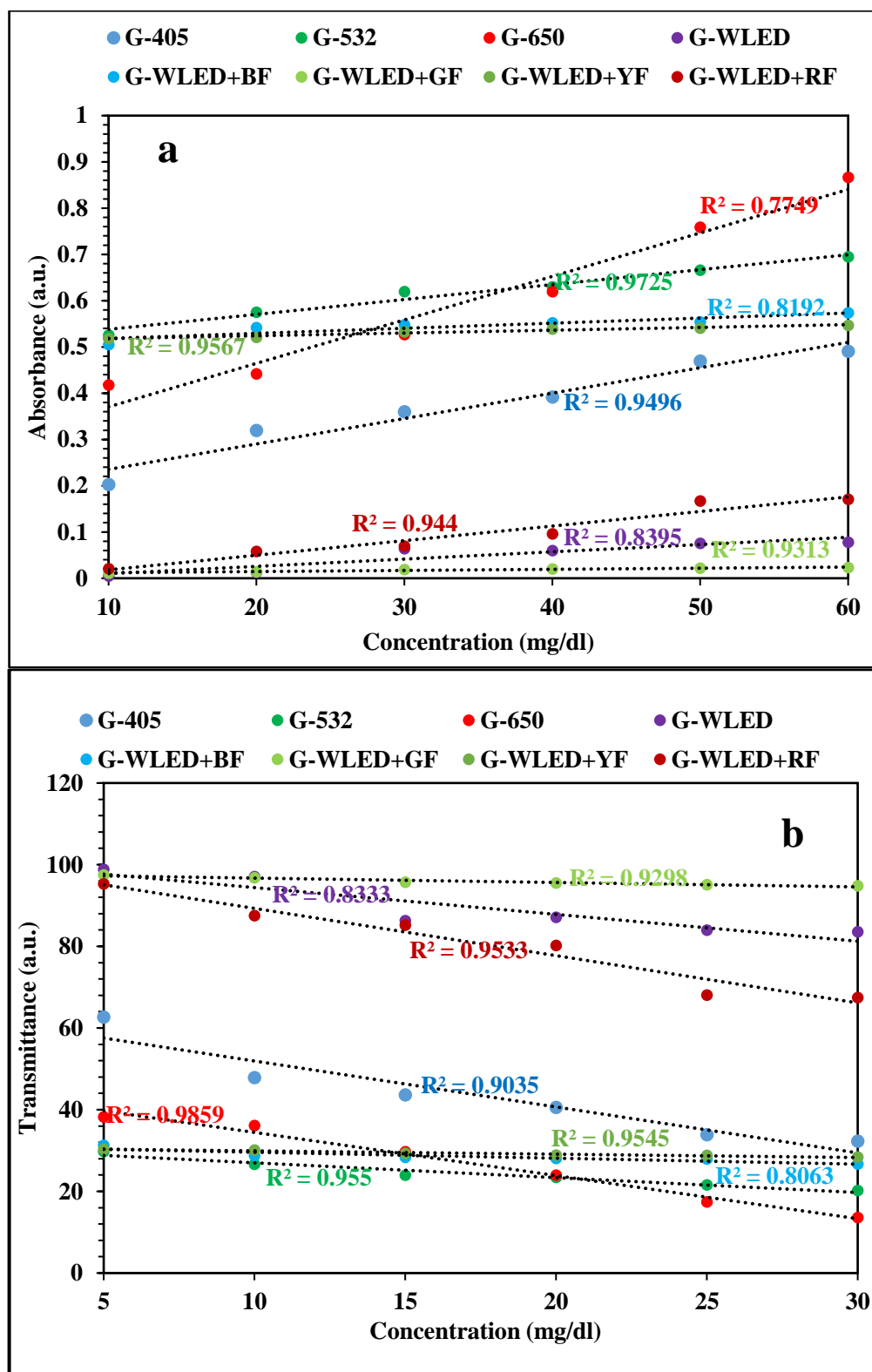


Figure 3.17: Absorbance (a) and transmittance (b) measurement of triglycerides using the smartphone adapter with colorimetric sensing application in eight different illumination sources

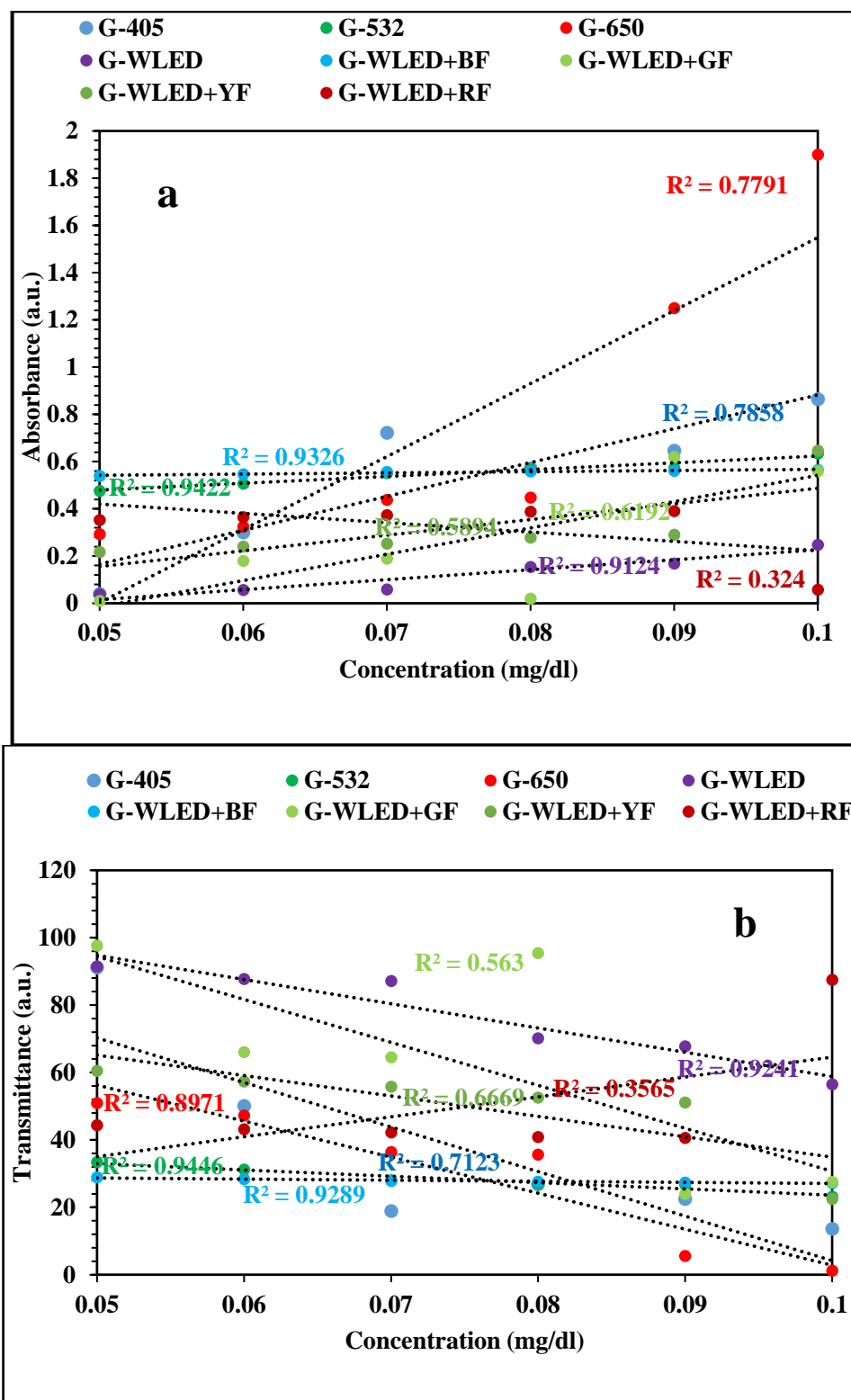


Figure 3.18: Absorbance (a) and transmittance (b) measurement of bilirubin using the smartphone adapter with colorimetric sensing application in eight different illumination sources

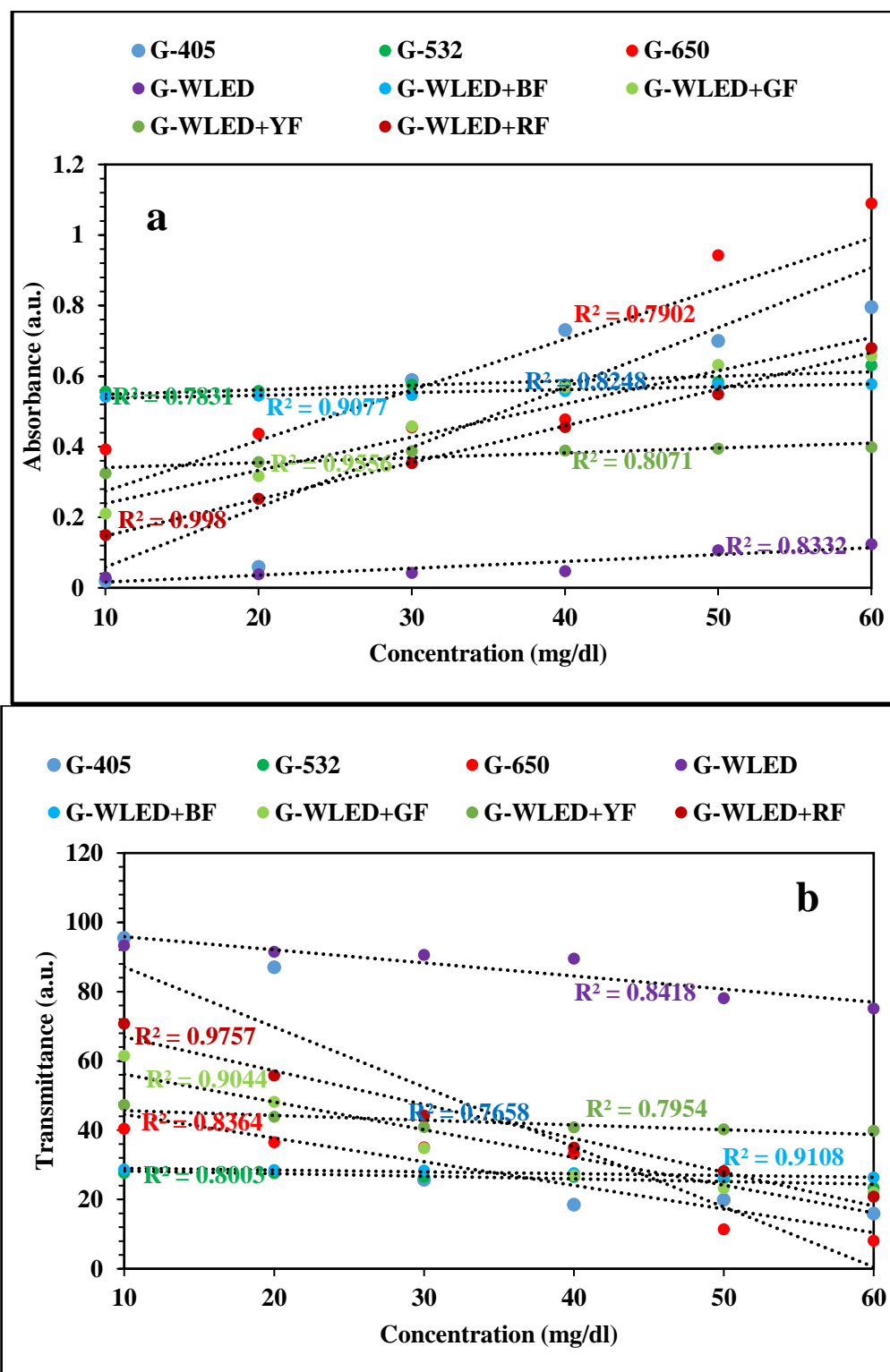


Figure 3.19: Absorbance (a) and transmittance (b) measurement HDL using the smartphone adapter with colorimetric sensing application in eight different illumination sources

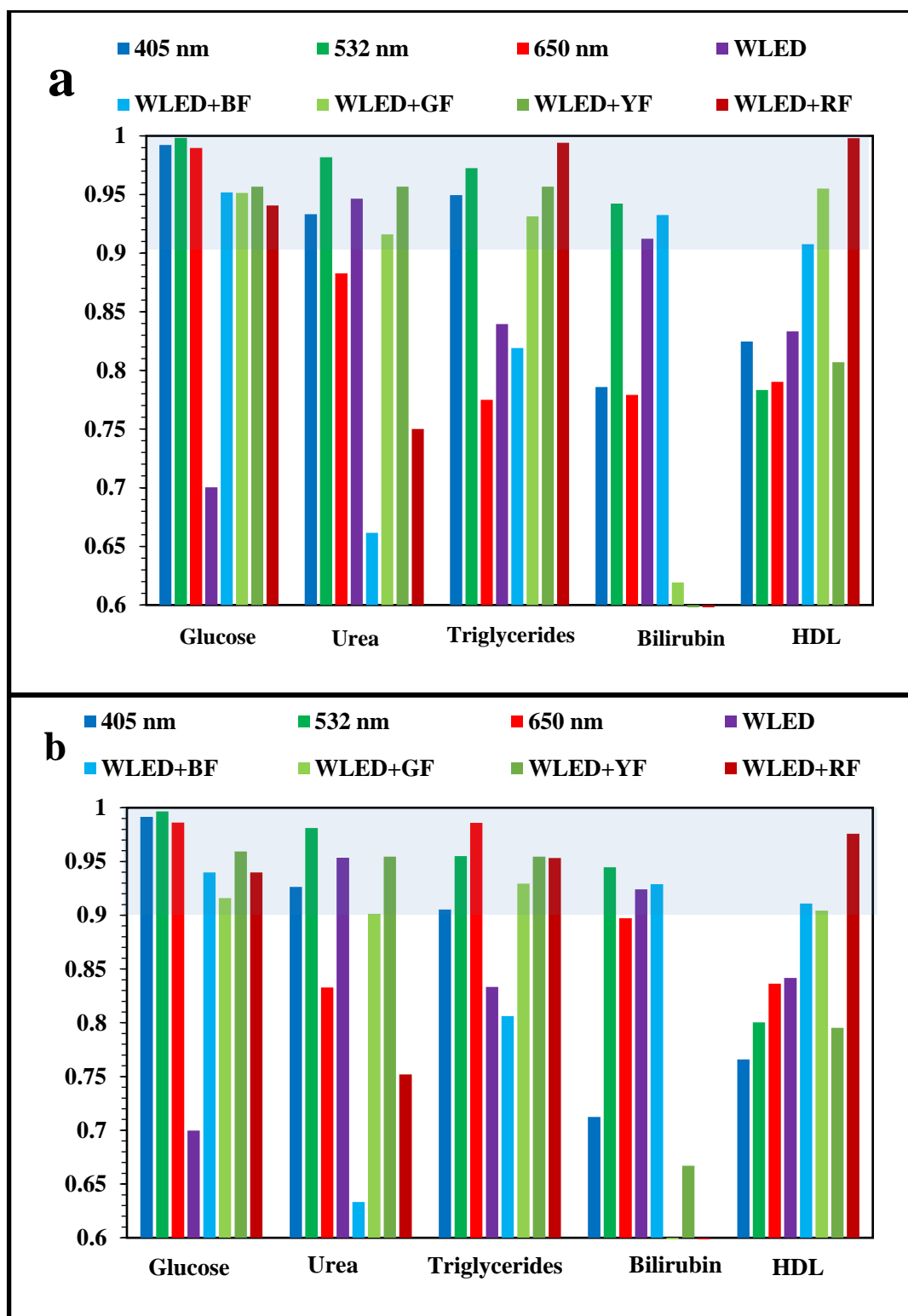


Figure 3.20: The regression coefficient of both absorbance (a) and transmittance (b) measurement of glucose, urea, triglycerides, bilirubin, and HDL using the smartphone adapter with colorimetric sensing application in eight different illumination sources

3.5. Performance Comparison

As a comparison, the cost for smartphone adapters in 3D printing was estimated, commercial point-of-care adapters, and standard point-of-care instruments and/or devices, and we plotted the results on a logarithmic scale, as shown in Figure 3.21. This resulted in a much more inexpensive environment for the most accurate, up-to-date accessories and software-programmed adapters with a cost of less than 2000 US dollars for the first prototype, including the optical components, mechanical components, 3D-printed adapters, electronics, and software design and simulation.

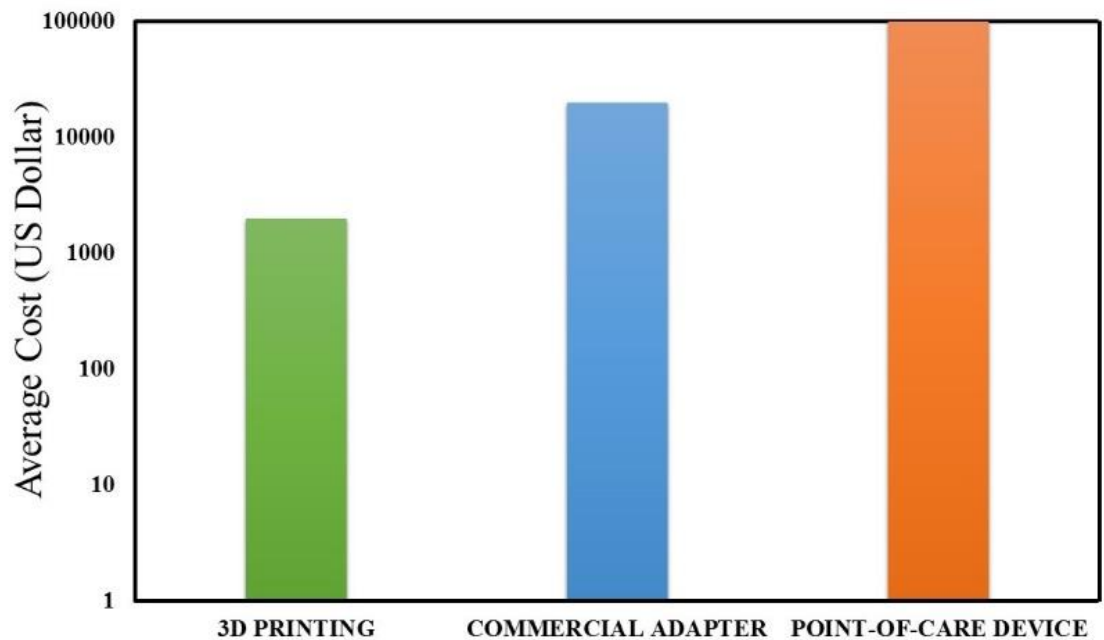


Figure 3.21: Price comparison among point-of-care devices [65]

The cost of smartphone-adapters for most of the reported literature is very low, lower than 100\$, offering great reliability and a cheap alternative to laboratory equipment, reducing the cost of testing if the smartphone-based adapters are adopted, as shown in Figure 3.22.

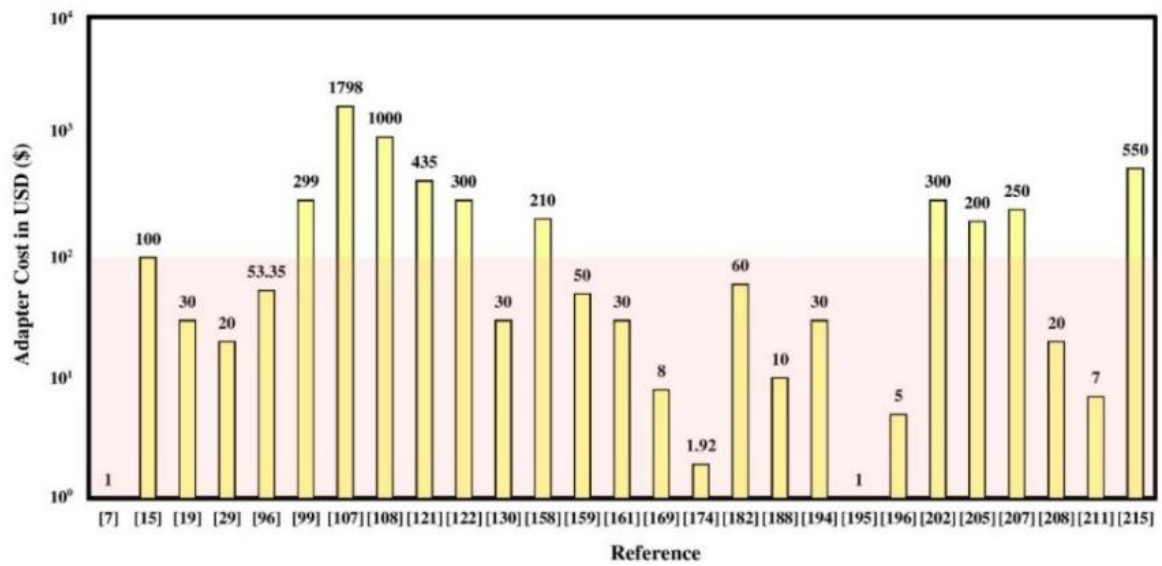


Figure 3.22: Price comparison in USD as a logarithmic scale for different adapters in reported literature [65]

The limit of detection for most of the reported literature is very low, offering low-sample-concentration samples in the range of μM and reaching even pM, which is very encouraging for point-of-care applications, as shown in Figure 3.23.

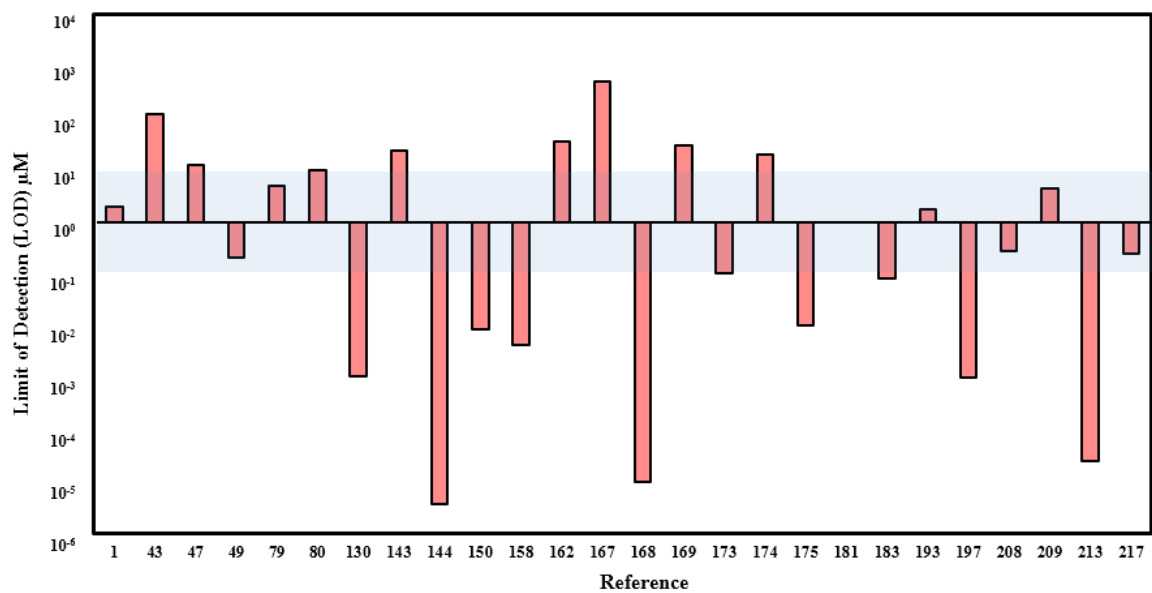


Figure 3.23: Limit of detection (LOD) in μM for reported literature [65]

The regression coefficient (R^2) is a correlation function ensuring the matching of the data with a standard model. In the case of smartphone-based adapters, the R^2 coefficient indicates a high level of matching between the smartphone-based adapters and laboratory equipment. For most of the reported research, the R^2 is in the range of 98%-100%, as shown in Figure 3.24.

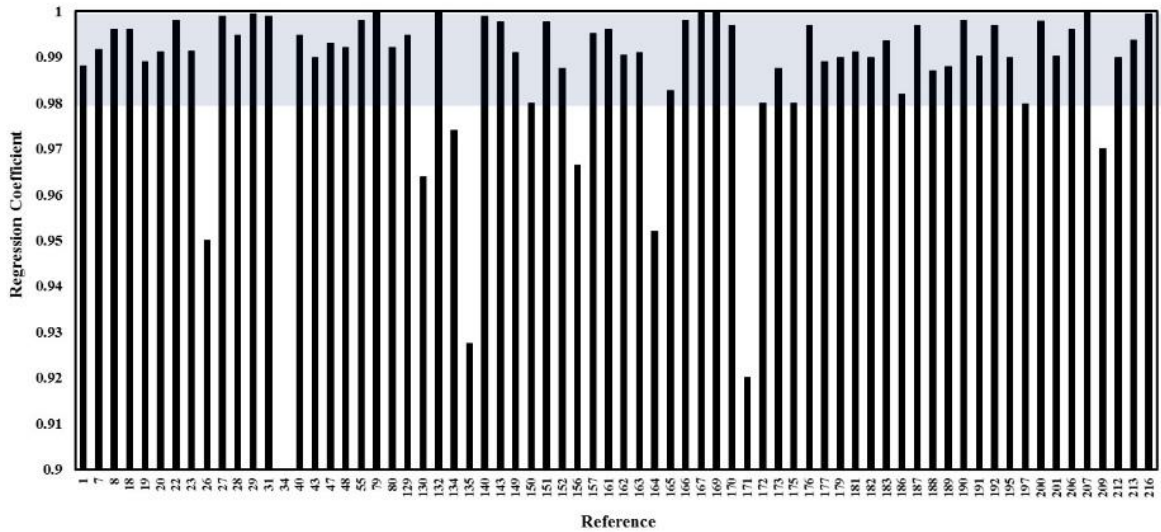


Figure 3.24: Regression coefficient for reported literature [65]

3.6. Conclusions

The colorimetric sensing application developed here can be a good candidate for a variety of biochemical materials that enable the interested users to perform rapid testing and measurement of material concentration based on the simple image capturing of the carefully prepared samples. It can be deduced that continuing this approach is of interest to rapid test, measurement, detection, and diagnosis studies that rely on the concept of colorimetry. The efficiency and reliability of the colorimetric sensing application with high accuracy concentration prediction is a promising application that can benefit researchers worldwide.

The smartphone imaging adapter with 532 nm laser proved to give the highest reliable image in terms of focusing and pixel resolution making it highly recommended for imaging in Whole blood and Urine imaging. The effects of the emission filter can greatly reduce the background noise of the system; therefore, it is recommended to use emission filters for bright and reliable imaging. The use of 3D printing with the smartphone and well-designed optical elements can provide various fields of applications with reliable imaging platforms for data collection, storage, image processing, and acquisition.

Using the custom-designed 3D printed smartphone adapter with the developed Android application (colorimetric sensing) resulting in dominant performance over the previous reports in terms of prediction accuracy, all-smartphone based measurement, cost-effectiveness, eco-friendly PLA material, and a very low limit of detection. To the best of current knowledge, this is the first report on the effects of multiple illumination sources on multiple biomarkers with a complete set of results depending solely on the smartphone. This enables reliable use of the compatible system in biomarker testing.

3.7. Future Work

Use the 3D design in another set of applications with the possibility of minor modifications; these applications include:

1. Bacterial detection and recognition.
2. Colorimetric sensing of other materials like cholesterol, creatinine, lipids and other biochemical materials.
3. Fluorescence analysis of laser dyes.
4. Using optical fiber sensing for physical parameter sensing like temperature and humidity.
5. Include Networking with IoT platforms.
6. Design smartphone sensors for food safety applications.
7. Use the adapter for big data collection and analysis for medical diagnostics.
8. Use machine learning to recognize biological samples.
9. Use the ELISA technique with a custom-designed 3D printed design to predict a wide range of biomaterials concentrations.

References

References:

- [1] G. Kendall, “Apollo 11 anniversary: Could an iPhone fly me to the moon?,” Commentary in the Independent Journal, Tuesday 09 July 2019.
- [2] B. Patra, M. Sharma, W. Hale, and M. Utz, “Time-resolved non-invasive metabolomic monitoring of a single cancer spheroid by microfluidic NMR,” *Scientific Reports*, vol. 11, no. 1, pp. 1–11, 2021.
- [3] C. C. Stemple, S. V. Angus, T. S. Park, and J. Y. Yoon, “Smartphone-Based Optofluidic Lab-on-a-Chip for Detecting Pathogens from Blood,” *J. Lab. Autom.*, vol. 19, no. 1, pp. 35–41, 2014.
- [4] J. R. Mejía-Salazar, K. R. Cruz, E. M. M. Vásques, and O. N. de Oliveira, “Microfluidic point-of-care devices: New trends and future prospects for ehealth diagnostics,” *Sensors (Switzerland)*, vol. 20, no. 7, pp. 1–19, 2020.
- [5] M. Pateraki et al., “Biosensors and Internet of Things in smart healthcare applications: challenges and opportunities,” *Wearable Implant. Med. Devices*, pp. 25–53, 2020.
- [6] S. Mittal, and V. Mattela, “A survey of techniques for improving efficiency of mobile web browsing,” *Concurrency Computat Pract Exper.* vol. 31, pp. e5126, 2019.
- [7] S. Majumder, and M.J. Deen, “Smartphone Sensors for Health Monitoring and Diagnosis,” *Sensors (Switzerland)*, vol. 19, pp. 2164, 2019.
- [8] Lucio Vision Labs, “Understanding the digital image sensor,” accessed March, 2021.
- [9] Perkins Precision Development (PPD) manufactures, “A guide of the optical components,” Colorado, United States, accessed March, 2021.
- [10] E.D. Kimberly, “Light Emitting Diodes,” University of California at Irvine, United States. pp. 2. Retrieved, Feb 12, 2019.

- [11] Lighting Research Center, “How is white light made with LEDs?,” Rensselaer Polytechnic Institute. Retrieved, Jan 12, 2019.
- [12] H. Kaushal, and G. Kaddoum, “Optical Communication in Space: Challenges and Mitigation Techniques,” in *IEEE Communications Surveys & Tutorials*, vol. 19, no. 1, pp. 57-96, 2017.
- [13] M. Yafia, A. Ahmadi, M. Hoorfar, and H. Najjaran, “Ultra-portable smartphone controlled integrated digital microfluidic system in a 3D-printed modular assembly,” *Micromachines*, vol. 6, no. 9, pp. 1289–1305, 2015.
- [14] N. Shahrubudin, T. C. Lee, and R. Ramlan, “An overview on 3D printing technology: Technological, materials, and applications,” *Procedia Manuf.*, vol. 35, pp. 1286–1296, 2019.
- [15] B. Evans, “*Practical 3D Printers: The Science and Art of 3D Printing*,” Apress Publishers, United States, 2012.
- [16] Y. D. Liang, “Introduction to programming using python,” Chapter 1, Georgia Southern University, Pearson Education, United Kingdom, 2013.
- [17] G. C. Onwubolu, “*Introduction to SolidWorks: A Comprehensive Guide with Applications in 3D Printing*,” CRC Press, United States, 2017.
- [18] T. Hagos, “*Learn Android Studio 4: Efficient Java-Based Android Apps Development*,” Apress Publishers, United States, 2020.
- [19] J. Vetelino, and A. Reghu, “*Introduction to Sensors*,” CRC Press, United States, 2011.
- [20] Rampwise Inc., “Delivering on smart things,” accessed March 2021.
- [21] Electronics Project Focus, “What is a Biosensor, Types of Biosensors and Applications,” accessed March 2021.
- [22] M. R. Younis, C. Wang, M. A. Younis, and X. Xia, “Smartphone-Based Biosensors,” *Nanobiosensors*, pp. 357–387, 2020.
- [23] R. Singh, M. Das Mukherjee, G. Sumana, R. K. Gupta, S. Sood, and B. D. Malhotra, “Biosensors for pathogen detection: A smart approach towards

- clinical diagnosis,” *Sensors Actuators, B Chem.*, vol. 197, pp. 385–404, 2014.
- [24] W. Chen, Y. Yao, T. Chen, W. Shen, S. Tang, and H. K. Lee, “Application of smartphone-based spectroscopy to biosample analysis: A review,” *Biosens. Bioelectron.*, vol. 172, no. November 2020, pp. 112788, 2021.
- [25] E. Rary, S. M. Anderson, B. D. Philbrick, T. Suresh, and J. Burton, “Smart sanitation—biosensors as a public health tool in sanitation infrastructure,” *Int. J. Environ. Res. Public Health*, vol. 17, no. 14, pp. 1–14, 2020.
- [26] M. S. Hirsch, and W. Jacly, “A Comprehensive Review of Biomarker Use in the Gynecologic Tract Including Differential Diagnoses and Diagnostic Pitfalls,” *Advances In Anatomic Pathology*, vol. 27, no. 3, pp. 164-192, 2020.
- [27] Biomarkers Definitions Working Group, “Biomarkers and surrogate endpoints: Preferred definitions and conceptual framework,” *Clinical Pharmacology and Therapeutics*, vol. 69, no. 3, 2021.
- [28] R. F. Dods, “Understanding Diabetes,” John Wiley & Sons, 2013.
- [29] A. O. Hosten, “BUN and Creatinine,” In: H. K. Walker, W. D. Hall, J. W. Hurst, editors. *Clinical Methods: The History, Physical, and Laboratory Examinations*. 3rd edition. Boston: Butterworths; 1990. Chapter 193, <https://www.ncbi.nlm.nih.gov/books/NBK305/>.
- [30] P. P. Toth, S. Philip, M. Hull, and C. Granowitz, “Elevated Triglycerides (≥ 150 mg/dL) and High Triglycerides (200–499 mg/dL) Are Significant Predictors of New Heart Failure Diagnosis: A Real-World Analysis of High-Risk Statin-Treated Patients,” *Vasc Health Risk Manag*, vol. 15, pp. 533-538, 2019.
- [31] L. B. VanWagner, and R. M. Green, “Evaluating Elevated Bilirubin Levels in Asymptomatic Adults,” *JAMA*, vol. 313, no. 5, pp. 516–517, 2015.

- [32] T. Kurth, B. M. Everett, J. E. Buring, C. S. Kase, P. M. Ridker, and J. M. Gaziano, "Lipid levels and the risk of ischemic stroke in women," *Neurology*, vol. 68, no. 8, pp. 556-562, 2007.
- [33] The Editors of Encyclopaedia Britannica, "Colorimetry," 2014, Encyclopedia Britannica, www.britannica.com/science/colorimetry.
- [34] R. Horikoshi, "Teaching chemistry with LEGO® bricks," *Chemistry Teacher International*, 2020. (Published Ahead of Print / Just Accepted).
- [35] T. Smith, and J. Guild, "The C.I.E. colorimetric standards and their use. Transactions of the Optical Society," vol. 33, no. 3, pp. 73–134, 1931.
- [36] W. S. Stiles, and J. M. Burch, "N.P.L. Colour-matching Investigation: Final Report (1958)," *Optica Acta: International Journal of Optics*, vol. 6, no. 1, pp. 1–26, 1959.
- [37] W. D. Wright, "A re-determination of the trichromatic coefficients of the spectral colours. Transactions of the Optical Society," vol. 30, no. 4, pp. 141–164, 1929.
- [38] J. Guild, "The colorimetric properties of the spectrum," *Philosophical Transactions of the Royal Society A*, vol. 230, pp. 681-693, 1931.
- [39] R. C. Gonzalez, and R. E. Woods, "Digital Image Processing," Pearson international edition, (3rd Edition), 2009.
- [40] R. M. Rangayyan, B. Acha, and C. Serrano, "Color Image Processing with Biomedical Applications" SPIE Press Book, 2011.
- [41] J.-Y. Yoon, "Basic principles of optical biosensing using a smartphone," *Smartphone Based Medical Diagnostics*, pp. 11–28, 2020.
- [42] J. Jiang, X. Wang, R. Chao, Y. Ren, C. Hu, Z. Xu, and G. L. Liu, "Smartphone based portable bacteria pre-concentrating microfluidic sensor and impedance sensing system," *Sensors and Actuators B: Chemical*, vol. 193, pp. 653–659, 2014.

- [43] K. Wu, T. Klein, V. D. Krishna, D. Su, A. M. Perez, and J.-P. Wang, “Portable GMR handheld platform for the detection of influenza a virus,” *ACS Sensors*, vol. 2, no. 11, pp. 1594–1601, 2017.
- [44] M. A. Saeed, and A. Jabbar, ““smart diagnosis” of parasitic diseases by use of smartphones,” *Journal of Clinical Microbiology*, vol. 56, no. 1, pp. e01469-17, 2017.
- [45] D.-H. Park, C. J. Han, Y.-G. Shul, and J.-H. Choy, “Avatar DNA nanohybrid system in chip-on-a-phone,” *Scientific Reports*, vol. 4, no. 1, pp. 4879, 2014.
- [46] M. Sajid, A. Osman, G. U. Siddiqui, H. B. Kim, S. W. Kim, J. B. Ko, Y. K. Lim, and K. H. Choi, “All-printed highly sensitive 2d MoS₂ based multireagent immunosensor for smartphone based point-of-care diagnosis,” *Scientific Reports*, vol. 7, no. 1, pp. 5802(1–11), 2017.
- [47] L. Guan, J. Tian, R. Cao, M. Li, Z. Cai, and W. Shen, “Barcode-like paper sensor for smartphone diagnostics: An application of blood typing,” *Analytical Chemistry*, vol. 86, no. 22, pp. 11362–11367, 2014.
- [48] P. E. Araque, I. M. P. de Vargas Sansalvador, N. L. Ruiz, M. M. E. Rodriguez, M. A. C. Rodriguez, and A. M. Olmos, “Non-invasive oxygen determination in intelligent packaging using a smartphone,” *IEEE Sensors Journal*, vol. 18, no. 11, pp. 4351–4357, 2018.
- [49] V. Turbè, E. R. Gray, V. E. Lawson, E. Nastouli, J. C. Brookes, R. A. Weiss, D. Pillay, V. C. Emery, C. T. Verrips, H. Yatsuda, D. Athey, and R. A. McKendry, “Towards an ultra-rapid smartphone- connected test for infectious diseases,” *Scientific Reports*, vol. 7, no. 1, pp. 1-11, 2017.
- [50] M. Samandari, M. G. Julia, A. Rice, A. Chronopoulos, and A. E. del Rio Hernandez, “Liquid biopsies for management of pancreatic cancer,” *Translational Research*, vol. 201, pp. 98–127, 2018.

- [51] G. Choi, D. Song, S. Shrestha, J. Miao, L. Cui, and W. Guan, "A field-deployable mobile molecular diagnostic system for malaria at the point of need," *Lab on a Chip*, vol. 16, no. 22, pp. 4341–4349, 2016.
- [52] T. F. Scherr, S. Gupta, D. W. Wright, and F. R. Haselton, "Mobile phone imaging and cloud-based analysis for standardized malaria detection and reporting," *Scientific Reports*, vol. 6, no. 1, pp. 1-9, 2016.
- [53] J. Liu, Y. Fan, Z. Kong, Y. Wang, J. Luo, S. Xu, H. Jin, and X. Cai, "Smartphone-based rapid quantitative detection of luteinizing hormone using gold immunochromatographic strip," *Sensors and Actuators B: Chemical*, vol. 259, pp. 1073–1081, 2018.
- [54] S. Choi, S. Kim, J.-S. Yang, J.-H. Lee, C. Joo, and H.-I. Jung, "Real-time measurement of human salivary cortisol for the assessment of psychological stress using a smartphone," *Sensing and Bio-Sensing Research*, vol. 2, pp. 8–11, 2014.
- [55] K. Hogenelst, M. Soeter, and V. Kallen, "Ambulatory measurement of cortisol: Where do we stand, and which way to follow?," *Sensing and Bio-Sensing Research*, vol. 22, pp. 100249, 2019.
- [56] R. A. Faris, Z. F. Bawi, and M. D. AbdHusein, "Nanoelisa for highly sensitive ca-15-3 tumor marker detection," *SYLWAN journal*, vol. 163, pp. 1–13, 2019.
- [57] R. A. Faris, Z. F. Bawi, M. D. AbdHusein, and W. A. Salah, "Fast, low cost and sensitive detection of breast cancer serum biomarkers ca15-3 using gold nanostar plasmonic elisa biosensor," *SYLWAN journal*, vol. 162, pp. 127–139, 2018.
- [58] B. Udugama, P. Kadhiresan, A. Samarakoon, and W. C. W. Chan, "Simplifying assays by tableting reagents," *Journal of the American Chemical Society*, vol. 139, no. 48, pp. 17341–17349, 2017.

- [59] A. Skandarajah, C. D. Reber, N. A. Switz, and D. A. Fletcher, “Quantitative imaging with a mobile phone microscope,” *PLoS ONE*, vol. 9, no. 5, pp. e96906, 2014.
- [60] S. Huang, K. Abe, S. Bennett, T. Liang, P. D. Ladd, L. Yokobe, C. E. Anderson, K. Shah, J. Bishop, M. Purfield, P. C. Kauffman, S. Paul, A. E. Welch, B. Strelitz, K. Follmer, K. Pullar, L. Sanchez-Erebia, E. Gerth-Guyette, G. Domingo, E. Klein, J. A. Englund, and E. Fu, P. Yager, “Disposable autonomous device for swab-to-result diagnosis of influenza,” *Analytical Chemistry*, vol. 89, no. 11, pp. 5776–5783, 2017.
- [61] M. You, M. Lin, Y. Gong, A. Ma, X. Li, and F. Xu, “Household fluorescent lateral flow strip platform for sensitive and quantitative prognosis of heart failure using dual-color upconversion nanoparticles,” *ACS Nano*, vol. 11, no. 6, pp. 6261–6270, 2017.
- [62] R. Álvarez-Diduk, J. Orozco, and A. Merkoçi, “Paper strip-embedded graphene quantum dots: a screening device with a smartphone readout,” *Scientific Reports*, vol. 7, no. 1, pp. 976, 2017.
- [63] A. Roda, E. Michelini, L. Cevenini, D. Calabria, M. M. Calabretta, and P. Simoni, “Integrating Biochemiluminescence Detection on Smartphones: Mobile Chemistry Platform for Point-of-Need Analysis,” *Analytical Chemistry*, vol. 86, no. 15, pp. 7299–7304, Jul. 2014.
- [64] W. Cui, M. He, L. Mu, Z. Lin, Y. Wang, W. Pang, M. Reed, and X. Duan, “Cellphone-enabled microwell-based microbead aggregation assay for portable biomarker detection,” *ACS Sensors*, vol. 3, no. 2, pp. 432–440, 2018.
- [65] T. Alawsi, and Z. Al-Bawi, “A review of smartphone point-of-care adapter design,” *Engineering Reports*, vol. 1, no. 2, Sep. 2019.

- [66] J. I. Hong, and B.-Y. Chang, “Development of the smartphone-based colorimetry for multi-analyte sensing arrays,” *Lab Chip*, vol. 14, no. 10, pp. 1725–1732, 2014.
- [67] Y. Jung, J. Kim, O. Awofeso, H. Kim, F. Regnier, and E. Bae, “Smartphone-based colorimetric analysis for detection of saliva alcohol concentration,” *Applied Optics*, vol. 54, no. 31, pp. 9183, Oct. 2015.
- [68] K. Choi, I. Chang, J. C. Lee, D.K. Kim, S. Noh, H. Ahn, J. H. Cho, Y. H. Kwak, S. Kim, and H. C. Kim, “Smartphone-based urine reagent strip test in the emergency department,” *Telemed. e-Health*, vol. 22, no. 6, pp. 534–540, 2016.
- [69] T. S. Kuntzleman, and E. C. Jacobson, “Teaching Beer’s Law and Absorption Spectrophotometry with a Smart Phone: A Substantially Simplified Protocol,” *Journal of Chemical Education*, vol. 93, no. 7, pp. 1249–1252, Jan. 2016.
- [70] M. Ra, M. S. Muhammad, C. Lim, S. Han, C. Jung, and W. Y. Kim, “Smartphone-Based Point-of-Care Urinalysis under Variable Illumination,” *IEEE J. Transl. Eng. Heal. Med.*, vol. 6, no. March 2017, pp. 1–11, 2018.
- [71] B. S. Hosker, “Demonstrating Principles of Spectrophotometry by Constructing a Simple, Low-Cost, Functional Spectrophotometer Utilizing the Light Sensor on a Smartphone,” *Journal of Chemical Education*, vol. 95, no. 1, pp. 178–181, Nov. 2017.
- [72] L. Barnes, D. M. Heithoff, S. P. Mahan, G. N. Fox, A. Zambrano, J. Choe, L. N. Fitzgibbons, J. D. Marth, J. C. Fried, H. T. Soh, and M. J. Mahan, “Smartphone-based pathogen diagnosis in urinary sepsis patients,” *EBioMedicine*, vol. 36, pp. 73–82, 2018.
- [73] A. Soni, R. K. Surana, and S. K. Jha, “Smartphone based optical biosensor for the detection of urea in saliva,” *Sensors and Actuators B: Chemical*, vol. 269, pp. 346–353, Sep. 2018.

- [74] M. V. Bills, B. T. Nguyen, and J. Y. Yoon, "Simplified White Blood Cell Differential: An Inexpensive, Smartphone- and Paper-Based Blood Cell Count," *IEEE Sens. J.*, vol. 19, no. 18, pp. 7822–7828, 2019.
- [75] K. Yun, J. Choi, I. U. Song, and Y. A. Chung, "Smartphone-based point-of-care cholesterol blood test performance evaluation compared with a clinical diagnostic laboratory method," *Appl. Sci.*, vol. 9, no. 16, 2019.
- [76] J. Lee, J. Song, J.-H. Choi, S. Kim, U. Kim, V.-T. Nguyen, J.-S. Lee, and C. Joo, "A Portable Smartphone-linked Device for Direct, Rapid and Chemical-Free Hemoglobin Assay," *Scientific Reports*, vol. 10, no. 1, pp. 1–10, 2020.
- [77] M. Hattori, S. Shirane, T. Matsuda, K. Nagayama, and T. Nagai, "Smartphone-based portable bioluminescence imaging system enabling observation at various scales from whole mouse body to organelle," *Sensors (Switzerland)*, vol. 20, no. 24, pp. 1–12, 2020.
- [78] Y. Xing, Q. Zhu, X. Zhou, and P. Qi, "A dual-functional smartphone-based sensor for colorimetric and chemiluminescent detection: A case study for fluoride concentration mapping," *Sensors and Actuators B: Chemical*, vol. 319, pp. 128254, Sep. 2020.
- [79] D. Kim, S. J. Kim, H. T. Ha, and S. Kim, "Smartphone-based image analysis coupled to paper-based colorimetric devices," *Curr. Appl. Phys.*, vol. 20, no. 9, pp. 1013–1018, 2020.
- [80] T. Liu, S. Zhang, W. Liu, S. Zhao, Z. Lu, Y. Wang, G. Wang, P. Zou, X. Wang, Q. Zhao, and H. Rao, "Smartphone based platform for ratiometric fluorometric and colorimetric determination H_2O_2 and glucose," *Sensors Actuators, B Chem.*, vol. 305, pp. 127524, 2020.
- [81] E. Vidal, A. S. Lorenzetti, C. D. Garcia, and C. E. Domini, "Use of universal 3D-Printed smartphone spectrophotometer to develop a time-based analysis for hypochlorite," *Analytica Chimica Acta*, vol. 1151, pp. 338249, 2021.

- [82] O. B. Mercan, V. Kılıç, and M. Sen, "Machine learning-based colorimetric determination of glucose in artificial saliva with different reagents using a smartphone coupled μ PAD," *Sensors and Actuators: B. Chemical*, vol. 329, pp. 129037, 2021.
- [83] V. Kılıç, N. Horzum, and M. Ertugrul Solmaz, "From Sophisticated Analysis to Colorimetric Determination: Smartphone Spectrometers and Colorimetry," *Color Detection*, Apr. 2020.
- [84] H.-C. Wang, F.-Y. Chang, and T.-M. Tsai, "Design, fabrication, and feasibility analysis of a colorimetric detection system with a smartphone for self-monitoring blood glucose," *Journal of Biomedical Optics*, vol. 24, no. 02, pp. 1, Feb. 2019.
- [85] H.-C. Wang, F.-Y. Chang, T.-M. Tsai, C.-H. Chen, and Y.-Y. Chen, "Development and clinical trial of a smartphone-based colorimetric detection system for self-monitoring of blood glucose," *Biomedical Optics Express*, vol. 11, no. 4, pp. 2166, Mar. 2020.
- [86] R. S. Tabatabaee, H. Golmohammadi, and S. H. Ahmadi, "Easy diagnosis of jaundice: A smartphone-based nanosensor bioplatfrom using photoluminescent bacterial nanopaper for point-of-care diagnosis of hyperbilirubinemia," *ACS Sensors*, vol. 4, pp. 1063–1071, 2019.
- [87] P. Martinkova, and M. Pohanka, "Colorimetric sensor based on bubble wrap and camera phone for glucose determination," *J. Appl. Biomed.*, vol. 14, pp. 315–319, 2016.
- [88] T. Alawsi, G. P. Mattia, Z. Al-Bawi, and R. Beraldi, "Smartphone-Based Colorimetric Sensor Application for Measuring Biochemical Material Concentration," *Sens. & Bio-Sens. Res.* vol. 32, no. 2, pp. 1-9. 2021.
- [89] P. B. M. Silva, K. Oliveira, and W. K. T. Coltro, "Colorimetric detection of glucose in biological fluids using toner-based microzone plates," *J. Braz. Chem. Soc.*, vol. 28, no. 1, pp. 197-201, 2017.

- [90] J. Li, Y. Sun, C. Chen, T. Sheng, P. Liu, and G. Zhang, "A smartphone-assisted microfluidic chemistry analyzer using image-based colorimetric assays for multi-index monitoring of diabetes and hyperlipidemia," *Anal. Chim. Acta*, vol. 1052, pp. 105–112, 2019.
- [91] E. V. Woodburn, K. D. Long, and B. T. Cunningham, "Analysis of paper-based colorimetric assays with a smartphone spectrometer," *IEEE Sens. J.*, vol. 19, pp. 508–514, 2019.
- [92] J. Xiao, Y. Liu, L. Su, D. Zhao, L. Zhao, and X. Zhang, "Microfluidic chip-based wearable colorimetric sensor for simple and facile detection of sweat glucose," *Anal. Chem.*, vol. 91, pp. 14803–14807, 2019.
- [93] T. T. Wang, C. kit Lio, H. Huang, R. Y. Wang, H. Zhou, P. Luo, and L. Sen Qing, "A feasible image-based colorimetric assay using a smartphone RGB camera for point-of-care monitoring of diabetes," *Talanta*, vol. 206, pp. 120211, 2020.
- [94] T. Golcez, V. Kilic, and M. Sen, "A Portable smartphone-based platform with an offline image processing tool for rapid paper-based colorimetric detection of glucose in artificial saliva," *Anal. Sci.*, pp. 1–25, 2020.
- [95] A. K. Yetisen, J. L. Martinez-Hurtado, A. Garcia-Melendrez, F. Da Cruz Vasconcellos, and C. R. Lowe, "A smartphone algorithm with inter-phone repeatability for the analysis of colorimetric tests," *Sensors Actuators, B Chem.*, vol. 196, pp. 156–160, 2014.
- [96] M. Y. Jia, Q. S. Wu, H. Li, Y. Zhang, Y. F. Guan, and L. Feng, "The calibration of cellphone camera-based colorimetric sensor array and its application in the determination of glucose in urine," *Biosens. Bioelectron.*, vol. 74, pp. 1029–1037, 2015.
- [97] Y. Wu, A. Boonloed, N. Sleszynski, M. Koesdjojo, C. Armstrong, S. Bracha, and V. T. Remcho, "Clinical chemistry measurements with commercially

- available test slides on a smartphone platform: Colorimetric determination of glucose and urea,” *Clin. Chim. Acta*, vol. 448, pp. 133–138, 2015.
- [98] S. Singhal, P. Ralhan, and N. Jatana, “Smartphone-based colorimetric detection to measure Blood Glucose Levels,” 2015 8th Int. Conf. Contemp. Comput. IC3, vol. 2015, pp. 269–274, 2015.
- [99] M. S. Coutinho, C. L. M. Morais, A. C. O. Neves, F. G. Menezes, and K. M. G. Lima, “Colorimetric determination of ascorbic acid based on its interfering effect in the enzymatic analysis of glucose: An approach using smartphone image analysis,” *J. Braz. Chem. Soc.*, vol. 28, pp. 2500–2505, 2018.
- [100] I. W. Mahdiasanti, A. Sabarudin, and H. Sulistyarti, “Simultaneous determination of bun-creatinine as kidney function biomarkers in blood using a microfluidic paper-based analytical devices,” *IOP Conf. Ser. Mater. Sci. Eng.*, vol. 546, no. 3, pp. 03, 2019.
- [101] A. Phonchai, S. Rattana, and K. Thongprajukaew, “A portable sol-gel urea colorimetric method for the determination of urea in feedstuffs,” *Food Chem.*, vol. 319, pp. 126545, 2020.
- [102] S. Parween, and A. Asthana, “An affordable, rapid determination of total lipid profile using paper-based microfluidic device,” *Sensors Actuators, B Chem.*, vol. 285, pp. 405–412, 2019.
- [103] W. Tan, L. Zhang, J. C. G. Doery, and W. Shen, “Study of paper-based assaying system for diagnosis of total serum bilirubin by colorimetric diazotization method,” *Sensors Actuators, B Chem.*, vol. 305, pp. 127448, 2020.
- [104] R. P. Edachana, A. Kumaresan, V. Balasubramanian, R. Thiagarajan, B. G. Nair, and S. B. T. Gopalakrishnan, “Paper-based device for the colorimetric assay of bilirubin based on in-situ formation of gold nanoparticles,” *Microchim. Acta*, vol. 187, no. 1, pp. 60, 2020.

- [105] L. De Greef, M. Goel, M. J. Seo, E. C. Larson, and S. N. Patel, “BiliCam: Using mobile phones to monitor newborn jaundice,” *UbiComp 2014 - Proc. 2014 ACM Int. Jt. Conf. Pervasive Ubiquitous Comput.*, pp. 331–342, 2014.
- [106] A. Mariakakis, M. Banks, L. Phillipi, L. Yu, J. Taylor, and S. Patel, “BiliScreen: smartphone-based scleral jaundice monitoring for liver and pancreatic disorders,” *Proc. ACM Inter., Mob., W. Ubi. Technol.*, vol. 1, pp. 1–26, 2017.
- [107] S. B. Munkholm, T. Krøgholt, F. Ebbesen, P. B. Szecsi, and S. R. Kristensen, “The smartphone camera as a potential method for transcutaneous bilirubin measurement,” *PLoS One*, vol. 13, pp. 1–11, 2018.
- [108] A. Aune, G. Vartdal, H. Bergseng, L. L. Randeberg, and E. Darj, “Bilirubin estimates from smartphone images of newborn infants’ skin correlated highly to serum bilirubin levels,” *Acta Paediatr. Int. J. Paediatr.*, vol. 109, pp. 2532–2538, 2020.

Appendices

Appendix A: Cura Ultimaker Software

The software version and the main window with all additional options are showed in both Figure A.1 and A.2

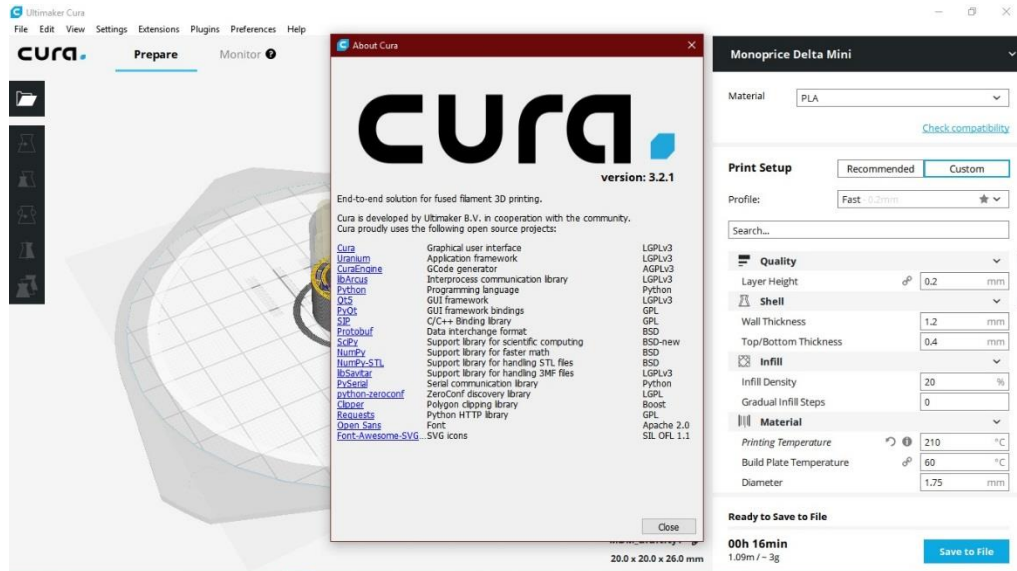


Figure A.1: Cura Ultimaker software environment

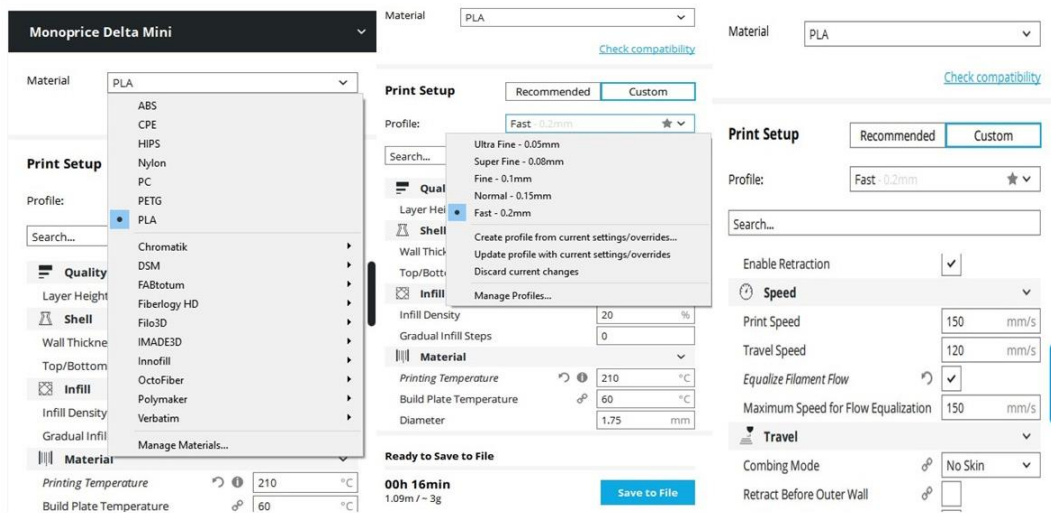


Figure A.2: Control parameters of Cura Ultimaker software

Appendix B: Detailed Design Parts of Smartphone Adapter

All design parts are shown separately for the design of the smartphone adapter in bioimaging (Chapter Four) as shown in Figures B.1 to B.6

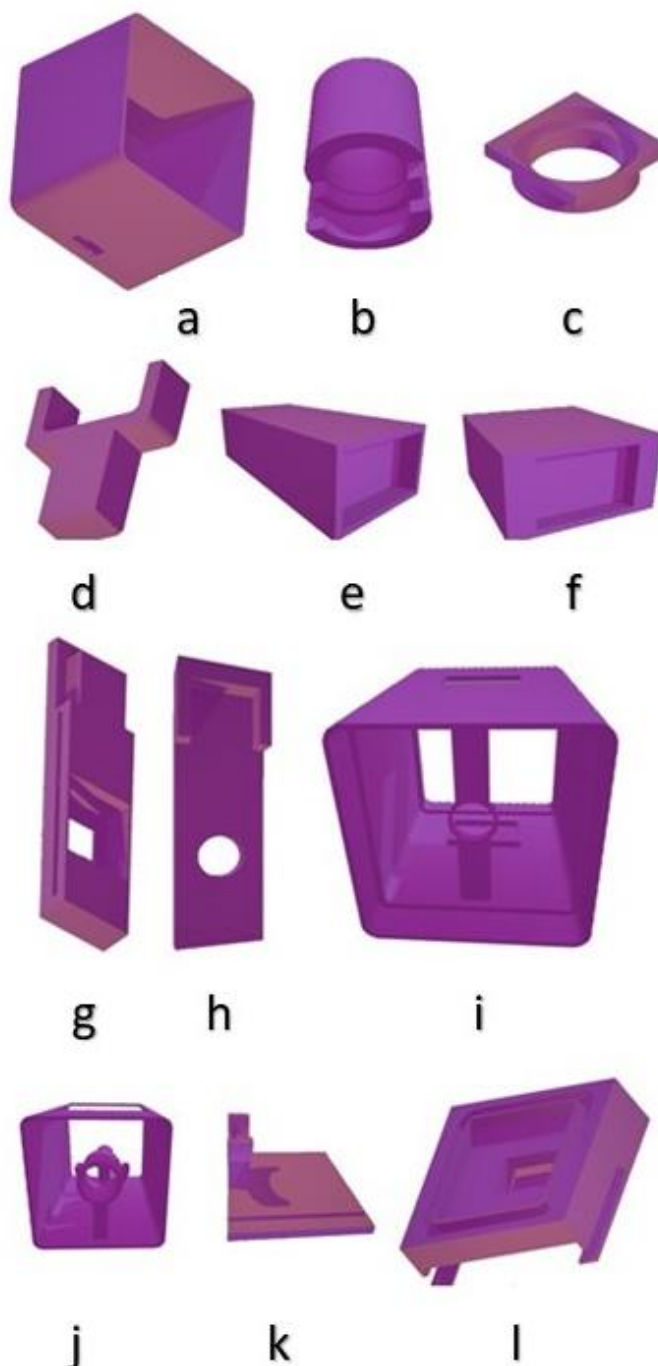


Figure B.1: 3D model of (a) Laser casing (b) Ring holder (c) Optical density filter ring (d) Adapter holder (e) Extended support (f) Ground support (g) Sample holder (h) Sample cover (i) Sample casing (j) Optics casing (k) Slide cover of optics casing (l) Smartphone holder

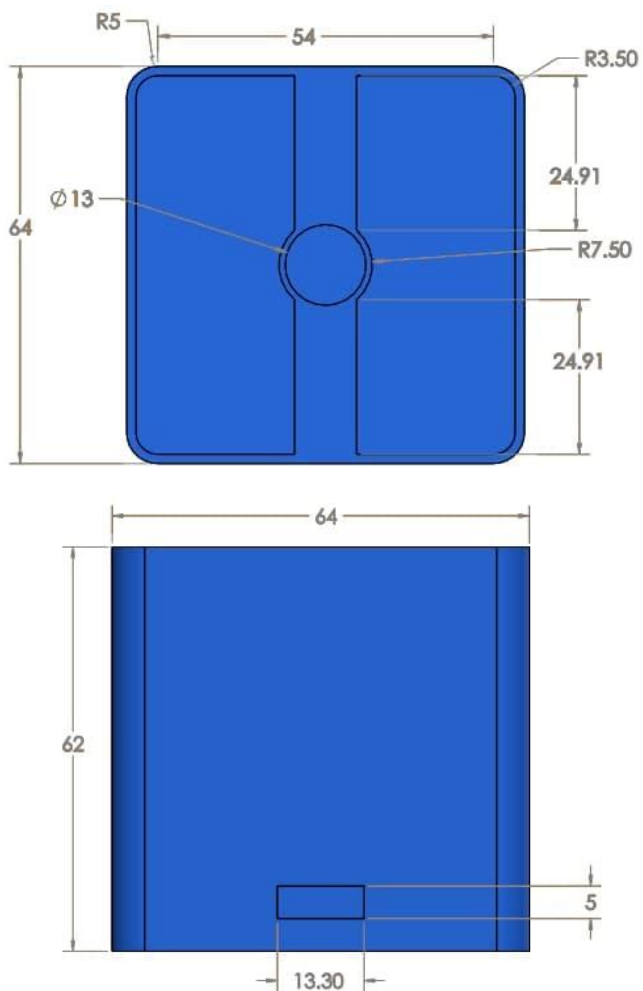


Figure B.2: Smartphone-based 3D printed adapter: source case dimensions

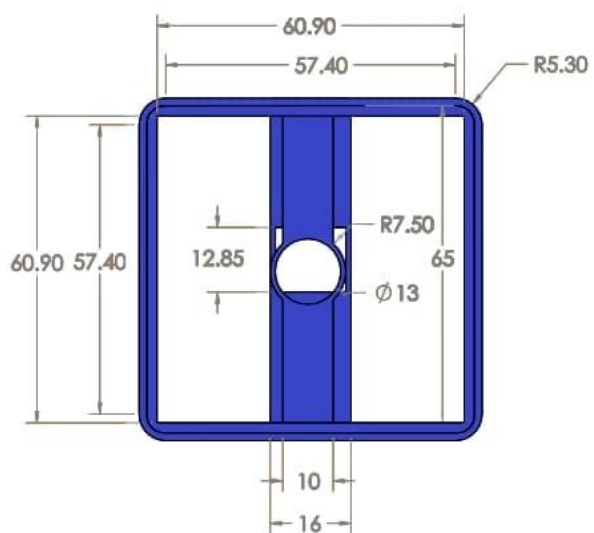


Figure B.3: Smartphone-based 3D printed adapter: sample case dimensions

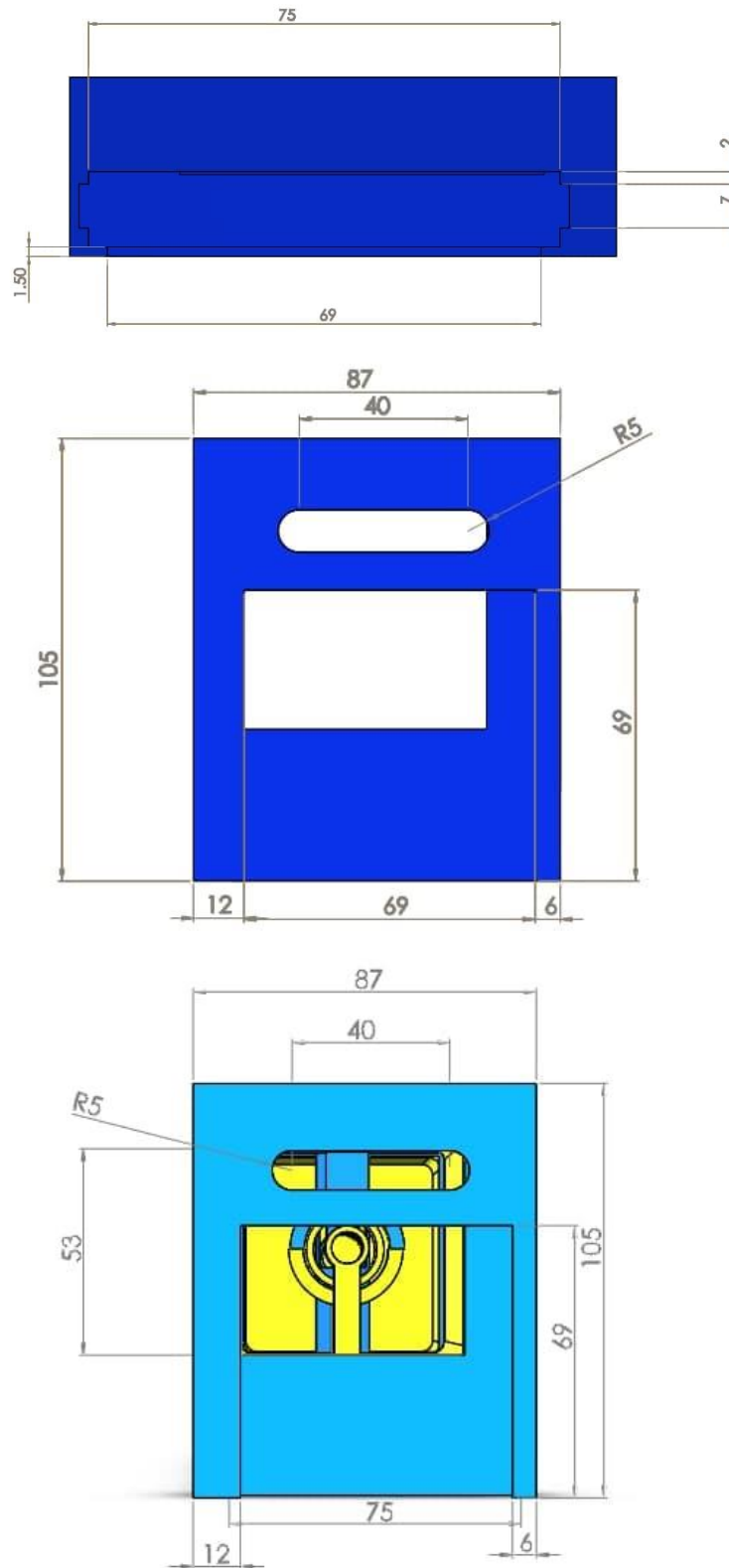


Figure B.4: Smartphone-based 3D printed adapter: smartphone holder dimensions

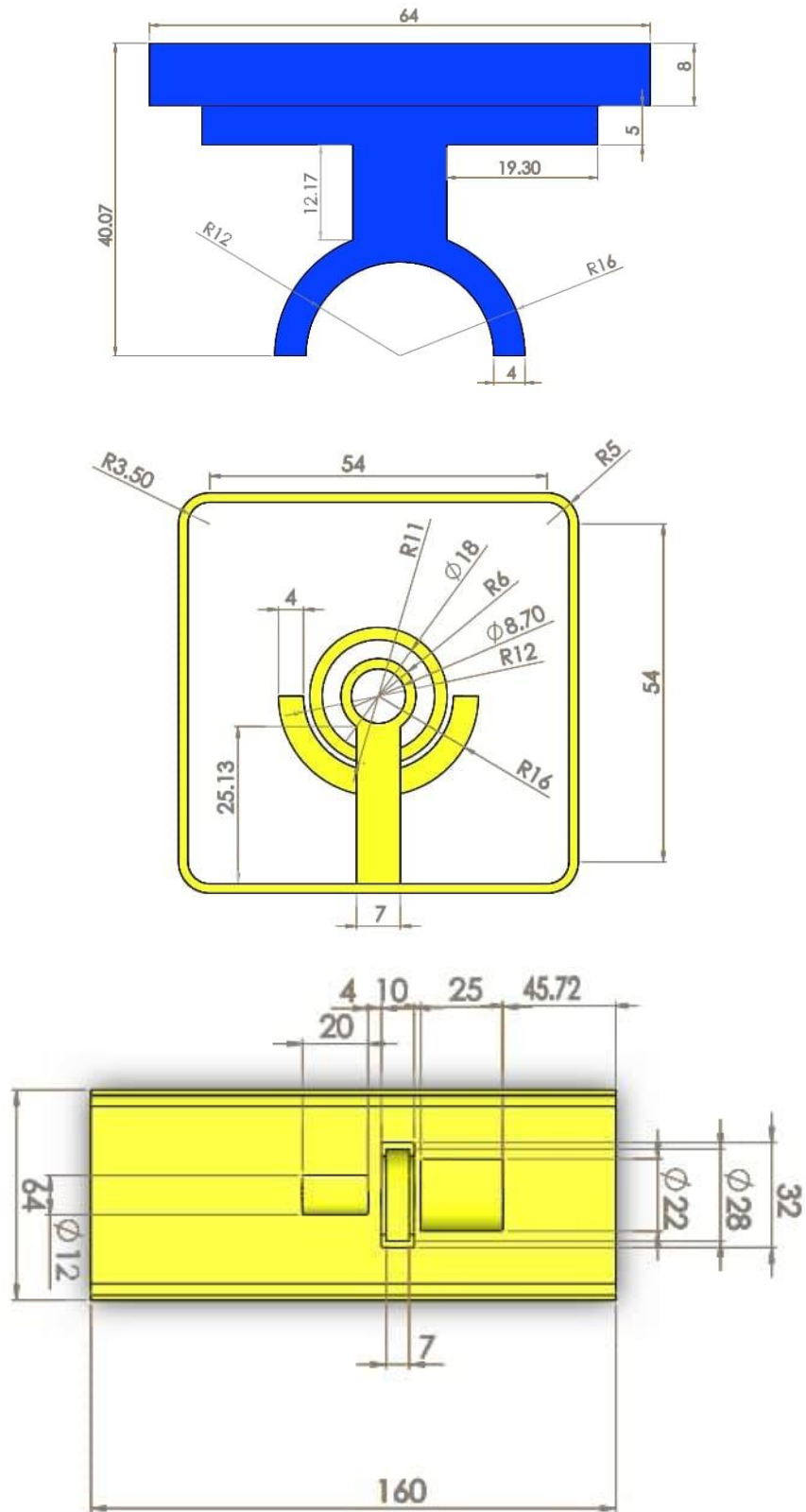


Figure B.5: Smartphone-based 3D printed adapter: optics case dimensions

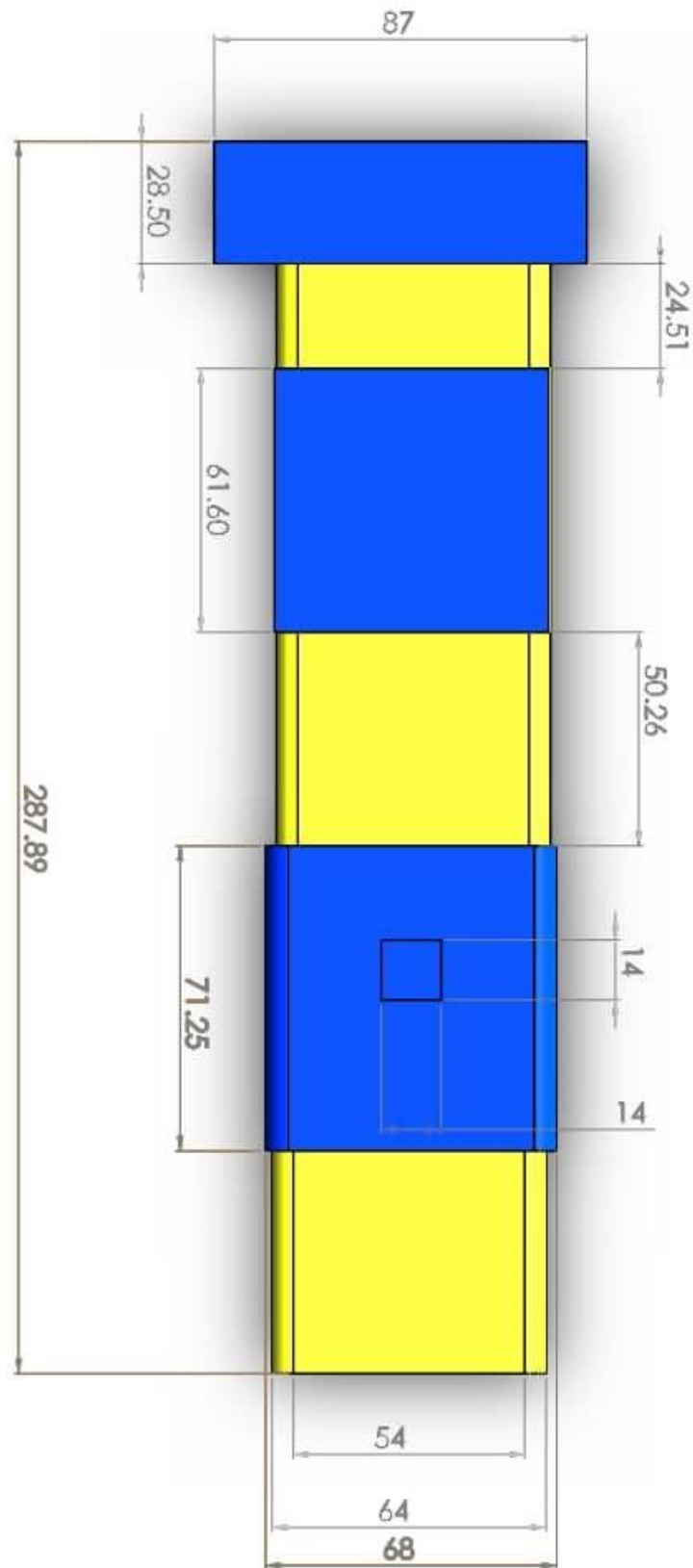


Figure B.6: Smartphone-based 3D printed adapter: overall dimensions

Appendix C: Materials and Devices Additional Figures

All materials and devices used which are not shown in the main text of the thesis, are shown in Figures C.1, C.2, C.3, C.4 and C.5. The datasheets of the prepared biomarkers are also shown in Figures C.6 to C.10.



Figure C.1: Laboratory devices (a) Centrifuge (b) Optical Microscope



Figure C.2: (a) Slide coloring (b) Left to dry



Figure C.3: Chemical dyes used in sample preparation



Figure C.4: Chemical pigments (a) Leishman Stain (b) Phosphate Buffer (c) Slide treatment chemical solution



Figure C.5: 3D printer AnyCubic i3 Mega

COD 11803 1 x 50 mL	COD 11503 1 x 200 mL	COD 11504 1 x 500 mL	COD 11538 1 x 1 L
STORE AT 2-8°C			
Reagents for measurement of glucose concentration Only for in vitro use in the clinical laboratory			

GLUCOSE
GLUCOSE OXIDASE/PEROXIDASE

PRINCIPLE OF THE METHOD

Glucose in the sample originates, by means of the coupled reactions described below, a coloured complex that can be measured by spectrophotometry¹.

$$\text{Glucose} + \frac{1}{2} \text{O}_2 + \text{H}_2\text{O} \xrightarrow{\text{glucose oxidase}} \text{Gluconate} + \text{H}_2\text{O}_2$$

$$2 \text{H}_2\text{O}_2 + 4 - \text{Aminoantipyrine} + \text{Phenol} \xrightarrow{\text{peroxidase}} \text{Quinoneimine} + 4 \text{H}_2\text{O}$$

Cerebrospinal fluid²:

Adult	40-70 mg/dL = 2.22-3.89 mmol/L
-------	--------------------------------

These ranges are given for orientation only; each laboratory should establish its own reference ranges.

According to the National Diabetes Data Group (US)³, elevation of fasting plasma glucose values over 140 mg/dL (7.77 mmol/L) on more than one occasion is diagnostic of diabetes mellitus.

CONTENTS

	COD 11803	COD 11503	COD 11504	COD 11538
A. Reagent	1 x 50 mL	1 x 200 mL	1 x 500 mL	1 x 1 L
S. Standard	1 x 5 mL	1 x 5 mL	1 x 5 mL	1 x 5 mL

COMPOSITION

A. Reagent: Phosphate 100 mmol/L, phenol 5 mmol/L, glucose oxidase > 10 U/mL, peroxidase > 1 U/mL, 4-aminoantipyrine 0.4 mmol/L, pH 7.5

S. Glucose/Urea/Creatinine Standard: Glucose 100 mg/dL (5.55 mmol/L), urea 50 mg/dL, creatinine 2 mg/dL. Aqueous primary standard.

STORAGE

Store at 2-8°C.

Reagent and Standard are stable until the expiry date shown on the label when stored tightly closed and if contaminations are prevented during their use.

Indications of deterioration:

- Reagent: Presence of particulate material, turbidity, absorbance of the blank over 0.150 at 500 nm (1 cm cuvette).
- Standard: Presence of particulate material, turbidity.

WARNING AND PRECAUTIONS

Exercise the normal precautions required for handling all laboratory reagents. Safety data sheet available for professional user on request. Disposal of all waste material should be in accordance with local guidelines.

REAGENT PREPARATION

Reagent and Standard are provided ready to use.

ADDITIONAL EQUIPMENT

- Thermostatic water bath at 37°C
- Analyzer, spectrophotometer or photometer able to read at 500 ± 20 nm

SAMPLES

Serum or plasma collected by standard procedures. Serum or plasma must be separated from the red cells promptly to prevent glycolysis. The addition of sodium fluoride to the blood sample prevent glycolysis.

Glucose in serum or plasma is stable for 5 days at 2-8°C. Heparin, EDTA, oxalate and fluoride may be used as anticoagulants.

Cerebrospinal fluid collected by standard procedures. Cerebrospinal fluid may be contaminated with bacteria or other cells and should therefore be analyzed for glucose immediately.

PROCEDURE

- Bring the Reagent to room temperature.
- Pipette into labelled test tubes: (Note 1)

	Blank	Standard	Sample
Glucose Standard (S)	---	10 µL	---
Sample	---	---	10 µL
Reagent (A)	1.0 mL	1.0 mL	1.0 mL

- Mix thoroughly and incubate the tubes for 10 minutes at room temperature (16-25°C) or for 5 minutes at 37°C.
- Measure the absorbance (A) of the Standard and the Sample at 500 nm against the Blank. The colour is stable for at least 2 hours.

CALCULATIONS

The glucose concentration in the sample is calculated using the following general formula:

$$\frac{A_{\text{Sample}}}{A_{\text{Standard}}} \times C_{\text{Standard}} = C_{\text{Sample}}$$

If the Glucose Standard provided has been used to calibrate (Note 2):

$\frac{A_{\text{Sample}}}{A_{\text{Standard}}}$	x 100 = mg/dL glucose	
	x 5.55 = mmol/L glucose	

REFERENCE VALUES

Serum and plasma²:

Children, adult	60-100 mg/dL = 3.30-5.60 mmol/L
-----------------	---------------------------------

QUALITY CONTROL

It is recommended to use the Biochemistry Control Serum level I (cod. 18005, 18009 and 18042) and II (cod. 18007, 18010 and 18043) to verify the performance of the measurement procedure. Each laboratory should establish its own internal Quality Control scheme and procedures for corrective action if controls do not recover within the acceptable tolerances.

METROLOGICAL CHARACTERISTICS

- Detection limit: 0.23 mg/dL = 0.0126 mmol/L
- Linearity limit: 500 mg/dL = 27.5 mmol/L. For higher values dilute sample 1/4 with distilled water and repeat measurement.
- Repeatability (within run):

Mean Concentration	CV	n
68 mg/dL = 4.84 mmol/L	1.2 %	20
328 mg/dL = 17.93 mmol/L	0.9 %	20

- Reproducibility (run to run):

Mean Concentration	CV	n
68 mg/dL = 4.84 mmol/L	2.7 %	25
328 mg/dL = 17.93 mmol/L	1.9 %	25

- Sensitivity: 4 mA dL/mg = 0.22 mA L/mmol
- Trueness: Results obtained with this reagent did not show systematic differences when compared with reference reagents (Note 2). Details of the comparison experiments are available on request.
- Interferences: Hemolysis (hemoglobin up to 300 mg/dL), bilirubin (up to 10 mg/dL) and lipemia (triglycerides up to 125 mg/dL) do not interfere. Ascorbic acid (up to 25 mg/dL) does not interfere. Other drugs and substances may interfere⁴.

These metrological characteristics have been obtained using an analyzer. Results may vary if a different instrument or a manual procedure are used.

DIAGNOSTIC CHARACTERISTICS

Glucose is the major source of energy in the body. Insulin, produced by islet cells in the pancreas, facilitates glucose entry into the tissue cells. A deficiency of insulin or a decrease of its effectiveness increases blood glucose.

Elevated serum or plasma glucose concentration is found in diabetes mellitus (insulin dependent, non-insulin dependent) and in other conditions and syndromes^{5,6}.

Hypoglycemia can occur in response to fasting, or it may be due to drugs, poisons, inborn errors of metabolism or previous gastrectomy^{7,8}.

Clinical diagnosis should not be made on the findings of a single test result, but should integrate both clinical and laboratory data.

NOTES

- These reagents may be used in several automatic analysers. Specific instructions for application in many of them are available on request.
- Calibration with the provided aqueous standard may cause a matrix related bias, specially in some analyzers. In these cases, it is recommended to calibrate using a serum based standard (Biochemistry Calibrator, cod. 18011 and 18044).

BIBLIOGRAPHY

- Trinder P. Determination of glucose in blood using glucose oxidase with an alternative oxygen acceptor. Ann Clin Biochem 1969; 6: 24-27.
- Tietz Textbook of Clinical Chemistry and Molecular Diagnostics, 5th ed. Burtis CA, Ashwood ER, Bruns DE. WB Saunders Co, 2012.
- National Diabetes Data Group: Classification and diagnosis of diabetes mellitus and other categories of glucose intolerance. Diabetes 1979; 28:1039-1057.
- Young DS. Effects of drugs on clinical laboratory tests, 5th ed. AACC Press, 2000.
- Friedman and Young. Effects of disease on clinical laboratory tests, 4th ed. AACC Press, 2001.

M11503-18

BioSystems S.A. Costa Brava, 30. 08030 Barcelona (Spain)
www.biosystems.es
Quality System certified according to

02/2020

Figure C.6: Glucose Biosystems Datasheet

COD 11536 4 x 50 mL	COD 11537 2 x 250 mL
STORE AT 2-8°C	
Reagents for measurement of urea concentration Only for <i>in vitro</i> use in the clinical laboratory	

UREA/BUN - COLOR

UREA/BUN - COLOR
UREASE/SALICYLATE

PRINCIPLE OF THE METHOD

Urea in the sample originates, by means of the coupled reactions described below, a coloured complex that can be measured by spectrophotometry^{1,2,3}.



CONTENTS

	COD 11536	COD 11537
A1. Reagent	2 x 48 mL	1 x 240 mL
A2. Reagent	2 x 2 mL	1 x 10 mL
B. Reagent	2 x 50 mL	1 x 250 mL
S. Standard	1 x 5 mL	1 x 5 mL

COMPOSITION

A1. Reagent: Sodium salicylate 62 mmol/L, sodium nitroprusside 3.4 mmol/L, phosphate buffer 20 mmol/L, pH 6.9.

A2. Reagent: Urea > 500 U/ml

B. Reagent Sodium hypochlorite 7 mmol/L, sodium hydroxide 150 mmol/L.

WARNING: H315: Causes skin irritation. H319: Causes serious eye irritation. P280: Wear protective gloves/protective clothing/eye protection/face protection. P305+P351+P338: IF IN EYES: Rinse cautiously with water for several minutes. Remove contact lenses, if present and easy to do. Continue rinsing. P332+P313: If skin irritation occurs: Get medical advice/attention.

S. Glucose/Urea/Creatinine Standard. Glucose 100 mg/dL, urea 50 mg/dL (8.3 mmol/L), BUN 23.3 mg/dL, creatinine 2 mg/dL. Aqueous primary standard.

For further warnings and precautions, see the product safety data sheet (SDS).

STORAGE

Store at 2-8°C.

Reagents and Standard are stable until the expiry date shown on the label when stored tightly closed and if contaminations are prevented during their use.

Indications of deterioration:

- Reagents: Presence of particulate material, turbidity, absorbance of the blank over 0.250 at 600 nm (1 cm cuvette).
- Standard: Presence of particulate material, turbidity.

REAGENT PREPARATION

Reagent (B) and Standard (S) are provided ready to use.

Reagent (A): Transfer the contents of one Reagent A2 vial into a Reagent A1 bottle (Note 1). Mix thoroughly. Other volumes can be prepared in the proportion: 1 mL Reagent A2 + 24 mL Reagent A1. Stable for 2 months at 2-8°C (Note 2).

ADDITIONAL EQUIPMENT

- Thermostatic water bath at 37°C
- Analyzer, spectrophotometer or photometer able to read at 600 ± 20 nm.

SAMPLES

Serum, plasma or urine collected by standard procedures. Dilute urine 1/50 with distilled water before measurement.

Urea in serum or plasma is stable for 7 days at 2-8°C. Heparin is recommended as anticoagulant.

Urea in urine is stable for 3 days at room temperature if microbial growth is prevented.

PROCEDURE

- Bring the Reagents to room temperature.
- Pipette into labelled test tubes:

	Blank	Standard	Sample
Urea Standard (S)	—	10 µL	—
Sample	—	—	10 µL
Reagent (A)	1.0 mL	1.0 mL	1.0 mL

- Mix thoroughly and incubate the tubes for 10 minutes at room temperature (16-25°C) or for 5 minutes at 37°C.

4. Pipette:

	Blank	Standard	Sample
Reagent (B)	1.0 mL	1.0 mL	1.0 mL

- Mix thoroughly and incubate the tubes for 10 minutes at room temperature (16-25°C) or for 5 minutes at 37°C.

6. Read the absorbance (A) of the Standard and the Sample at 600 nm against the Blank. The colour is stable for at least 2 hours.

CALCULATIONS

The urea concentration in the sample is calculated using the following general formula:

$$\frac{A_{\text{Sample}}}{A_{\text{Standard}}} \times C_{\text{Standard}} \times \text{Sample dilution factor} = C_{\text{Sample}}$$

If the Urea Standard provided has been used to calibrate (Note 3):

	Serum and plasma	Urine
A Sample	x 50 = mg/dL urea x 23.3 = mg/dL BUN	x 2500 = mg/dL urea x 1165 = mg/dL BUN
A Standard	x 8.3 = mmol/L urea	x 415 = mmol/L urea

REFERENCE VALUES

Serum and plasma⁴: 15-39 mg/dL urea = 7-18 mg/dL BUN = 2.5-6.5 mmol/L urea. Concentrations in the neonatal period are lower, and in adults over 60 years of age are higher than in adults. Concentrations also tend to be slightly higher in males than in females.

Urine⁴: 26-43 g/24-h urea = 12-20 g/24 h BUN = 428-714 mmol/24-h urea

These ranges are given for orientation only; each laboratory should establish its own reference ranges.

QUALITY CONTROL

It is recommended to use the Biochemistry Control Serum level I (cod. 18005, 18009 and 18042), level II (cod. 18007, 18010 and 18043) and the Biochemistry Control Urine (cod. 18054) to verify the performance of the measurement procedure.

Each laboratory should establish its own internal Quality Control scheme and procedures for corrective action if controls do not recover within the acceptable tolerances.

METROLOGICAL CHARACTERISTICS

- Detection limit 1.3 mg/dL urea = 0.60 mg/dL BUN = 0.21 mmol/L urea
- Linearity limit: 300 mg/dL = 140 mg/dL BUN = 50 mmol/L urea. For higher values dilute sample 1/5 with distilled water and repeat measurement.
- Repeatability (within run):

Mean urea concentration	CV	n
26 mg/dL = 4.3 mmol/L	1.6 %	20
86 mg/dL = 14.2 mmol/L	0.8 %	20

- Reproducibility (run to run):

Mean urea concentration	CV	n
26 mg/dL = 4.3 mmol/L	2.4 %	25
86 mg/dL = 14.2 mmol/L	1.3 %	25

- Sensitivity: 8.6 mA·dL/mg = 0.143 mA·L/mmol
- Trueness: Results obtained with this reagent did not show systematic differences when compared with reference reagents (Note 3). Details of the comparison experiments are available on request.
- Interferences: Lipemia (triglycerides 10 g/L) and bilirubin (20 mg/dL) do not interfere. Hemolysis (hemoglobin 2 g/L) and elevated ammonia interfere. Other drugs and substances may interfere⁵.

These metrological characteristics have been obtained using an analyzer. Results may vary if a different instrument or a manual procedure are used.

DIAGNOSTIC CHARACTERISTICS

Urea is synthesized in the liver as a by-product of the deamination of amino acids. Its elimination in the urine represents the major route for nitrogen excretion.

Elevated urea concentration in plasma is found as a result of a high-protein diet, increased protein catabolism, after a gastrointestinal hemorrhage, mild dehydration, shock and heart failure or treatment with glucocorticoids (pre-renal uremia)^{4,6}.

Post-renal uremia is caused by conditions that obstruct urine outflow: nephrolithiasis, tumor or prostatic hypertrophy. The usefulness of urea as an indicator of renal function is limited by the variability of its plasma concentration as a result of nonrenal factors^{4,6}.

Clinical diagnosis should not be made on the findings of a single test result, but should integrate both clinical and laboratory data.

NOTES

- It is advisable to wash the Reagent A2 vial with a small volume of the prepared mixture in order to completely rinse the vial and avoid any losses.
- The stability of Reagent A may be drastically reduced when it is not stored at 2-8°C.
- Calibration with the provided aqueous standard may cause a matrix related bias, specially in some analyzers. In these cases, it is recommended to calibrate using a serum based standard (Biochemistry Calibrator, cod. 18011 and 18044).

BIBLIOGRAPHY

- Chaney AL, Marbach EP. Modified reagents for determination of urea and ammonia. *Clin Chem* 1962; 8:130-132.
- Searcy RL, Reardon JE, Foreman JA. A new photometric method for serum urea nitrogen determination. *Amer J Med Technol* 1967; 33:15-20.
- Tabacco A, Meattini F, Moda E, Tarli P. Simplified enzymic/colorimetric serum urea nitrogen determination. *Clin Chem* 1979; 25: 336-337.
- Tietz Textbook of Clinical Chemistry and Molecular Diagnostics, 4th ed. Burtis CA, Ashwood ER, Bruns DE. WB Saunders Co, 2005.
- Young DS. Effects of drugs on clinical laboratory tests, 5th ed. AACCPress, 2000.
- Friedman and Young. Effects of disease on clinical laboratory tests, 4th ed. AACCPress, 2001.

COD 11828 1 x 50 mL	COD 11528 4 x 50 mL	COD 11529 2 x 250 mL
STORE AT 2-8°C		
Reagents for measurement of triglycerides concentration Only for in vitro use in the clinical laboratory		

TRIGLYCERIDES
GLYCEROL PHOSPHATE OXIDASE/PEROXIDASE

PRINCIPLE OF THE METHOD

Triglycerides in the sample originates, by means of the coupled reactions described below, a coloured complex that can be measured by spectrophotometry^{1,2}.

$$\begin{array}{l}
 \text{Triglycerides} + \text{H}_2\text{O} \xrightarrow{\text{lipase}} \text{Glycerol} + \text{Fatty acids} \\
 \text{Glycerol} + \text{ATP} \xrightarrow{\text{glycerol kinase}} \text{Glycerol-3-P} + \text{ADP} \\
 \text{Glycerol-3-P} + \text{O}_2 \xrightarrow{\text{G-3-P-oxidase}} \text{Dihydroxyacetone-P} + \text{H}_2\text{O}_2 \\
 2 \text{H}_2\text{O}_2 + 4 \text{-Aminopyrine} + 4 \text{-Chlorophenol} \xrightarrow{\text{peroxidase}} \text{Quinonimine} + 4 \text{H}_2\text{O}
 \end{array}$$

CONTENTS

	COD 11828	COD 11528	COD 11529
A. Reagent	1 x 50 mL	4 x 50 mL	2 x 250 mL
S. Standard	1 x 5 mL	1 x 5 mL	1 x 5 mL

COMPOSITION

A. Reagent: Pipes 45 mmol/L, magnesium acetate 5 mmol/L, 4-chlorophenol 6 mmol/L, lipase > 100 U/ml, glycerol kinase > 1.5 U/ml, glycerol-3-phosphate oxidase > 4 U/ml, peroxidase > 0.8 U/ml, 4-aminopyrine 0.75 mmol/L, ATP 0.9 mmol/L, pH 7.0.

S. Triglycerides Standard: Glycerol equivalent to 200 mg/dL (2.26 mmol/L) triolein. Aqueous primary standard.

STORAGE

Store at 2-8°C.

Reagent and Standard are stable until the expiry date shown on the label when stored tightly closed and if contaminations are prevented during their use.

Indications of deterioration:

- Reagent: Presence of particulate material, turbidity, absorbance of the blank over 0.150 at 500 nm (1 cm cuvette).
- Standard: Presence of particulate material, turbidity.

REAGENT PREPARATION

Reagent and Standard are provided ready to use.

ADDITIONAL EQUIPMENT

- Thermostatic water bath at 37°C.
- Analyzer, spectrophotometer or photometer able to read at 500 ± 20 nm.

SAMPLES

Serum or plasma collected by standard procedures.

Triglycerides in serum or plasma are stable for 5 days at 2-8°C. Heparin, EDTA, oxalate and fluoride may be used as anticoagulants.

PROCEDURE

1. Bring the Reagent to room temperature.
2. Pipette into labelled test tubes: (Note 1)

	Blank	Standard	Sample
Triglycerides Standard (S)	---	10 µL	---
Sample	---	---	10 µL
Reagent (A)	1.0 mL	1.0 mL	1.0 mL

3. Mix thoroughly and incubate the tubes for 15 minutes at room temperature (16-25°C) or for 5 minutes at 37°C.
4. Measure the absorbance (A) of the Standard and Sample at 500 nm against the Blank. The colour is stable for at least 2 hours.

CALCULATIONS

The triglycerides concentration in the sample is calculated using the following general formula:

$$\frac{A_{\text{Sample}}}{A_{\text{Standard}}} \times C_{\text{Standard}} = C_{\text{Sample}}$$

If the Triglycerides Standard provided has been used to calibrate (Note 2):

$\frac{A_{\text{Sample}}}{A_{\text{Standard}}}$	x 200 = mg/dL triglycerides
	x 2.26 = mmol/L triglycerides

REFERENCE VALUES

The following uniform cut-off points have been established by the US National Institutes of Health and have also been adopted in many other countries for the evaluation of risk³.

Up to 150 mg/dL = 1.7 mmol/L	Normal
150-199 mg/dL = 1.70-2.25 mmol/L	Borderline-high
200-499 mg/dL = 2.26-5.64 mmol/L	High
≥ 500 mg/dL = ≥ 5.65 mmol/L	Very high

QUALITY CONTROL

It is recommended to use the Biochemistry Control Serum level I (cod. 18005, 18009 and 18042) and II (cod. 18007, 18010 and 18043) to verify the performance of the measurement procedure. Each laboratory should establish its own internal Quality Control scheme and procedures for corrective action if controls do not recover within the acceptable tolerances.

METROLOGICAL CHARACTERISTICS

- Detection limit: 1.6 mg/dL = 0.018 mmol/L
- Linearity limit: 600 mg/dL = 6.78 mmol/L. For higher values dilute sample 1/4 with distilled water and repeat measurement.
- Repeatability (within run):

Mean Concentration	CV	n
100 mg/dL = 1.13 mmol/L	1.7%	20
245 mg/dL = 2.77 mmol/L	0.7%	20

- Reproducibility (run to run):

Mean Concentration	CV	n
100 mg/dL = 1.13 mmol/L	2.6%	25
245 mg/dL = 2.77 mmol/L	1.7%	25

- Trueness: Results obtained with this reagent did not show systematic differences when compared with reference reagents (Note 2). Details of the comparison experiments are available on request.
- Interferences: Hemoglobin (10 g/L) does not interfere. Bilirubin (2.5 mg/dL) may interfere. Other drugs and substances may interfere⁴.

These metrological characteristics have been obtained using an analyzer. Results may vary if a different instrument or a manual procedure are used.

DIAGNOSTIC CHARACTERISTICS

Triglycerides are esters of glycerol and fatty acids coming from the diet or obtained by synthesis mainly in the liver. Triglycerides are transported in plasma by lipoproteins and used by adipose tissue, muscle and other. Their primary function is to provide energy to the cell.

Elevated serum triglycerides levels can be caused by liver disease, diabetes mellitus, nephrosis, hypothyroidism, alcoholism, familial hyperlipoproteinemia IV and V, and other^{4,5}.

Clinical diagnosis should not be made on the findings of a single test result, but should integrate both clinical and laboratory data.

NOTES

1. This reagent may be used in several automatic analysers. Instructions for many of them are available on request.
2. Calibration with the provided aqueous standard may cause a matrix related bias, specially in some analyzers. In these cases, it is recommended to calibrate using a serum based standard (Biochemistry Calibrator, cod. 18011 and 18044).

BIBLIOGRAPHY

1. Bucolo G and David H. Quantitative determination of serum triglycerides by use of enzymes. *Clin Chem* 1973; 19: 476-482.
2. Fossati P and Prencipe L. Serum triglycerides determined colorimetrically with an enzyme that produces hydrogen peroxide. *Clin Chem* 1982; 28: 2077-2080.
3. National Cholesterol Education Program Expert Panel. Third report of the National Cholesterol Education Program (NCEP) Expert Panel on Detection, Evaluation, and Treatment of High Blood Cholesterol in Adults (ATP III). NIH Publication. Bethesda: National Heart, Lung, and Blood Institute; 2001.
4. Young DS. Effects of drugs on clinical laboratory tests, 5th ed. AACC Press, 2000.
5. Friedman and Young. Effects of disease on clinical laboratory tests, 4th ed. AACC Press, 2001.

M11528-21

BioSystems S.A. Costa Brava 30, 08030 Barcelona (Spain)
Quality System certified according to
EN ISO 13485 and EN ISO 9001 standards

08/2017

Figure C.8: Triglycerides Biosystems Datasheet

AGAPPE

BILIRUBIN TOTAL & DIRECT - TAB (Part-1: Bilirubin Direct)

4 x 50 mL
51003004

Procedure Notes

Laboratory Procedure for Sample Blank Mode		
	Sample Blank	Test
Direct Bilirubin Reagent	1000 µL	1000 µL
Activator Direct	-	20 µL
Serum / Calibrator	50 µL	50 µL

Mix well and incubate for 5 minute at room temperature. Measure the absorbance of calibrator and test against respective blank at 546 nm

Calculation

With Factor:

Direct Bilirubin = OD of Test - OD of Sample Blank X 16

With Calibrator:

Bilirubin Concentration = $\frac{\text{OD of Test} - \text{OD of Sample Blank}}{\text{OD of Calibrator} - \text{OD of Calib. Blank}} \times \text{Conc. of Calib.}$

Laboratory Procedure for Without Blank Mode		
	Reagent Blank	Test
Direct Bilirubin Reagent	1000 µL	1000 µL
Activator Direct	20 µL	20 µL
Serum / Calibrator	-	50 µL

Mix well and incubate for 5 minute at room temperature. Measure the absorbance of calibrator and test against respective blank at 546/650 nm

Calculation

With Factor:

Direct Bilirubin = OD of Test - OD of Reagent Blank X 20

With Calibrator:

Bilirubin Concentration = $\frac{\text{OD of Test} - \text{OD of Reagent Blank}}{\text{OD of Calibrator} - \text{OD of Reagent Blank}} \times \text{Conc. of Calib.}$

Quality Control

It is recommended to use Agappe Qualicheck Norm & Path (51601001) to verify the performance of the assay. Each laboratory has to establish its own internal quality control scheme and procedure for corrective action, if control do not recover within the acceptable range.

Reference Range

It is recommended that each laboratory should establish its own reference values. The following value may be used as guide line.

Direct Bilirubin upto 0.4 mg/dL

Results obtained for patient samples are to be correlated with clinical findings of patient for interpretation and diagnosis.

Performance

1. Linearity

The procedure is linear upto 20 mg/dL.

If the concentration is greater than linearity (20 mg/dL), dilute the sample with normal saline and repeat the assay. Multiply the result with dilution factor.

2. Comparison

A comparison study has been performed between Agappe reagent and another internationally available reagent yielded a correlation coefficient of $r^2 = 0.99$ and a regression equation of $y = 1.1051x$.

3. Precision

Intra Run		
	Control Level 1	Control Level 2
n	20	20
Mean (mg/dL)	0.60	1.67
SD	0.02	0.07
CV(%)	3.76	4.39

Inter Run		
	Control Level 1	Control Level 2
n	20	20
Mean (mg/dL)	0.6	1.7
SD	0.02	0.08
CV(%)	3.76	4.35

Accuracy (mg/dL)

Control	Expected Value	Measured Value
Control Level 1	0.34 ± 0.24	0.4
Control Level 2	1.4 ± 0.84	1.2
Qualicheck Norm	0.4 ± 0.26	0.4
Qualicheck Path	2.0 ± 0.40	2.0

4. Sensitivity

Lower detection Limit is 0.02 mg/dL

Bibliography

1. Walter, M., Gerard, H.; MICROCHEM J M 15, 251 (1980)
2. Annino J. S.; C. C. Principles and procedure, 1960
3. A. A. A. C. C.: Clin. Chem. 8 : 405, 196

SYMBOLS USED ON THE LABELS

IVD IN VITRO DIAGNOSTIC USE SEE PACKAGE INSERT FOR PROCEDURE LOT NUMBER MANUFACTURER'S ADDRESS MANUFACTURING DATE EXPIRY DATE TEMPERATURE LIMIT

AGAPPE DIAGNOSTICS SWITZERLAND GmbH

Knonerstrasse 54 - 6530 Cham Switzerland
Tel. +41 41 780 60 10 Fax: +41 41 780 60 11
info@agappeswiss.com | www.agappeswiss.com

REV. NO.: ADS/IFU/TDTB/CHEM/R04

CE ISO 9001:2015
EN ISO 13485:2016

Figure C.9: Bilirubin Agappe Diagnostics Datasheet

AGAPPE

BILIRUBIN TOTAL & DIRECT - TAB (Part-1: Bilirubin Direct)

4 x 50 mL
51003004

Intended Use

This reagent is intended for *in vitro* quantitative determination of Bilirubin in serum or plasma.
 - Modified Diazo Method
 - Linear up to 20 mg/dL
 - Fast incubation 5 minutes at room temperature
 - With out sample blank procedure also included
 - Sample volume only 50 µL.

Clinical Significance

Bilirubin is formed by the breakdown of RBC's in the spleen, liver & bone marrow. Small amount of bilirubin circulates in the plasma loosely bound to albumin, which is not water soluble. This is referred to as indirect or unconjugated bilirubin. In the liver bilirubin is conjugated with glucuronic acid, which forms a soluble compound. This is referred as direct bilirubin. Elevated levels are found in Hepatitis, Cirrhosis, Haemolytic jaundice, obstruction of biliary tract & drug induced reactions.

Principle

Sulfanilic acid reacts with sodium nitrite to form diazotized sulfanilic acid. Direct Bilirubin reacts with diazotized sulfanilic acid to form azobilirubin.

Kit Components

Reagent/Component	Product Code	Description
Direct Bilirubin Reagent	2 x 50 mL 51003004	Sulfanilic Acid 28.9 mmol/L Hydrochloric Acid 165 mmol/L Preservatives and Stabilizers
Direct Bilirubin Activator	1 x 4 mL	Sodium nitrite (1.0g/L)

Risk & Safety

Material safety data sheets (MSDS) will be provided on request.

Reagent Preparation

Direct Bilirubin Reagent and Direct Bilirubin Activator are ready to use.

Reagent Storage and Stability

The sealed reagents are stable up to the expiry date stated on the label, when stored at room temperature. The activator should be stored at 2 - 8°C

Open Vial Stability

Once opened, the reagent is stable up to 20 days if contamination is avoided.

Onboard Calibration Stability

On board Calibration stability is 15 days.

Reagent Deterioration

Turbidity or precipitation in any kit component indicates deterioration and the component must be discarded. Values outside the recommended acceptable range for the Agappe Qualicheck Norm & Path control may also be an indication of reagent instability and associated results are invalid. Sample should be retested, using fresh vial of reagent.

Precaution

To avoid contamination, use clean laboratory wares. Use clean, dry disposable pipette tips for dispensing. Close reagent bottles immediately after use.

Avoid direct exposure of reagent to light.

Do not blow into the reagent bottles.

This reagent is only for IVD use and follow the normal precaution required for handling all laboratory reagents.

Waste Management

Reagents must be disposed off in accordance with local regulations.

Sample

Serum / Plasma (free of hemolysis)

Interferences

No interference for

Ascorbic Acid up to 50 mg/dL

Hemoglobin up to 1000 mg/dL

Materials Provided

Direct Bilirubin Reagent and Direct Bilirubin Activator

Materials Required but Not Provided

- Pipettes & Tips
- Test Tubes & racks
- Timer
- Incubator
- Analyzer

Test Parameters

1. Sample Blank Mode	
Mode of Reaction	End Point
Slope of Reaction	Increasing
Wavelength	546 nm
Temperature	30° C
Factor (Direct)	16
Blank	Sample Blank
Linearity	20 mg/dL
Reaction Time	5 min
Sample Volume	50 µL
Reagent Volume	1000 µL
Activator	20 µL
Cuvette	1 cm light path

2. Without Sample Blank Mode	
Mode of Reaction	End Point
Slope of Reaction	Increasing
Wavelength I	546 nm
Wavelength II	650 nm
Temperature	30° C
Factor (Direct)	20
Blank	Reagent Blank
Linearity	20 mg/dL
Reaction Time	5 min
Sample Volume	50 µL
Reagent Volume	1000 µL
Activator	20 µL
Cuvette	1 cm light path

Application parameters for various instrument are available on request. Please contact customer support department for specific information.

Unit Conversion

Traditional Unit	SI Unit	Conversion from Traditional to SI
mg/dL	µmol/L	x 17.1

Calibration

Agappe Multicalibrator (51610002) is recommended for calibration of this assay on fully auto analyzers.

Use provided factor for estimation of this assay on semi auto analyzers.

SYMBOLS USED ON THE LABELS
 IVD IN VITRO DIAGNOSTIC USE SEE PACKAGE INSERT FOR PROCEDURE LOT LOT NUMBER MANUFACTURER'S ADDRESS MANUFACTURING DATE EXPIRY DATE TEMPERATURE LIMIT

AGAPPE DIAGNOSTICS SWITZERLAND GmbH
 Knomauerstrasse 54 - 6350 Cham Switzerland
 Tel. +41 41 780 60 10 Fax: +41 41 780 60 11
 info@agappeswiss.com | www.agappeswiss.com

REV. NO.: ADS/TFU/TDTB/CHEM/R04

CE ISO 9001:2015
EN ISO 13485:2016

Figure C.9: continued

AGAPPE

HDL CHOLESTEROL

4 x 25 mL
51010001**Intended Use**

This reagent is intended for *in vitro* quantitative determination of HDL in serum or plasma.

- Precipitation method, Phosphotungstate magnesium acetate reagent

- Linear up to 125 mg/dL.

Clinical Significance

Lipoproteins are the proteins, which mainly transport lipids in the blood stream. They are (HDL) High density lipoproteins, (LDL) Low density lipoproteins, (VLDL) Very low density lipoproteins & chylomicrons. LDL carries cholesterol to the peripheral tissues where it can be deposited & increase the risk of atherosclerotic heart & peripheral vascular disease. Hence high levels of LDL are atherogenic. HDL transports cholesterol from peripheral tissues to the liver & then for excretion, hence HDL has a protective effect. Hence the determination of serum HDL cholesterol is a useful tool to identify patients at risk of developing coronary heart disease.

Principle

The chylomicrons, Very low density lipoproteins (VLDL) and Low density lipoproteins (LDL) of serum are precipitated by phosphotungstic acid and magnesium ions. After centrifugation, High density lipoproteins (HDL) are in the supernatant. HDL content of supernatant is measured by an enzymatic Method.

Kit Components

Reagent/Component	Product Code	Description
HDL Cholesterol Reagent	4 x 25 mL 51010001	Phosphotungstate 14 mmol/L Magnesium Chloride 1 mmol/L Preservative
HDL Cholesterol Standard	1 x 4 mL	HDL Cholesterol Standard Concentration 50 mg/dL

Risk & Safety

Material safety data sheets (MSDS) will be provided on request.

Reagent Preparation

HDL Cholesterol Reagent and HDL Cholesterol Standard are ready to use.

Reagent Storage and Stability

The sealed reagents are stable up to the expiry date stated on the label, when stored 2 - 8°C and protected from light.

Open Vial Stability

Once opened, the reagent is stable up to 4 weeks, if contamination is avoided.

Reagent Deterioration

Turbidity or precipitation in any kit component indicates deterioration and the component must be discarded. Values outside the recommended acceptable range for the Agappe Quali check Norm & Path control may also be an indication of reagent instability and associated results are invalid. Sample should be retested, using a fresh vial of reagent.

Precaution

To avoid contamination, use clean laboratory wares. Use clean, dry disposable pipette tips for dispensing. Close reagent bottles immediately after use.

Avoid direct exposure of reagent to light.

Do not blow into the reagent bottles.

This reagent is only for IVD use and follow the normal precaution required for handling all laboratory reagents.

Waste Management

Reagents must be disposed off in accordance with local regulations.

Sample

Serum / Plasma (free of hemolysis)

Interferences

No interference for

Bilirubin up to 10 mg/dL

Hemoglobin up to 1000 mg/dL

Materials Provided

HDL Cholesterol Reagent and HDL Cholesterol Standard

Materials Required but Not Provided

- Cholesterol Reagent
- Pipettes & Tips
- Test Tubes & racks
- Timer
- Incubator
- Analyzer

Test Parameters

Mode of Reaction	End Point
Slope of Reaction	Increasing
Wavelength I	505 nm (500-532nm)
Wavelength II	630 nm
Temperature	37°C
Standard Concentration	50 mg/dL
Blank	Cholesterol Reagent
Linearity	125 mg/dL
Incubation Time	5 min
Sample Volume	50 µL
Reagent Volume	1000 µL
Cuvette	1 cm light path

Unit Conversion

Traditional Unit	SI Unit	Conversion from Traditional to SI
mg/dL	mmol/L	x 0.026

Calibration

Agappe HDL Cholesterol standard is recommended for calibration of this assay.

Procedure Notes**Laboratory Procedure for Semi Auto Analyzer****1. Precipitation**

Sample	300 µL	
HDL Reagent	300 µL	

Mix well, allow to stand for 10 min. at room temperature, mix again and centrifuge for 10 min, at 4000 rpm.

After centrifugation, separate the clear supernatant from the precipitate within 1 hour and determine the HDL concentration using the cholesterol reagent (which is not provided along with the kit)

2. HDL Cholesterol Determination

	Blank	Standard	Sample
Cholesterol Reagent	1000 µL	1000 µL	1000 µL
HDL Standard	-	50 µL	-
HDL Supernatant	-	-	50 µL

Mix well and incubate for 5 minute at 37°C. Measure the absorbance of standard and sample against the reagent blank.

SYMBOLS USED ON THE LABELS

IVD IN VITRO DIAGNOSTIC USE SEE PACKAGE INSERT FOR PROCEDURE LOT LOT NUMBER MANUFACTURER'S ADDRESS MANUFACTURING DATE EXPIRY DATE TEMPERATURE LIMIT

AGAPPE DIAGNOSTICS SWITZERLAND GmbH

Knonauerstrasse 54 - 6530 Cham Switzerland
Tel. +41 41 780 60 10 Fax: +41 41 780 60 11
info@agappeswiss.com | www.agappeswiss.com

REV. NO.: ADS/IFU/HDL/CHEM/R01

CE ISO 9001:2015
EN ISO 13485:2016

Figure C.10: HDL Agappe Diagnostics Datasheet

AGAPPE**HDL CHOLESTEROL**4 x 25 mL
51010001**Calculation**

$$\text{HDL Cholesterol Conc. (mg/dL)} = \frac{\text{Absorbance of Sample}}{\text{Absorbance of Standard}} \times \text{Conc. of Standard} \times 2$$

where, 2 = dilution factor of the sample

LDL Chol. Conc in mg/dL = Total Cholesterol - (HDL Chol. + Triglycerides/5)

Quality Control

It is recommended to use Agappe Qualicheck Norm & Path (51601001) to verify the performance of the assay. Each laboratory has to establish its own internal quality control scheme and procedure for corrective action, if control do not recover within the acceptable range.

Reference Range

It is recommended that each laboratory should establish its own reference values. The following value may be used as guide line.

HDL Cholesterol

Men : 35 - 55 mg/dL

Women : 45 - 65 mg/dL

LDL Cholesterol

Suspicious : 150 mg/dL

Elevated : 190 mg/dL

Results obtained for patient samples are to be correlated with clinical findings of patient for interpretation and diagnosis.

Performance**1. Linearity**

The reagent is linear upto 125 mg/dL

If the concentration is greater than linearity (125 mg/dL), dilute the sample with normal saline and repeat the assay. Multiply the result with dilution factor.

2. Precision**Accuracy (mg/dL)**

Control	Expected Value	Measured Value
Qualicheck Norm	30 ± 4.5	32
Qualicheck Path	70 ± 10	68.51

3. Sensitivity

Lower detection Limit is 1.0 mg/dL

Bibliography

1. Assmann, G.; Internist 20 (1979), 559
2. Gordon, T., *et al.*; Med 62 (1977), 707
3. Friedewald, W. T., *et al.*; Clin.Chem.18 (1972), 499.

SYMBOLS USED ON THE LABELS

IVD IN VITRO DIAGNOSTIC USE SEE PACKAGE INSERT FOR PROCEDURE LOT LOT NUMBER MANUFACTURER'S ADDRESS MANUFACTURING DATE EXPIRY DATE TEMPERATURE LIMIT

AGAPPE DIAGNOSTICS SWITZERLAND GmbH

Knonaerstrasse 54 - 6330 Cham Switzerland
Tel. +41 41 780 60 10 Fax: +41 41 780 60 11
info@agappeswiss.com | www.agappeswiss.com

REV. NO.: ADS/IFU/HDL/CHEM/R01

CE ISO 9001:2015
EN ISO 13485:2016

Figure C.10: continued

Appendix D: Optical Component Datasheets



www.vishay.com

VLHW5100

Vishay Semiconductors

Ultrabright White LED, Ø 5 mm Untinted Non-Diffused Package



19223

DESCRIPTION

The VLHW5100 is a clear, non-diffused 5 mm LED for high end applications where supreme luminous intensity required.

These lamps with clear untinted plastic case utilize the highly developed ultrabright InGaN technologies.

The lens and the viewing angle is optimized to achieve best performance of light output and visibility.

PRODUCT GROUP AND PACKAGE DATA

- Product group: LED
- Package: 5 mm
- Product series: standard
- Angle of half intensity: $\pm 10^\circ$

FEATURES

- Untinted non-diffused lens
- Utilizing ultrabright InGaN technology
- High luminous intensity
- Luminous intensity and color categorized for each packing unit
- ESD-withstand voltage: up to 4 kV according to JESD22-A114-B
- Circuit protection by Zener diode
- Material categorization: for definitions of compliance please see www.vishay.com/doc?99912



RoHS
COMPLIANT
HALOGEN
FREE
GREEN
IS-20051

APPLICATIONS

- Interior and exterior lighting
- Outdoor LED panels
- Instrumentation and front panel indicators
- Replaces incandescent lamps
- Light guide compatible

PARTS TABLE

PART	COLOR	LUMINOUS INTENSITY (mcd)			at I_F (mA)	COORDINATE (x, y)			at I_F (mA)	FORWARD VOLTAGE (V)			at I_F (mA)	TECHNOLOGY
		MIN.	TYP.	MAX.		MIN.	TYP.	MAX.		MIN.	TYP.	MAX.		
VLHW5100	White	5600	-	11 200	20	-	0.33, 0.33	-	20	2.8	-	3.6	20	InGaN and converter

ABSOLUTE MAXIMUM RATINGS ($T_{amb} = 25^\circ\text{C}$, unless otherwise specified)

PARAMETER	TEST CONDITION	SYMBOL	VALUE	UNIT
Reverse voltage		V_R	5	V
DC forward current		I_F	30	mA
Peak forward current	at 1 kHz, $t_p/T = 0.1$	I_{FSM}	0.1	A
Power dissipation		P_V	100	mW
Zener reverse current		I_Z	100	mA
Junction temperature		T_j	100	$^\circ\text{C}$
Operating temperature range		T_{amb}	-40 to +100	$^\circ\text{C}$
Storage temperature range		T_{stg}	-40 to +100	$^\circ\text{C}$
Soldering temperature	$t \leq 5$ s	T_{sd}	260	$^\circ\text{C}$
Thermal resistance junction-to-ambient		R_{thJA}	400	K/W

Rev. 1.3, 20-May-2019

1

Document Number: 81159

For technical questions, contact: LED@vishay.com

THIS DOCUMENT IS SUBJECT TO CHANGE WITHOUT NOTICE. THE PRODUCTS DESCRIBED HEREIN AND THIS DOCUMENT ARE SUBJECT TO SPECIFIC DISCLAIMERS, SET FORTH AT www.vishay.com/doc?91000

Figure D.1: Light Emitting Diode Datasheet



www.vishay.com

VLHW5100

Vishay Semiconductors

OPTICAL AND ELECTRICAL CHARACTERISTICS (T _{amb} = 25 °C, unless otherwise specified)							
WHITE VLHW5100							
PARAMETER	TEST CONDITION	PART	SYMBOL	MIN.	TYP.	MAX.	UNIT
Luminous intensity	I _F = 20 mA	VLHW5100	I _V	5600	-	11 200	mcd
Chromaticity coordinate x acc. to CIE 1931	I _F = 20 mA		x	-	0.33	-	
Chromaticity coordinate y acc. to CIE 1931	I _F = 20 mA		y	-	0.33	-	
Angle of half intensity	I _F = 20 mA		φ	-	± 10	-	°
Forward voltage	I _F = 20 mA		V _F	2.8	-	3.6	V
Reverse current	V _R = 5 V		I _R	-	-	50	μA
Temperature coefficient of V _F	I _F = 20 mA		TC _{V_F}	-	-4	-	mV/K
Temperature coefficient of I _V	I _F = 20 mA		TC _{I_V}	-	-0.5	-	% / K

CHROMATICITY COORDINATED CLASSIFICATION				
GROUP	X		Y	
	MIN.	MAX.	MIN.	MAX.
3A	0.2900	0.3025	y = 1.4x - 0.121	y = 1.4x - 0.071
3B	0.3025	0.3150	y = 1.4x - 0.121	y = 1.4x - 0.071
3C	0.2900	0.3025	y = 1.4x - 0.171	y = 1.4x - 0.121
3D	0.3025	0.3150	y = 1.4x - 0.171	y = 1.4x - 0.121
4A	0.3150	0.3275	y = 1.4x - 0.121	y = 1.4x - 0.071
4B	0.3275	0.3400	y = 1.4x - 0.121	y = 1.4x - 0.071
4C	0.3150	0.3275	y = 1.4x - 0.171	y = 1.4x - 0.121
4D	0.3275	0.3400	y = 1.4x - 0.171	y = 1.4x - 0.121
5A	0.3400	0.3525	y = 1.4x - 0.121	y = 1.4x - 0.071
5B	0.3525	0.3650	y = 1.4x - 0.121	y = 1.4x - 0.071
5C	0.3400	0.3525	y = 1.4x - 0.171	y = 1.4x - 0.121
5D	0.3525	0.3650	y = 1.4x - 0.171	y = 1.4x - 0.121

Note

- Chromaticity coordinate groups are tested with a tolerance of ± 0.01

LUMINOUS INTENSITY CLASSIFICATION		
GROUP	LIGHT INTENSITY (mcd)	
	MIN.	MAX.
STANDARD		
DB	5600	7100
EA	7100	9000
EB	9000	11 200

Note

- Luminous intensity is tested with an accuracy of ± 11 %.
- The above type numbers represent the order groups which include only a few brightness groups. Only one group will be shipped on each reel (there will be no mixing of two groups on each reel). In order to ensure availability, single brightness groups will not be orderable.
- In a similar manner for colors where color groups are measured and binned, single color groups will be shipped on any one reel.
- In order to ensure availability, single color groups will not be orderable.

FORWARD VOLTAGE CLASSIFICATION		
GROUP	FORWARD VOLTAGE (V)	
	MIN.	MAX.
0	2.8	3.0
1	3.0	3.2
2	3.2	3.4
3	3.4	3.6

Note

- Forward voltage is tested with an accuracy of ± 0.1 V

Figure D.1: continued

GDL-7050L


Key Features:

Mini Size
 Low Cost
 Auto Power Control Function
 High Reliability

Applications:

Biotechnology
 Laser Display
 Laser Printing
 Surveying Equipments

Model Number		GDL-7050L			
Optical Parameters		Specs			Conditions
		Min	Typ	Max	
Wavelength		531nm	532nm	533nm	
Output Power		40mW	50mW	60mW	
Power Stability	2hours @ Constant Temp	-	+/-2%	+/-5%	APC
Operating Temperature (Case)		-	20~35°C ^①	-	
Residual IR		-	-	1%	
Beam Diameter		-	0.1mm	-	At output window
Beam Divergence		-	8mrad	10.5mrad	Full angle, 1/e ²
Roundness		90%	95%	100%	
M-Square		-	1.1	1.2	
RMS Noise(20Hz~20MHz)		-	0.30%	0.50%	At recommended temperature
Polarization Extinction Ratio		100:1	-	-	
Electrical Parameters					
LD Working Current		-	350mA	600mA	
LD Working Voltage		-	2.0V	2.3V	
Monitor Current		200uA	400uA	700uA	50mW at recommended temperature
GDL Power Consumption		-	0.7W	1.38W	
Mechanical Parameters					
Laser Head Dimensions	Length	-	-	15.5mm	
	Diameter	10.48mm	10.50mm	10.52mm	
Beam Alignment Tolerance	Position(Δr)	-	0.1mm	0.3mm	
	Angle	-	7mrad	15mrad	
Laser Weight		-	3.3g	-	
Reliability					
Operating Humidity		-	5%~85% R.H.	-	
Storage Temperature		-	-40 to +85 °C	-	
Shock		-	1500g, 0.5ms, 6 shocks	-	3 axes, 2 shocks/axis
Vibration		-	20~2000Hz, 0.02g ² /Hz	-	3 axes, 1hr/axis
Expected Lifetime (MTTF)		10000hrs	-	-	

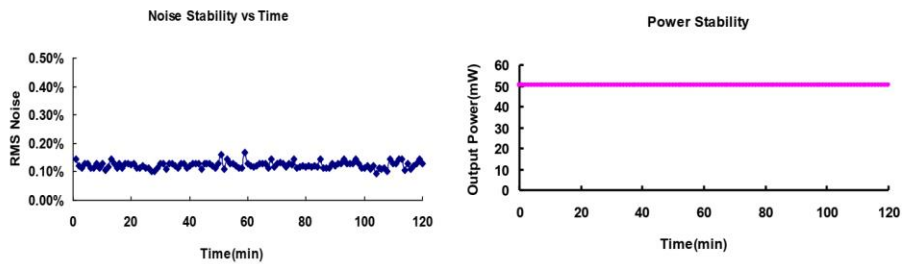
Note: ^① Recommended temperature

Add: 2F, Building 65, 421 Hong Cao Road, Shanghai 200233, China
 Tel: +86-21-64853978 Fax: +86-21-64850389 Email: laser@phototech.com
 Website: www.phototech.com

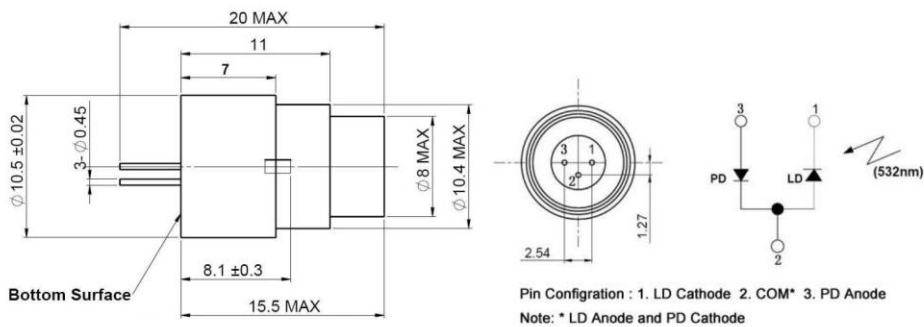
Rev. B

Figure D.2: 532 nm Laser Diode Datasheet

Typical Output Performance



Dimensions and Pin Configuration (Unit: mm)



Add: 2F, Building 65, 421 Hong Cao Road, Shanghai 200233, China
Tel: +86-21-64853978 Fax: +86-21-64850389 Email: laser@phototech.com
Website: www.phototech.com

Rev. B

Figure D.2: continued



405nm Laser Diode



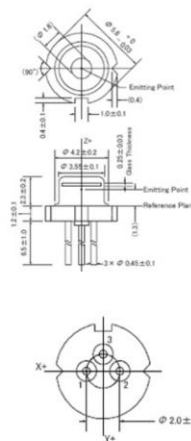
■ Features

- Output Power: 100mW (CW)
- Efficient Quantum Well Structure
- Standard TO-18 Package



Outline Dimension

TO-18 Package



(Unit: mm)

■ Absolute Maximum Ratings

(Tc=25°C)

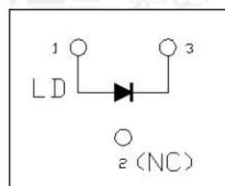
Item	Symbol	Absolute Maximum Ratings	Unit
Optical Output Power	Po	100	mW
LD Reverse Voltage	Vr (LD)	5	V
PD Reverse Voltage	Vr (PD)	-	V
Storage Temperature	Tstg	-40~85	°C
Operating Case Temperature	Tc	-10~70	°C

■ Initial Electrical/Optical Characteristics

(Tc=25°C)

Item	Condition	Symbol	Typ.	Unit
Optical Output	CW	Po	100	mW
Peak Wavelength*	Po=100mW	λ_p	405	nm
Threshold Current	CW	Ith	≤ 0.035	A
Operating Current	Po=100mW	Iop	≤ 0.12	A
Slope Efficiency	CW	η	≥ 1.3	W/A
Operating Voltage	Po=100mW	Vop	≤ 4.6	V
FWHM Beam Divergence	Po=100mW	$\theta_{//}$	≤ 9	deg.
		θ_{\perp}	≤ 20	deg.
Wavelength Temperature Coefficient	Po=100mW		0.3	nm/°C
Polarization	Po=100mW		TE	

Pin Connection



* Measuring specifications.

All figures in this specification are measured by CNI's method and may contain measurement deviations

The above specifications are for reference purpose only and subjected to change without prior notice.



Changchun New Industries Optoelectronics Tech. Co., Ltd

<http://www.cnilaser.com>

◆ CONTACT

No.668, Chuangxin Road, High-tech zone, Changchun 130012, China

Phone: 0086-431-85603799

Fax: 0086-431-87020258

Figure D.3: 405 nm Laser Diode Datasheet

U-LD-650543A

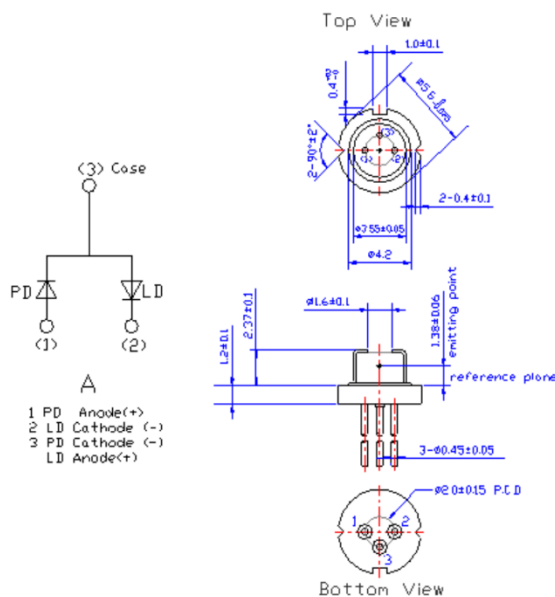
UNION OPTRONICS CORP.

650nm Laser Diode**650nm Red Laser Diode****U-LD-650543A**

■ Specifications

- (1) Device: Laser Diode
 (2) Structure: TO-18(ϕ 5.6mm), With no glass cap, PD

■ External dimensions(Unit : mm)



■ Absolute Maximum Ratings($T_c=25^\circ\text{C}$)

Parameter	Symbol	Value	Unit	
Optical Output	Po	5	mW	
Reverse Voltage	Laser	Vr	2	V
	PIN PD	Vr(PIN)	30	V
Operating Temperature	Top	-10~+40	$^\circ\text{C}$	
Storage Temperature	Tstg	-15~+85	$^\circ\text{C}$	

友嘉科技股份有限公司

桃園縣楊梅鎮3鄰高獅路156號

UNION OPTRONICS CORP.

No.156, Gaoshih Rd., Yangmei Township, Taoyuan County 326, Taiwan (R.O.C.)

TEL : 886-3-485-2687

FAX : 886-3-475-4378

E-mail : sales@uocnet.com

Ver.9 2008/12

Figure D.4: 650 nm Laser Diode Datasheet

650nm Laser Diode

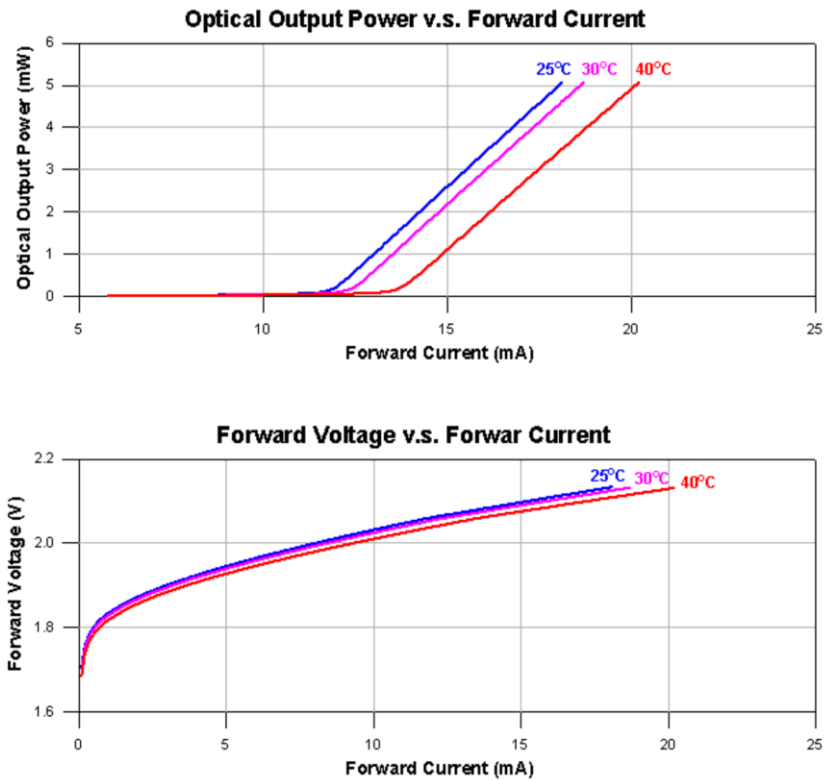
UNION OPTRONICS CORP.

■ Electrical and Optical Characteristics(Tc=25°C)

Parameter	Symbol	Condition	Min.	Typ.	Max.	Unit	
Threshold Current	I _{th}	P _o =5mW	-	12	25	mA	
Operating Current	I _{op}	P _o =5mW	-	18	25	mA	
Operating Voltage	V _{op}	-	-	2.1	2.5	Volt	
Slope Efficiency	η	4mW-1mW	0.4	0.8	-	mW/mA	
		I _{4mW} -I _{1mW}					
Monitor Current	I _m	P _o =5mW	0.05	0.3	0.5	mA	
Beam Divergence (FWHM)	Parallel	$\theta_{//}$	P _o =5mW	5	9	12	deg.
	Perpendicular	θ_{\perp}	P _o =5mW	30	36	42	deg.
Lasing Wavelength	λ	P _o =5mW	640	655	660	nm	

◎ $\theta_{//}$ and θ_{\perp} are defined as the angle within which the intensity is 50% of the peak value.

■ Typical characteristic curves



UNION OPTRONICS CORP.

Figure D.4: continued

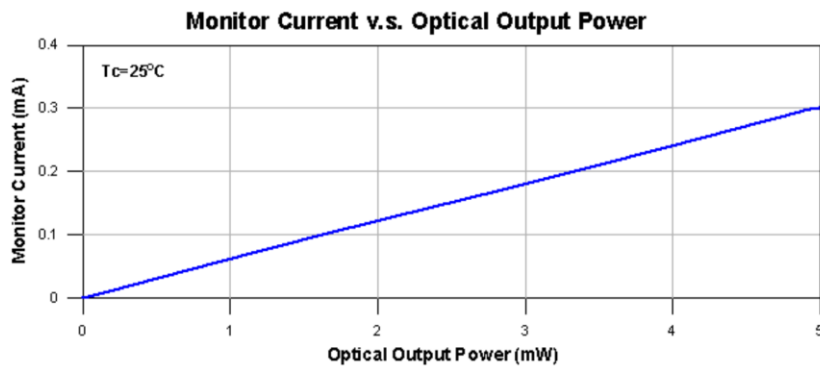
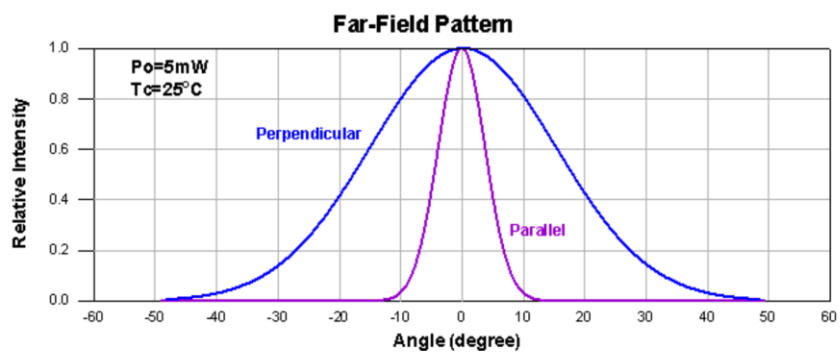
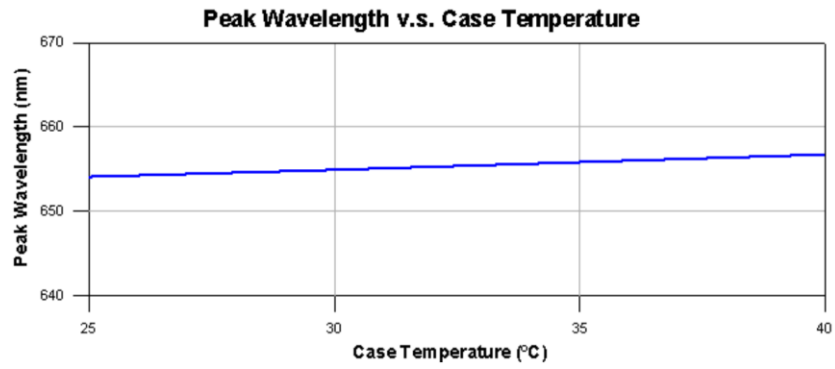


Figure D.4: continued

5/8/2021

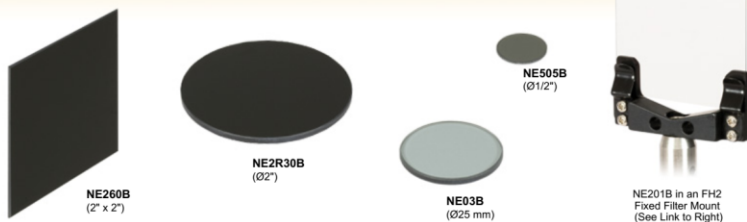
Unmounted Absorptive Neutral Density Filters



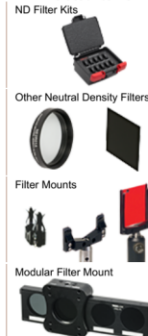
Products Home / Optical Elements / Optical Filters / Neutral Density Filters / Neutral Density Filters: Absorptive/Reflective / Unmounted Absorptive Neutral Density Filters

Unmounted Absorptive Neutral Density Filters

- ▶ Optical Densities from 0.1 to 8.0
- ▶ Attenuate Visible Light
- ▶ Ø1/2", Ø25 mm, Ø2", and 2" x 2" Sizes Available



Related Items



Overview Specs Graphs Damage Thresholds LIDT Calculations Feedback Selection Guide

Filter Sizes	Ø1/2"	Ø25 mm	Ø2"	2" x 2"
Dimensional Tolerance	+0.0 / -0.25 mm (Diameter)			+0.0 / -0.25 mm (H, L)
Clear Aperture	90% Outer Diameter			>90% of Total Area
Surface Flatness (@ 633 nm)	<λ/4 (OD = 0.7, 0.8, 0.9, 1.5) λ/4 (All Other ODs)	<λ (OD = 0.7, 0.8, 0.9, 1.5) λ (All Other ODs)		<2λ (OD = 0.7, 0.8, 0.9, 1.5) 2λ (All Other ODs)
Surface Quality	40-20 Scratch-Dig			
Parallelism	<3 arcmin (OD = 0.7, 0.8, 0.9, 1.5); 3 arcmin (All Other ODs)	<10 arcsec (OD = 0.7, 0.8, 0.9, 1.5) 10 arcsec (All Other ODs)		
Substrates	NG1, NG4, NG9, or NG11 (Schott Glass)			

Damage Thresholds		
Optical Density		Damage Threshold
0.2	Pulsed	10 J/cm ² (532 nm, 10 ns, 10 Hz, Ø0.456 mm)
1.0	Pulsed	10 J/cm ² (532 nm, 10 ns, 10 Hz, Ø0.504 mm)
2.0	CW ^{a,b}	12 W/cm (532 nm, Ø1.0 mm)
4.0	Pulsed	5 J/cm ² (532 nm, 10 ns, 10 Hz, Ø0.340 mm)
6.0	Pulsed	5 J/cm ² (532 nm, 10 ns, 10 Hz, Ø0.340 mm)

a. The power density of your beam should be calculated in terms of W/cm. For an explanation of why the linear power density provides the best metric for long pulse and CW sources, please see the Damage Thresholds tab.
b. CW testing for these filters was performed using a 60 second exposure at each test site.

Optical Density (@ 633 nm)	Theoretical Transmission ^a (@ 633 nm)	Substrate Thickness ^b	Substrate
0.1 ± 0.01	77.6 to 81.3%	0.6 mm	NG11
0.2 ± 0.01	61.7 to 64.6%	1.4 mm	NG11
0.3 ± 0.015	50%	2.3 mm	NG11
0.4 ± 0.02	40%	0.7 mm	NG4
0.5 ± 0.03	32%	0.9 mm	NG4
0.6 ± 0.04	25%	1.1 mm	NG4
0.7 ± 0.04	20%	1.3 mm	NG4
0.8 ± 0.05	16%	1.5 mm	NG4
0.9 ± 0.05	13%	1.7 mm	NG4
1.0 ± 0.06	10%	1.9 mm	NG4
1.3 ± 0.08	5%	2.5 mm	NG4
1.5 ± 0.08	3%	2.9 mm	NG4
2.0 ± 0.10	1%	1.4 mm	NG9
3.0 ± 0.15	0.1%	2.1 mm	NG9
4.0 ± 0.20	1.0x10 ⁻² %	2.8 mm	NG9
5.0 ± 0.25	1.0x10 ⁻³ %	3.6 mm	NG9
6.0 ± 0.30	1.0x10 ⁻⁴ %	1.5 mm	NG1
7.0 ± 0.35	1.0x10 ⁻⁵ %	1.7 mm	NG1
8.0 ± 0.40	1.0x10 ⁻⁶ %	1.9 mm	NG1

a. If desired, Thorlabs can measure the transmission of most of these filters prior to shipment. Please contact [Technical Support](#) for a quote.
b. The actual thickness of each ND filter depends upon the optical density of the lot of glass used to manufacture the filter.

Optical Density

Optical density (OD) indicates the attenuation factor provided by an optical filter, i.e. how much it reduces the optical power of an incident beam. OD is related to the transmission, T, by the equation

$$OD = \log_{10} \left(\frac{1}{T} \right), \text{ or } T = 10^{-OD}$$

where T is a value between 0 and 1. Choosing an ND filter with a higher optical density will translate to lower transmission and greater absorption of the incident light. For higher transmission and less absorption, a lower optical density would be appropriate. As an example, if a filter with an OD of 2 results in a transmission value of 0.01, this means the filter attenuates the beam to 1% of the incident power. Please note that the transmission data for our neutral density filters is provided in percent (%).

Figure D.5: Optical Density Filter Datasheet

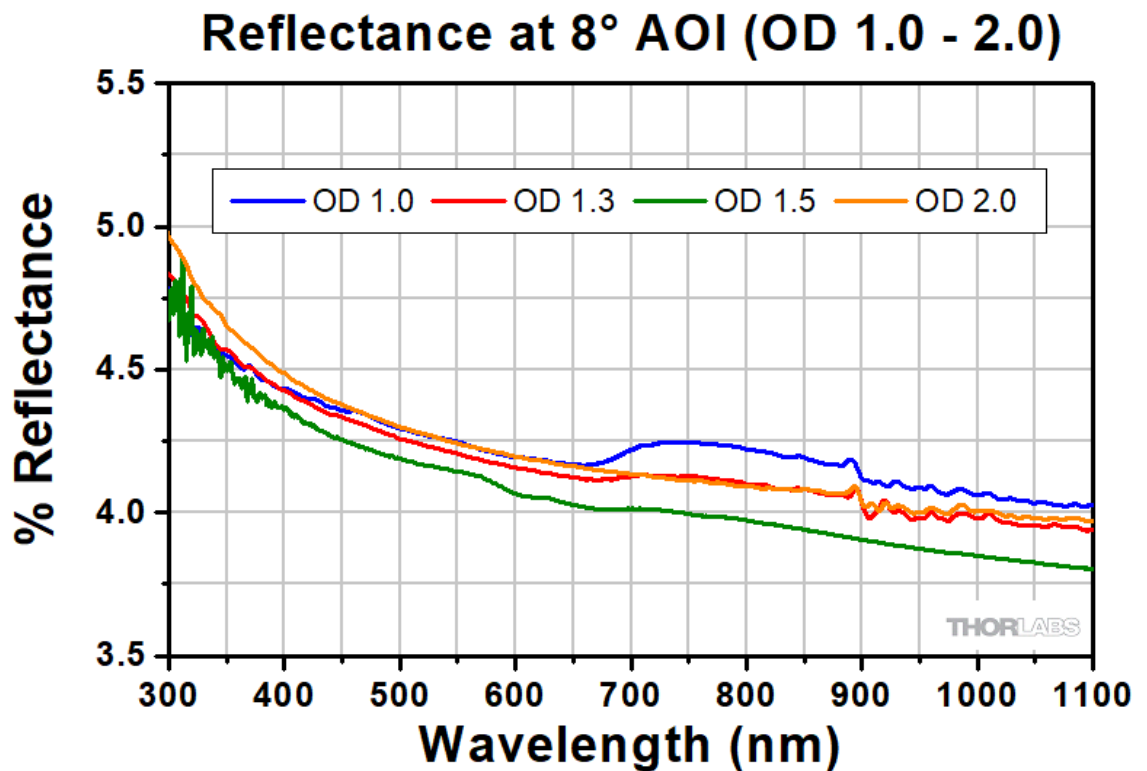
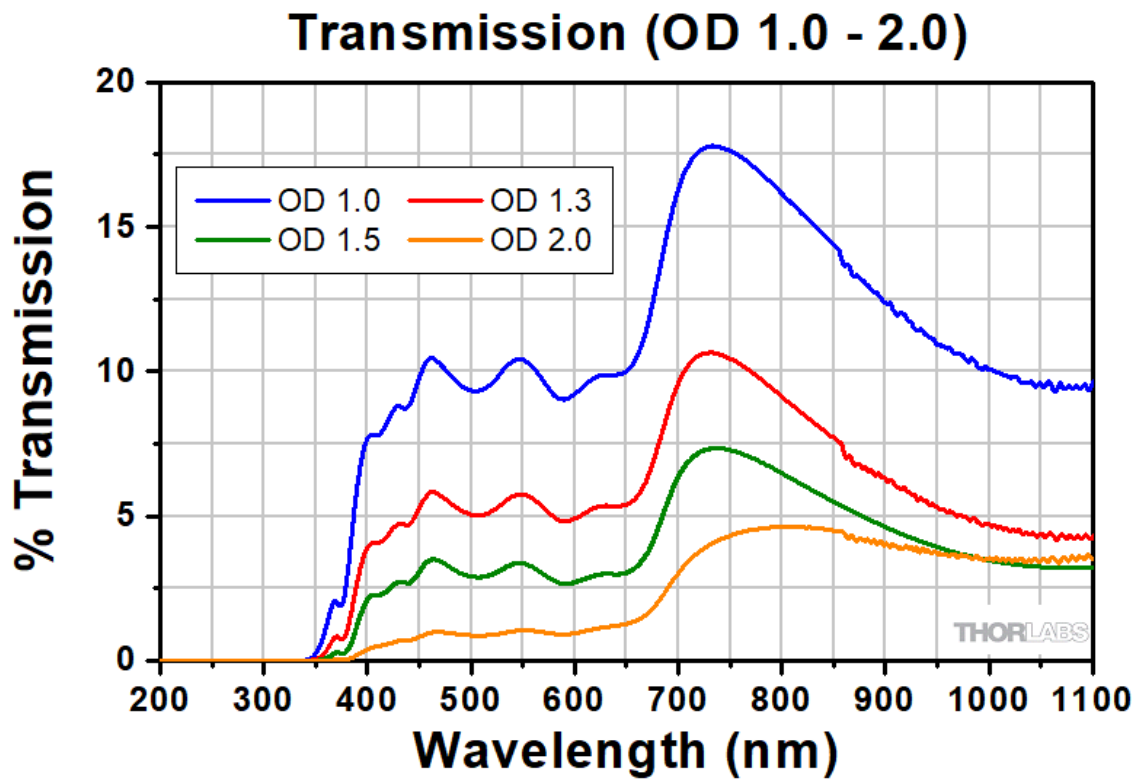


Figure D.5: continued



Products Home / Optical Elements / Optical Filters / Spectral Filters / UV/VIS Bandpass & Laser Line Filters: 340 - 694.3 nm Center Wavelength

UV/VIS Bandpass & Laser Line Filters: 340 - 694.3 nm Center Wavelength

- ▶ Pass Regions Between 1 nm and 40 nm FWHM
- ▶ Ø1/2" and Ø1" Mounted Filters
- ▶ <0.01% Transmission in Blocking Region



FKB-VIS-40



Related Items



Overview Specs Tutorial Feedback

Features

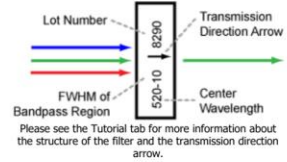
- Central Wavelengths from 340 nm to 694.3 nm
- 1, 3, 10, or 40 nm Bandpass Regions
- Ø1/2" or Ø1" Mounted Filters
- Edge Scribed for Superb Long-Term Stability
- Typical Transmission Plots Available for Every Filter
- Laser Line Filters for Popular Laser Diode, Argon, Krypton, HeCd, HeNe, and Nd:YAG Laser Lines



Optic Handling and Cleaning Tutorial



Click to Enlarge
FL532-1 Filter Mounted in a TRF90 Flip Mount Using a Retaining Ring



The bandpass and laser line filters shown on this page feature center wavelengths shorter than 700 nm. Transmission curves for individual filters are available by viewing the Spec sheet for an individual filter. Each filter is mounted in an unthreaded black anodized aluminum ring with an outer diameter of Ø1/2" or Ø1" and a maximum edge thickness of 6.3 mm. Please note that Ø1/2" filter options are highlighted in green in the tables below.

Thorlabs' bandpass filters provide one of the simplest ways to transmit a well-defined wavelength band of light, while rejecting other unwanted radiation. Their design is essentially that of a thin film Fabry-Perot Interferometer formed by vacuum deposition techniques and consists of two reflecting stacks, separated by an even-order spacer layer. These reflecting stacks are constructed from alternating layers of high and low refractive index materials, which can have a reflectance in excess of 99.99%. By varying the thickness of the spacer layer and/or the number of reflecting layers, the central wavelength and bandwidth of the filter can be altered.

This type of filter displays very high transmission in the bandpass region, but the spectral range of blocked light on either side of the bandpass region is narrow. To compensate for this, an additional blocking component is added, which is either an all dielectric or a metal-dielectric depending on the requirements of the filter. Although this additional blocking component will eliminate any unwanted out-of-band radiation, it also reduces the filter's overall transmission throughput. For applications with demanding wavefront requirements, such as imaging, please consider our [premium bandpass filters](#).

Each filter is housed in a black anodized aluminum ring that is labeled with an arrow indicating the design transmission direction. The ring makes handling easier and enhances the blocking OD by limiting scattering. These filters can be mounted in our extensive line of [filter mounts and wheels](#). As the mounts are not threaded, [retaining rings](#) will be required to mount the filters in one of our internally-threaded [lens tubes](#) or filter mounts, as shown above. We do not recommend removing the filter from its mount, as the filter consists of several layers of glass that are held together with epoxy and the mounting ring. These glass layers are necessary to protect the dielectric coating from the atmosphere; exposure would significantly reduce the filter's transmission efficiency over time.

Please note that due to the gradual breakdown of the dielectric coatings, our bandpass filters have a typical lifetime of two years. Older filters will experience a decrease in overall transmission in the passband.

Additional Bandpass Filters

UV/Visible Bandpass Filters 340 - 694.3 nm CWLs	NIR Bandpass Filters 700 - 1650 nm CWLs	MIR Bandpass Filters 1750 - 9500 nm CWLs	Premium Bandpass Filters 300 - 1550 nm CWLs	Bandpass Filter Kits
--	--	---	--	--------------------------------------

We also offer custom bandpass filters with other central wavelengths or FWHM. To request a quote, contact [Tech Support](#).

340 - 390 nm Bandpass Filters

Item #	CWL ^a	FWHM ^b	T (Min) ^c	Blocking ^d	Transmission/ OD Data ^e	Laser Line	Size
FB340-10	340 ± 2 nm	10 ± 2 nm	25%	200 - 3000 nm	ⓘ	N/A	Ø1"
FB350-10	350 ± 2 nm	10 ± 2 nm	25%	200 - 3000 nm	ⓘ	N/A	Ø1"
FL355-10	355 ± 2 nm	10 ± 2 nm	25%	200 - 1150 nm	ⓘ	Nd:YAG	Ø1"
FB360-10	360 ± 2 nm	10 ± 2 nm	25%	200 - 3000 nm	ⓘ	N/A	Ø1"
FB370-10	370 ± 2 nm	10 ± 2 nm	25%	200 - 3000 nm	ⓘ	N/A	Ø1"
FB380-10	380 ± 2 nm	10 ± 2 nm	25%	200 - 3000 nm	ⓘ	N/A	Ø1"
FB390-10	390 ± 2 nm	10 ± 2 nm	30%	200 - 3000 nm	ⓘ	N/A	Ø1"

a. Center Wavelength
b. Full Width Half Max
c. Minimum Transmission at Center Wavelength

Figure D.6: Bandpass Emission Filter Datasheet

5/8/2021

UV/VIS Bandpass & Laser Line Filters: 340 - 694.3 nm Center Wavelength



Products Home / Optical Elements / Optical Filters / Spectral Filters / UV/VIS Bandpass & Laser Line Filters: 340 - 694.3 nm Center Wavelength

UV/VIS Bandpass & Laser Line Filters: 340 - 694.3 nm Center Wavelength

- Pass Regions Between 1 nm and 40 nm FWHM
- Ø1/2" and Ø1" Mounted Filters
- <0.01% Transmission in Blocking Region

Related Items

- Filter Mounts
- Fast-Change Filter Mount
- Fast Filter Wheel
- Liquid Crystal Tunable Filter

Overview **Specs** Tutorial Feedback

Common Specifications	
Out of Band Transmission	<0.01%
Housing Diameter	1/2" (Laser Line) 1" (Bandpass)
Housing Diameter Tolerance	+0.0 / -0.2 mm
Clear Aperture	Ø8.6 mm (Min) for Ø1/2" Ø21 mm (Min) for Ø1"
Thickness	<6.3 mm
Surface/Coating Quality	80-50 Scratch-Dig
Edge Treatment	Mounted in Black Anodized Aluminum Ring
Edge Markings	CWL-FWHM † Lot Number; The Arrow Points in the Direction of the light transmission
Substrates	Schott Borofloat and Soda Lime
Optimum Operating Temperature	23 °C
Operating Temperature	-50 to 80 °C

340 - 390 nm Bandpass Filters

Item #	CWL ^a	FWHM ^b	T (Min) ^c	Blocking ^d	Transmission/ OD Data ^e	Laser Line	Size
FB340-10	340 ± 2 nm	10 ± 2 nm	25%	200 - 3000 nm		N/A	Ø1"
FB350-10	350 ± 2 nm	10 ± 2 nm	25%	200 - 3000 nm		N/A	Ø1"
FL355-10	355 ± 2 nm	10 ± 2 nm	25%	200 - 1150 nm		Nd:YAG	Ø1"
FB360-10	360 ± 2 nm	10 ± 2 nm	25%	200 - 3000 nm		N/A	Ø1"
FB370-10	370 ± 2 nm	10 ± 2 nm	25%	200 - 3000 nm		N/A	Ø1"
FB380-10	380 ± 2 nm	10 ± 2 nm	25%	200 - 3000 nm		N/A	Ø1"
FB390-10	390 ± 2 nm	10 ± 2 nm	30%	200 - 3000 nm		N/A	Ø1"

^a Center Wavelength
^b Full Width Half Max
^c Minimum Transmission at Center Wavelength
^d <0.01% (<40 dB)
^e Click on for a plot and downloadable data. Measured data accounts for all losses including Fresnel reflections. Please note that transmission is only guaranteed for the specified center wavelength and that the data in the plots is typical. Performance may vary from lot to lot.

Based on your currency / country selection, your order will ship from Newton, New Jersey

+1	Qty	Docs	Part Number - Universal	Price	Available
	<input type="text"/>		FB340-10 Ø1" Bandpass Filter, CWL = 340 ± 2 nm, FWHM = 10 ± 2 nm	\$146.08	Today
	<input type="text"/>		FB350-10 Ø1" Bandpass Filter, CWL = 350 ± 2 nm, FWHM = 10 ± 2 nm	\$146.08	Today
	<input type="text"/>		FL355-10 Ø1" Laser Line Filter, CWL = 355 ± 2 nm, FWHM = 10 ± 2 nm	\$153.67	5-8 Days
	<input type="text"/>		FB360-10 Ø1" Bandpass Filter, CWL = 360 ± 2 nm, FWHM = 10 ± 2 nm	\$146.08	Today
	<input type="text"/>		FB370-10 Ø1" Bandpass Filter, CWL = 370 ± 2 nm, FWHM = 10 ± 2 nm	\$146.08	Today
	<input type="text"/>		FB380-10 Ø1" Bandpass Filter, CWL = 380 ± 2 nm, FWHM = 10 ± 2 nm	\$146.08	Today
	<input type="text"/>		FB390-10 Ø1" Bandpass Filter, CWL = 390 ± 2 nm, FWHM = 10 ± 2 nm	\$146.08	Today

Add To Cart

Figure D.6: continued

5/8/2021

UV/VIS Bandpass & Laser Line Filters: 340 - 694.3 nm Center Wavelength



FB400-10	400 ± 2 nm	10 ± 2 nm	37%	200 - 3000 nm		N/A	Ø1"
FB400-40	400 ± 8 nm	40 ± 8 nm	45%	200 - 1150 nm		N/A	Ø1"
FB405-10	405 ± 2 nm	10 ± 2 nm	37%	200 - 3000 nm		N/A	Ø1"

Copyright © 1999-2021 Thorlabs, Inc.

Careers

Site Index

Privacy Policy

English ^

 USD ^

FB460-10	460 ± 2 nm	10 ± 2 nm	45%	200 - 3000 nm		N/A	Ø1"
FB470-10	470 ± 2 nm	10 ± 2 nm	45%	200 - 3000 nm		N/A	Ø1"
FB480-10	480 ± 2 nm	10 ± 2 nm	45%	200 - 3000 nm		N/A	Ø1"
FL488-1	488 ± 0.2 nm	1 ± 0.2 nm	40%	200 - 1150 nm		Argon	Ø1"
FL488-3	488 ± 0.6 nm	3 ± 0.6 nm	45%	200 - 1150 nm		Argon	Ø1"
FL05488-10	488 ± 2 nm	10 ± 2 nm	65%	200 - 1100 nm		Argon	Ø1/2"
FL488-10	488 ± 2 nm	10 ± 2 nm	65%	200 - 1150 nm		Argon	Ø1"
FB490-10	490 ± 2 nm	10 ± 2 nm	45%	200 - 3000 nm		N/A	Ø1"

- a. Center Wavelength
- b. Full Width Half Max
- c. Minimum Transmission at Center Wavelength
- d. <0.01% (<40 dB)
- e. Click on for a plot and downloadable data. Measured data accounts for all losses including Fresnel reflections. Please note that transmission is only guaranteed for the specified center wavelength and that the data in the plots is typical. Performance may vary from lot to lot.

Based on your currency / country selection, your order will ship from Newton, New Jersey

+1	Qty	Docs	Part Number - Universal	Price	Available
	<input type="text"/>		FB400-10 Ø1" Bandpass Filter, CWL = 400 ± 2 nm, FWHM = 10 ± 2 nm	\$135.27	Today
	<input type="text"/>		FB400-40 Ø1" Bandpass Filter, CWL = 400 ± 8 nm, FWHM = 40 ± 8 nm	\$122.28	Today
	<input type="text"/>		FB405-10 Ø1" Bandpass Filter, CWL = 405 ± 2 nm, FWHM = 10 ± 2 nm	\$108.21	Today
	<input type="text"/>		FB410-10 Ø1" Bandpass Filter, CWL = 410 ± 2 nm, FWHM = 10 ± 2 nm	\$108.21	Today
	<input type="text"/>		FB420-10 Ø1" Bandpass Filter, CWL = 420 ± 2 nm, FWHM = 10 ± 2 nm	\$108.21	Today
	<input type="text"/>		FB430-10 Ø1" Bandpass Filter, CWL = 430 ± 2 nm, FWHM = 10 ± 2 nm	\$107.13	Today
	<input type="text"/>		FB440-10 Ø1" Bandpass Filter, CWL = 440 ± 2 nm, FWHM = 10 ± 2 nm	\$107.13	Today
	<input type="text"/>		FL441.6-10 Ø1" Laser Line Filter, CWL = 441.6 ± 2 nm, FWHM = 10 ± 2 nm	\$108.21	Today
	<input type="text"/>		FB450-10 Ø1" Bandpass Filter, CWL = 450 ± 2 nm, FWHM = 10 ± 2 nm	\$107.13	Today
	<input type="text"/>		FB450-40 Ø1" Bandpass Filter, CWL = 450 ± 8 nm, FWHM = 40 ± 8 nm	\$103.89	Today
	<input type="text"/>		FL457.9-10 Ø1" Laser Line Filter, CWL = 457.9 ± 2 nm, FWHM = 10 ± 2 nm	\$108.21	Today
	<input type="text"/>		FL460-10 Ø1" Laser Line Filter, CWL = 460 ± 2 nm, FWHM = 10 ± 2 nm	\$108.21	Today
	<input type="text"/>		FB460-10 Ø1" Bandpass Filter, CWL = 460 ± 2 nm, FWHM = 10 ± 2 nm	\$101.72	Today
	<input type="text"/>		FB470-10 Ø1" Bandpass Filter, CWL = 470 ± 2 nm, FWHM = 10 ± 2 nm	\$101.72	Today
	<input type="text"/>		FB480-10 Ø1" Bandpass Filter, CWL = 480 ± 2 nm, FWHM = 10 ± 2 nm	\$101.72	Today
	<input type="text"/>		FL488-1 Ø1" Laser Line Filter, CWL = 488 ± 0.2 nm, FWHM = 1 ± 0.2 nm	\$228.33	Today
	<input type="text"/>		FL488-3 Ø1" Laser Line Filter, CWL = 488 ± 0.6 nm, FWHM = 3 ± 0.6 nm	\$195.86	Today
	<input type="text"/>		FL05488-10 Ø1/2" Laser Line Filter, CWL = 488 ± 2 nm, FWHM = 10 ± 2 nm	\$51.14	Today
	<input type="text"/>		FL488-10 Ø1" Laser Line Filter, CWL = 488 ± 2 nm, FWHM = 10 ± 2 nm	\$101.72	Today
	<input type="text"/>		FB490-10 Ø1" Bandpass Filter, CWL = 490 ± 2 nm, FWHM = 10 ± 2 nm	\$99.56	Today

Add To Cart

500 - 590 nm Bandpass Filters

Item #	CWL ^a	FWHM ^b	T (Min) ^c	Blocking ^d	Transmission/ OD Data ^e	Laser Line	Size
FB500-10	500 ± 2 nm	10 ± 2 nm	50%	200 - 1200 nm		N/A	Ø1"
FB500-40	500 ± 8 nm	40 ± 8 nm	70%	200 - 1150 nm		N/A	Ø1"
FL508.5-10	508.5 ± 2 nm	10 ± 2 nm	65%	200 - 1150 nm		Argon	Ø1"
FB510-10	510 ± 2 nm	10 ± 2 nm	50%	200 - 3000 nm		N/A	Ø1"
FL05514.5-1	514.5 ± 0.2 nm	1 ± 0.2 nm	45%	200 - 1100 nm		Argon	Ø1/2"
FL514.5-1	514.5 ± 0.2 nm	1 ± 0.2 nm	45%	200 - 1150 nm		Argon	Ø1"
FL514.5-3	514.5 ± 0.6 nm	3 ± 0.6 nm	55%	200 - 1150 nm		Argon	Ø1"
FL514.5-10	514.5 ± 2 nm	10 ± 2 nm	65%	200 - 1150 nm		Argon	Ø1"
FB520-10	520 ± 2 nm	10 ± 2 nm	50%	200 - 3000 nm		N/A	Ø1"
FB530-10	530 ± 2 nm	10 ± 2 nm	50%	200 - 3000 nm		N/A	Ø1"

Figure D.6: continued

5/8/2021

UV/VIS Bandpass & Laser Line Filters: 340 - 694.3 nm Center Wavelength



FL532-3	532 ± 0.6 nm	3 ± 0.6 nm	60%	200 - 1150 nm		Nd:YAG	Ø1"
FL05532-10	532 ± 2 nm	10 ± 2 nm	70%	200 - 1100 nm		Nd:YAG	Ø1/2"
FL532-10	532 ± 2 nm	10 ± 2 nm	70%	200 - 1150 nm		Nd:YAG	Ø1"
FB540-10	540 ± 2 nm	10 ± 2 nm	50%	200 - 3000 nm		N/A	Ø1"

Copyright © 1999-2021 Thorlabs, Inc.

Careers

Site Index

Privacy Policy

English USD

c. Minimum Transmission at Center Wavelength
d. <0.01% (<40 dB)

e. Click on for a plot and downloadable data. Measured data accounts for all losses including Fresnel reflections. Please note that transmission is only guaranteed for the specified center wavelength and that the data in the plots is typical. Performance may vary from lot to lot.

Based on your currency / country selection, your order will ship from Newton, New Jersey

+1	Qty	Docs	Part Number - Universal	Price	Available
	<input type="text"/>		FB500-10 Ø1" Bandpass Filter, CWL = 500 ± 2 nm, FWHM = 10 ± 2 nm	\$99.56	Today
	<input type="text"/>		FB500-40 Ø1" Bandpass Filter, CWL = 500 ± 8 nm, FWHM = 40 ± 8 nm	\$99.56	Today
	<input type="text"/>		FL508.5-10 Ø1" Laser Line Filter, CWL = 508.5 ± 2 nm, FWHM = 10 ± 2 nm	\$101.72	Today
	<input type="text"/>		FB510-10 Ø1" Bandpass Filter, CWL = 510 ± 2 nm, FWHM = 10 ± 2 nm	\$95.77	Today
	<input type="text"/>		FL05514.5-1 Ø1/2" Laser Line Filter, CWL = 514.5 ± 0.2 nm, FWHM = 1 ± 0.2 nm	\$98.75	Today
	<input type="text"/>		FL514.5-1 Ø1" Laser Line Filter, CWL = 514.5 ± 0.2 nm, FWHM = 1 ± 0.2 nm	\$228.33	Today
	<input type="text"/>		FL514.5-3 Ø1" Laser Line Filter, CWL = 514.5 ± 0.6 nm, FWHM = 3 ± 0.6 nm	\$149.33	Today
	<input type="text"/>		FL514.5-10 Ø1" Laser Line Filter, CWL = 514.5 ± 2 nm, FWHM = 10 ± 2 nm	\$101.72	Today
	<input type="text"/>		FB520-10 Ø1" Bandpass Filter, CWL = 520 ± 2 nm, FWHM = 10 ± 2 nm	\$93.61	Today
	<input type="text"/>		FB530-10 Ø1" Bandpass Filter, CWL = 530 ± 2 nm, FWHM = 10 ± 2 nm	\$93.61	Today
	<input type="text"/>		FL05532-1 Ø1/2" Laser Line Filter, CWL = 532 ± 0.2 nm, FWHM = 1 ± 0.2 nm	\$98.75	Today
	<input type="text"/>		FL532-1 Ø1" Laser Line Filter, CWL = 532 ± 0.2 nm, FWHM = 1 ± 0.2 nm	\$228.33	Today
	<input type="text"/>		FL532-3 Ø1" Laser Line Filter, CWL = 532 ± 0.6 nm, FWHM = 3 ± 0.6 nm	\$149.33	Today
	<input type="text"/>		FL05532-10 Ø1/2" Laser Line Filter, CWL = 532 ± 2 nm, FWHM = 10 ± 2 nm	\$51.14	Today
	<input type="text"/>		FL532-10 Ø1" Laser Line Filter, CWL = 532 ± 2 nm, FWHM = 10 ± 2 nm	\$101.72	Today
	<input type="text"/>		FB540-10 Ø1" Bandpass Filter, CWL = 540 ± 2 nm, FWHM = 10 ± 2 nm	\$93.61	Today
	<input type="text"/>		FL543.5-10 Ø1" Laser Line Filter, CWL = 543.5 ± 2 nm, FWHM = 10 ± 2 nm	\$101.72	Today
	<input type="text"/>		FB550-10 Ø1" Bandpass Filter, CWL = 550 ± 2 nm, FWHM = 10 ± 2 nm	\$93.61	Today
	<input type="text"/>		FB550-40 Ø1" Bandpass Filter, CWL = 550 ± 8 nm, FWHM = 40 ± 8 nm	\$109.29	Today
	<input type="text"/>		FB560-10 Ø1" Bandpass Filter, CWL = 560 ± 2 nm, FWHM = 10 ± 2 nm	\$93.61	Today
	<input type="text"/>		FB570-10 Ø1" Bandpass Filter, CWL = 570 ± 2 nm, FWHM = 10 ± 2 nm	\$93.61	Today
	<input type="text"/>		FB580-10 Ø1" Bandpass Filter, CWL = 580 ± 2 nm, FWHM = 10 ± 2 nm	\$93.61	Today
	<input type="text"/>		FB590-10 Ø1" Bandpass Filter, CWL = 590 ± 2 nm, FWHM = 10 ± 2 nm	\$93.61	Today

Add To Cart

600 - 694.3 nm Bandpass Filters

Item #	CWL ^a	FWHM ^b	T (Min) ^c	Blocking ^d	Transmission/ OD Data ^e	Laser Line	Size
FB600-10	600 ± 2 nm	10 ± 2 nm	50%	200 - 1200 nm		N/A	Ø1"
FB600-40	600 ± 8 nm	40 ± 8 nm	70%	200 - 1150 nm		N/A	Ø1"
FB610-10	610 ± 2 nm	10 ± 2 nm	50%	200 - 3000 nm		N/A	Ø1"
FB620-10	620 ± 2 nm	10 ± 2 nm	50%	200 - 3000 nm		N/A	Ø1"
FB630-10	630 ± 2 nm	10 ± 2 nm	50%	200 - 3000 nm		N/A	Ø1"
FL05632.8-1	632.8 ± 0.2 nm	1 ± 0.2 nm	50%	200 - 1100 nm		HeNe	Ø1/2"
FL632.8-1	632.8 ± 0.2 nm	1 ± 0.2 nm	50%	200 - 1150 nm		HeNe	Ø1"
FL05632.8-3	632.8 ± 0.6 nm	3 ± 0.6 nm	65%	200 - 1100 nm		HeNe	Ø1/2"
FL632.8-3	632.8 ± 0.6 nm	3 ± 0.6 nm	65%	200 - 1150 nm		HeNe	Ø1"
FL05632.8-10	632.8 ± 2 nm	10 ± 2 nm	70%	200 - 1100 nm		HeNe	Ø1/2"
FL632.8-10	632.8 ± 2 nm	10 ± 2 nm	70%	200 - 1150 nm		HeNe	Ø1"
FL05635-10	635 ± 2 nm	10 ± 2 nm	70%	200 - 1100 nm		Diode	Ø1/2"
FL635-10	635 ± 2 nm	10 ± 2 nm	70%	200 - 1150 nm		Diode	Ø1"
FB640-10	640 ± 2 nm	10 ± 2 nm	50%	200 - 1200 nm		N/A	Ø1"
FL647.1-10	647.1 ± 2 nm	10 ± 2 nm	70%	200 - 1150 nm		Krypton	Ø1"
FB650-10	650 ± 2 nm	10 ± 2 nm	50%	200 - 1200 nm		N/A	Ø1"

https://www.thorlabs.com/newgrouppage9.cfm?objectgroup_id=1001&pn=FB530-10

3/5

Figure D.6: continued

Appendix E: Software code

```

package com.example.myapplication;

import androidx.annotation.NonNull;
import androidx.annotation.Nullable;
import androidx.appcompat.app.AppCompatActivity;

import android.Manifest;
import android.content.Intent;
import android.content.pm.PackageManager;
import android.graphics.Bitmap;
import android.net.Uri;
import android.os.Build;
import android.os.Bundle;
import android.provider.MediaStore;
import android.view.View;
import android.widget.Button;
import android.widget.ImageView;
import android.widget.Switch;
import android.widget.Toast;

import java.security.Permissions;

public class MainActivity extends AppCompatActivity {

    ImageView mImageView;
    Button mChooseBtn;

    private static final int IMAGE_PICK_CODE = 1000;
    private static final int PERMISSION_CODE = 1001;

    @Override
    protected void onCreate(Bundle savedInstanceState) {
        super.onCreate(savedInstanceState);
        setContentView(R.layout.activity_main);

        //VIEWS
        mImageView = findViewById(R.id.image_view);
        mChooseBtn = findViewById(R.id.choose_image_btn);

        //handle button click
        mChooseBtn.setOnClickListener(new View.OnClickListener() {
            @Override
            public void onClick(View v) {
                //check runtime permission
                if (Build.VERSION.SDK_INT >= Build.VERSION_CODES.M){
                    if
                    (checkSelfPermission(Manifest.permission.READ_EXTERNAL_STORAGE)
                        == PackageManager.PERMISSION_DENIED){
                        //permission not granted, request it.
                        String[] permissions =
                        {Manifest.permission.READ_EXTERNAL_STORAGE};
                        //show popup for runtime permission
                        requestPermissions(permissions, PERMISSION_CODE);
                    }
                    else {
                        //permission already granted
                        pickImageFromGallery();
                    }
                }
            }
        });
    }
}

```

```

    }
}
else {
    //system os is less then marshmallow
    pickImageFromGallery();
}
}
});
}

private void pickImageFromGallery() {
    //intent to pick image
    Intent intent = new Intent(Intent.ACTION_PICK);
    intent.setType("image/*");
    startActivityForResult(intent, IMAGE_PICK_CODE);
}

//handle result of runtime permission
@Override
public void onRequestPermissionsResult(int requestCode, @NonNull String[]
permissions, @NonNull int[] grantResults) {
    switch (requestCode){
        case PERMISSION_CODE:{
            if (grantResults.length >0 && grantResults[0] ==
                PackageManager.PERMISSION_GRANTED){
                //permission was granted
                pickImageFromGallery();
            }
            else {
                //permission was denied
                Toast.makeText(this, "Permission denied...!",
                    Toast.LENGTH_SHORT).show();
            }
        }
    }
}

//handle result of picked image
@Override
protected void onActivityResult(int requestCode, int resultCode, Intent
data) {
    if (resultCode == RESULT_OK && requestCode == IMAGE_PICK_CODE){
        //set image to image view
        mImageView.setImageURI(data.getData());
    }
}
}

package com.example.multipleimage;

import androidx.annotation.NonNull;
import androidx.annotation.Nullable;
import androidx.appcompat.app.AppCompatActivity;

import android.content.Intent;
import android.os.Bundle;
import android.view.View;
import android.widget.ImageView;

```

```

public class MainActivity extends AppCompatActivity {
    private ImageView img1, img2;
    private final int CODE_IMG_GALLERY = 1;
    private final int CODE_MULTIPLE_IMG_GALLERY = 2;

    @Override
    protected void onCreate(Bundle savedInstanceState) {
        super.onCreate(savedInstanceState);
        setContentView(R.layout.activity_main);

        init();
        img1.setOnClickListener(new View.OnClickListener(){
            @Override
            public void onClick (View V){
                startActivityForResult(Intent.createChooser(new Intent().
                    setAction(Intent.ACTION_GET_CONTENT).
                    setType("image/*"), "select one image"),
                    CODE_IMG_GALLERY);
            }
        });

        img2.setOnClickListener(new View.OnClickListener(){
            @Override
            public void onClick (View V){
                Intent intent = new Intent();
                intent.setType("Image/*");
                intent.putExtra(Intent.EXTRA_ALLOW_MULTIPLE, true);
                intent.setAction(Intent.ACTION_GET_CONTENT);
                startActivityForResult(Intent.createChooser(intent,
                    "Select Multiple Images"),
                    CODE_MULTIPLE_IMG_GALLERY);
            }
        });

        private void init() {
            this.img1= findViewById(R.id.img1);
            this.img2= findViewById(R.id.img2);
        }

    @Override
    protected void onActivityResult(int requestCode, int
resultCode, @Nullable Intent data) {
        super.onActivityResult(requestCode, resultCode, data);

        if(requestCode == CODE_IMG_GALLERY && resultCode == Result_OK){
            Uri imageUri = data.getdata();
            if(imageUri==Null){
                img1.setimageUri(imageUri);
            }
            else if(requestCode == CODE_MULTIPLE_IMG_GALLERY &&
resultCode == Result_OK){
                Clipdata clipdata=data.getClipdata();
                if(clipdata=null){
                    img1.setImageUri(clipData.getItemAt(0).getUri());
                }
            }
        }
    }
}

```

```

        img2.setImageUri(clipData.getItemAt(1).getUri());

        for(int i=0; i < clipData.getItemCount(), i++){
            ClipData.Item item= clipData.getItemAt(i);
            Uri uri = item.getUri();
            Log.e(tag: "MAS.IMGS",uri.toString())

        }

    }
}
}

package com.example.mycamera;

import androidx.annotation.Nullable;
import androidx.appcompat.app.AppCompatActivity;

import android.Manifest;
import android.content.Intent;
import android.content.pm.PackageManager;
import android.graphics.Bitmap;
import android.net.Uri;
import android.os.Build;
import android.os.Bundle;
import android.provider.MediaStore;
import android.view.View;
import android.widget.Button;
import android.widget.ImageView;

import java.security.Permission;
import java.security.Permissions;

public class MainActivity extends AppCompatActivity {

    Button btnCaptueImage;
    Button btnChooseImage;
    ImageView imageDisplay;

    private static final int IMAGE_PICK_CODE = 1000;
    private static final int PERMISSION_CODE = 1001;

    @Override
    protected void onCreate(final Bundle savedInstanceState) {
        super.onCreate(savedInstanceState);
        setContentView(R.layout.activity_main);
        btnCaptueImage = (Button)findViewById(R.id.btn_captureImage);
        btnChooseImage = (Button) findViewById(R.id.btn_chooseImage);
        imageDisplay = (ImageView)findViewById(R.id.imageCapture);

        btnCaptueImage.setOnClickListener(new View.OnClickListener() {
            @Override
            public void onClick(View v) {

                Intent intent = new Intent(MediaStore.ACTION_IMAGE_CAPTURE);

```

```

        startActivityForResult(intent, 0);
    }
});

}

@Override
protected void onActivityResult(int requestCode, int resultCode,
@Nullable Intent data) {
    super.onActivityResult(requestCode, resultCode, data);

    Bitmap bitmap = (Bitmap) data.getExtras().get("data");
    imageDisplay.setImageBitmap(bitmap);
}

}

package com.example.mycolorhex;

import androidx.appcompat.app.AppCompatActivity;

import android.annotation.SuppressLint;
import android.graphics.Bitmap;
import android.graphics.Color;
import android.os.Bundle;
import android.view.MotionEvent;
import android.view.View;
import android.widget.ImageView;
import android.widget.TextView;

import com.example.mycolorhex.R;

public class MainActivity extends AppCompatActivity {

    ImageView mImageView;
    TextView mResultTv;
    Bitmap bitmap;
    double XX;

    @SuppressLint("ClickableViewAccessibility")
    @Override
    protected void onCreate(Bundle savedInstanceState) {
        super.onCreate(savedInstanceState);
        setContentView(R.layout.activity_main);

        mImageView = findViewById(R.id.imageView);
        mResultTv = findViewById(R.id.resultTv);

        mImageView.setDrawingCacheEnabled(true);
        mImageView.buildDrawingCache(true);

        mImageView.setOnTouchListener(new View.OnTouchListener(){
            @Override
            public boolean onTouch(View view, MotionEvent event) {
                if (event.getAction()==MotionEvent.ACTION_DOWN ||
event.getAction()==MotionEvent.ACTION_MOVE)
                    bitmap = mImageView.getDrawingCache();
                int pixel =
bitmap.getPixel((int)event.getX(),(int)event.getY());

                int r= Color.red(pixel);
                int g= Color.green(pixel);

```

```

int b= Color.blue(pixel);

String hex = "#"+Integer.toHexString(pixel);

if (g>=200 || r>=200 || b<=150) {
    XX=(550);
}

if (r<=50 || b>=200) {
    XX=(490-(50*(1-g)));
}

if (r<=50 || g>=200) {
    XX=(510-20*b);
}

if (g==1 || b==0) {
    XX=(580-70*(1-r));
}

if (r>=250 || b==0){
    XX=(640-60*g);
}

if (g==0 || b==0 || r==255) {
    XX=(650);
}

if (g==0 || b==0) {
    XX=(780-(80/0.65)*(0.35-r));
}

mResultTv.setText("RGB:"+r +" "+g +" "+b
    +"\nHEX:"+ hex
    +"\nWaveLength:"+XX);

return true;
});
}
}

```

List of Publications

1. **T. Alawsi** and Z. Al-Bawi, “*A review of smartphone point-of-care adapter design,*” Engineering Reports, vol. 1, no. 2, pp. 1-30, Sep. (2019).
<https://doi.org/10.1002/eng2.12039>
2. **T. Alawsi**, G. P. Mattia, Z. Al-Bawi, and R. Beraldi, "*Smartphone-Based Colorimetric Sensor Application for Measuring Biochemical Material Concentration,*" Sens. & Bio-Sens. Res., vol. 32, no. 2, pp. 1-9, 100404, (2021).
<https://doi.org/10.1016/j.sbsr.2021.100404>
3. **T. Alawsi**, Z. Al-Bawi, R. Beraldi, G. P. Mattia, and R. A. Faris, “*A Custom 3D Printed Design of Smartphone-Based Adapter With Android Application for Colorimetric Glucose Concentration Measurements,*” ACS Omega, (2021). (Under Review).

Citations

1. Richard A. Crocombe, Pauline E. Leary, Brooke Kammrath, **“Portable Spectroscopy and Spectrometry 1: Technologies and Instrumentation,”** In Chapter 9: **“Smartphone Technology - Instrumentation and Applications,”** John Wiley & Sons, Jun 14, 2021.
2. Richard A. Crocombe, Pauline E. Leary, Brooke Kammrath, **“Portable Spectroscopy and Spectrometry 2: Applications,”** In Chapter 10: **“Toward Clinical Applications of the Smartphone in Low-Cost and Point-of-Care Settings,”** John Wiley & Sons, Jun 14, 2021.
3. Delamarche, E., Temiz, Y., Lovchik, R..D., Christiansen, M.G. and Simone, S. (2021), **“Capillary microfluidics for monitoring medication adherence,”** Angew. Chem. Int. Ed.. Accepted Author Manuscript. <https://doi.org/10.1002/anie.202101316>
4. T. Alawsi, G. P. Mattia, Z. Al-Bawi, and R. Beraldi, **"Smartphone-Based Colorimetric Sensor Application for Measuring Biochemical Material Concentration,"** Sens. & Bio-Sens. Res., vol. 32, no. 2, pp. 1-9, 100404, (2021). <https://doi.org/10.1016/j.sbsr.2021.100404>
5. Brady Hunt, Alberto J. Ruiz, and Brian W. Pogue, **"Smartphone-based surgical image guidance: future or fantasy?"**, Proc. SPIE 11625, Molecular-Guided Surgery: Molecules, Devices, and Applications VII, 116250K (8 March 2021); <https://doi.org/10.1117/12.2591503>
6. Ezequiel Vidal, Anabela S. Lorenzetti, Carlos D. Garcia, Claudia E. Domini, **“Use of universal 3D-Printed smartphone spectrophotometer to develop a time-based analysis for hypochlorite,”** Analytica Chimica Acta, Volume 1151, 2021, 338249, <https://doi.org/10.1016/j.aca.2021.338249>
7. N. Sathishkumar, Bhushan J. Toley, **“Development of an experimental method to overcome the hook effect in sandwich-type lateral flow immunoassays guided by computational modelling,”** Sensors and Actuators B: Chemical, Volume 324, 2020, 128756, <https://doi.org/10.1016/j.snb.2020.128756>
8. Nath, P.; Kabir, A.; Khoubarfarin Doust, S.; Kreais, Z.J.; Ray, A. **“Detection of Bacterial and Viral Pathogens Using Photonic**

- Point-of-Care Devices,”** *Diagnostics* 2020, 10, 841.
<https://doi.org/10.3390/diagnostics10100841>
9. N, Sathishkumar; Toley, Bhushan (2020): “**Transport Phenomena at Test and Control Lines in Lateral Flow Immunoassays Reveal a Path to Expanding Their Dynamic Range,**” *ChemRxiv*. Preprint.
<https://doi.org/10.26434/chemrxiv.12240338.v1>
10. Vinoth Kumar Rajendran, Padmavathy Bakthavathsalam, Peter L. Bergquist & Anwar Sunna (2021) “**Smartphone technology facilitates point-of-care nucleic acid diagnosis: a beginner’s guide,**” *Critical Reviews in Clinical Laboratory Sciences*, 58:2, 77-100, DOI: <https://doi.org/10.1080/10408363.2020.1781779>
11. G. P. da Nóbrega, M. S. Valença, T. M. S. Nunes, T. M. P. de Silans, C. A. de Souza Filho, “**Characterization and Mitigation of the Influence of Temperature on the Light Source of Surface Plasmon Resonance Biosensors Based on Smartphones,**” *The Brazilian Society of Automation (SBA)*, Vol 2 No 1 (2020): CBA2020, <https://doi.org/10.48011/asba.v2i1.1200>
12. Anderson Luis do Valle, “**Nanocrystals in Glyphosate Detection,**” Ph.D. Thesis in Genetics and Biochemistry, Federal University of Uberlândia: Brazil, 23-Oct-2019, [https://repositorio.ufu.br/bitstream/123456789/27380/1/Nanocrystals GlyphosateDetection.pdf](https://repositorio.ufu.br/bitstream/123456789/27380/1/Nanocrystals%20GlyphosateDetection.pdf)

الخلاصة

في الآونة الأخيرة ، أتاح التصوير والاستشعار المستند إلى الهواتف الذكية إمكانية وصول تطبيقات المجالات متعددة التخصصات من خلال منصة فريدة تحدث فيها جميع العمليات بسرعة وسلاسة. حقق استخدام الأساليب القائمة على الهواتف الذكية تقدماً كبيراً باعتباره أداة موثوقة للاختبار السريع والتشخيص والقياس والمراقبة في الموقع.

في هذا البحث ، تم تحقيق مستشعر لوني قائم على الهاتف الذكي والتحقق منه تجريبياً وإثباته ، تم تنفيذ المستشعر اللوني لكل من جوانب الأجهزة والبرامج بشكل تجريبي لقياس وتصوير المواد الحيوية المتعددة بما في ذلك الدم الكامل والبول والجلوكوز والدهون الثلاثية واليوريا ، HDL ، والبيليروبين. تم إجراء هذه القياسات والتصوير على أجهزة المختبر الحالية ، بالإضافة إلى البرامج فقط ومع كل من أجهزة وبرامج الاستشعار اللونية القائمة على الهاتف الذكي.

بالنسبة للبرنامج (تطبيق الاستشعار اللوني) فقط وعمل الأجهزة المعملية ، تم تحضير عينات الجلوكوز والدهون الثلاثية بتركيزات (100 ، 200 ، 300 ، 400 ، 500 مجم / ديسيلتر) وتركيزات اليوريا (10 ، 30 ، 50 ، 100 ، 150 مجم / ديسيلتر). كانت نطاقات الطول الموجي المقاسة للجلوكوز (350-640 نانومتر) ، والدهون الثلاثية (400-680 نانومتر) ، واليوريا (500-780 نانومتر). نتج عن معامل انحدار الامتصاص والنفاذية (R^2) لتطبيق الاستشعار اللوني 0.9825 و 0.9899 ؛ 0.9405 و 0.9502 ؛ 0.9431 و 0.8597 على التوالي. بينما بالنسبة لمقياس الطيف الضوئي كانت قيم $R^2 @ 560$ 0.9973 (نانومتر) و 0.9793 عند 600 نانومتر. 0.952 عند 620 نانومتر و 0.9364 عند 410 نانومتر ؛ 0.9948 @ 570 نانومتر و 0.9827 @ 530 نانومتر ، على التوالي.

تم توضيح جدوى التصميم الجديد المطبوع ثلاثي الأبعاد المستند إلى الهاتف الذكي بمساعدة البرنامج المصمم بتطبيقات Android التي تهدف فقط إلى قياس تركيز عينات العلامات الحيوية المتعددة بناءً على نهج الكشف اللوني. توفر العناصر البصرية والإلكترونية داخل المحول منصة تصوير موثوقة للحصول على الصور وتحليلها واختبارها وقياساتها السريعة. تم تنفيذ واختبار تصميم المحول المستند إلى الهاتف الذكي المطبوع ثلاثي الأبعاد لتطبيقات قياس الألوان في المؤشرات الحيوية بما في ذلك الجلوكوز واليوريا والدهون الثلاثية والبيليروبين و HDL.

أظهرت النتائج ان قيم معامل الانحدار الخطي (R^2) لمنحنى امتصاص الجلوكوز باستخدام مصادر الإضاءة 405 نانومتر ؛ 532 نانومتر ؛ 650 نانومتر ؛ WLED. WLED + BF ؛ WLED + GF ؛ WLED + YF ؛ WLED + RF هي 0.9922 ؛ 0.9983 ؛ 0.9898 ؛

0.7004 ؛ 0.9518 ؛ 0.9313 ؛ 0.9567 ؛ و 0.9407 على التوالي. باتباع نفس ترتيب مصادر الإضاءة ، فإن R^2 لليوريا 0.9332 ؛ 0.9818 ؛ 0.8829 ؛ 0.9464 ؛ 0.6615 ؛ 0.9161 ؛ 0.9567 ؛ و 0.7502. بالنسبة للدهون الثلاثية ، تكون قيم R^2 0.9496 ؛ 0.9725 ؛ 0.7749 ؛ 0.8395 ؛ 0.8192 ؛ 0.9313 ؛ 0.9567 ؛ و 0.944. بالنسبة إلى البيليروبين ، تكون قيم R^2 0.7858 ؛ 0.9422 ؛ 0.7791 ؛ 0.9124 ؛ 0.9326 ؛ 0.6192 ؛ 0.5894 ؛ و 0.324. بالنسبة لـ HDL ، تكون قيم R^2 هي 0.8248 ؛ 0.7831 ؛ 0.7902 ؛ 0.8332 ؛ 0.9077 ؛ 0.8071 ؛ و 0.998.

بالنسبة لمنحنيات النفاذية ، كانت قيم R^2 بنفس ترتيب مصادر الإضاءة والعلامات الحيوية (0.9915 ؛ 0.9965 ؛ 0.9862 ؛ 0.6997 ؛ 0.9398 ؛ 0.916 ؛ 0.9545 ؛ و 0.9398) ، (0.9263 ؛ 0.9818 ؛ 0.8829 ؛ 0.9464 ؛ 0.6615 ؛ 0.9161 ؛ 0.9567 ؛ و 0.752) ، (0.9035 ؛ 0.955 ؛ 0.9859 ؛ 0.8333 ؛ 0.8063 ، 0.9298 ، 0.9545 ، و 0.9533) ، (0.7123 ؛ 0.9446 ؛ 0.8971 ، 0.9241 ، 0.9289 ، 0.563 ، 0.6669 ، 0.3565) (0.7658 ؛ 0.8003 ، 0.8364 ، 0.8418 ؛ 0.9108 ؛ 0.9044 ؛ 0.7954 ؛ و 0.9575 على التوالي.

كان حد الكشف (LOD) للجلوكوز واليوريا والدهون الثلاثية والبيليروبين و HDL 0.57 مجم / ديسيلتر أو 0.03135 ملي مولاري ، 1.34 مجم / ديسيلتر أو 0.2278 ملي مولاري ، 7.79 مجم / ديسيلتر أو 0.0879 ملي مولاري ، 0.008 مجم / ديسيلتر أو 0.14 ميكرومولاري. و 0.86 مجم / ديسيلتر أو 0.02224 ملي مولاري على التوالي.



وزارة التعليم العالي و البحث العلمي
جامعة بغداد
معهد الليزر للدراسات العليا

تصميم و تحقيق اداء متحسس لوني مبني على الهاتف الذكي

أطروحة مقدمة الى

معهد الليزر للدراسات العليا \ جامعة بغداد \ لاستكمال متطلبات نيل شهادة
دكتوراه فلسفة في الليزر \ الهندسة الالكترونية و الاتصالات

من قبل

طيف عائد فيصل

بكالوريوس هندسة الليزر و الالكترونيات البصرية -2013

ماجستير هندسة الليزر و الالكترونيات البصرية -2017

باشراف

الأستاذ المساعد الدكتورة زينب فاضل مهدي